SIMILARITY SOLUTIONS OF BOUNDARY LAYER FLOWS IN A CHANNEL FILLED BY NON-NEWTONIAN FLUIDS

JAWAD RAZA

DOCTOR OF PHILOSOPHY
UNIVERSITI UTARA MALAYSIA
2018

Awang Had Salleh
Graduate School
of Arts And Sciences

Universiti Utara Malaysia

PERAKUAN KERJA TESIS / DISERTASI
(Certification of thesis / dissertation)

Kami, yang bertandatangan, memperakukan bahawa
(We, the undersigned, certify that)

JAWAD RAZA

calon untuk Ijazah   **PhD**
(candidate for the degree of)

telah mengemukakan tesis / disertasi yang bertajuk:
(has presented his/her thesis / dissertation of the following title):

"SIMILARITY SOLUTIONS OF BOUNDARY LAYER FLOWS IN A CHANNEL FILLED BY NON-NEWTONIAN FLUIDS"

seperti yang tercatat di muka surat tajuk dan kulit tesis / disertasi.
(as it appears on the title page and front cover of the thesis / dissertation).

Bahawa tesis/disertasi tersebut boleh diterima dari segi bentuk serta kandungan dan meliputi bidang ilmu dengan memuaskan, sebagaimana yang ditunjukkan oleh calon dalam ujian lisan yang diadakan pada : **13 Februari 2018.**
That the said thesis/dissertation is acceptable in form and content and displays a satisfactory knowledge of the field of study as demonstrated by the candidate through an oral examination held on:
February 13, 2018.

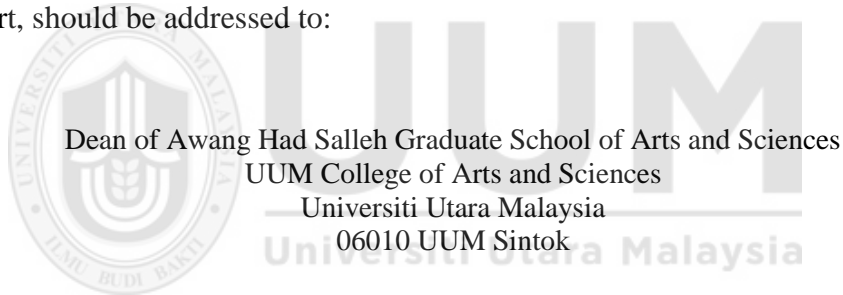|		
Pengerusi Viva: *(Chairman for VIVA)*	**Assoc. Prof. Dr. Rahela Abdul Rahim**	Tandatangan *(Signature)*
Pemeriksa Luar: *(External Examiner)*	**Prof. Dr.Ishak Hashim**	Tandatangan *(Signature)*
Pemeriksa Dalam: *(Internal Examiner)*	**Assoc. Prof. Dr. Azizan Saaban**	Tandatangan *(Signature)*
Nama Penyelia/Penyelia-penyelia: *(Name of Supervisor/Supervisors)*	**Dr. Azizah Mohd Rohni**	Tandatangan *(Signature)*
Nama Penyelia/Penyelia-penyelia: *(Name of Supervisor/Supervisors)*	**Prof. Dr. Zurni Omar**	Tandatangan *(Signature)*

Tarikh:
(Date) **February 13, 2018**

Permission to Use

In presenting this thesis in fulfilment of the requirements for a postgraduate degree from Universiti Utara Malaysia, I agree that the Universiti Library may make it freely available for inspection. I further agree that permission for the copying of this thesis in any manner, in whole or in part, for scholarly purpose may be granted by my supervisor(s) or, in their absence, by the Dean of Awang Had Salleh Graduate School of Arts and Sciences. It is understood that any copying or publication or use of this thesis or parts thereof for financial gain shall not be allowed without my written permission. It is also understood that due recognition shall be given to me and to Universiti Utara Malaysia for any scholarly use which may be made of any material from my thesis.

Requests for permission to copy or to make other use of materials in this thesis, in whole or in part, should be addressed to:

Dean of Awang Had Salleh Graduate School of Arts and Sciences
UUM College of Arts and Sciences
Universiti Utara Malaysia
06010 UUM Sintok

Abstrak

Penyelesaian keserupaan bagi bendalir tak-Newtonan semakin mendapat perhatian para penyelidik kerana kepentingan praktikal dalam bidang sains dan kejuruteraan. Pada masa ini, kebanyakan penyelidik menumpukan kajian terhadap bendalir tak-Newtonan pada permukaan helaian. Walau bagaimanapun, hanya segelintir penyelidik sahaja yang memberi perhatian kepada geometri saluran disebabkan kekompleksan persamaan menakluk. Oleh itu, kajian ini berhasrat untuk mengkaji penyelesaian berangka bagi masalah baharu dalam bendalir nano, bendalir Casson dan bendalir mikropolar tak termampat lamina di bawah pelbagai keadaan aliran bendalir. Setiap bendalir yang dipertimbang melibatkan dinding saluran berliang, dinding meregang atau mengecut, dan dinding mengembang atau menguncup dengan pengaruh pelbagai parameter fizikal. Rumusan matematik seperti hukum pemuliharaan, momentum atau momentum sudut, pemindahan haba dan jisim dilakukan terhadap masalah baharu. Setelah rumusan matematik dibangunkan, persamaan menakluk bagi aliran bendalir berbentuk persamaan pembezaan separa kemudiannya dijelmakan kepada masalah nilai sempadan (MNS) persamaan pembezaan biasa (PPB) tak linear dengan menggunakan penjelmaan keserupaan yang sesuai. Selepas menukarkan MNS peringkat tinggi kepada sistem MNS peringkat pertama yang setara, fungsi *shootlib* dalam perisian Maple 18 digunakan bagi mendapatkan penyelesaian keserupaan PPB tak linear. Keputusan berangka dalam kajian ini dibandingkan dengan penyelesaian sedia ada dalam kajian lepas bagi tujuan pengesahan. Keputusan yang diperolehi amat bertepatan sekali dengan penyelesaian sedia ada. Penyelesaian berbilang untuk beberapa masalah terutamanya dalam saluran berliang dengan dinding mengembang atau menguncup juga wujud untuk kes sedutan kuat. Kajian ini berjaya menemui penyelesaian berangka bagi masalah baharu untuk pelbagai keadaan aliran bendalir. Keputusan yang diperolehi daripada kajian ini boleh dijadikan rujukan teori dalam bidang berkaitan.

Kata Kunci: Bendalir Casson, Bendalir micropolar, Bendalir nano, Penyelesaian berbilang, Saluran berliang.

Abstract

Similarity solutions of non-Newtonian fluids are getting much attention to researchers because of their practical importance in the field of science and engineering. Currently, most of researchers focus their work on non-Newtonian fluids over a sheet. However, only a few of them pay their attention towards the geometry of channel due to the complexity of governing equations. Therefore, this study attempts to investigate the numerical solutions of new problems of laminar incompressible Nanofluids, Casson fluids and Micropolar fluids under various fluid flow conditions. Each considered fluid involves porous channel walls, stretching or shrinking walls, and expanding or contracting walls with the influence of various physical parameters. Mathematical formulations such as the law of conservation, momentum or angular momentum, heat and mass transfer are performed on the new problems. After the mathematical formulation is developed, the governing fluid flow equations of partial differential equations are then transformed into boundary value problems (BVPs) of nonlinear ordinary differential equations (ODEs) by using the suitable similarity transformations. After converting high order BVPs into the equivalent first order system of BVPs, *shootlib* function in Maple 18 software is employed to obtain the similarity solutions of nonlinear ODEs. The numerical results in this study are compared with the existing solutions in literature for the purpose of validation. The results are found to be in good agreement with the existing solutions. Multiple solutions of some of the problems particularly in porous channel with expanding or contracting walls also exist for the case of strong suction. This study has successfully find the numerical solutions of the new problems for various fluid flow conditions. The results obtained from this study can serve as a theoretical reference in related fields.

Keywords: Casson fluid, Micropolar fluid, Multiple solutions, Porous channel, Nanofluid.

Acknowledgement

I find even the most powerful words devoid of all power while expressing my gratitude. I would bow myself before Almighty Allah who is the entire source of knowledge and wisdom and next to His messenger Hazrat Muhammad (pbuh) who is the only source of guidance for human beings for the completion of this hard task.

My grateful thanks are given to honorable and cooperative supervisors Dr. Azizah Mohd. Rohni and Prof. Dr. Zurni Omar, for providing valuable suggestions, cooperation and guidance throughout the studies. It is not enough to thank them for their guidance to help me to achieve my goal. Without their valuable support, my thesis would not have been possible.

I extend my warm thanks to my very loving and caring family, fiancée and all family members who provided a constant financial and moral support without which I was unable to do the research like that.

I had a very enjoyable study at Universiti Utara Malaysia (UUM). Not only, it does have a beautiful natural environment, but the university also has helpful staff. Finally, I would like to thank all my friends for their encouragement during my study.

JAWAD RAZA

List of Publication

Raza, J., Rohni, A. M., Omar, Z., & Awais, M. (2016). Heat and mass transfer analysis of MHD nanofluid flow in a rotating channel with slip effects. *Journal of Molecular Liquids*, *219*, 703-708 (**ISI journal).**

Raza, J., Rohni, A. M., & Omar, Z. (2016). MHD Flow and Heat Transfer of Cu-Water Nanofluids in a Semi Porous Channel with Stretching Walls, *International Journal of Heat and Mass Transfer,* 103, 336 – 340 (**ISI journal)**

Raza, J., Rohni, A. M., Omar, Z., & Awais, M. (2017), Rheology of the Cu-H2O nanofluid in porous channel with heat transfer: Multiple solutions, *Physica E: Low-dimensional Systems and Nanostructures*, 86, 248-252. (**ISI journal)**

Raza, J., Rohni, A. M., & Omar, Z. (2016). A Note on Some Solutions of Copper-Water (Cu-Water) Nanofluids in a Channel with Slowly Expanding or Contracting Walls with Heat Transfer. *Mathematical and Computational Applications*, *21*(2), 24. (**SCOPUS)**

Raza, J., Rohni, A. M., & Omar, Z. (2016). Multiple Solutions of Mixed Convective MHD Casson fluid flow in a Channel. *Journal of Applied Mathematics,* 2016, 1-10 (**SCOPUS)**

Raza, J., Rohni, A. M., & Omar, Z. (2016), Rheology of micropolar fluid in a channel with changing walls: Investigation of multiple solutions, *Journal of Molecular liquids* 223, 890-902 (**ISI journal)**

Raza, J., Rohni, A. M., & Omar, Z. (2017). A Note on Some Solutions of Micropolar Fluid in a Channel with Permeable Walls, *Multidiscipline Modeling in Materials and Structures.* (**SCOPUS)**

Raza, J., Rohni, A. M., & Omar, Z. (2017), Unsteady Flow of a Casson Fluid between Two Orthogonally Moving Porous Disks: A Numerical Investigation, *Journal of Communications in Numerical Analysis*, 2 (2017), 109-124.

Raza, J., Rohni, A. M., Omar, Z., & Awais, M. (2016), Physicochemical and Rheological Properties of Titania & Carbon Nanotube in a channel with Changing walls: Investigation of Critical points, *Multidiscipline Modeling in Materials and Structures*, 12 (4), 619 – 634. (**SCOPUS)**

Raza, J., Rohni, A. M., & Omar, Z. (2016), Numerical Investigation of Copper-Water (Cu-Water) Nanofluid with Different Shapes of Nanoparticles in a Channel with Stretching Wall: Slip Effects, *Mathematical and Computational Applications,* 21(4), 43. (**SCOPUS)**

Raza, J., Rohni, A. M., & Omar, Z. (2017, November). Triple solutions of Casson fluid flow between slowly expanding and contracting walls. In *AIP Conference Proceedings* (Vol. 1905, No. 1, p. 030029). AIP Publishing.

Raza, J., Rohni, A. M., & Omar, Z. (2018). A note on some solutions of micropolar fluid in a channel with permeable walls. *Multidiscipline Modeling in Materials and Structures*, *14*(1), 91-101. **(SCOPUS)**

Table of Contents

List of Tables

List of Figures

Nomenclature

$a(t)$	Height of the channel
$\bar{V}$	Velocity field
p	Pressure
$\bar{l}$	Body couple per unit mass
$\lambda, \mu, \alpha, \beta, \gamma$ and κ	Micropolar material constants
T	Temperature of the fluid
(x, y)	Coordinate axes
$\kappa_\circ$	Thermal conductivity
g	Component of micro-rotation
N	Micro-inertia spin parameter
θ	Dimensionless temperature
$B_\circ$	External uniform magnetic field
p	Pressure (Pa)
k_s	Thermal conductivity of the solid fraction (W/m.K)
k_{nf}	Thermal conductivity of the nanofluid (W/m.K)
ρ_s	Density of the solid fraction (Kg/m³)
$\bar{v}$	Micro-rotation vector
ρ	Density
$\bar{f}$	Body force
j	Micro-inertia
t	Time
(u, v)	Velocity component of the fluid

Pr	Prandtl number
C_p	Specific heat
C_1	Vortex viscosity parameter
η	Similarity variable
R	Reynolds number
T	Fluid temperature (K or ^{0}C)
$v_\circ$	Injection/suction
k_f	Thermal conductivity of the fluid (W/m.K)
n	Shape factor through H-C Model
c_p	Specific heat at constant pressure (J/(kg K)
$(c_p)_{nf}$	Specific heat of nanofluid
(u, v)	Velocity component in Cartesian coordinate

Dimensionless number

$R = \dfrac{a^2 b}{v_f}$	Stretching Reynolds number
$Pr = \dfrac{a^2 b (\rho C_p)_f}{\kappa_f}$	Prandtl number
$\rho_{nf} = \rho_f(1 - \varphi) + \rho_s$	Density of the nanofluid
$M^2 = \dfrac{\sigma B_\circ^2 a^2}{\mu_f}$	Magnetic parameter
$\mu_{nf} = \dfrac{\mu_f}{(1 - \varphi)^{2.5}}$	Dynamic viscosity of the nanofluid (Pa.s)
$\dfrac{\sigma_{nf}}{\sigma_f} = 1 + \dfrac{3\left(\dfrac{\sigma_s}{\sigma_f} - 1\right)\varphi}{\left(\dfrac{\sigma_s}{\sigma_f} + 2\right) - \left(\dfrac{\sigma_s}{\sigma_f} - 1\right)\varphi}$	Ratio of effective electrical conductivity of nanofluid to the base fluid

Greek symbols

η	Scaled boundary layer coordinate
σ_{nf}	effective electrical conductivity of nanofluid

xviii

μ		Dynamic viscosity
k_{nf}		Thermal conductivity of the nanofluid (W/m.K)
θ		Self-similar temperature
φ		Nanoparticle volume fraction parameter
μ_{nf}		Effective dynamic viscosity of nanofluid
ρ		Density (kg/m³)

Subscripts

nf	Nanofluid
s	Solid phase
2	Upper wall
f	Fluid phase
1	Lower wall

List of Appendices

CHAPTER ONE

INTRODUCTION

1.1 Background

Mechanics is a branch of science that deals with the motion and properties of the rigid bodies that are either at rest or in motion. Mechanics is divided into two main categories: classic and quantum mechanics. In the classical mechanics, which is introduced by the Newton's laws of motion, demonstrates the theory of motion, the energy conservative principle, the forces, the movement of heavy bodies (comets, galaxies, planets, stars), the features of rigid bodies, the movement of fluids; gases as well as liquids, spacecraft navigation and soils mechanical behavior. On the other hand, the quantum mechanics explores the structure, responses and movement of particles (Marsden & Ratiu, 1999).

Nonetheless, fluid is a substance that cannot sustain its shape when shear stresses are applied on it. Therefore, fluid mechanics is the study of gases and liquids at rest or in motion. This area of physics is divided into two parts: fluid statics, the study of the behavior of stationary fluids; and fluid dynamics, the study of the behavior of moving and flowing fluids. Hauke and Moreau (2008) on the other hand examined the behavior of stationary fluid and dynamics of fluid that is dissimilar from the two-aforementioned behavior. Lastly, the flow of fluid is branched into hydrodynamics as well. This part concerns about the mechanical properties of the fluid and has many applications in flight science, air flow analysis and water stream exploration.

According to Pritchard and Mitchell (2011), the copious uses of fluid mechanics demonstrate its importance and principles of all structures and associations with exploratory studies. Exploration of fluid apparatus, for example, pumps, heat exchangers, flow compressors, rocket motors established the importance of fluid mechanics to mechanical engineering. The flow of air entities i.e. aerodynamics, is a great interest to aerospace and space approaches in the framework of air ship and rockets.

In the next section, some useful definitions and concepts are highlighted which are used throughout this research.

1.2 Flow Characteristics

Flow may be classified in many ways such as laminar, turbulent, real, ideal, steady, unsteady, uniform, non-uniform, irrotational and rotational.

1.2.1 Laminar flow

In laminar flow, fluid particles move along smooth paths in laminas, or layers, with one layer gliding smoothly over an adjacent layer.

1.2.2 Turbulent flow

The fluid flow in which fluid particles move in very irregular paths, causing an exchange of momentum from one portion of the fluid to another in a manner similar to the molecular momentum from one portion of the fluid to another, is known as turbulent flow.

1.2.3 Ideal flow

An ideal fluid is frictionless and incompressible. The assumption of an ideal fluid is helpful in analyzing flow situations involving large expanses of fluids, as in the motion of an airplane of a submarine.

1.2.4 Steady flow

Steady flow occurs when conditions at any instant in the fluid do not change with the time. In mathematical form it can be expressed as:

$$\frac{\partial \overline{V}}{\partial t} = 0, \qquad \frac{\partial \rho}{\partial t} = 0, \qquad \frac{\partial p}{\partial t} = 0, \qquad \frac{\partial T}{\partial t} = 0.$$

where $\overline{V}$ is the velocity, ρ is the density, p is the pressure and T is the temperature. Water being pumped through a fixed system at a constant rate is an example of steady flow.

1.2.5 Unsteady flow

If the velocity of fluid particles passing through a point in space does not remain the same at all times, the flow is known as unsteady flow. Water being pumped through a fixed system at an increasing or decreasing rate is an example of unsteady flow.

1.2.6 Uniform flow

If all the particles in a fluid stream have the same velocity both in magnitude and direction $\left(\frac{\partial \overline{V}}{\partial s} = 0 \right)$, the flow is known as uniform flow. The only requirement for uniform flow is that, for any chosen time, the velocity must be the same for the entire mass of the fluid under consideration. A modified definition for uniform flow is: if the average velocity at each cross section is the same at a given instant, the flow is considered uniform.

1.2.7 Non-uniform flow

Flow such that the velocity vector varies from place to place at any instant $\left(\dfrac{\partial \overline{V}}{\partial s} \neq 0 \right)$ is known

as non-uniform flow. A liquid flowing through a reducing section or through a curved pipe has

non-uniform flow.

1.2.8 Rotational flow

If, in a given flow field, the velocity gradients exist and are continuous at each point, and the

curl of the velocity vector is not zero, then the flow in the field under consideration is known

to be rotational flow.

$$\text{Curl } (\overline{V}) = \nabla \times \overline{V} = \begin{vmatrix} \hat{i} & \hat{j} & \hat{k} \\ \dfrac{\partial}{\partial x} & \dfrac{\partial}{\partial y} & \dfrac{\partial}{\partial z} \\ u & v & w \end{vmatrix} \neq 0 .$$

1.2.9 Irrotational flow

If the curl of the velocity vector is zero, then the flow in that field is known as an irrotational

flow i.e. $\nabla \times \overline{V} = 0$

$$\Rightarrow \frac{\partial u}{\partial y} = \frac{\partial v}{\partial x}, \quad \frac{\partial v}{\partial z} = \frac{\partial w}{\partial y}, \quad \frac{\partial w}{\partial x} = \frac{\partial u}{\partial z}.$$

The following section considers the types of non-Newtonian fluids which will be

discussed in the current study.

1.3 Non-Newtonian Fluids

Fluid can be characterized into two types: Newtonian fluids and non-Newtonian fluids.

Before differentiating those two types, it is better to understand the concept of viscosity.

Viscosity is a physical property of the fluid's resistance to flow. This is a vital property of the fluid which resists deformation when some shear stresses are applied to it. Newton examined that force on rigid body F is directly proportional to the product of the moving body area A that contacts with the fluid and the velocity gradient $\dfrac{U}{d}$ for steady, laminar fluid flow. Mathematically, this can be expressed as

$F \propto A\,\dfrac{U}{d}, \quad \Rightarrow F = \mu\,\dfrac{U}{d}\,A$. As such μ is proportionality constant known as the *coefficient of viscosity*. Similarly, shear stress τ_{xy} works in such a manner that the force per unit area becomes shear stress. Hence, it can be written mathematically as:

$$\tau_{xy} = \frac{F}{A} = \mu\,\frac{U}{d} = \mu\,\frac{du}{dy} \tag{1.1}$$

Equation (1.1) is known as Newton's law of viscosity or Newton's law of fluid friction. Therefore, any fluid that fulfils Newton's law of viscosity is known as Newtonian fluid. More precisely, it can be argued that if the rate of change of deformation of the fluid is directly proportional to the applied shear stress then such kind of the fluid is known as Newtonian fluids. Many common fluids such as air and water are Newtonian fluids.

On the other hand, if there exists a nonlinear relation between the applied shear stress and the rate of deformation, then such fluids are known as non-Newtonian fluids which will be addressed in the current study. In this regard, some examples of non-Newtonian fluids are second grade fluids, viscoelastic fluids, micropolar fluids, Casson fluids, dusty fluids, nanofluids, Carreau fluids and upper convected Maxwell fluids. Due to the complexity of such fluids, many non-Newtonian fluid models are presented. However, in this study of nanofluid, Casson fluid and micropolar fluids are being addressed as studies of this sort are scarce leaving glaring gaps to be investigated. The applications

5

of non-Newtonian fluid models considered in the current study are in chemical, biomedical and engineering sciences. The application includes ketchup, custard, toothpaste, starch suspensions, maizena, paint, blood and cleanser which are the best examples of non-Newtonian fluids. The following section deals with the types of non-Newtonian fluids concerning the current study.

1.3.1 Nanofluids

A nanofluid is the combination of the nanoparticles having less than 100nm size. The nanoparticles are usually made of metals, carbides, oxides or carbon nanotubes and the base fluids is normally conductive fluid such as water, oil and ethylene glycol as shown in Figure 1.1.

Nanofluids have numerous applications in heat transfer, fuel cells, hybrid engine cooling and thermal management, chillers and regenerative heat exchangers because it has notable properties that make them conceivably helpful.
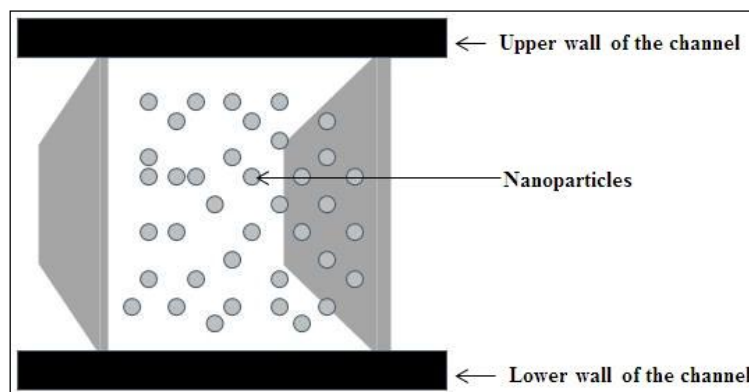
Figure 1.1. Nanofluids with Nano particles

Similarly, the study of convective heat transfer in nanofluids has indicated great applications in various industrial problems such as heat exchanger, automotive coolant,

6

electronic component and solar energy. The choice of base fluid-particle combination depends on the application for which the nanofluid is intended. Nanofluids commonly contain up to a 5% volume fraction of nanoparticles to ensure effective heat transfer enhancements. One of the main objectives of using nanofluids is to achieve the best thermal properties with the least possible (<1%) volume fraction of nanoparticles in the base fluid (Eldabe et al., 2013).

1.3.2 Casson Fluids

Casson fluid is classified as a non-Newtonian fluid due to its rheological characteristics (Makanda, Shaw & Sibanda, 2015). This type of non-Newtonian fluid deals with yield and shear stresses. Mukhopadhyay (2013) postulated that for a general viscoplastic model, Casson fluid model is the best to support this concept because it exhibits yield stress; if shear stresses are less than the yield stress when certain forces were applied to the fluid, then it behaves like solids otherwise it will behave like liquids.
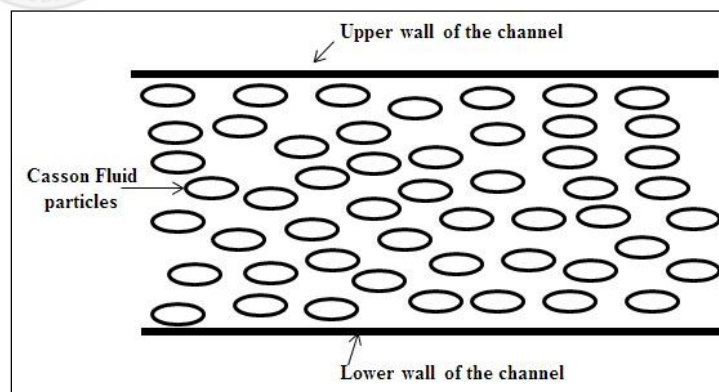
Figure 1.2. Casson fluids in a channel

The study of Casson fluid has captured the attention of many researchers due to its applications in the field of metallurgy, food processing, drilling operations and bioengineering operations. Its application extends to the manufacturing of

7

pharmaceutical products, coal in water, china clay, paints, synthetic lubricants and biological fluids such as synovial fluids, sewage sludge, jelly, tomato sauce, honey, soup and blood due to its contents such as plasma, fibrinogen, and protein; thus making Casson fluid being a crucial study in fluid dynamics.

1.3.3 Micropolar Fluids

Micropolar fluids belong to the class of the fluids with non-symmetric stress tensor. They contain small particles having rotation as well as motion. For determining the rotational fluid, the current research was supposed to use the curl of velocity vector if it became the non-zero which meant that the flow have rotation. It was Eringen (1964) who for the very first time introduced the micro fluids which are subclass of generalized fluids. These fluids have microscopic effects, coming from the local structure and micro motions of the fluid elements. These fluids are influenced by spin inertia and can support stress momentum and body momentum. However, complicated fluid problems can be solved with the help of Eringen's theory, including the flow of low concentration suspensions, blood, liquid crystals and turbulent shear flows.
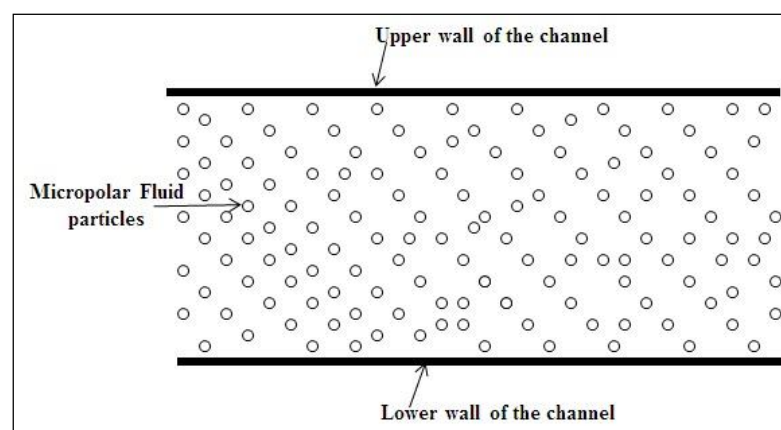
Figure 1.3. Micropolar fluid in a channel

Micropolar fluids have five additional coefficients of viscosity as compared to classical Newtonian fluids. Physically, micropolar fluids may represent fluids consisting of rigid, randomly oriented (or spherical) particles suspended in a viscous medium, where the deformation of fluid particles is ignored. The fluids consisting of bar-like elements and certain anisotropic fluids, for example, liquid crystals which are made up of dumbbell molecules are of this type. Animal blood also falls into this category. Moreover, the mathematical model of polymeric fluids and fluids with certain additive may resemble the mathematical model of the micropolar fluids (Ashraf, Kamal & Syed, 2009).

1.4 Channel

Channel is the passage consists of two parallel plates in which liquid flows. Nowadays, researchers having great intention to the channels due to the implications of channel in our daily life such as flow in a pipe, blood flow in vessels and drip irrigation. Listed below are some types of channel.

1.4.1 Stretching or Shrinking Channel

In this type of channel, parallel plates of the channel passage are stretching in the direction of the flow or shrinking opposite the direction of the fluid flow. This type of channel has vast applications in several manufacturing processes such as extrusion of molten polymers through a slit die to produce plastic sheets, hot rolling, wire and fiber coating, processing of food stuffs as well as metal spinning.
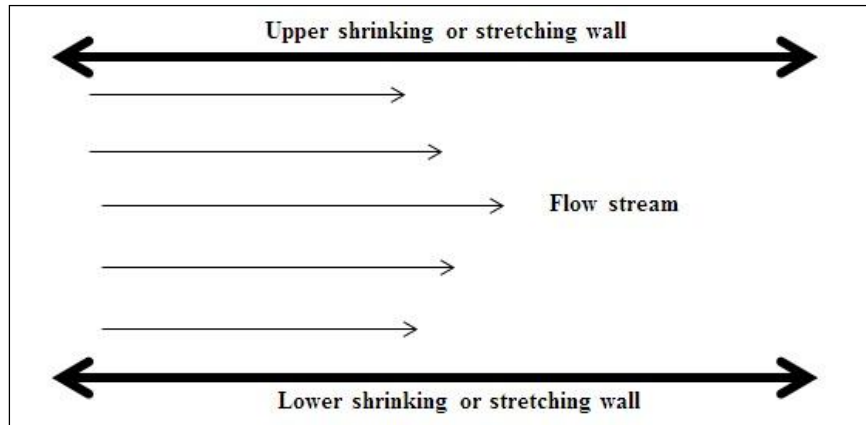
Figure 1.4. Flow in a stretching or shrinking channel

1.4.2 Open or Close Channel

The analysis of flow patterns of water surface, shape, velocity, shear stress and discharge through a stream falls under the Open Channel Flow.

Open Channel Flow is defined as fluid flow with a free surface open to the atmosphere. Examples include streams, rivers and culverts not flowing full as shown in Figure 1.5. Open channel flow assumes that the pressure at the surface is constant and the hydraulic grade line is at the surface of the fluid. The best examples of open channel flow are the flow in canals, drainage ditches, sewers and the flow of rainwater in the gutters.
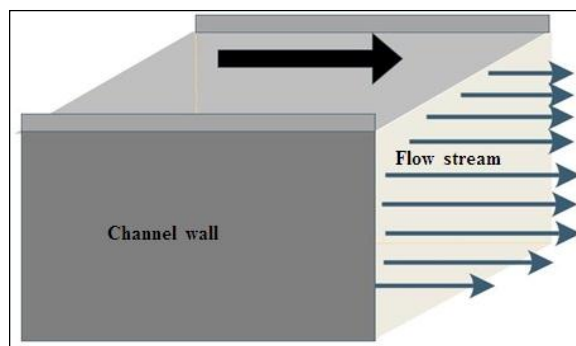
Figure 1.5. Open channel fluid flow

10

Meanwhile, the Closed channel flow is a type of liquid flow within a closed conduit. This type of flow is confined to the parallel walls or plates as depicted in Figure 1.6. The best example of closed channel flow is flow in a pipe or blood flow in arteries.
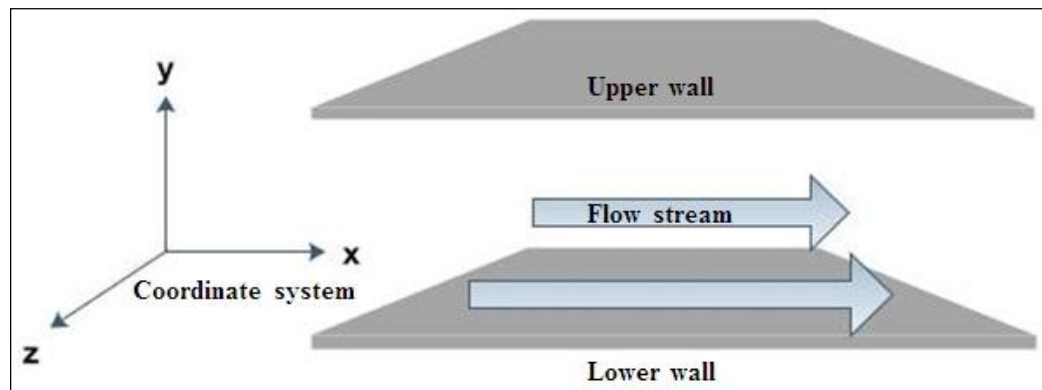
Figure 1.6. Closed channel fluid flow

Open channel flow and closed channel flow are similar in many ways, yet differ to each other in one significant respect. In closed channel flow, fluid is confined within the premises of the channel and does not exert direct atmospheric pressure, but hydraulic pressure exists on the conduit (see Figure 1.7).
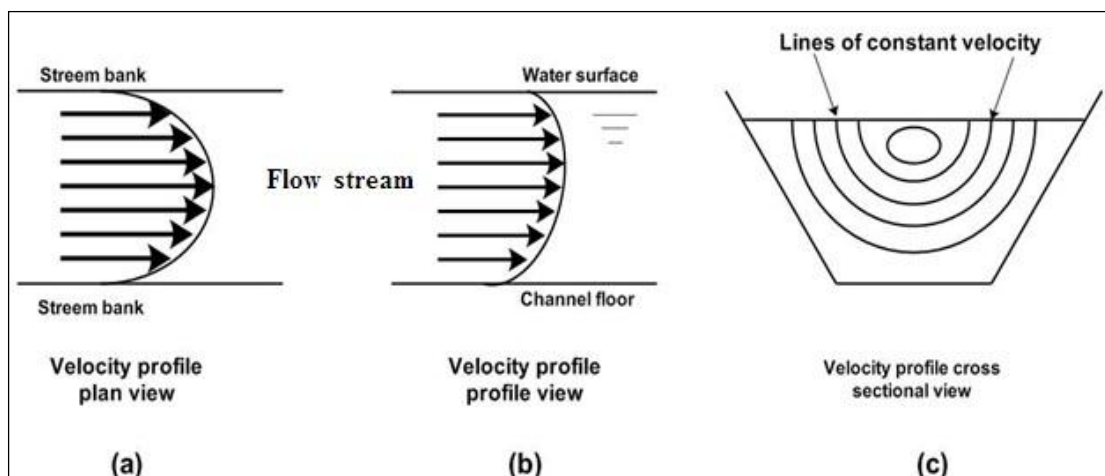
Figure 1.7. Stream lines of channel flow

At a perceptible level, a close channel has more applications in the real life (Ashraf et al., 2009). For instance, ground water movements in irrigation sector, blood flows in vessels and arteries, flows in pipes are most prominent applications of closed channel. Keeping in view of these applications, this thesis confined into closed channel.

1.4.3 Squeezing (Expanding and Contracting) Channel

Squeezing channel is similar to a close channel. Channel walls are located within some distance to each other and slowly expand or contract at constant rate. Such kind of channel has received considerable attentions of researchers in recent years because of its applications in physiological pumps, peristaltic motion, blood flows in vessels and many more.
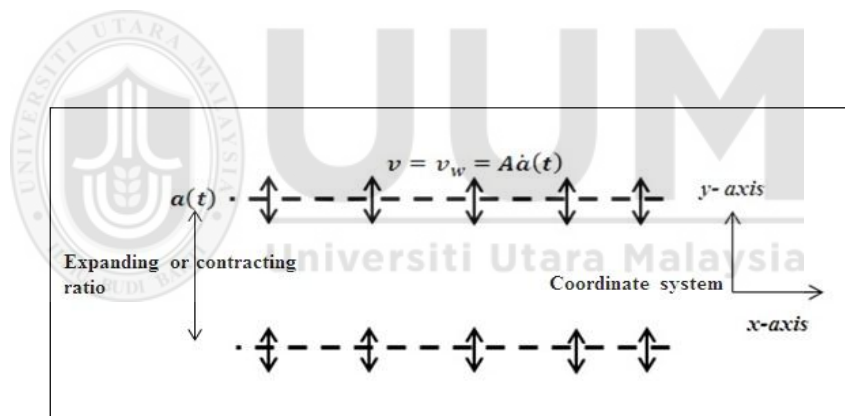
Figure 1.8. Squeezing channel

1.5 Boundary Layer Flows

A fluid layer near to the walls of channel where velocity of the fluid tends to be zero is known as boundary layer. In a same vein, we can say that viscosity and frictional effects near the channel walls cannot be negligible and these effects offer great reduction in the velocity of fluid near the rigid body (See Figure 1.9).
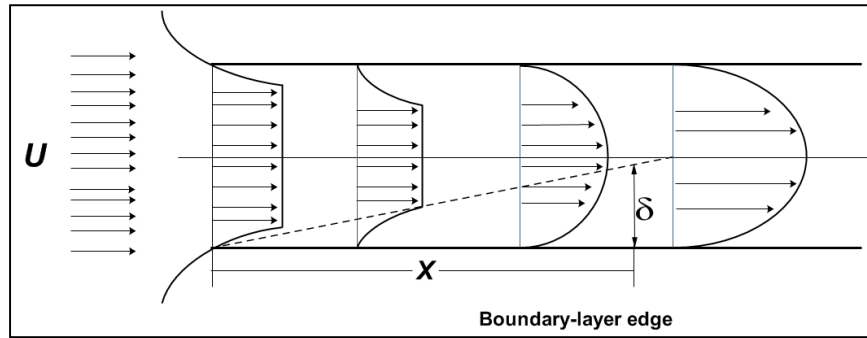
Figure 1.9: Boundary layer stream line profile

According to Prandtl, flow outside the premises of boundary layer is known as inviscid. However, flow within the boundary layer is known to be viscous flow. Moreover, the region from the solid wall of the channel to the point where viscous stream velocity is 99% of the free stream velocity is known as boundary layer thickness (i.e. $u(y) = 0.99U$).

The next section covers the concept of similarity solution and highlights the previous studies who had effectively incorporated this concept.

1.6 Similarity Solution

The basic idea of similarity solution is to simplify the governing equations of a physical problem by reducing the number of independent variables and utilizing a coordinate transformation. This transformation is known as similarity transformation and the independent variables x and y involving in partial differential equations is combined properly as a new independent variable $\eta(x, y)$ known as "similarity variables".

In 1908, Blasius introduced the term "similarity solution" to solve Prandtl's boundary layer equations. On the other hand, the system of equations for boundary layer flow problems in the form of partial differential equations is often difficult to be solved as compared to ordinary differential equations (Rohni, 2013). Therefore, reducing the

partial differential equations into ordinary differential equations using similarity transformation is a better choice. In the same manner, solutions of boundary layer flow problems have been comprehensively studied by numerous researchers such as Ishak and Nazar (2010), Shehzad et al. (2013) and many others.

The next section shall deal with the inspiration of the current study and highlights as to why the current study is important.

1.6 Motivation of the Study

Fluid through a permeable channel for steady and laminar flow was examined by Berman (1953). Furthermore, fluid can be exerted or injected from the channel walls that are permeable. The study of similarity solution of Navier-Stoke equations depicts a two-dimensional flow of a viscous incompressible fluid through a channel with one permeable wall to determine and to analyze the number of solutions in various cases according to the high order boundary conditions at the impermeable walls of the channel. Moreover, flow in a channel with one or two accelerating walls was addressed by Cox (1991). The exact solution of two dimensional flow through a permeable channel (Berman, 1953) was further generalized under the various conditions by Brady (1984), Shrestha & Terrill (1968). A fluid flow problem of a viscous incompressible fluid in a channel with uniformly wall acceleration was also presented by Watson, Banks, Zaturska, & Drazin (1990). They also assumed that channel walls were permeable such that suction, and injection can be taken place. Hewitt, Duck and Al-Azhari (2003) investigated three-dimensional stagnation point over a sheet by extended the solution structure of previous investigations (Watson, Banks, Zaturska, & Drazin, 1990). Fan and Chao (1965) considered the theoretical solution for the velocity profile of steady fully developed laminar flow of a viscous incompressible fluid. The

investigations of the literatures quoted above are restricted to Newtonian fluids only. The classical Navier-Stokes model is insufficient to describe some modern engineering structures which are often made up of materials possessing an internal structure. Fluids containing additives, materials with fibrous or coarse grain structures and polycrystalline materials containing internal structure fall in this category.

On the contrary, experimental examination for fluids that does not belong to the category of Newtonian fluids offer great reduction in the shear stress near the rigid body (Hoyt & Fabula, 1964), which was further generalized to micropolar fluid model introduced by Eringen (1964). From these investigations, non-Newtonian fluids imminently show having more applications as compared to classical Navier-Stoke model. Moreover, Magnetohydrodynamic (MHD) fluid flow in a channel involves more applications which are not only theoretical but also practical in MHD generators, accelerators and blood flow measurements (Ashraf et al., 2009).

Nonetheless, the phenomenon of fluid movement through permeable media is critical in the fields of compound, biomedical, natural designing and science. This phenomenon has applications in the production of oil and gas from topographical structures, filtration, ground water development, regenerative heat exchangers, surface catalysis of synthetic responses and biting the dust and so forth.

Therefore, problems to be investigated in the current research deals with the flow of some non-Newtonian fluids (Nanofluids, Casson Fluids, Micropolar) in a porous channel dealing specifically with:

- Incompressible non-Newtonian fluids
- Steady/Unsteady flow

15

- Laminar flow

1.7 Problem Statement

Among other applications, the study of Non-Newtonian fluid in a semi-porous channel and stretching channel simulate the subsurface drip irrigation system in addition to simulating the blood flow in arteries. Characterization of steady fluid motions in the porous channels can be followed back to 1953 when some of the works were carried out by Berman (1953) to examine the laminar two-dimensional flow of an incompressible fluid determined by uniform injection inside a rectangular channel with porous walls. Later, Shrestha and Terrill (1968), Brady (1984), Watson, Banks, Zaturska, and Drazin (1990) and Cox (1991) extended this research under the different fluid flow conditions. However, these studies only focused on Newtonian fluids which are inadequate to describe the physical phenomenon in real life. Therefore, nowadays many researchers are focusing on non-Newtonian fluids.

Among the non-Newtonian fluids, Casson fluid models and micropolar fluid models have pulled in more attention of the researchers due to their applications in the field of engineering, chemical, biomedical and environmental sciences. Especially the fluid flow problems in a channel filled by non-Newtonian fluids which has many applications in the production of oil and gasses, filtration, ground water movement and chemical reactions. The Casson constitutive mathematical formulation was inferred by Casson (1959) which demonstrates that the rate of strain and stress relationship is nonlinear. On the other hand, micropolar fluid model was described by Eringen (1964).

Recently many researchers such as Shateyi and Prakash, (2014), Hossain, Roy and Hossain (2013), Kumar et al., (2014), Kumar, Jain and Gupta (2012), Rohni et al.,

16

(2008), Jat et al., (2013), Kishan and Jagadha, (2013), Hussain and Ahmad, (2014), Hayat et al., (2014), Sheikholeslami et al., (2016a), Sheikholeslami et al., (2016b), Sheikholeslami et al., (2016c), Sheikholeslami et al., (2015a), Kandelousi, (2014), Sheikholeslamit et al., (2015b), Sheikholeslami and Ganji, (2015) focused for non-Newtonian fluids over a sheet and channel. Hence, it has become explicitly clear that there is scarcity of investigation regarding the geometry of channels for non-Newtonian fluids particularly for Casson fluid and nanofluids. Therefore, the focus of the current research was to develop a mathematical formulation of the new physical phenomenon in the geometry of the channel which so far has been the most neglected area. Furthermore, we investigated and presented new branches of the solution graphically and numerically for the various non-Newtonian fluids under the variations of different physical parameters which have never been addressed in the geometry of channels. It is due to the fact that multiple solution cannot be seen experimentally, although only first solution is stable and physically realizable in the most of the cases, is still of mathematical interest since the solutions are also part of solution to the system of differential equations from mathematical point of view.

1.8 Research Questions

Based on the research problem the following research questions have been formulated as a basis for this study.

- Does magnetic field effects on thermal conductivity of the copper water nanofluid confined within two parallel walls?

- Do multiple solutions occur in the geometry of the porous channel?

- Do multiple solutions depend upon heat transfer and wall expansion ratio in a channel with slowly expanding or contracting walls?

- Does thermal buoyancy, concentration buoyancy, Casson parameter and Reynolds number effects significantly on velocity profile?

- Do multiple solutions exist for the case of steady laminar incompressible Casson fluid in a porous channel?

- Do multiple solutions exist for the flow of Casson fluid in a channel with expanding or contracting walls?

- Does velocity of micropolar fluid near a rigid wall decrease by increasing vortex viscosity parameter for the case of multiple solutions?

- Do multiple solutions exist for the flow of micropolar fluid in a channel with slowly expanding or contracting walls?

- Do multiple solutions depend upon suction Reynolds number of micropolar fluid in a porous channel?

1.9 Objectives of the Study

The objectives of the current study were to develop mathematical models, to derive boundary layer equations, to transform governing partial differential equations into similarity equations, to solve similarity equations numerically for the following problems:

1) Flow of Nanofluids in a channel

18

This objective is further discretized into the three sub problems. In the first problem, we will investigate the problem of Cu-Water nanofluid in a semi-porous channel with stretching walls under the influence of magnetic field. The second problem is depend upon the solution of heat transfer effects on Cu-Water nanofluid in a channel with porous walls. Water base copper nanofluid in a channel with slowly expanding or contracting walls with heat transfer will be studied in the third problem.

2) Flow of Casson fluids in a Channel

The first problem of the current objective is to study the problem of heat and mass transfer analysis of MHD mixed convection Casson fluid in a channel with shrinking channel walls embedded in a porous medium. Multiple solutions of mixed convection MHD Casson fluid flow in a porous channel will be investigated in the second problem and the problem of Casson fluid flow between slowly expanding or contracting walls will investigate in the next problem. Multiple solutions will be investigated and stability analysis will be performed in order to check which solution is physically stable.

3) Flow of micropolar fluid in a channel

Multiple solutions of MHD micropolar fluid in a channel with heat transfer will investigate in the first problem of the current objective. Moreover, stability analysis will employ to determine the physical reliability of the solutions. The problem of micropolar fluid in a channel with expanding or contracting walls will be investigated in the second problem of the current objective. The third problem is consist of the problem of micropolar fluid in a channel with permeable walls. The occurrence of multiple solutions should be investigated and stability analysis will be performed.

1.10 Significance of the Study

Problems of fluid flow in a permeable tube or channels received much attentions of researchers due to its distinctive applications in biomedical engineering like blood flow in arteries, blood oxygenators, dialysis of blood in kidney, filtration, underground fluid movement, irrigation, heat exchangers and many more. In the same vein, flow in a channel with expanding or contracting walls has also numerous applications in blood flow in artificial kidneys and flow in respiratory system. Based on the applications identified from above and previous sections which are deemed important in the specific context of the study, this research seeks to extend non-Newtonian fluid flow in a channel by addressing the gaps mentioned in the above sections. This study is confined to the channels which are permeable; channel walls can be stretched or shrinked and the channels with expanding or contracting walls that can be heated under the influence of transverse magnetic field.

1.11 Scope of the Study

The scope of the study is limited to two-dimensional steady, laminar and incompressible flows of Casson fluids, Micropolar fluids and Nanofluids in a horizontal channel. Governing boundary layer equations were transformed into ordinary differential equations (ODEs) by using suitable similarity transformation. Reduce the resulting ODEs into first order initial value problem and then solved numerically by employing the shooting method.

1.12 Techniques for Solving Boundary Value Problems

There are many methods for solving boundary value problems but some of them are analytical and others are numerical. Yet some of them involve finite difference,

20

shooting method, Runge-Kutta-Fehlberg method, homotopy analysis method (HAM), finite element method and Keller box method. However, in this study we addressed only the shooting method.

1.12.1 Shooting Method

For numerical method, shooting method is used to solve boundary value problems by reducing it into initial value problems. The current study employed the trial and error approach to get closer to the boundary conditions and the nonlinear governing equations are reduced to system of equation by using reduction of order. Afterwards, the initial conditions were guessed to manipulate the results by comparing them with the boundary conditions such that if the difference between initial guess and the boundary condition remains smaller and afterwards it stops. However, this recursive process of guessing values is continued until the required accuracy could not be achieved. This method for this study is inspired by several renowned researchers such as Mukhopadhyay (2013), Kameswaran et al. (2014) and Eldabe et al. (2013) who have successfully employed the shooting method for solving boundary value problems. Features of shooting method can be found in (Na, 1980) and (Jaluria, 2002). Since it has been noticed in the past that the shooting method has numerous advantages for instance, it is easy to program in a general form, stable scheme, less storage required and efficient for solving both initial value problems (IVPs) and boundary value problems (BVPs).

1.12.2 Runge-Kutta-Fehlberg Method

Runge-Kutta-Fehlberg method guarantees the accuracy in solution of the initial value problem $\frac{dy}{dx} = f(x,y), y(x_j) = y_j$ using appropriate step size. For each step, two

different approximations to the solution are computed and then checked by comparing calculated value with the given terminal point. The step size discretized into much smaller if the compared numerical value are not asymptotic to the required accuracy. In each step the following six steps are required to compute:

$$I_1 = hf(x_i, y_i),$$

$$I_2 = hf\left(x_i + \frac{1}{4}h, y_i + \frac{1}{4}I_i\right),$$

$$I_3 = hf\left(x_i + \frac{3}{8}h, y_i + \frac{3}{32}I_i + \frac{9}{32}I_2\right),$$

$$I_4 = hf\left(x_i + \frac{12}{13}h, y_i + \frac{1932}{2197}I_i - \frac{7200}{2197}I_2 + \frac{7296}{2197}I_3\right),$$

$$I_5 = hf\left(x_i + h, y_i + \frac{439}{216}I_1 - 8I_2 + \frac{3680}{513}I_3 - \frac{845}{4104}I_4\right),$$

$$I_6 = hf\left(x_i + \frac{1}{2}h, y_i - \frac{8}{27}I_1 + 2I_2 - \frac{3544}{2565}I_3 + \frac{1859}{4104}I_4 - \frac{11}{40}I_5\right),$$

The approximation of 4th order solution is

$$y_{i+1} = x_i + \frac{25}{216}I_1 + \frac{1408}{2565}I_3 + \frac{2197}{4101}I_4 - \frac{1}{5}I_5,$$

The better approximated 5th order solution is given by

$$\sigma_{i+1} = y_i + \frac{16}{135}I_i + \frac{6656}{12825}I_3 + \frac{28561}{56430}I_4 - \frac{9}{50}I_5 + \frac{2}{55}I_6$$

Furthermore, optimal step size dh can be determined by multiplying h with a scalar

$d = 0.84\left(\frac{tol\, h}{2|\sigma_{i+1} - y_{i+1}|}\right)^{\frac{1}{4}}$, where, tol is tolerance error.

1.13 Thesis organization

Similarity solutions of boundary layer flows of non-Newtonian fluids in channels are presented in this study for different fluid flow conditions containing six chapters where Chapter One is based on the basic concepts which involved the current research.

Literature reviews related to the problems considered for nanofluid, casson fluid and micropolar fluid, in the current study is discussed in Chapter Two.

In each of Chapter Three to Five, the chapters are discretized into four sections. First section is Mathematical formulation of the problem considered in the chapters, numerical solution is given in the second section, third and fourth sections are for stability analysis, results and discussion section which comprises the analysis of the numerical findings of the problems. Chapter Three is concerned with the derivation of boundary layer flows of nanofluid in a channel with heat transfer. Tiwari and Dass (2007) model for nanofluid is employed on the problems considered for stretching channel, porous channel and expanding or contracting channel. Three different problems of nanofluid in a closed channel is considered in this chapter. In Chapter Four, Non-Newtonian Casson fluid model is presumed for different problems in a closed channel. Problems of micropolar fluid in a closed channel under the various fluid flow conditions are presented in Chapter Five. Conclusion of the study and future research are given in Chapter Six, which is the final chapter of this thesis.

Chapter Two discusses the existing literatures concerning the phenomenon under discussion to provide its better understanding.

CHAPTER TWO
LITERATURE REVIEW

2.1 Introduction

This chapter reviews the studies that have been carried out concerning fluid flow in channels under various fluid flow conditions. Section 2.2 presents the studies regarding the boundary layer flow. The next three subsections review several selected researches of boundary layer flow for nanofluids, Casson fluid and micropolar fluid, respectively.

2.2 Boundary Layer Flow in a Channel

The characterization of steady fluid motions in porous channels can be followed back to 1953 when some of the works were carried out by Berman (1953) to examine the laminar two-dimensional flow of an incompressible fluid determined by uniform injection inside a rectangular channel with porous walls. This exact solution was further generalized by Cox (1991), Brady (1984), Shrestha and Terrill (1968), Watson et al. (1990) and Robinson (1976) under various conditions.

Accordingly, Cox (1991) considered the flow in a channel with one permeable and different nonporous yet quickening walls. Shrestha and Terrill (1968) inspected the laminar course through a channel with consistently permeable walls of distinctive porousness for small Reynolds number and thought about their arrangement and numerical arrangements. A predictable scientific issue of the flow of a thick incompressible fluid driven along a channel with permeable and consistently quickening walls was researched by Watson et al. (1990). Likewise, Robinson (1976) succeeded to find the solution of steady, incompressible fluid flow problem in a porous

channel with constant fluid density, whereby uniform suction was applied at both upper and lower walls. Similarly, the investigation of heat and mass transfer in a vertical channel filled with viscous immiscible fluids was analyzed by Kumar et al. (2014). Numerical analysis for blood flow through aneurismal artery and symmetric stenotic was presented by Sadek et al. (2013).

2.3 Boundary Layer Flow of Nanofluid

Many industrial processes involve heat transfer phenomenon. From these processes, heat must be added, removed or transferred from one system to another. These procedures give a source to vitality recuperation and procedure liquid warming or cooling.

Many methods have existed to improve the efficiency of heat transfer in these processes. One of the most common methods is to add some high thermal conductive solid particles into the fluids. These types of particles are known as nanoparticles and the fluid is known as nanofluid. In the event that particle molecule cooperation in the suspension prompt accumulation, the consequences for the thickness can be dynamic, since not exclusively are the totals greater than the individual particles, and henceforth more impervious to flow, however they likewise encase, thus immobilize a portion of the fluid stage. This enhancement in the solid volume fraction results in a higher than expected viscosity at low applied shear stress, therefore, with the suspension exhibiting non-Newtonian shear-thinning behavior (Richmond et al., 1998).

However, mathematical models of nanofluids flow incorporate two fundamental approaches; a single-phase model or a two-phase model. Single-phase model considers nanoparticles and base fluid as a single homogeneous fluid with respect to its effective properties. On the other hand, mathematical formulation of two-phase nanofluids was

simplified by Buongiomo (2006) who stated that the basic mechanics contributing to thermal enhancement are Brownian diffusion and thermophoresis. This study was generalized into boundary layer model for free convective flows of nanofluids by Kuznetsov & Nield (2010). Hamad, Pop, & Ismail (2011) then trailed the investigation of MHD boundary layer flow of nanofluids. Chamkha and Aly (2010) investigated further about magneto nanofluid flow using Blottner implicit difference method with heat generation effects.

Likewise, nanofluids are used for increasing thermophysical properties, for instance, thermal conductivity, thermal diffusivity, thickness, and convective heat transfer coefficients diverged from those of the base fluids like water, ethylene or triethylene-glucose and diverse coolants, biofluids, and polymer game plans, as clarified by Choi (2009) and Wong and De Leon (2010). Sheikholeslami *et al*. (2013) have analytically investigated flow of laminar nanofluid in a semi-porous channel. This analysis was done during the presence of transverse magnetic field. Results showed that the Reynolds number and the velocity boundary layer thickness has inverse relation whereas the Hartmann number and the velocity boundary layer thickness are directly related. Sheikholeslami et al. (2012) have used finite element method which is best known for control volumes. During the study, they noticed a natural convection for transfer of heat by using semi-annulus enclosure having nanofluid. Their findings suggested that the angle of turn has significant positive effect on variation in values of local Nusselt number, isotherms and streamlines. A steady magneto-hydrodynamic (MHD) free convection boundary layer flow past a vertical semi-infinite flat plate embedded in water filled with a nanofluid has been theoretically studied by Hamad et al. (2011). In this case, the cooling performance of copper and silver nanoparticles is

26

the highest. This study found that application in heat exchanger where conduction in the solid wall is under the influence of convection in fluid.

2.4 Boundary Layer Flow of Casson fluid

The investigation of non-Newtonian fluids has remarkably increased because of their colossal scope of pragmatic applications in engineering and industries. Various specialists of the field have examined differing fluid flow problems identified with a few non-Newtonian fluids (Makanda et al. 2015). Among the non-Newtonian fluids, Casson fluid has pulled more consideration of specialists because of its applications in the fields of metallurgy, sustenance preparing, boring operations and bioengineering operations (Ramesh & Devakar, 2015; Nichols et al. 2011). Some more applications can be found in the assembling of pharmaceutical items, coal in water, china mud, paints, manufactured ointments and organic liquids, synovial liquids, sewage slop, jam, tomato sauce, nectar, soup, blood , plasma, fibrinogen and protein (Merrill et al.1965).

In the same vein, the Casson constitutive mathematical formulation was inferred by Casson (1959) which demonstrates that the rate of strain and stress relationship is nonlinear. The flow of Casson fluid between two turning chambers was examined by Eldabe et al. (2001). Attia and Sayed-Ahmed (2010) considered the Couette flow of electrically directing Casson fluid between parallel plates. The impact of mass exchange on MHD flow of Casson fluid was addressed by Shehzad et al. (2013). Taylor's series was utilized with a specific end goal to explain nonlinear differential mathematical equations. Unequivocal limited distinction strategy for unsteady Casson fluid course through parallel plates was examined by Afikuzzaman et al. (2015). In a recent study, Reddy et al. (2015) investigated the impacts of Joule heating and Hall

27

effects with the expectation of free convection in an electrically conducting Casson fluid in a vertical direct in the nearness of gooey dispersal. Mathematical results were found with the assistance of Homotopy Analysis Method (HAM) and contrasted with Adomian Decomposition Method (ADM). Walawender et al. (1975), Batra and Jena (1991), Ahmed and Attia (1998), Kataria & Patel (2016) and Das et al. (2015) have accounted for the flow of Casson fluid under various fluid flow conditions.

2.5 Boundary Layer Flow of Micropolar fluid

Fluid flow behavior in a channel has generous applications in the field of biomedical, engineering, environmental, chemical engineering and science. Particularly for fluids having nonlinear relationship between shear stresses and rate of change of deformation. Among these fluids, micropolar fluid is one of the most prominent. Micropolar fluid with microstructure molecular bounding is the class of the fluid with nonsymmetrical stress tensor. In 1953, the theory of micropolar fluid was firstly introduced by Eringen. He stated that the impact of microration on microstructure model depicts micropolar fluid. These fluids have microscopic effects, coming from the local structure and micro motions of the fluid elements. These fluids are influenced by spin inertia and can support stress momentum and body momentum. Complicated fluid problems can be solved with the help of Eringen's theory including the flow of low concentration suspensions, blood, liquid crystals and turbulent shear flows. Micropolar fluids have five additional coefficients of viscosity as compared to classical Newtonian fluids. Physically micropolar fluids may represent fluids consisting of rigid, randomly oriented (or spherical) particles suspended in a viscous medium, where the deformation of fluid particles is ignored. The fluids consisting of bar-like elements and certain anisotropic fluids, for example, liquid crystals which are made up of dumbbell molecules are of

28

this type. Animal blood also falls into this category. Moreover, the mathematical model of polymeric fluids and fluids with certain additive may resemble the mathematical model of the micropolar fluids.

Consequently, the problem of fully developed laminar pulse flow of an incompressible fluid through rectangular channels was analyzed by Qi et al. (2008). The investigation of the problem of laminar flow of micropolar fluid in a rectangular microchannel was done by Shangjun et al. (2006). They used Chebyshev collection method for solving nonlinear differential equation of their proposed study. Two-dimensional flows of micropolar fluids in a porous channel with mass transfer were studied by Kelson et al. (2003). Misra et al. (2008) proposed the problem of steady incompressible viscoelastic electrically conducting fluid and heat transfer in a channel with stretching walls. They examined that reverse flow occurs near the center of the channel due to the stretching walls of the channel. Two-dimensional steady flows of an incompressible micropolar fluid through the channel bounded by a permeable bed over a rigid plate was presented by Sreenadh et al. (2012). The fluid was injected from the permeable bed. The flow in the channel was governed by Eringen's micropolar fluid model. Kumar et al. (2010) investigated the problems of fully developed free-convective flow in a vertical channel where one region was filled by micropolar fluids and other was by viscous fluids. Sheikholeslami et al. (2014) presented the effects of heat and mass transfer of micropolar fluid in a porous channel analytically. The problem of two-dimensional flow of a micropolar fluid in a permeable channel with high mass transfer was studied by Ziabakhsh and Domairry (2008).

An analytical investigation of the problem of micropolar fluid in a porous channel with suction/injection has been made by Aski et al. (2014). Consequently, an approximate

29

solution of micropolar fluid in a channel subject to heat transfer and chemical reaction was presented by Sheikholeslami et al. (2014). Homotopy perturbation method (HPM) was used to find approximate solution of governing nonlinear differential equations of micropolar fluid. Sajid et al. (2009) analyzed the boundary layer flow of a micropolar fluid in a porous channel. Fluid is injected or exerted from the porous walls of the channel with constant velocity. Fakour et al. (2015) considered the heat transfer analysis on micropolar fluid in a channel analytically and numerically. An approximate solution was obtained by least square method (LSM) and compared to Runge–Kutta of fourth-order. The study revealed that boundary layer thickness of velocity decreased by increasing the values of Reynolds number R. Moreover, fluid temperature increased with the increasing of the strength of Peclet number Pe. Hydromagnetic flow of a micropolar fluid between parallel plates with heat transfer was examined by Mehmood et al. (2016). Resulting coupled nonlinear governing equations were solved by Optimal Homotopy Analysis Method (OHAM). The study revealed that coupling parameter increased the vortex viscosity of the fluid; thus, reducing the fluid velocity.

In short, the already existing literature related to the phenomenon under discussion have revealed that the flow of non-Newtonian fluids in a channel have numerous applications in the field of engineering, biomedical and science. Nonetheless, the literatures depicted are lacking the study of the geometrical channel for non-Newtonian fluids. Therefore, this thesis aims to conduct the research on this part. In the view of the literature discussed in the current chapter, this thesis intended to address the boundary layer flows in a channel, boundary layer flows of nanofluid, casson fluid and micropolar fluid. The following chapter will deal with the formulation of the different problems of nanofluid in a channel.

CHAPTER THREE
BOUNDARY LAYER FLOWS OF NANOFLUIDS IN A CHANNEL WITH HEAT TRANSFER

The previous chapter discussed the literature of the field to limit the scope of the study to provide enough understanding about the issues under investigation. The current chapter shall deal with nanofluids in different topological structure (e.g. porous channel, stretching channel, expanding or contracting channel). Particularly, an incompressible nanofluid is taken in different geometries to obtain numerical results. The impact of different physical parameters on the rheology of nanofluids is also examined. Mathematical models of nanofluids flow incorporate two fundamental approaches; to specify a single-phase model or a two-phase model. Single-phase approach is easier to implement and requires less computational time. The results are strongly based on the specific thermophysical model especially those for thermal conductivity and viscosity of the observed nanoparticles. There are many thermophysical models to analyse the thermal conductivity of the nanofluids. On the other hand, ultrafine particle can be easily fluidize and significant effects on motion of the fluid due to the Brownian motion and thermophoresis effects are observed. Recently, two-phase models have been used by the researchers due to better accuracy, however, it provides less detail about each phase. The fluids scattered with ultrafine particles (nanoparticles) known as nanofluids are promising for heat transfer enhancement because of their high thermal conductivity.

In recent decades, metallic nanoparticles have been extensively utilised in several industries due to their vast applications (Parveen et al., 2012). They possess distinctive properties such as chemical, electrical, physical and optical (Phillips et al., 2011). In a same vein, various branches of modern engineering are using copper and its alloys.

31

Copper nanoparticles have wide range of applications is an outcome of enhancement thermal and electrical conductivity (Konieczny & Rdzawski, 2012). Due to the enhancement in thermal and electrical conductivity, the copper nanoparticles have been employed in the field of chemical, biomedical and engineering (Muraviev et al., 2006). In addition, copper is having multifaceted attributes, for instance, it is cheaper compared to other precious metals including gold and silver and also having high antibacterial properties (Khodashenas & Ghorbani, 2014). Therefore, the current chapter discusses problems in a channel associated with Tiwari and Dass (2007) model pertinent to the copper-water nanoparticles.

3.1 Tiwari model

Low thermal conductivity of customary heat transfer fluid, for example, water, oil, and ethylene glycol blend is an essential confinement in improving the execution and the smallness of numerous designing electronic gadgets. To conquer this downside, there is a solid inspiration to create propelled heat transfer fluids with considerably higher conductivities to improve thermal qualities. In that capacity, an inventive path in enhancing thermal conductivities of a fluid is to suspend metallic nanoparticles inside it. In 2007, Tiwari and Dass investigated the behaviour of nanofluids inside a two-sided-lid-driven heated square. Mathematical model is developed to examine the behaviour of nanofluids with the help of solid volume fraction. The study revealed that heat transfer capacity of base fluid increased as enhancement in the strength of solid volume fraction. Furthermore, fluid flow pattern changed from natural convection to force convection due to the immersion of nanoparticles in the base fluid. Ahmad and Pop (2010) investigated the problems of mixed convection boundary layer flow over a flat plate using Tiwari and Dass model. The study revealed that skin friction and heat

transfer coefficients increased as nanoparticles induced into base fluid. Sheremet et al. (2015) examined the water based nanofluid flow in a square porous cavity with isothermal vertical walls. Recently, many researchers focused their intention towards the problem of MHD and nanoparticles effects on flow and heat transfer. For instance, Dogonchi et al. (2017), Sheikholeslami et al. (2013), AbdEl-Gaied and Hamad (2013), Sheikholeslami and Ganji (2013), Sheikholeslami and Bhatti (2017), Bhatti et al. (2016), Sheikholeslami et al. (2015) are most prominent.

3.1.1   Mathematical Description of Tiwari and Dass

Governing equations of Newtonian nanofluids are taken into account by Navier-Stokes equation.

$$\frac{\partial \rho_{nf}}{\partial t} + \nabla \cdot \left(\rho_{nf}\bar{V}\right) = 0 \tag{3.1}$$

$$\rho_{nf}\left(\frac{\partial \bar{V}}{\partial t} + \bar{V} \cdot \nabla\bar{V}\right) = -\nabla p + \nabla \cdot \left(\mu_{nf}(\nabla\bar{V} + (\nabla\bar{V})^T) - \frac{2}{3}\mu_{nf}(\nabla \cdot \bar{V})I\right) + \bar{F} \tag{3.2}$$

$$\rho_{nf}C_p\left[\frac{\partial T}{\partial t} + \bar{V} \cdot \nabla T\right] = k\nabla^2 T + \emptyset \tag{3.3}$$

$$\nabla \cdot \bar{B} = 0 \tag{3.4}$$

$$\nabla \times \bar{B} = \mu_m \bar{J} \tag{3.5}$$

$$\nabla \times \bar{E} = 0 \tag{3.6}$$

$$\bar{J} = \sigma_{nf}(\bar{E} + \bar{V} \times \bar{B}) \tag{3.7}$$

Where $\bar{V}$ is the fluid velocity, p is the fluid pressure, ρ_{nf} is the density of the nanofluid, μ_{nf} is the dynamic viscosity of the nanofluid, $\bar{F}$ is the external forces applied to the nanofluid, $\bar{J}$ is the current density and $\bar{B}$ is total magnetic field so that $\bar{B} = \bar{B}_\circ + \bar{b}$, $\bar{b}$ is the conductivity of the fluid. Moreover, $\nabla \cdot \bar{J} = 0$ is obtained from Eqs. (3.4) - (3.7). The uniform stationary magnetic field $\bar{B}$ is applied transverse in direction and magnetic

Reynolds number is taken small (Shercliff, 1965). As a consequence the induced magnetic field $\bar{b}$ is negligible. Furthermore, since there is no applied polarization voltage, therefore, an electric field (i.e. $\bar{E} = 0$) has vanished. This means that fluid follows conservation of energy (No energy is extracted or added to the fluid). Applying these assumptions, electromagnetic body force occurs in Eq. (3.2) takes the following linearized form (Rossow, 1958):

$$\bar{F} = \bar{J} \times \bar{B} = \sigma_{nf}[(\bar{V} \times \bar{B_\circ}) \times \bar{B_\circ}] = \left(-\sigma_{nf}B_\circ^2 u, 0, 0\right)$$

Components of the velocity vector $\bar{V} = (u(x,y,z), v(x,y,z), w(x,y,z))$ and in the light of said assumptions, the governing equations (3.1) – (3.3) in the component form can be written as:

$$\frac{\partial u}{\partial t} + \frac{\partial u}{\partial x} + \frac{\partial v}{\partial y} + \frac{\partial w}{\partial x} = 0 \tag{3.8}$$

$$\rho_{nf}\frac{\partial u}{\partial t} + \rho_{nf}\left(u\frac{\partial u}{\partial x} + v\frac{\partial u}{\partial y} + w\frac{\partial u}{\partial z}\right) = -\frac{\partial p}{\partial x} + \mu_{nf}\left(\frac{\partial^2 u}{\partial x^2} + \frac{\partial^2 u}{\partial y^2} + \frac{\partial^2 u}{\partial z^2}\right)$$

$$- \sigma_{nf}B_\circ^2 u \tag{3.9}$$

$$\rho_{nf}\frac{\partial v}{\partial t} + \rho_{nf}\left(u\frac{\partial v}{\partial x} + v\frac{\partial v}{\partial y} + w\frac{\partial v}{\partial z}\right) = -\frac{\partial p}{\partial y} + \mu_{nf}\left(\frac{\partial^2 v}{\partial x^2} + \frac{\partial^2 v}{\partial y^2} + \frac{\partial^2 v}{\partial z^2}\right) \tag{3.10}$$

$$\rho_{nf}\frac{\partial w}{\partial t} + \rho_{nf}\left(u\frac{\partial w}{\partial x} + v\frac{\partial w}{\partial y} + w\frac{\partial w}{\partial z}\right) = -\frac{\partial p}{\partial z} + \mu_{nf}\left(\frac{\partial^2 w}{\partial x^2} + \frac{\partial^2 w}{\partial y^2} + \frac{\partial^2 w}{\partial z^2}\right) \tag{3.11}$$

$$u\frac{\partial T}{\partial x} + v\frac{\partial T}{\partial y} = \frac{k_{nf}}{\left(\rho C_p\right)_{nf}}\frac{\partial^2 T}{\partial y^2} \tag{3.12}$$

where u and v are the velocity component along x and y-axes respectively, σ_{nf} is effective electrical conductivity of nanofluid, ρ_{nf} is effective density, μ_{nf} is the effective dynamic viscosity, $\left(\rho C_p\right)_{nf}$ is heat capacitance and k_{nf} thermal conductivity of the nanofluid. These physical quantities described mathematically as:

$$\rho_{nf} = \rho_f(1 - \varphi) + \rho_s \tag{3.13}$$

$$\mu_{nf} = \frac{\mu_f}{(1 - \varphi)^{2.5}} \tag{3.14}$$

$$\left(\rho C_p\right)_{nf} = \left(\rho C_p\right)_f(1 - \varphi) + \left(\rho C_p\right)_s\varphi \tag{3.15}$$

$$\frac{k_{nf}}{k_f} = \frac{k_s + 2k_f - 2\varphi(k_f - k_s)}{k_s + 2k_f + \varphi(k_f - k_s)} \tag{3.16}$$

$$\frac{\sigma_{nf}}{\sigma_f} = 1 + \frac{3\left(\frac{\sigma_s}{\sigma_f} - 1\right)\varphi}{\left(\frac{\sigma_s}{\sigma_f} + 2\right) - \left(\frac{\sigma_s}{\sigma_f} - 1\right)\varphi} \tag{3.17}$$

Furthermore, the relationship between physical quantities of our interest are:

$$A_1 = \frac{\rho_{nf}}{\rho_f} = (1 - \varphi) + \frac{\rho_s}{\rho_f}\varphi \tag{3.18}$$

$$A_2 = \frac{(\rho C_p)_{nf}}{(\rho C_p)_f} = (1 - \varphi) + \frac{(\rho C_p)_s}{(\rho C_p)_f}\varphi \tag{3.19}$$

$$A_3 = \frac{\kappa_{nf}}{\kappa_f} = \frac{\kappa_s + 2\kappa_f - 2\varphi(\kappa_f - \kappa_s)}{\kappa_s + 2\kappa_f + 2\varphi(\kappa_f - \kappa_s)} \tag{3.20}$$

3.2 MHD Nanofluid Flow in a Semi Porous Channel with Stretching Walls

This problem deals with heat transfer analysis on MHD nanofluids in a channel with stretching walls. An incompressible nanofluid with nanoparticles of Copper (Cu) are filled in a channel with water is treated as a based fluid. The governing partial differential equations are firstly transformed into ordinary differential equations by using suitable similarity transformation for stretching walls of the channel. The resulting nonlinear ordinary differential equations are then solved numerically by shooting method. Findings are well explained through pictorial representation and tabulation as well. Abbasi et al. (2014) investigated the problem of laminar incompressible viscous fluid flow in a channel with stretching walls under the influence of magnetic field. However, in the current problem we investigate copper water nanofluid under the same conditions, therefore, Abbasi et al. (2014) is the most appropriate reference of the current problem.

35

3.2.1 Mathematical Formulation

A steady laminar incompressible two-dimensional boundary layer flow in a channel is considered. Cartesian coordinate system is used such that the x-axis is taken in the direction of the flow and y-axis is perpendicular to the channel. Moreover, the upper wall is located at y= a, which is static and non-permeable, and the lower wall is located at y= -a, which is permeable as well as stretching in the direction of x-axis with stretching velocity $u = bx$ as shown in Figure 3.1. Flow is subjected to a constant applied magnetic field $B_\circ$ in the direction of y-axis. Temperature of lower and upper wall is T_1 and T_2 respectively and considered to be constant. From section 3.1.1, the governing boundary layer equations based on law of conservation, momentum and energy for the current problem are as follows (see equations 3.8 - 3.12):
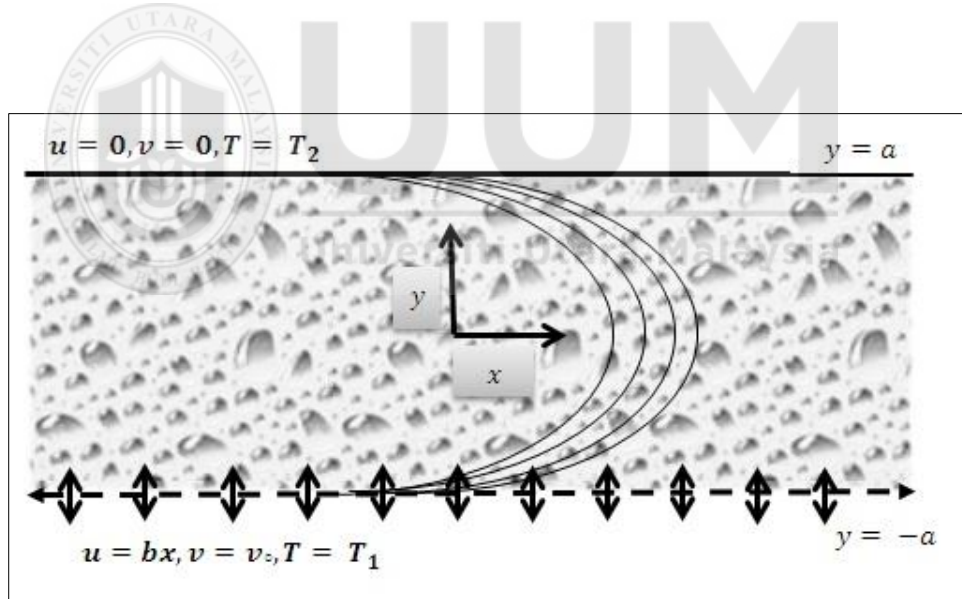
Figure 3.1. Physical model of the proposed problem

$$\frac{\partial u}{\partial x} + \frac{\partial v}{\partial y} = 0 \tag{3.21}$$

$$\rho_{nf}\left(u\frac{\partial u}{\partial x} + v\frac{\partial u}{\partial y}\right) = -\frac{\partial p}{\partial x} + \mu_{nf}\frac{\partial^2 u}{\partial y^2} - \sigma_{nf}B_\circ^2 u \tag{3.22}$$

$$\rho_{nf}\left(u\frac{\partial v}{\partial x} + v\frac{\partial v}{\partial y}\right) = -\frac{\partial p}{\partial y} + \mu_{nf}\frac{\partial^2 v}{\partial x^2} \tag{3.23}$$

$$u \frac{\partial T}{\partial x} + v \frac{\partial T}{\partial y} = \frac{k_{nf}}{\left(\rho C_p\right)_{nf}} \frac{\partial^2 T}{\partial y^2} \qquad (3.24)$$

where u and v are the velocity component along x and y axes respectively. σ_{nf} is effective electrical conductivity of nanofluid, ρ_{nf} is effective density, μ_{nf} is the effective dynamic viscosity, $\left(\rho C_p\right)_{nf}$ is heat capacitance and k_{nf} thermal conductivity of the nanofluid. These physical quantities were described mathematically in section 3.1.1 (see equations 3.13 - 3.17). The subjected boundary conditions are:

$$u = bx, \ v = \ - v_\circ \ T = \ T_1 \ at \ y = -a \ (Lower \ Wall) \qquad (3.25)$$

$$u = 0, \ v = 0, \ T = \ T_2 \ at \ y = a \ (Upper \ Wall) \qquad (3.26)$$

Moreover, $b<0$ is for shrinking of the channel walls and $b>0$ is for stretching of the channel wall. Introducing similarity variables to convert governing equations (3.21) - (3.24) into ordinary differential equations by Misra, Shit, & Rath (2008).

$$\eta = \frac{y}{a} \ , u = bx f'(\eta) \ , v = \ -ab f(\eta), \theta(\eta) = \frac{T - T_2}{T_1 - T_2}$$

Substituting similarity variables into equation (3.21) - (3.24) and by using the equations (3.13) - (3.17), the results are :

$$f'''' - M^2 B^\circ (1 - \varphi)^{2.5} f'' - A_1 R (1 - \varphi)^{2.5} (f' f'' - f f''') = 0 \qquad (3.27)$$

$$\frac{1}{Pr} \theta'' + \frac{A_2}{A_3} f \theta' = 0 \qquad (3.28)$$

where $R = \frac{a^2 b}{v_f}$ is stretching Reynolds number, $M^2 = \frac{\sigma B_\circ^2 a^2}{\mu_f}$ is Hartman number, $Pr = \frac{a^2 b (\rho C_p)_f}{\kappa_f}$ is the Prandtl number, λ is suction parameter. The values of A_1, A_2, A_3 are given in section 3.1.1 (see 3.18 – 3.20).

The appropriate boundary conditions become:

$$f'(-1) = 1, f'(1) = 0, \theta(-1) = 1\rbrace$$
$$f(-1) = \lambda, f(1) = 0, \theta(1) = 0 \ \rbrace \tag{3.29}$$

3.2.2 Solution of the Problem

Equations (3.27) and (3.28) were solved subjected to the boundary condition in Eq. (3.29) numerically using shooting method. A standard methodology is to compose the nonlinear ODEs inform of a first order initial value problem as follows:

By putting:

$$f' = p \tag{3.30}$$

$$p' = q \tag{3.31}$$

$$q' = s \tag{3.32}$$

$$s' = M^2 B^{\circ}(1 - \varphi)^{2.5} q + A_1 R (1 - \varphi)^{2.5} (pq - fs) \tag{3.33}$$

$$\theta' = z \tag{3.34}$$

$$z' = -Pr \frac{A_2}{A_3} fz \tag{3.35}$$

The boundary conditions are:

$$p(-1) = 1, \theta(-1) = 1, q(-1) = \alpha \rbrace$$
$$f(-1) = \lambda, s(-1) = \beta, z(-1) = \gamma \rbrace \tag{3.36}$$

where α, β, γ are unknown initial conditions. Hence, shooting the values of missing initial values of α, β, γ is crucial such that solution satisfies the boundary conditions $f(1) = 0$, $p(1) = 0$ and $\theta(1) = 0$ of the original boundary value. This computation is done with the aid of *shootlib* function in Maple software (Meade, Haran & White, 1996).

3.2.3 Results and Discussions

This section is devoted to present the numerical results in tabulation form and pictorial representation. The performance of solid volume fraction on velocity profile can be depicted by Figure 3.2 for the fixed value of $M = 0.4, R = 10, \lambda = 0.5$. The figure presented that prior to the center of the channel, solid volume fraction velocity profile increases. Afterwards, a reversed phenomenon can be observed. In Figure 3.3, reversible flow occurs for the variation of stretching Reynolds number for fixed values of the other parameters $\varphi = 0.03, M = 0.4, \lambda = 0.5$. This is in accordance with the variation of stretching Reynolds number. Figure 3.4 is the representation of consequences of suction parameter on velocity profile. Apart from the upper wall of the channel, velocity profile enhances speedily. The effect of magnetic field on velocity profile is observed in Figure 3.5 for fixed values of $\varphi = 0.03, R = 10, \lambda = 0.5$. Increasing the values of magnetic parameter M will increase the velocity profile $f'(\eta)$ near the channel walls and decreases at the center. This is the effect of magnetic field is normal in the direction of the channel wall; therefore, the effect of magnetic field is dominant near the walls. Physically speaking, when magnetic field is applied to the nanofluid, then the fluids' apparent viscosity decreases due to the chain formation of the nanoparticles. The chainlike structures speed up the flow and accelerate the motion. This result is caused by the fact that the flow of nanofluid can be controlled very efficiently by applying and varying magnetic field; an advantage where many possible control based applications can be used for instance in MHD power generation, casting of metals and ion propulsion.
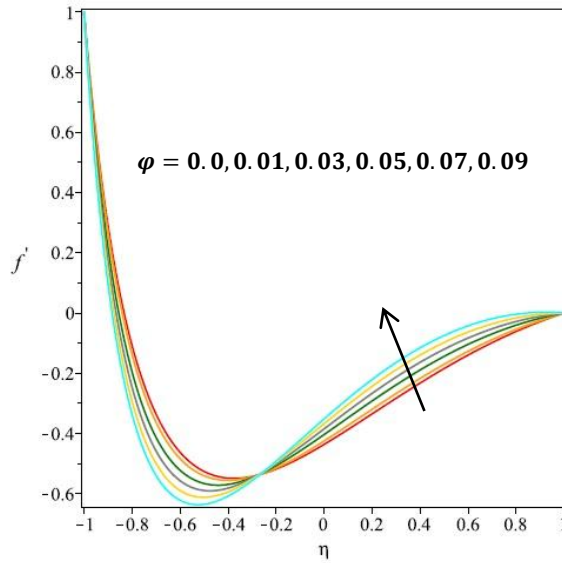
Figure 3.2. Effects of φ on f' for $M = 0.4, R = 10, \lambda = 0.5$
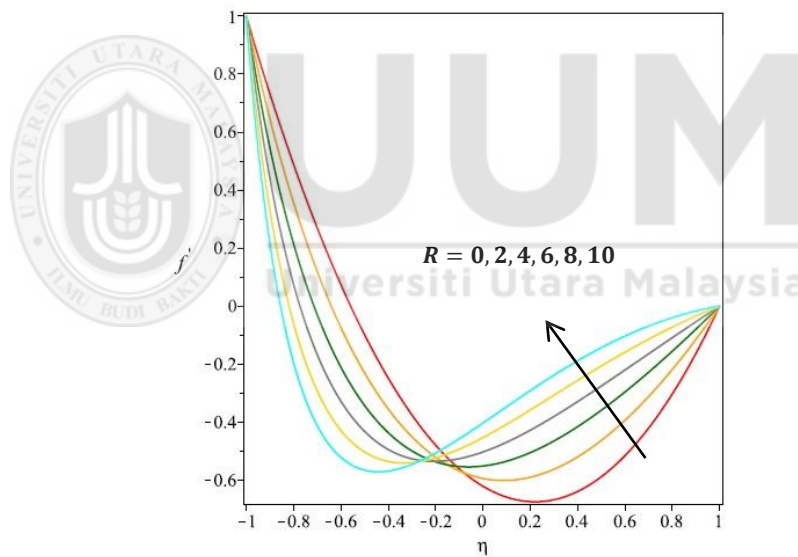
Figure 3.3. Effect of R on f' for $\varphi = 0.03,\ M = 0.4,\ \lambda = 0.5$

The effect of Prandtl number on $\theta(\eta)$ for fixed values of $M = 0.4, R = 10, \lambda = 0.5, \varphi = 0.03$ is represented in Figure 3.6. which demonstrated that an increased value in Prandtl number will decrease the profile of $\theta(\eta)$. Hence, Figure 3.6 concluded that thermal diffusivity decreases by increasing Prandtl number; implying that heat diffuses slowly farther from the heated surface. Figure 3.7 presented the comparison of the present

40

results with previously published results of Abbasi et al. (2014) in the form of qualitative and found good agreement with the published literature.

Table 3.1 represents some thermophyscial properties of water and nanoparticles. Numerical values of the effect of Reynolds number, magnetic field, suction parameter and solid volume fraction on skin friction and heat transfer are illustrated in Table 3.2. The magnitude values of skin friction and heat transfer increase and decrease respectively by increasing in the values of solid volume fraction from 0 to 0.09. Skin friction increases numerically as stretching Reynolds number increases, however, heat transfer rate decreases for the fixed values of other parameters. Trend of the numerical values of skin friction and heat transfer rate increases as suction parameter increases from 0 to 0.5.
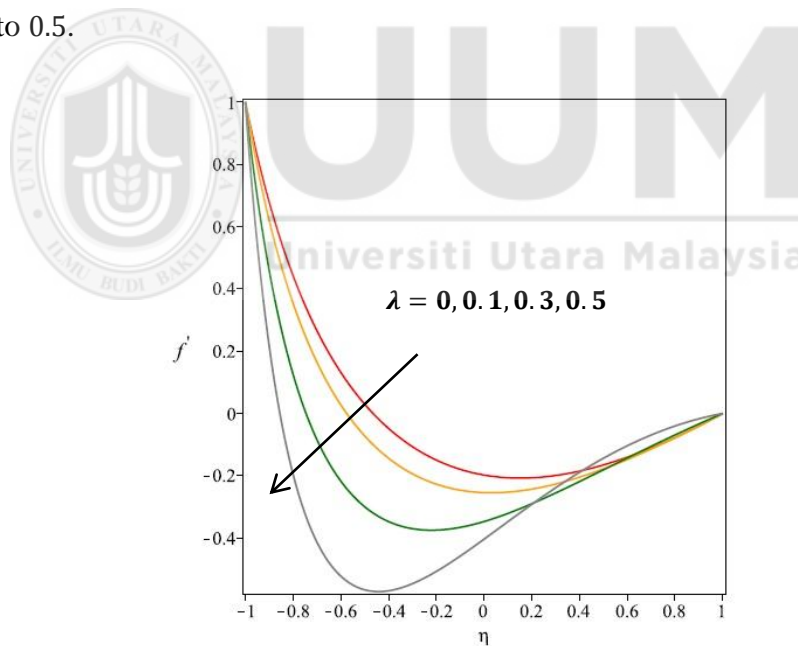
Figure 3.4. Effect of λ on f' for $\varphi = 0.03, R = 10, M = 0.4$

An increasing value in magnetic field will decrease the skin friction and heat transfer rate. The magnetic field applied perpendicularly to the channel is opposing the fluid motion, therefore heat is produced. This phenomenon is depicted in Table 3.2. In fact, magnetic nanoparticles are stronger than tumor cells, therefore, it absorbs more power

41

than microparticles in alternating current magnetic fields endurable in humans (Hayat et al., 2014). Heat transfer rate increases by increase the values of Prantl number by setting $M = 0.4, R = 10, \lambda = 0.5, \varphi = 0.03$.
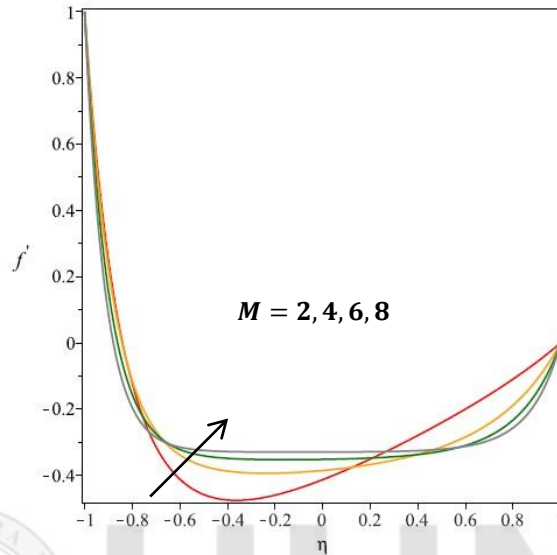
Figure 3.5. Effects of M on f' for $\varphi = 0.03, R = 10, \lambda = 0.5$
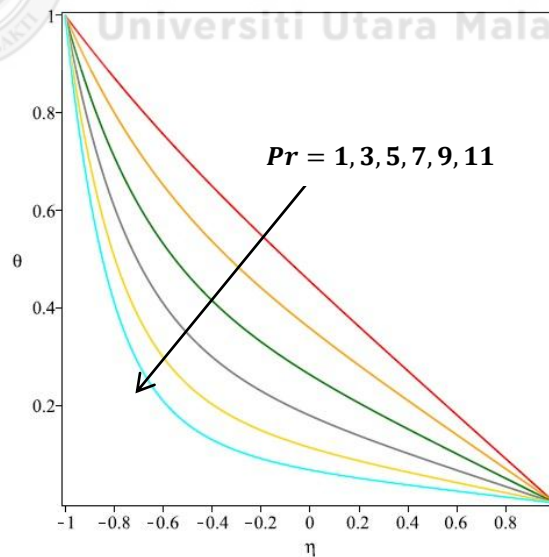
Figure 3.6. Effects of Pr on $\theta(\eta)$ for $M = 0.4, R = 10, \lambda = 0.5, \varphi = 0.03$

Numerical results validation is performed by comparing the results from Runge-Kutta-Fehlberg method. The following table shows the numerical results in tabulation representing shooting method and Runge-Kutta-Fehlberg method. (See Table 3.3).
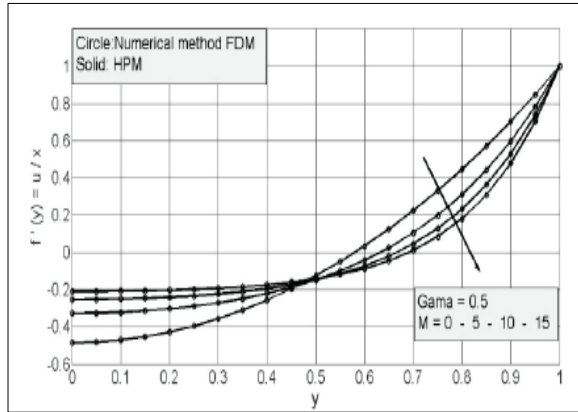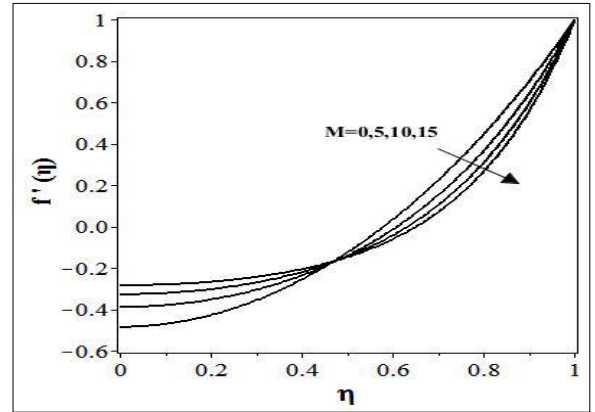
| Abbasi et al. (2014) | Present results $R = 2, M = 0,5,10,15, \varphi = 0$ |

$$f''(0) = 0, f(0) = 0, f'(1) = 1, f(1) = 0$$

Figure 3.7. Validation of the physical model

Table 3.1

Thermophysical properties of water and nanoparticles

Nanofluids	$\rho/_{kg.m^{-3}}$	$C_p/_{j.kg^{-1}.k}$	$k/_{W.m^{-1}.k}$	$\beta \times 10^5/_{K^{-1}}$
Pure water	991.1	4179	0.613	21
Copper (Cu)	8933	385	401	1.67
Alumina (Al_2O_3)	3970	765	40	0.85
Silver (Ag)	10500	235	429	1.89
Titanium Oxide (TiO_2)	4250	686.2	8.9538	0.9

43

Table 3.2

Effect of different parameters on skin friction & heat transfer rate for Nanoparticle (Copper Cu)

R	M	Pr	λ	φ	$f''(-1)$	$\theta'(-1)$
10	0.4	1.0	1.0	0	-9.384752739	-0.709290125
				0.01	-9.846596801	-0.694623691
				0.03	-10.71745956	-0.668955131
				0.05	-11.51701997	-0.647222635
				0.07	-12.24689148	-0.628538897
				0.09	-12.91298929	-0.612199712
0	0.4	1.0	1.0	0.03	-2.800909116	-0.787739677
2					-3.910754184	-0.759006092
4					-5.299500304	-0.732485523
6					-6.901388546	-0.709232644
8					-8.695953803	-0.688577949
10					-10.71745956	-0.668955131
10	0.4	1.0	0.0	0.03	-3.742085886	-0.562724070
			0.1		-4.543897119	-0.587615101
			0.3		-6.877754916	-0.633277452
			0.5		-10.71745956	-0.668955131
	0				-10.75677730	-0.667396680
	2				-10.48398313	-0.687931523
10	4	1.0	1.0	0.03	-11.49142634	-0.698915350
	6				-13.38986618	-0.698123028
	8				-15.57744388	-0.694903830
10	0.4	1	1.0	0.03		-0.668955132
		3				-1.142279804
		5			--	-1.816013339
		7				-2.676178601
		9				-3.669210781

Table 3.3

Comparison of the numerical results

R	M	Pr	λ	φ	f''(−1)	θ'(−1)	f''(−1)	θ'(−1)
					Shooting method		**Runge-Kutta-Fehlberg**	
0	0.4	1.0	1.0	0.03	-2.800909116	-0.787739677	-2.800909152	-0.798405957
2					-3.910754184	-0.759006092	-3.910754228	-0.768556325
4					-5.299500304	-0.732485523	-5.299500357	-0.741001284

3.3 Cu-Water Nanofluid in a Porous Channel: Triple Solutions

Fluid flow problem of a nanofluid comprising a base fluid (water) and copper (Cu) nanoparticles have been considered in a porous channel under the influence of magnetic field. The channel walls considered to be permeable. Governing partial differential equations are converted into system of nonlinear ordinary differential equation by using suitable similarity transformation and solved numerically using shooting method. Multiple solutions occur for the variation of suction Reynolds number, solid volume fraction and magnetic parameters considered. Problem considered in this section is most relevant to Ganesh and Krishnambal (2006). They considered the problem of steady laminar incompressible viscous fluid in a porous channel under the influence of magnetic field. Governing equations were solved numerically by R-K- Gill method. Moreover, Ganesh and Krishnambal (2006) focused to examine the one solution, however, this study has succeeded to find the multiple solutions of the problem for the fixed values of the different physical parameters.

3.3.1 Problem Formulation

This problem considers two-dimensional steady laminar incompressible flow of electrically conductive nanofluid in a porous channel $(-a \leq y \leq a)$ by Nouri et al. (2013) and uses Cartesian coordinate system such as the *x*-axis is taken in the direction

of the flow and *y*-axis is perpendicular to the channel. Moreover, fluid is taken

symmetric in the direction *y*-axis as shown in Figure 3.8. Flow is subjected to a constant

applied magnetic field $B_\circ$ in the direction of *y*-axis. Under these assumptions governing

equations of the law of conservation, momentum and energy equations defined in

section 3.1.1 are in the following form:
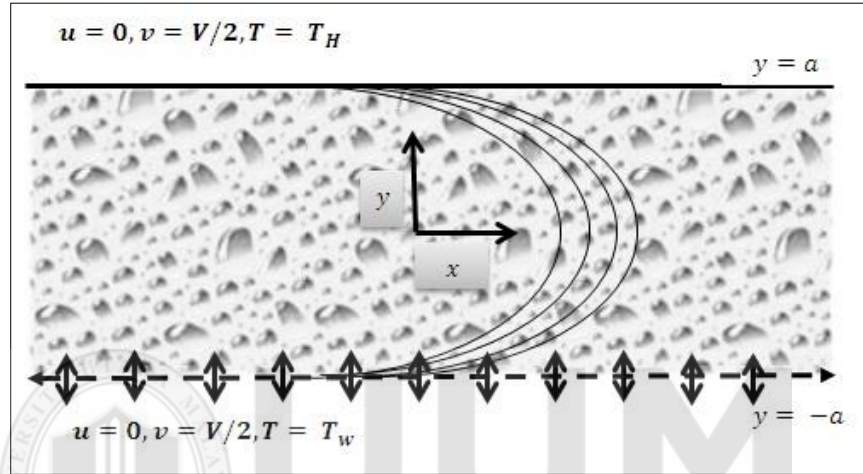
Figure 3.8. Physical model of the problem

$$\frac{\partial u}{\partial x} + \frac{\partial v}{\partial y} = 0 \tag{3.37}$$

$$\rho_{nf}\left(u\frac{\partial u}{\partial x} + v\frac{\partial u}{\partial y}\right) = -\frac{\partial p}{\partial x} + \mu_{nf}\frac{\partial^2 u}{\partial y^2} - \sigma_{nf}B_\circ^2 u \tag{3.38}$$

$$\rho_{nf}\left(u\frac{\partial v}{\partial x} + v\frac{\partial v}{\partial y}\right) = -\frac{\partial p}{\partial y} + \mu_{nf}\frac{\partial^2 v}{\partial x^2} \tag{3.39}$$

$$u\frac{\partial T}{\partial x} + v\frac{\partial T}{\partial y} = \frac{k_{nf}}{\left(\rho C_p\right)_{nf}}\frac{\partial^2 T}{\partial y^2} \tag{3.40}$$

where u and v are the velocity component along x and y axes respectively. σ_{nf} is

effective electrical conductivity of nanofluid, ρ_{nf} is effective density, μ_{nf} is effective

dynamic viscosity, $(\rho C_p)_{nf}$ is heat capacitance and k_{nf} is thermal conductivity of the nanofluid. These physical quantities described mathematically in section 3.1.1.

This research prefers to solve equations (3.37) - (3.40) through equations (3.13) - (3.17) with boundary conditions of:

$$u = 0, v = \frac{V}{2}, \qquad T = T_w, C = C_w \ at \ y = a \tag{3.41}$$

$$\frac{\partial u}{\partial y} = 0, v = 0, \qquad T = T_H, C = C_H \ at \ y = 0 \tag{3.42}$$

The stream function is introduced such that:

$$\bar{u} = \frac{\partial \psi}{\partial y}, \bar{v} = \frac{-\partial \psi}{\partial x} \tag{3.43}$$

The system of equations (3.37) - (3.40) were solved and eliminating the pressure term from Eq. (3.38) - (3.39) by introducing vorticity ω:

$$\frac{\partial \omega}{\partial t} + u \frac{\partial \omega}{\partial x} + v \frac{\partial \omega}{\partial y} = v \left(1 + \frac{1}{\beta}\right) \left(\frac{\partial^2 \omega}{\partial x^2} + \frac{\partial^2 \omega}{\partial y^2}\right) - \frac{\sigma B_\circ^2 u'}{\rho} \tag{3.44}$$

Where

$$\omega = \left(\frac{\partial \bar{v}}{\partial x} - \frac{\partial \bar{u}}{\partial y}\right) \tag{3.45}$$

Defining

$$x^* = \frac{x}{a}, y^* = \frac{y}{a}, u = -Vx^*f'(y^*), v = Vf(y^*),$$

$$\theta(y^*) = \frac{T - T_H}{T_w - T_H}, \vartheta(y^*) = \frac{C - C_H}{C_w - C_H}$$

proposed by Hayat and Abbas (2008). Then the governing nonlinear momentum and energy equations of nanofluids in a channel can be written as:

$$f^{iv} + RA_1(1 - \varphi)^{2.5}(f'f'' - ff''') + M^2(1 - \varphi)^{2.5}f'' = 0 \tag{3.46}$$

$$\frac{1}{Pr}\theta'' + \frac{A_2}{A_3}f\theta' = 0 \tag{3.47}$$

47

where $R = \frac{Va}{\nu}$ is Reynolds number ($R > 0$ for suction $R < 0$ for injection), $M^2 = \frac{\sigma B_\circ^2 a^2}{\mu_f}$

is Hartman number, $Pr = \frac{Va(\rho C_p)_f}{\kappa_f}$ is the Prandtl number and the values of A_1, A_2, A_3 are

defined in section 3.1.1.

Moreover, boundary conditions become

$$\left.\begin{array}{l} f(1) = 1/2, f'(1) = 0, \theta(1) = 1 \\ f''(0) = 0, f(0) = 0, \theta(0) = 0 \end{array}\right\} \tag{3.48}$$

3.3.2 Stability Analysis

The stability analysis of the steady flow solution $f(\eta) = f_\circ(\eta)$ and $\theta(\eta) = \theta_\circ(\eta)$ which

satisfies the boundary conditions in Eq. (3.48) is from (Merkin 1986, Rosca & Pop

2013),

$$f(\eta) = f_\circ(\eta) + e^{-\lambda t} F(\eta, t) \tag{3.49}$$

$$\theta(\eta) = \vartheta_\circ(\eta) + e^{-\lambda t} G(\eta, t) \tag{3.50}$$

where

$0 < F(\eta, t) \ll 1$, $0 < G(\eta, t) \ll 1$ and λ is the unknown eigenvalues, $F(\eta, t)$ and $G(\eta, t)$

are the smallest relative to $f_\circ(\eta)$ and $\theta_\circ(\eta)$ respectively.

The governing equations of (3.46) – (3.47) for unsteady case ($\tau = t$) are as follows:

$$\frac{\partial^4 f}{\partial \eta^4} + RA_1(1 - \varphi)^{2.5}\left[\frac{\partial f}{\partial \eta}\frac{\partial^2 f}{\partial \eta^2} - f\frac{\partial^3 f}{\partial \eta^3}\right] + M^2(1 - \varphi)^{2.5}\frac{\partial^2 f}{\partial \eta^2} = \frac{\partial^3 f}{\partial \tau \partial \eta^2} \tag{3.51}$$

$$\frac{\partial^2 \theta}{\partial \eta^2} + Pr\frac{A_2}{A_3}f\frac{\partial \theta}{\partial \eta} = \frac{\partial \theta}{\partial \tau} \tag{3.52}$$

Substituting Equations (3.49) - (3.50) into Equations (3.51) - (3.52) and setting $\tau = 0$

(Merkin, 1986), will get;

$$\left.\begin{array}{l} F'''' + RA_1(1 - \varphi)^{2.5}[f_\circ' F'' + f_\circ'' F' - f_\circ F''' - F f_\circ'''] \\ + \\ M^2(1 - \varphi)^{2.5}F'' + \lambda F'' = 0 \end{array}\right\} \tag{3.53}$$

48

$$G'' + Pr\frac{A_2}{A_3}(f_\circ G' + F\theta'_\circ) + \lambda G = 0 \tag{3.54}$$

The research of the current study envisioned to analyse the stability of the steady

state. Therefore, in Equations (3.53) – (3.54), we set $\tau = 0$ as suggested by Merkin

(1986) with the boundary conditions of:

$$\left.\begin{array}{l} F(1) = 0, F'(1) = 0, G(1) = 1 \\ \quad F''(0) = 0, F(0), G(0) = 0 \end{array}\right\} \tag{3.55}$$

$f_\circ(\eta)$ and $\theta_\circ(\eta)$ can be determined by the smallest eigenvalue λ due to the steady state

flow solution. Therefore, the range of the possible eigenvalues can be determined by

relaxing the boundary conditions on $f_\circ(\eta)$ and $\theta_\circ(\eta)$ as prescribed by Harris et al. (2009).

Therefore, the boundary condition $G(1) \to 0$ are relaxed and thereby solved the system

of differential equation with the new boundary condition $G'(0) = 1$.

3.3.3 Numerical Method for Solution

The ODEs for stability (3.53) – (3.54) subjected to the boundary conditions in Eq.

(3.55) were solved numerically by using of the program "*bvp4c*" in MATLAB. "*bvp4c*"

is a finite difference method that implements the three-stage Lobatto IIIa formula,

which is a collocation method of fourth-order accuracy. In this approach, the

differential equations are firstly reduced to a system of first-order equations by

introducing new variables. Mesh selection and error control are based on the residual

of the continuous solution. In this study, the relative error tolerance is to 10^{-8}.

Equations (3.46) and Eq. (3.47) subjected to the boundary condition in Eq. (3.48) are

solve numerically using shooting method. A standard methodology is supposed to

compose the nonlinear ODEs of a first order initial value problem by putting:

$$f' = p \tag{3.56}$$

$$p' = q \tag{3.57}$$

$$q' = s \tag{3.58}$$

$$s' = -M^2(1 - \varphi)^{2.5}q - A_1 R(1 - \varphi)^{2.5}(pq - fs) \tag{3.59}$$

$$\theta' = z \tag{3.60}$$

$$z' = -Pr\frac{A_2}{A_3}fz \tag{3.61}$$

with boundary conditions of:

$$\left. \begin{array}{l} f(1) = 1/2, p(1) = 0, \theta(1) = 0 \\ q(1) = s_1, s(1) = s_2, z(1) = s_3 \end{array} \right\} \tag{3.62}$$

Here s_1, s_2 and s_3 are unknown initial conditions. The missing values of initial conditions that satisfy equation (3.62) of the original boundary conditions are determined using shooting method. Integrating equations (3.56) – (3.61) as an initial value problem requires the values of $q(1), s(1)$. Since these values are not given in the boundary condition (3.62), by trial and error, suitable guess values are made and integration is carried out. Afterwards, the calculated values are compared for $f'(0)$ with the given boundary conditions in equation (3.62) with accuracy of 10^{-8}.

3.3.4 Results and Discussions

In this section, Figures (3.9) - (3.15) are displayed to evaluate the effect of different parameters on velocity profile $f'(\eta)$ and skin friction. The objective of this study is to investigate multiple solutions of nanofluids in a porous channel. Table 3.4shows the thermophysical properties of nanofluid. Table 3.5 shows the numerical results with two different methods and validate our numerical solutions. Table 3.6 presents the smallest eigenvalues γ at several values of Reynolds number. This table presented that the eigenvalues of the 1st solution is positive and negative for the 2nd and third solutions.

Therefore, this stability analysis shows that the 1st solution is stable and physically reliable but the 2nd and 3rd solutions are unstable and physically unreliable.

Present study reveals that multiple solutions exists only for the case of suction $R > 0$ for the fixed values of $M = 0.4$ and $\varphi = 0.03$. Based on the finding of multiple solutions, conclusion is made such that there is only one solution in the case of $R \in (-\infty, 21.1)$. However, multiple solutions exist for the values of suction $R \geq 21.1$. This phenomenon is well explained in Figure 3.9 which depicted the occurrence of multiple solutions for the different values of suction on skin friction for $M = 0.4, \varphi = 0.03$.
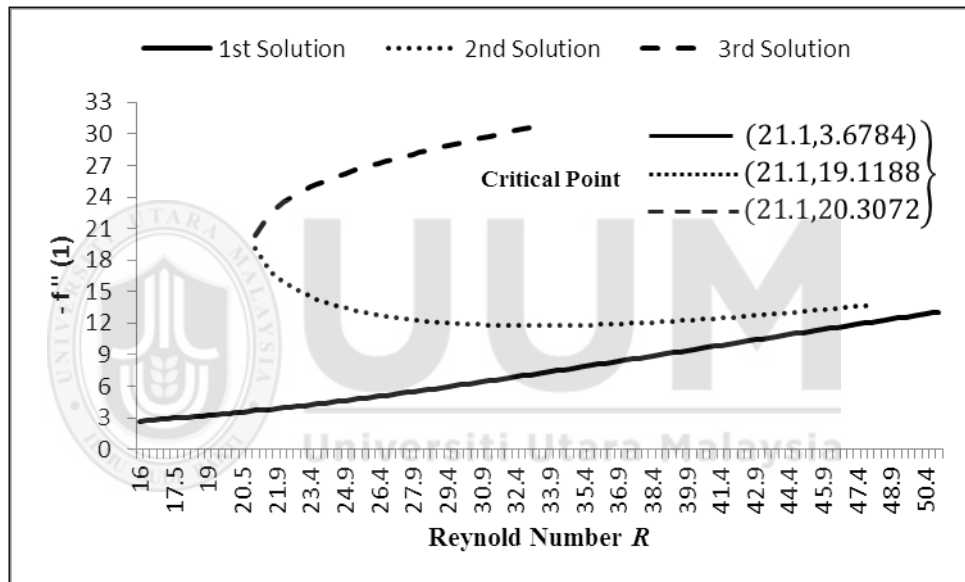
Figure 3.9. Effect of suction on skin friction $f''(\eta)$ *for* $M = 0.4, \varphi = 0.03$

Figure 3.10 elucidates the effects of solid volume fraction φ on velocity profile $f'(\eta)$ of different solutions. Enhancement of the strength of solid volume fraction φ decreases the velocity profile $f'(\eta)$ for the 1st and the 3rd solutions and increases for the 2nd solution in the quarter half of the channel. However, changes in velocity profile $f'(\eta)$ for the 1st and the 2nd solutions are smaller than the 3rd solution. Increasing the values of Reynolds number in the case of suction, decreases the velocity profile $f'(\eta)$ for the 1st and the 3rd solutions but increases for the 2nd solution for $0 \leq \eta < 0.5$ as presented in

Figure 3.11. The effects of magnetic field M on velocity profile $f'(\eta)$ for $\varphi = 0.03, R = 30, Pr = 6.2$ are presented in Figure 3.12. Velocity profile $f'(\eta)$ for the 1st and the 2nd solutions increases as the enhancement of magnetic field M but decreases for the 3rd solution. this trend is observed in the quarter half of the channel and afterwards.

Figure 3.13 demonstrates the effects of Prandtl number Pr on $\theta(\eta)$ which concluded that temperature profile decreases by the increasing of Prandtl number for the 1st and the 2nd solutions near the center of the channel. However, a totally inverse phenomenon is observed for 3rd solution. The effects of solid volume fraction φ on temperature profile $\theta(\eta)$ are presented in Figure 3.14. Increasing the strength of solid volume fraction φ increases monotonically the 1st and the 2nd solutions but decreases for the 3rd solution. Physically speaking, solid volume fraction φ for nanofluids will increase the thermal conductivity of nanofluids for the 1st and the 2nd solutions was already an established fact. Figure 3.15 represented the effects of Reynolds number on temperature $\theta(\eta)$. Thermal diffusivity increases by increasing the strength of suction for the 1st and the 3rd solutions. Figure 3.16 illustrated the effects of Lorentz force on temperature $\theta(\eta)$ which demonstrated an increase in the magnetic field will decrease the temperature. Figure 3.17 showed the qualitative comparison with the previously published results of Ganesh and Krishnambal (2006). From the graphical representation it is found an excellent agreement of the present results with the previously published results.
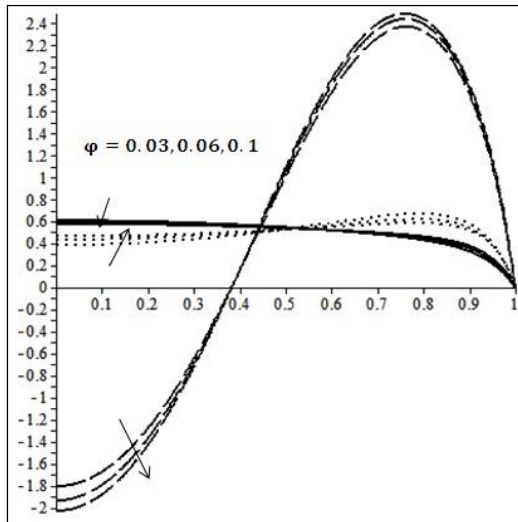
Figure 3.10. Effect of solid volume fraction φ on velocity profile $f'(\eta)$ for suction $R = 30, M = 0.4, Pr = 6.2$
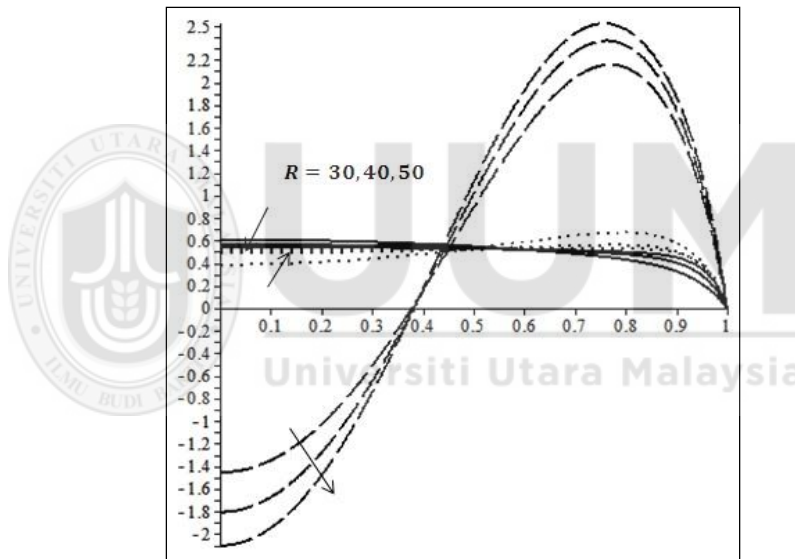
Figure 3.11. Effect of suction on velocity profile $f'(\eta)$ for suction $\varphi = 0.03$, $M = 0.4, Pr = 6.2$
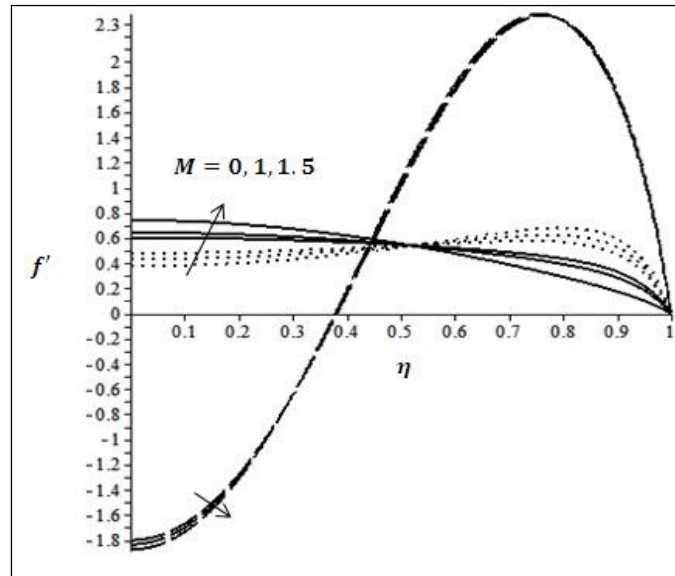
Figure 3.12. Effect of magnetic field M on velocity profile $f'(\eta)$ for suction $\varphi = 0.03, R = 30, Pr = 6.2$
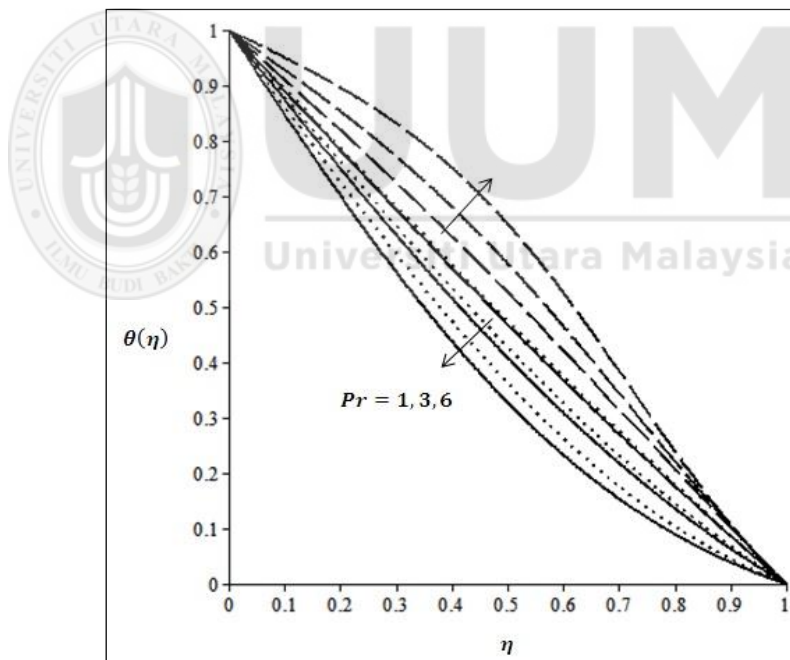
Figure 3.13. Effect of Prandtl number on $\theta(\eta)$ for $\varphi = 0.03, R = 30, M = 0.4$
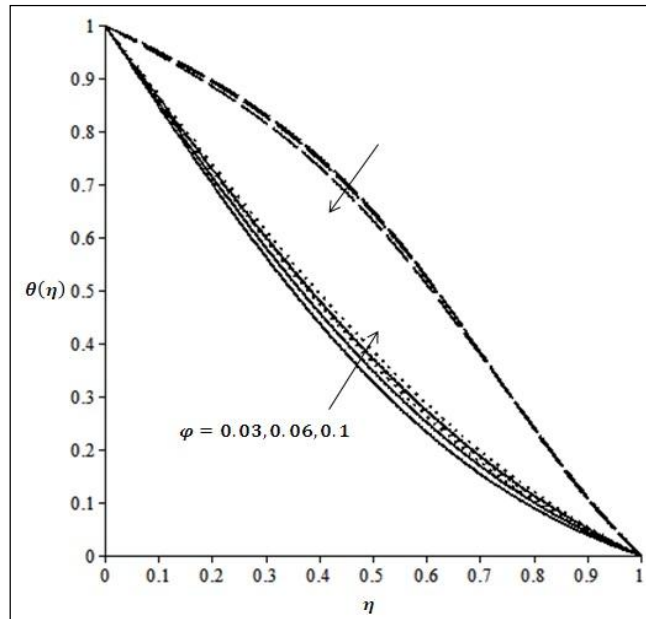
Figure 3.14. Effect of Solid volume fraction on temperature profile $\theta(\eta)$ for $Pr = 6.2$, $R = 30$, $M = 0.4$
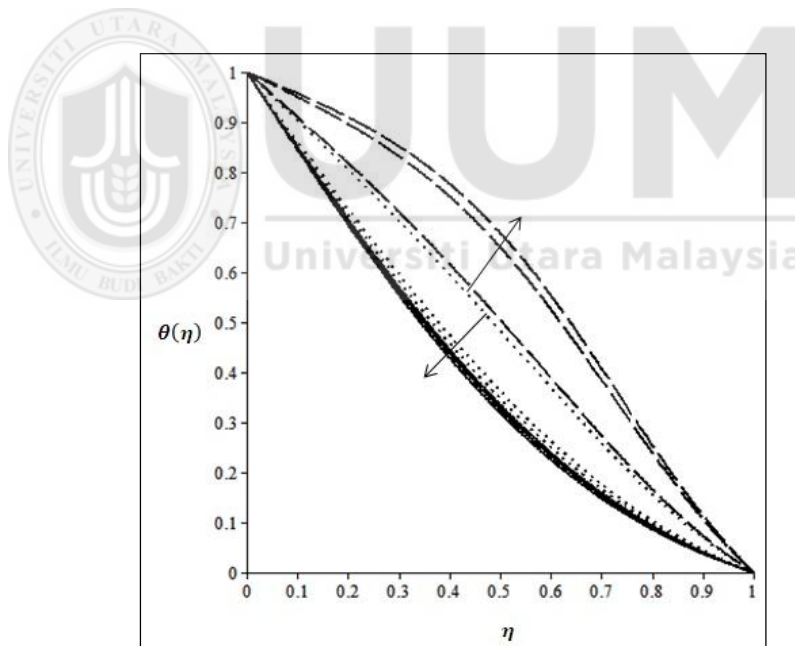
Figure 3.15. Effect of Reynolds number on temperature profile $\theta(\eta)$ for $Pr = 6.2$, $\varphi = 0.03$, $M = 0.4$
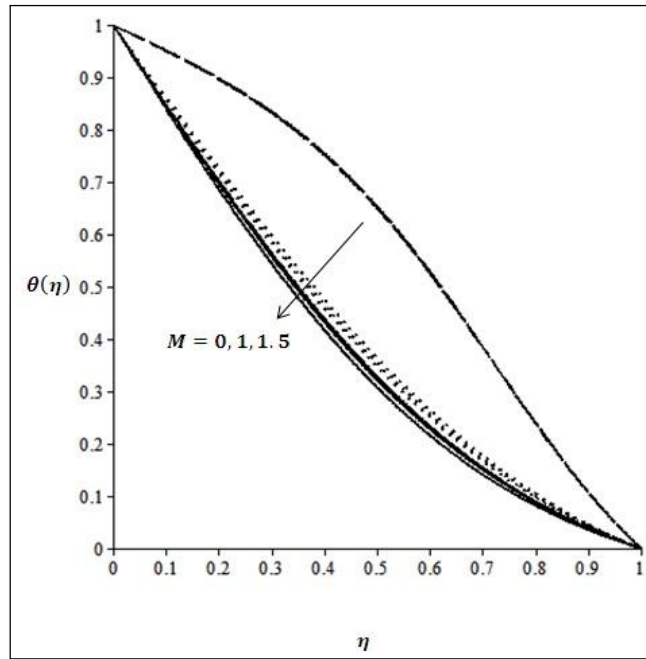
Figure 3.16. Effect of Magnetic field on temperature profile $\theta(\eta)$ for $Pr = 6.2$, $\varphi = 0.03$, $R = 30$
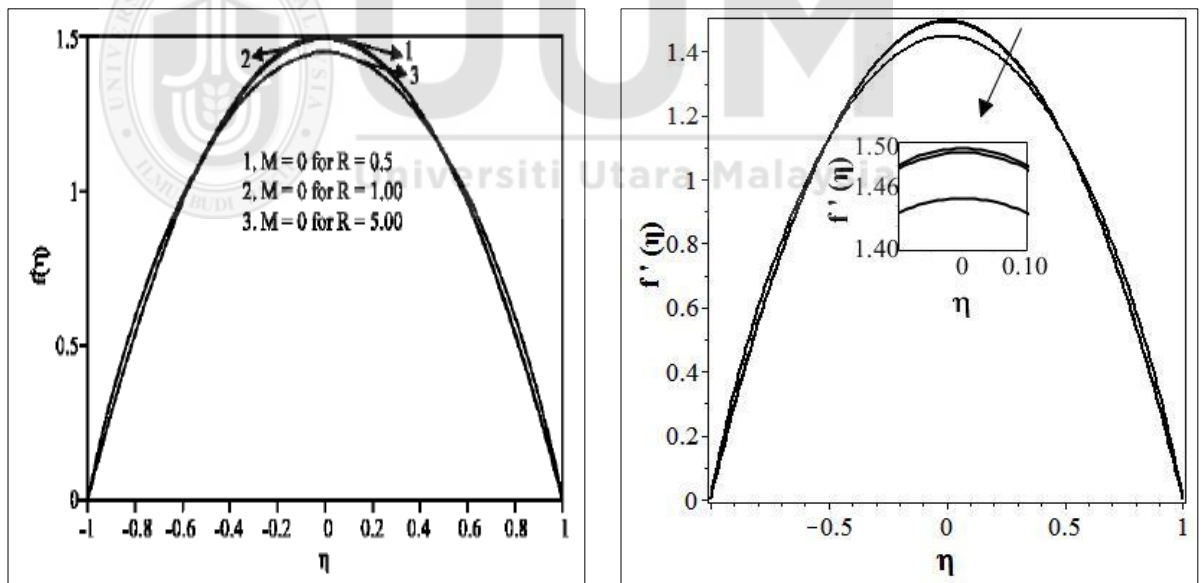
Velocity Profile for Ganesh and Krishnambal   Present results for

(2006) $\varphi = 0, f(1) = 1, f(-1) = -1$

Figure 3.17. Validation of the physical model with Ganesh and Krishnambal (2006)

56

Table 3.4

Thermophysical properties of water and nanoparticles

	$\rho/{kg.m^{-3}}$	$C_p/{j.kg^{-1}.k}$	$k/{W.m^{-1}.k}$	$\beta \times 10^5/{K^{-1}}$
Pure water	991.1	4179	0.613	21
Copper (Cu)	8933	385	401	1.67
Alumina (Al_2O_3)	3970	765	40	0.85
Silver (Ag)	10500	235	429	1.89
Titanium Oxide (TiO_2)	4250	686.2	8.9538	0.9

Table 3.5

Validation of numerical results

R	M	Pr	φ	$f''(-1)$ Shooting method	$f''(-1)$ Runge-Kutta-Fehlberg
0	0.4	1.0	0.03	-1.485109908	-1.485109914
3				-1.571249086	-1.571249083
6				-1.699887651	-1.699887682

Table 3.6

Smallest eigenvalues λ at several values of Reynolds number

R	φ	M	Pr	1st Solution λ	2nd Solution λ	3rd Solution λ
21.1				4.2965	-5.0736	-5.9199
24				4.3458	-5.5422	-6.1633
27	0.03	0.4	6.2	4.4537	-5.7458	-6.4317
30				4.7172	-5.9273	-6.4956
33				4.9495	-5.9930	-6.7513

3.4 Copper-Water (Cu-Water) Nanofluids in a Channel with Slowly Expanding or Contracting Walls: Triple Solutions

This study has been carried out to examine the occurrence of multiple solutions for Copper-Water nanofluids flows in a porous channel with slowly expanding and contracting walls. The governing equations are firstly transformed to similarity equations by using similarity transformation. The resulting equations are then solved numerically by using shooting method. The effects of wall expansion ratio and solid volume fraction on velocity and temperature profile have been studied. Numerical results are presented graphically for the variations of different physical parameters. The study reveals that triple solutions exist only for the case of suction. The problem considered by Hatami et al. (2015) is the most relevant reference of the current problem. To validate our physical model, we set physical parameter $\varphi = 0.04, I: \alpha = R = 5, II: \alpha = 1, R = 4, III: \alpha = -0.5, R = -2, IV: \alpha = -1, R = 1$ and found an excellent agreement with the published results.

3.4.1 Mathematical Formulation

This study considers two-dimensional flow of unsteady, laminar and incompressible nanofluids in a porous channel where the channel walls are variant in the direction of y-axis and can be expanded or contracted with respect to the time dependent rate $\dot{a}$. Moreover, both channel walls are assumed to have the same permeability, and uniform wall suction/injection is imposed at the walls. The fluid is considered symmetric about y-axis as shown in Figure 3.18.
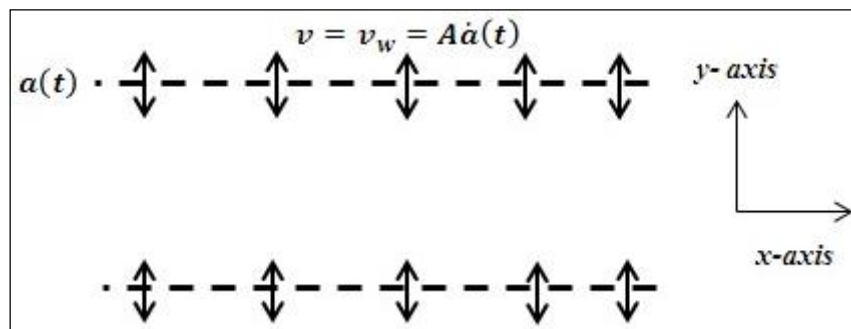
Figure 3.18. Physical model of the proposed problem.

58

The governing equations of the problem are given below:

$$\frac{\partial u}{\partial x} + \frac{\partial v}{\partial y} = 0 \tag{3.63}$$

$$\frac{\partial \bar{u}}{\partial t} + \rho_{nf}\left(\bar{u}\frac{\partial \bar{u}}{\partial x} + \bar{v}\frac{\partial \bar{u}}{\partial y}\right) = -\frac{\partial p}{\partial x} + \mu_{nf}\left(2\frac{\partial^2 \bar{u}}{\partial x^2} + \frac{\partial^2 \bar{u}}{\partial y^2} + \frac{\partial^2 \bar{u}}{\partial x \partial y}\right) \tag{3.64}$$

$$\frac{\partial \bar{v}}{\partial t} + \rho_{nf}\left(\bar{u}\frac{\partial \bar{v}}{\partial x} + \bar{v}\frac{\partial \bar{v}}{\partial y}\right) = -\frac{\partial p}{\partial y} + \mu_{nf}\left(2\frac{\partial^2 \bar{v}}{\partial x^2} + \frac{\partial^2 \bar{v}}{\partial y^2} + \frac{\partial^2 \bar{v}}{\partial x \partial y}\right) \tag{3.65}$$

$$u\frac{\partial T}{\partial x} + v\frac{\partial T}{\partial y} = \frac{k_{nf}}{(\rho C_p)_{nf}}\left(\frac{\partial^2 T}{\partial x^2} + \frac{\partial^2 T}{\partial y^2}\right) \tag{3.66}$$

where u and v are the velocity component along x and y axes respectively. ρ_{nf} is effective density, μ_{nf} is the effective dynamic viscosity, $(\rho C_p)_{nf}$ is heat capacitance and k_{nf} thermal conductivity of the nanofluid.

The preference here is to solve equations (3.63) – (3.66) through equations (3.16) – (3.17) with boundary conditions of:

$$\bar{u}(x, a) = 0, \bar{v}(a) = -v_w = -A\dot{a}, T = T_H \tag{3.67}$$

$$\frac{\partial \bar{u}}{\partial y}(x, 0) = 0, \bar{v}(0) = 0, T = T_w \tag{3.68}$$

Fluid can be injected or sucked with uniform velocity v_w at the channel walls. Moreover, the injection/suction coefficient $A \cong {v_w}/{\dot{a}}$ that appears in equation (3.67) is a measure of wall permeability.

The stream functions are introduced such that

$$\bar{u} = \frac{\partial \psi}{\partial y}, \bar{v} = \frac{-\partial \psi}{\partial x} \tag{3.69}$$

59

The system of equations in Equations (3.63) – (3.66) are solved and the pressure term

from Equations (3.64) and (3.65) is eliminated by introducing vorticity ω. We will get:

$$\frac{\partial \omega}{\partial t} + u \frac{\partial \omega}{\partial x} + v \frac{\partial \omega}{\partial y} = \frac{\mu_{nf}}{\rho_{nf}} \left(\frac{\partial^2 \omega}{\partial x^2} + \frac{\partial^2 \omega}{\partial y^2} \right) \tag{3.70}$$

Where

$$\omega = \left(\frac{\partial \bar{v}}{\partial x} - \frac{\partial \bar{u}}{\partial y} \right)$$

Similarity solution can be developed from the mean flow stream function in the light of

boundary conditions Equations (3.67) and (3.68). For this, consider $y \equiv \frac{\bar{y}}{a}$ and stream

function can be written as:

$$\psi = \frac{v}{a(t)} \bar{x} \bar{F}(\eta, t), \qquad where \; \eta = \left. y \middle/ a(t) \right. \tag{3.71}$$

Putting Equation (3.71) into (3.69) we have:

$$\bar{u} = \frac{v \bar{x}}{a^2(t)} \bar{F}_\eta, \bar{v} = \frac{-v}{a(t)} \bar{F}(\eta, t), \theta(\eta) = \frac{T - T_H}{T_w - T_H} \tag{3.72}$$

where $\bar{F}_\eta$ is the partial derivative of $\bar{F}$ with respect to η. Using Equation (3.72) in

Equation (3.70), we get:

$$(\bar{F})_{\eta\eta\eta\eta} + \frac{v_f}{v_{nf}} \left(\alpha \left[\eta(\bar{F})_{\eta\eta\eta} + 3(\bar{F})_{\eta\eta} \right] + \bar{F}(\bar{F})_{\eta\eta\eta} - (\bar{F})_\eta(\bar{F})_{\eta\eta} \right)$$

$$- \left. a^2 \middle/ v \right. (\bar{F})_{\eta\eta t} = 0 \tag{3.73}$$

where $\alpha = \frac{\dot{a}a}{v}$ is the wall expansion ratio.

The boundary conditions are:

$$\bar{F}_\eta = 0, \bar{F} = R, \theta = 0, \qquad \eta = 1 \tag{3.74}$$

$$\overline{F_{\eta\eta}} = 0, \bar{F} = 0, \theta = 1, \qquad \eta = 0 \tag{3.75}$$

where $R = \frac{a v_w}{v}$ is the cross flow Reynolds number and $R > 0$ is for injection and $R < 0$

for suction through the walls.

For self-similar solution, we consider $f = \frac{\bar{F}}{R}$ by the transformation introduced by Uchida & Aoki (1990) and Dauenhauer & Majdalani (2003). This can lead us to consider the case where α is a constant and $f = f(\eta)$. Therefore, $f_{\eta\eta t} = 0$. So Equation (3.73) becomes:

$$f'''' + A_1(1-\varphi)^{2.5}\big(\alpha[\eta f''' + 3f''] + R(ff''' - f'f'')\big) = 0 \tag{3.76}$$

$$\theta'' + \frac{A_1}{A_2}(PrfR + \alpha\eta Pr)\theta' = 0 \tag{3.77}$$

With boundary conditions of:

$$\left.\begin{array}{l} f(0) = 0, f''(0) = 0, \theta(0) = 1 \\ f(1) = 1, f'(1) = 0, \theta(1) = 0 \end{array}\right\} \tag{3.78}$$

3.4.2 Stability Analysis

The stability analysis of the steady flow solution $f(\eta) = f_\circ(\eta)$, $\theta(\eta) = \theta_\circ(\eta)$ which satisfies the boundary conditions (3.78), (Merkin 1986, Rosca & Pop 2013),

$$f(\eta) = f_\circ(\eta) + e^{-\lambda t}F(\eta, t) \tag{3.79}$$

$$\theta(\eta) = \vartheta_\circ(\eta) + e^{-\lambda t}G(\eta, t) \tag{3.80}$$

where

$\tau = t$ and $0 < F(\eta, t) \ll 1$, $0 < G(\eta, t) \ll 1$ and λ is the unknown eigenvalues, $F(\eta, t)$ and $G(\eta, t)$ are the smallest relative to $f_\circ(\eta)$ and $\theta_\circ(\eta)$ respectively.

The governing equations of (3.76) – (3.77) for unsteady case are as follows:

$$\frac{\partial^4 f}{\partial \eta^4} + A_1(1-\varphi)^{2.5}\left[\alpha\left(\eta\frac{\partial^3 f}{\partial \eta^3} + 3\frac{\partial^2 f}{\partial \eta^2}\right) + R\left(f\frac{\partial^3 f}{\partial \eta^3} - \frac{\partial f}{\partial \eta}\frac{\partial^2 f}{\partial \eta^2}\right)\right] = \frac{\partial^3 f}{\partial \tau \partial \eta^2} \tag{3.81}$$

$$\frac{\partial^2 \theta}{\partial \eta^2} + Pr\frac{A_2}{A_3}(Rf + \alpha\eta)\frac{\partial \theta}{\partial \eta} = \frac{\partial \theta}{\partial \tau} \tag{3.82}$$

Substituting Equations (3.79) - (3.80) into Equations (3.81) - (3.82) and setting $\tau = 0$ (Merkin, 1986), will get:

$$F'''' + A_1(1-\varphi)^{2.5}\begin{bmatrix} \alpha(\eta f_\circ''' F'' + 3f_\circ'' F''') \\ + \\ R(f_\circ F''' + Ff_\circ''' - f_\circ' F'' - f_\circ'' F') \end{bmatrix} + \lambda F'' = 0 \qquad (3.83)$$

$$\theta'' + \frac{A_2}{A_3}[PrRf_\circ + \alpha\eta Pr]\theta_\circ' + \frac{A_2}{A_3}[PrRF + \alpha\eta Pr]G'' + \lambda G = 0 \qquad (3.84)$$

Along with the boundary conditions,

$$\left.\begin{array}{l} F(1) = 0, F'(1) = 0, G(1) = 0 \\ \quad F''(0) = 0, F(0), G(0) = 1 \end{array}\right\} \qquad (3.85)$$

$f_\circ(\eta)$ and $\theta_\circ(\eta)$ can be determined by the smallest eigenvalue λ due to the steady state flow solution. Therefore, the range of the possible eigenvalues can be determined by relaxing the boundary conditions on $f_\circ(\eta)$ and $\theta_\circ(\eta)$ as prescribed by Harris et al. (2009). Therefore, the boundary condition is relaxed $G(1) \to 0$ and system of differential equation with a new boundary condition $G'(0) = 1$ is solved.

3.4.3 Numerical Computation

The ODEs equations for stability in Equations (3.83) – (3.84) subjected to the boundary condition in Equations (3.85) were solved numerically using "*bvp4c*" from MATLAB. "*bvp4c*" is a finite difference method that implements the three-stage Lobatto IIIa formula, which is a collocation method of fourth-order accuracy. In this approach, the differential equations are firstly reduced to a system of first-order equations by introducing new variables. Mesh selection and error control are based on the residual of the continuous solution. In this study, the relative error tolerance is set to 10^{-8}.

In order to find the numerical solution of Equations (3.76) - (3.77) subjected to the boundary condition in Equation (3.78), the current study employed shooting method. It is important to notice that Equation (3.76) is fourth order nonlinear ODE and hence it has to be changed it into a system of 1st order ODEs such that:

$$f' = p, \ p' = q, \ q' = s, \ s' = -A_1(1-\varphi)^{2.5}\big(\alpha(\eta s + 3q) + R(fs - pq)\big) \qquad (3.86)$$

$$\theta' = r, \ r' = \frac{-A_1}{A_2}(Pr(\alpha\eta + Rf)r) \tag{3.87}$$

with boundary conditions of

$$\left.\begin{array}{l}f(1) = 1, \quad p(1) = 0, \quad \theta(1) = 0, \\ q(1) = \alpha_1, \quad s(1) = \alpha_2, r(1) = \alpha_3\end{array}\right\} \tag{3.88}$$

Here, α_1, α_2 and α_3 are unknown initial conditions. These initial conditions are determined using shooting strategy described by Meade et. al. (1996) that satisfy the given boundary conditions.

3.4.4 Results and Discussions

The present section represents the numerical solutions for the different values of parameters involved. Figure are prepared to find the multiple solutions for different values of Reynolds number R, solid volume fraction φ and wall expansion ratio α on skin friction, velocity and temperature profiles.
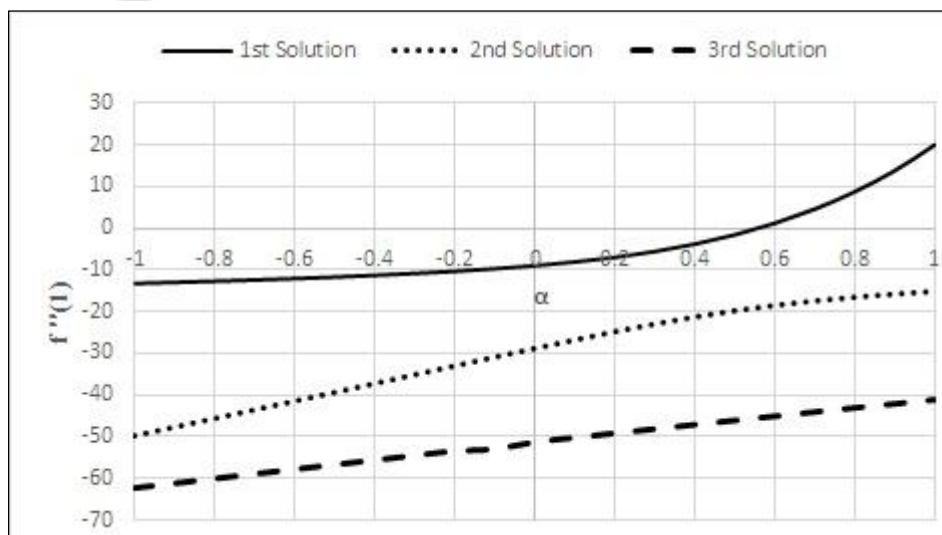
Figure 3.19. Skin friction $f''(1)$ against the variation of α (wall expansion or contraction ratio)

Table 3.7 shows the validity of the numerical results in comparison to the two different numerical approaches and Table 3.8 presents the smallest eigenvalues against the different values of the wall expansion ratio $\alpha > 0$ for the fixed values of Reynolds number R, solid volume fraction φ and Prandtl number Pr. The latter table illustrates that an increase in the wall expansion ratio $\alpha > 0$ resulting into positive eigenvalues for the 1st solution, but negative for the 2nd and the 3rd solutions. Thus, 1st solution is stable and rests of the other solutions are unstable. Physically speaking, the 1st solution is more reliable compared to the 2nd and the 3rd solutions. Consequently, the skin friction $f''(1)$ against wall expansion or contraction ratio α are plotted in Figure 3.19 which shows that skin friction $f''(1)$ increases monotonically by the variation of $\alpha \in [-1.0, 1.0]$. Physically, the variation of α from -1.0 to 1.0 (contracting walls to expanding walls) increases the wall drag. This behavior can be explained such that for the case of expanding walls $\alpha > 0$, flow towards the center become fast due to the space caused by wall expansion and slip regime exists near the wall. Therefore, for expanding walls $\alpha > 0$, skin friction increases numerically for all the solutions. Furthermore, from the achieved numerical results, there exits only single solution in the case of injection $(R > 0)$ for the considered problem. Moreover, multiple solutions exist only for the case of suction $(R < 0)$ with the fixed values of $R = -10$ and $\varphi = 0.1$.
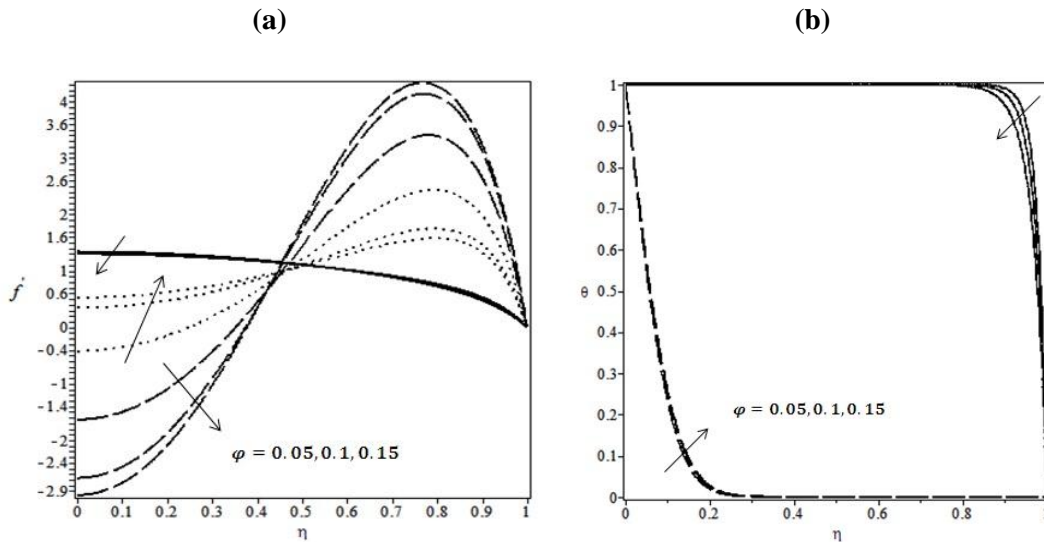
Figure 3.20. Effect of Solid Volume Fraction φ on Velocity Profile $f'(\eta)$ and Temperature Profile $\theta(\eta)$ for Expanding walls

Figure 3.20 depicts the behavior of velocity profile $f'(\eta)$ and temperature profile $\theta(\eta)$ for the variations of solid volume fraction φ, the fixed values of Reynolds number R, and wall expansion ratio $\alpha = 0.1$. The velocity profile $f'(\eta)$ decreases near the center of the channel for the 1st and the 3rd solutions. However, a total reverse phenomena in the case of 2nd solution is observed. Similar effect of solid volume fraction φ on temperature profile $\theta(\eta)$ is presented in the same figure. Temperature profile $\theta(\eta)$ is decreased as the strength of solid volume fraction φ increases. Moreover, asymptotical behavior is also observed for the 3rd solution. Figure 3.21 shows the effect of solid volume fraction φ for the fixed values of Reynolds number R and wall expansion ratio $\alpha = -0.1$ on velocity and temperature profile. This figure demonstrated that the behavior of fluid velocity and temperature profile are the same for expanding walls $\alpha > 0$, except the magnitude of the numerical values. Figure 3.22 clearly shows that velocity near the center of the channel increases for the 1st and the 2nd solutions but decreases for the 3rd solution. However, opposite occurrence near the wall is observed. This contrary is because the fluid moves freely near the center of the channel due to the space

generated by the wall expansion. Therefore, the fluid velocity $f'(\eta)$ increases gradually near the center of the channel $\eta \approx 0$. Furthermore, temperature profile decreases gradually by increasing the values of wall expansion and asymptotical behavior is observed for the 3rd solution.

(a)   **(b)**
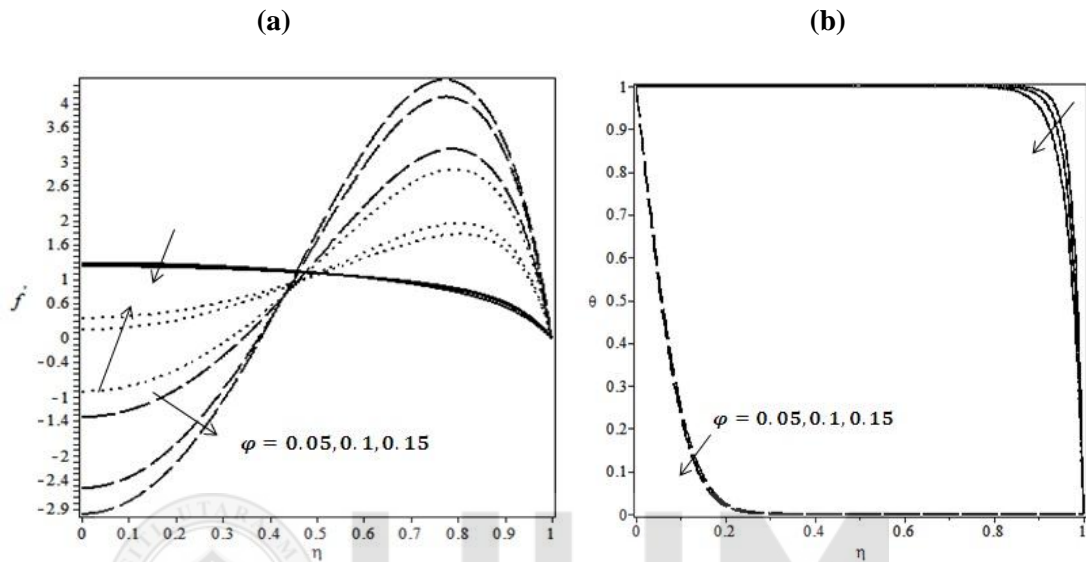
Figure 3.21. Effect of Solid Volume Fraction φ on Velocity Profile $f'(\eta)$ and Temperature Profile $\theta(\eta)$ for Contracting walls
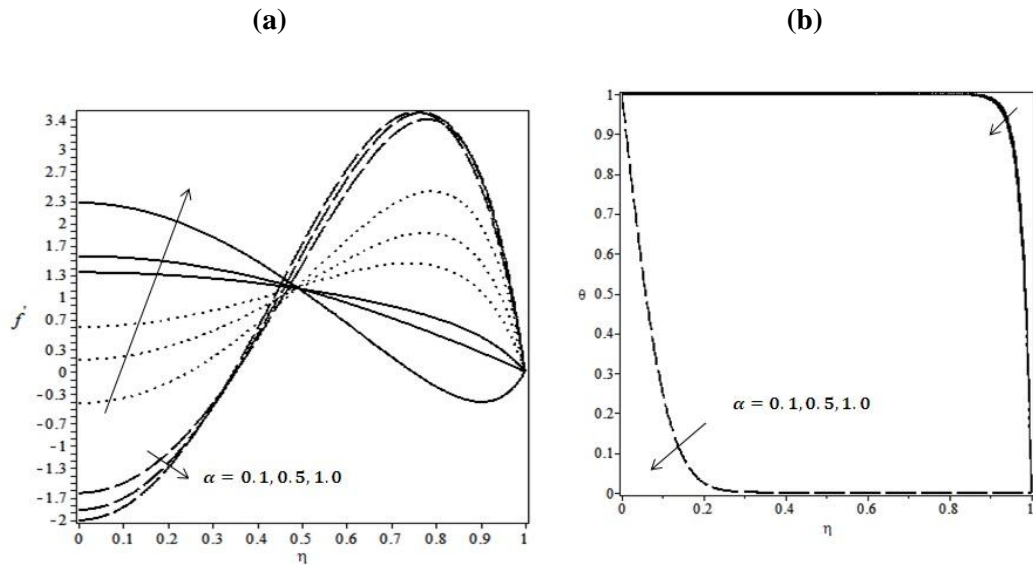
Figure 3.22. Effect of Wall expansion $\alpha > 0$ on Velocity Profile $f'(\eta)$ and Temperature Profile $\theta(\eta)$

Figure 3.23 exhibits the effect of wall contraction $\alpha < 0$ on velocity profile $f'(\eta)$ and temperature profile $\theta(\eta)$ for the fixed values of solid volume fraction φ and fixed values of Reynolds number R. The plot shows that the velocity profile $f'(\eta)$ decreases near the center of the channel but increases near the channel wall for the case of wall expansion ratio $\alpha < 0$. This is caused by the contracting walls $\alpha < 0$ which provide less space to the fluid to flow; hence, fluid velocity near the center of the channel decreases but the flow towards the channel wall increases as well the temperature profile in all solutions. Figure 3.24 showed the validation of the physical model of the present study in the form of graph and found good agreement with the literature published before (Hatami et al., 2015).

(a)   **(b)**
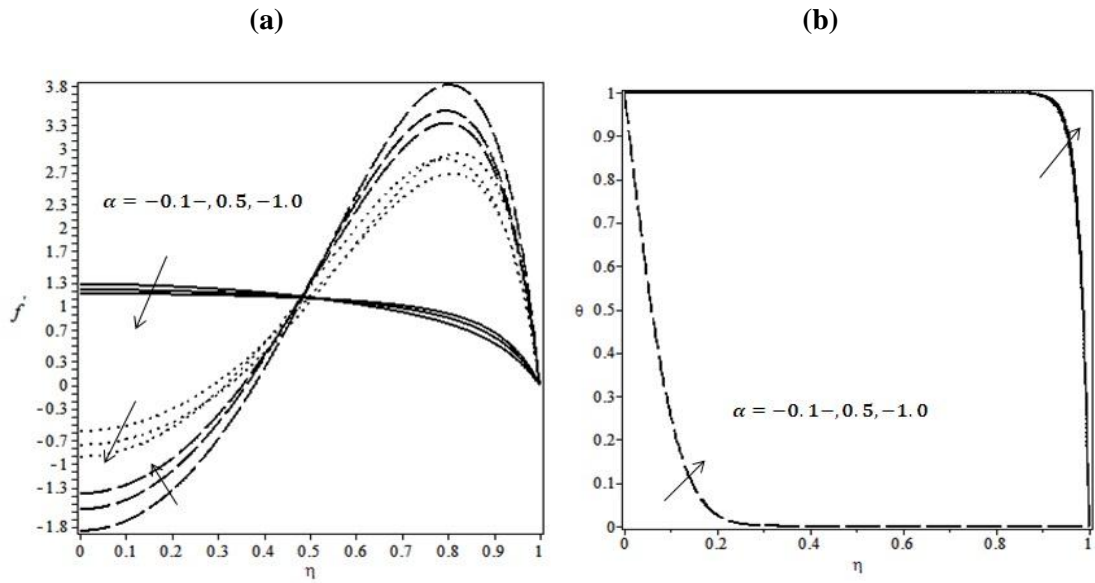
Figure 3.23. Effect of Wall contraction $\alpha < 0$ on Velocity Profile $f'(\eta)$ and Temperature Profile $\theta(\eta)$
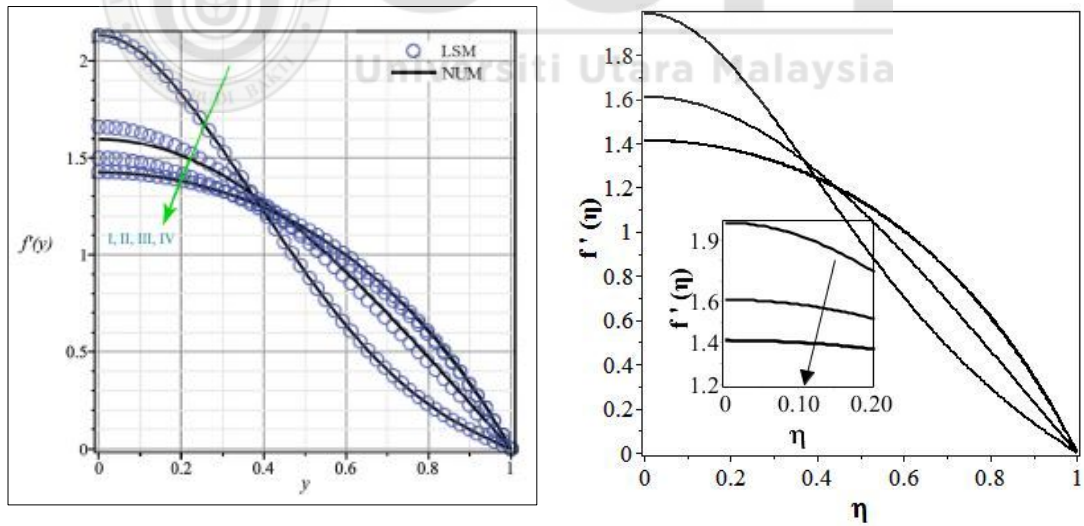
Present work for $\varphi = 0.04$,

$$I: \alpha = R = 5, II: \alpha = 1, R = 4,$$

Hatami et al. (2015)

$$III: \alpha = -0.5, R = -2, IV: \alpha = -1, R = 1$$

Figure 3.24. Validation of physical model with Hatami et al. (2015)

Table 3.7

Validation of numerical results

R	α	Pr	φ	$f''(-1)$ Shooting method	$f''(-1)$ Runge-Kutta-Fehlberg
0	-0.1	6.2	0.1	-3.110833618	-3.110833585
-10				-9.718933431	-9.718933671
-20				-25.93558737	-25.93558751
-10	-0.1	6.2	0.0	-6.369097305	-6.369097357
			0.05	-8.248977654	-8.248978262
			0.1	-9.718934067	-9.718933671

Table 3.8

Smallest eigenvalues λ at several values of Expansion ratio α

R	φ	Pr	α	1st Solution λ	2nd Solution λ	3rd Solution λ
			0	5.448	-0.5	-6.844
-10	0.05 (5%)	6.2	0.1	6.9873	-4.81	-8.8888
			0.5	8.5266	-14.2438	-15.0805
			1	10.0659	-19.479	-15.5839

Universiti Utara Malaysia

69

CHAPTER FOUR

HEAT AND MASS TRANSFER ANALYSIS ON CASSON FLUID IN A CHANNEL WITH VARIOUS FLUID FLOW CONDITIONS

This chapter deals with some problems of Casson fluid flow in a channel. The effects of magnetic field, heat transfer, mass transfer, suction on fluid flow are also considered. In problems 4.2-4.4, we studied the laminar incompressible Casson fluid model which characterized the non-Newtonian fluid behaviour. Trusting to the limited literature presented in Chapter 2, it is concluded that none of the authors succeeded to find the multiple solutions of the Casson fluid model in a channel for the problem considered in this Chapter. The studies reveal that the multiple solutions in the channel for porous wall, expanding or contracting walls exist only for the case of high suction for some fixed values of other physical parameters.

In recent decades, problems of laminar incompressible Casson fluid over sheet and surface got much attraction of researchers due to its vast applications in the field of food processing, biochemical industries and polymer processing (Saidulu & Lakshmi, 2016). The problem of Casson fluid flow in a tube filled by homogenous porous medium was examined by Dash et al. (1996). They employed Brinkman model to examine the resistance offered by porous medium in the fluid flow. Mukhopadhyay (2013) investigated the problem of boundary layer flows of Casson fluid over a nonlinear stretching sheet. Numerical solution is obtained by employing shooting method. The study revealed that velocity profile for the Casson fluid decreased by increasing in the enhancement of Casson parameter. This study was further generalized by Nadeem et al. (2013) for different fluid flow conditions. The problem of boundary layer flow of Non-Newtonian Casson fluid over a stretching surface solved numerically (Mukhopadhyay et al., 2014). Mustafa and Khan (2015) dealt with the problem of

70

Casson nanofluid past a nonlinear stretching sheet. Das et al. (2015) analyzed the effect of heat and mass transfer on Non-Newtonian Casson fluid over a sheet. They concluded that the fluid particles of Casson fluid offer great reduction in the velocity as Casson parameter increases. Numerical solution of Casson fluid past a permeable surface under the influence of thermal radiation was presented by Raju et al. (2016). Recently, Tamoor et al. (2017) investigated the problem of Non-Newtonian flow over a stretching cylinder. Casson fluid model is taken to characterized the Non-Newtonian flow and governing equations were solved by Homotopy Analysis Method (HAM). In this chapter, the problems is formulated into mathematical governing equations and then transformed into nonlinear ODEs as done in previously published literature (Rauf et al. 2016; Sajid et al. 2009; Shehzad et al. 2013) by using similarity transformation. In order to solve the problems considered in this chapter, the following mathematical model of Casson fluid flow is presented.

4.1 Mathematical Modelling for Casson fluid

Governing equation of Casson fluid model in vector form can be written as:

$$\frac{\partial \rho}{\partial t} + \nabla \cdot (\rho \bar{V}) = 0 \tag{4.1}$$

$$\rho \left[\frac{\partial \bar{V}}{\partial t} + (\bar{V} \cdot \nabla)\bar{V}\right] = -\nabla P + \mu \nabla^2 \bar{V} + \bar{J} \times \bar{B} \tag{4.2}$$

$$\rho C_p \left[\frac{\partial T}{\partial t} + \bar{V} \cdot \nabla T\right] = k \nabla^2 T + \emptyset \tag{4.3}$$

$$\left[\frac{\partial C}{\partial t} + \bar{V} \cdot \nabla C\right] = D_m \nabla^2 C \tag{4.4}$$

$$\nabla \cdot \bar{B} = 0 \tag{4.5}$$

$$\nabla \times \bar{B} = \mu_m \bar{J} \tag{4.6}$$

$$\nabla \times \bar{E} = 0 \tag{4.7}$$

$$\bar{J} = \sigma_{nf}(\bar{E} + \bar{V} \times \bar{B}) \tag{4.8}$$

Where $\bar{V}$ is the fluid velocity, p is the fluid pressure, ρ_{nf} is the density of the nanofluid, μ_{nf} is the dynamic viscosity of the nanofluid, $\bar{F}$ is the external forces applied to the nanofluid, $\bar{J}$ is the current density and $\bar{B}$ is total magnetic field so that $\bar{B} = \bar{B}_\circ + \bar{b}$, $\bar{b}$ is the conductivity of the fluid. Moreover, $\nabla \cdot \bar{J} = 0$ is obtained from Eqs. (4.5) - (4.8). The uniform stationary magnetic field $\bar{B}$ is applied transverse in direction and magnetic Reynolds number is taken small (Shercliff, 1965). As a consequence the induced magnetic field $\bar{b}$ is negligible. Furthermore, since there is no applied polarization voltage, therefore, an electric field (i.e. $\bar{E} = 0$) has vanished. This means that fluid follows conservation of energy (No energy is extracted or added to the fluid). Applying these assumptions, electromagnetic body force occurs in Eq. (4.2) takes the following linearized form (Rossow, 1958):

$$\bar{J} \times \bar{B} = \sigma_{nf}[(\bar{V} \times \bar{B}_\circ) \times \bar{B}_\circ] = (-\sigma_{nf}B_\circ^2 u, 0, 0) \tag{4.9}$$

Moreover, the rheological equation for Cauchy stress tensor can be written as:

$$\tau$$

$$= \tau_\circ + \mu\alpha \tag{4.10}$$

The constitutive equation for the Casson fluid can be written as Eldabe et al. (2001):

$$\tau_{ij} = \begin{cases} 2\left(\mu_B + \dfrac{\tau_y}{\sqrt{2\pi}}\right)e_{ij}, \pi > \pi_c, \\ 2\left(\mu_B + \dfrac{\tau_y}{\sqrt{2\pi_c}}\right)e_{ij}, \pi < \pi_c \end{cases} \tag{4.11}$$

where μ_B is the plastic dynamic viscosity of the non-Newtonian fluid, τ_y is the yield stress of the fluid, π is the product of the component of deformation rate with itself, and π_c is critical value of π based on non- Newtonian model.

$$p_y = \frac{\mu_B\sqrt{2\pi}}{\beta} \tag{4.12}$$

is yield stress. Some fluids require a gradually increasing shear stress to maintain a constant strain rate and are called Rheopectic, in the case of Casson fluid (Non-Newtonian) flow where $\pi > \pi_c$.

$$\mu = \mu_B + \frac{p_y}{\sqrt{2\pi}} \tag{4.13}$$

Substitute Eq. (4.12) into Eq. (4.13), then Kinematic viscosity can be written as:

$$\nu = \frac{\mu}{\rho} = \frac{\mu_B}{\rho}\left(1 + \frac{1}{\beta}\right) \tag{4.14}$$

Components of the velocity vector $\bar{V} = (u(x,y,z), v(x,y,z), w(x,y,z))$ and in the light of the said assumptions (Eqs. 4.14, 4.9), Eqs. (4.1) - (4.4) becomes:

$$\frac{\partial u}{\partial t} + \frac{\partial u}{\partial x} + \frac{\partial v}{\partial y} + \frac{\partial w}{\partial x} = 0 \tag{4.15}$$

$$\rho\frac{\partial u}{\partial t} + \rho\left(u\frac{\partial u}{\partial x} + v\frac{\partial u}{\partial y} + w\frac{\partial u}{\partial z}\right) = -\frac{\partial p}{\partial x} + \mu\left(1 + \frac{1}{\beta}\right)\left(\frac{\partial^2 u}{\partial x^2} + \frac{\partial^2 u}{\partial y^2} + \frac{\partial^2 u}{\partial z^2}\right)$$
$$- \sigma_{nf}B_\circ^2 u \tag{4.16}$$

$$\rho\frac{\partial v}{\partial t} + \rho\left(u\frac{\partial v}{\partial x} + v\frac{\partial v}{\partial y} + w\frac{\partial v}{\partial z}\right) = -\frac{\partial p}{\partial y} + \mu\left(1 + \frac{1}{\beta}\right)\left(\frac{\partial^2 v}{\partial x^2} + \frac{\partial^2 v}{\partial y^2} + \frac{\partial^2 v}{\partial z^2}\right) \tag{4.17}$$

$$\rho\frac{\partial w}{\partial t} + \rho\left(u\frac{\partial w}{\partial x} + v\frac{\partial w}{\partial y} + w\frac{\partial w}{\partial z}\right) = -\frac{\partial p}{\partial z} + \mu\left(1 + \frac{1}{\beta}\right)\left(\frac{\partial^2 w}{\partial x^2} + \frac{\partial^2 w}{\partial y^2} + \frac{\partial^2 w}{\partial z^2}\right) \tag{4.18}$$

$$u\frac{\partial T}{\partial x} + v\frac{\partial T}{\partial y} = \frac{k}{\rho C_p}\frac{\partial^2 T}{\partial y^2} \tag{4.19}$$

$$u\frac{\partial C}{\partial x} + v\frac{\partial C}{\partial y} = D_m\frac{\partial^2 C}{\partial y^2} \tag{4.20}$$

4.2 MHD Mixed Convective Casson Fluid in a Channel with Shrinking and Stationary Walls Embedded in a Porous Medium

Numerical investigation is carried out to present mixed convective Casson fluid in a channel under the influence of magnetic field. Concurrent effects of energy and concentration of the Casson fluid particles are considered and analyzed. Mathematical

73

formulation of conservation of mass, momentum, heat and mass transfer is performed. Governing PDEs are reduced into nonlinear ODEs by applying suitable similarity transformation and then solve numerically with the aid of Runge-Kutta-Fehlberg method (RFK45). Numerical results of different physical parameters, Reynolds number, Casson parameter, Magnetic number, porosity parameter, thermal buoyancy parameter, Prandtl number, Smith number and chemical reaction rate are presented in figures as well as in tables. The present investigation might be useful to the flow and heat control of polymeric preparing.

The problem considered by Sarojamma et al. (2014) is most relevant reference of the problem considered in this Section. Sarojamma et al. (2014) considered the flow of Casson fluid in a channel under the influence of magnetic field, heat transfer and mass transfer. The channel walls were stretching with the constant velocity along the flow of the fluid. In order to validate our physical model, we set $\lambda = 0, p = 0, f'(-1) = 1, f'(1) = 1$ and found the good agreement of the results. Nevertheless, for $\beta \to \infty$ the considered problem reduced into viscous fluid in a channel (Abbasi et al. 2014).

4.2.1 Problem Formulation

We considered steady, laminar and incompressible MHD flow of mixed convective Casson fluid in a channel. Lower and upper walls of the channel are located at $y = -a$ and $y = a$ respectively. However, the lower wall is shrinking with constant velocity while the upper wall remain stationary. A uniform magnetic field of strength $B_\circ$ is connected to the velocity field. The actuated magnetic field is insignificant as contrast to the forced field. The magnetic Reynolds number R, which is utilized to analyze the transport of magnetic lines of force in a directing fluid to the spillage of such lines from the fluid is low. At this low R, the magnetic field tends to unwind towards an absolute

74

diffusive state. As a result, the impelled magnetic field b is disregarded; hence, is no connected polarization voltage which infers that the electric field is zero. The electrical current streaming in the fluid offers ascend to an affected magnetic field which would exist if the fluid is an electrical separator. Moreover, the lower wall has temperature T_1 and concentration C_1 while the upper wall has temperature T_2 and concentration C_2.
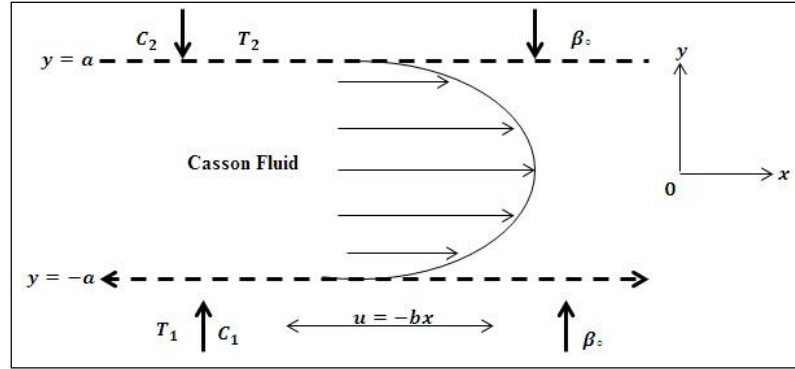
Figure 4.1: Physical Model of the Proposed Problem

Under these assumptions, the governing equations for MHD boundary layer flow of Casson fluid are expressed as the following equations:

$$\frac{\partial u}{\partial x} + \frac{\partial v}{\partial y} = 0 \tag{4.21}$$

$$u\frac{\partial u}{\partial x} + v\frac{\partial u}{\partial y} = -\frac{1}{\rho}\frac{\partial p}{\partial x} + v\left(1 + \frac{1}{\beta}\right)\frac{\partial^2 u}{\partial y^2} + g\beta_T\big((T - T_2) + \beta_C(C - C_2)\big)$$

$$-\frac{\sigma B_o^2 u}{\rho} + \frac{v}{r}u \tag{4.22}$$

$$u\frac{\partial v}{\partial x} + v\frac{\partial v}{\partial y} = -\frac{1}{\rho}\frac{\partial p}{\partial y} + v\left(1 + \frac{1}{\beta}\right)\frac{\partial^2 v}{\partial x^2} \tag{4.23}$$

$$u\frac{\partial T}{\partial x} + v\frac{\partial T}{\partial y} = \frac{k}{\rho C_p}\frac{\partial^2 T}{\partial y^2} \tag{4.24}$$

$$u\frac{\partial C}{\partial x} + v\frac{\partial C}{\partial y} = D\frac{\partial^2 C}{\partial y^2} - \kappa_1 \tag{4.25}$$

75

where ρ is density, μ is dynamic viscosity, ν is kinematic viscosity, σ is electrical conductivity, β is Casson fluid parameter, , r is permeability of the medium, T is temperature of the fluid, k is thermal conductivity, κ_1 is reaction rate, D is mass diffusion and C is the concentration field.

The boundary conditions are:

$$u(x, -a) = -bx, v(x, -a) = 0, T(x, -a) = T_1, C(x, -a) = C_1 \tag{4.26}$$

$$u(x, a) = 0, v(x, a) = 0, T(x, a) = T_2, C(x, a) = C_2 \tag{4.27}$$

where $b > 0$ is the shrinking rate of the channel wall, T_1, C_1, T_2 and C_2 are temperature and concentration at the lower and at the upper walls of the channel respectively. The following self-similar transformation are defined to convert governing partial differential equations into ordinary differential equations:

$$\eta = \frac{y}{a}, u = bxf'(\eta), v = -abf(\eta), \theta(\eta) = \frac{T - T_2}{T_1 - T_2}, \varphi(\eta) = \frac{C - C_2}{C_1 - C_2} \tag{4.28}$$

Inserting Equation (4.28) into Equations (4.21) - (4.25), we shall get:

$$\left(1 + \frac{1}{\beta}\right) f'''' - (M^2 - p) f'' - R(f'f'' - ff''') + \lambda(\theta' + N\phi') = 0, \tag{4.29}$$

$$\theta'' - PrRf\theta' = 0 \tag{4.30}$$

$$\varphi'' - RSc\gamma\varphi - RScf\varphi' = 0 \tag{4.31}$$

Here, $R = \frac{a^2 b}{\nu} > 0$ is the shrinking/stretching Reynolds number, $p = \frac{\rho a^2}{\kappa}$ is porosity parameter, $\lambda = \frac{Gr_x}{Re^2}$ is thermal buoyancy parameter with $Gr_x = \frac{a^4 g \beta_T (T_1 - T_2)}{x\nu^3}$ the Grashof number, $N = \frac{\beta_C (C_1 - C_2)}{T_1 - T_2}$ the concentration buoyancy parameter, $Pr = \frac{\mu C_p}{k_\circ}$ is Prandtl number, $Sc = \frac{\mu}{\rho D}$ is Smith number and $\gamma = \frac{k_1}{b}$ is chemical reaction rate.

Boundary conditions from Equation (4.26) and Eq. (4.27) in the view of Equation (4.28) is expressed by:

$$f(\pm 1) = 0, f'(-1) = -1, f'(1) = 0, \left.\begin{matrix}\\\end{matrix}\right\}$$
$$\theta(-1) = 1, \theta(1) = 0, \varphi(-1) = 1, \varphi(1) = 0 \tag{4.32}$$

4.1.2 Numerical Solution

Equations (4.29) - (4.31) are highly nonlinear twisted ODEs; therefore, finding the exact solution is hard and numerical technique must be executed. The numerical solution is employed using shooting method while Runge-Kutta-Fehlbergh fourth-fifth order (RKF45) is used to validate the numerical results. A usual approach to convert the equations into first order initial value problem is given as:

$$\begin{pmatrix} z_1 \\ z_2 \\ z_3 \\ z_4 \\ z_5 \\ z_6 \\ z_7 \\ z_8 \end{pmatrix} = \begin{pmatrix} f \\ f' \\ f'' \\ f''' \\ \theta \\ \theta' \\ \varphi \\ \varphi' \end{pmatrix} \tag{4.33}$$

$$\left(1 + \frac{1}{\beta}\right) z_4' - (M^2 - p) z_3 - R(z_2 z_3 - z_1 z_4) + \lambda(z_6 + N z_8) = 0 \tag{4.34}$$

$$z_6' - PrR z_1 z_6 = 0 \tag{4.35}$$

$$z_8' - RSc\gamma z_7 - RSc z_1 z_8 = 0 \tag{4.36}$$

The initial conditions are:

$$\begin{pmatrix} z_1(-1) \\ z_2(-1) \\ z_3(-1) \\ z_4(-1) \\ z_5(-1) \\ z_6(-1) \\ z_7(-1) \\ z_8(-1) \end{pmatrix} = \begin{pmatrix} 0 \\ -1 \\ s_1 \\ s_2 \\ 1 \\ s_3 \\ 1 \\ s_4 \end{pmatrix} \qquad (4.37)$$

where s_1, s_2, s_3 and s_4 are unknown initial conditions. These initial conditions are guessed with the help of shooting method and Newton-Raphson algorithms and then numerical integration is applied.

4.2.3 Results and Discussions

In this section the main objective is to discuss the influence of physical parameters such as Reynolds number R, Casson parameter β, porosity parameter p, thermal buoyancy parameter λ, concentration buoyancy parameter N, Prandtl number Pr, Smith number Sc and chemical reaction parameter γ on velocity, temperature and concentration fields. Tabulation representation and graphs are drawn by varying the numerical values of parameter one by one, keeping the other parameters invariant. The physical quantities like couple stress $f''(\pm 1)$, heat transfer $\theta'(\pm 1)$ and mass transfer $\varphi'(\pm 1)$ at the lower and upper walls of the channel are also presented.

The influence of Reynolds number, magnetic field, porosity parameter, thermal buoyancy parameter and Casson parameter on skin friction at the channel's walls are shown in Table 4.1. Couple stresses at the walls deteriorated numerically by increasing the values of Reynolds number. Couple stresses at both walls increased by the enhancement of magnetic field which produces a Lorentz forces that drag the fluid particles at the rest near the walls of the channel; hence, increasing the couple stresses.

78

Increment in the numerical values of porosity and Casson parameter decreased the couple stresses at the walls of the channel. However, a total opposite behavior is seen for the variation of thermal buoyancy parameter. Magnitude of couple stress for heat and mass transfer increased at the lower wall but decreased at the upper wall of the channel when the values of $\lambda \geq 0$ increased as shown in Table 4.2. Heat and mass transfer rate at walls for different values of Pr, Sc and γ are shown in Table 4.3. Numerical values of mass transfer at the channel wall decreased by the enhancement of Prandtl number and heat transfer at the lower walls asymptotically goes to zero at the lower wall but increased numerically at the upper wall of the channel. The influence of Smith number and chemical reaction on mass transfer rate behaves similarly to the numerical values.

Table 4.1

Couple stress at the walls for various values of R, M, p, λ and β

R	M	p	λ	β	$f''(-1)$	$f''(1)$
0	0.5	2	0.2	0.3	1.900228462	-1.018053327
10					1.489282916	-1.29620167
20					1.098548787	-1.672490826
20	0	2	0.2	0.3	1.080820996	-1.684972765
	1				1.151259666	-1.636254968
	2				1.355056526	-1.507705565
20	0.5	0	0.2	0.3	1.237538258	-1.579668445
		1			1.168672471	-1.624566845
		2			1.098548787	-1.672490826
20	0.5	2	0	0.3	1.093781352	-1.684963077
			0.5		1.105743608	-1.65375159
			1		1.117853576	-1.622436585
20	0.5	2	0.2	0.1	1.64252106	-1.208906326
				0.3	1.098548787	-1.672490826
				0.5	0.755074703	-2.12901968

Table 4.2

Effect of λ on couple stresses, heat and mass transfer at the walls

R	M	p	β	λ	$f''(-1)$	$f''(1)$	$\theta'(-1)$	$\theta'(1)$	$\varphi'(-1)$	$\varphi'(1)$
20	0.5	2	0.3	0	1.0937812	-1.6849637	-3.41E-03	-1.5164857	-1.2830283	-0.2824908
				0.5	1.1057436	-1.6537519	-3.52E-03	-1.5093768	-1.2838814	-0.2817262
				1	1.1178535	-1.6224365	-3.64E-03	-1.5021794	-1.2847656	-0.2799588

Table 4.3

Heat and Mass Transfer rate at the walls for the various values of Pr, Sc and γ

Pr	Sc	γ	$\theta'(-1)$	$\theta'(1)$	$\varphi'(-1)$	$\varphi'(1)$
0.1	0.3	0.5	-0.288760451	-0.68789913	-1.283561613	-0.281945285
0.5			-1.70E-02	-1.308810092	-1.28341278	-0.282083894
1			-2.94E-04	-1.750441868	-1.283325286	-0.282205545
0.7	0.1	0.5	-3.46E-03	-1.513595427	-0.836785711	-0.389890317
	0.5		-3.46E-03	-1.513595427	-1.610967549	-0.226676959
	1		-3.46E-03	-1.513737728	-2.225803443	-0.157501281
0.7	0.3	0	-3.46E-03	-1.513584957	-7.67E-02	-1.039084565
		0.5	-3.46E-03	-1.513646795	-1.283367579	-0.282143041
		1	-3.46E-03	-1.51374855	-2.046508543	-0.10306111

Table 4.4

Validation of the numerical results

R	M	p	λ	β	$f''(-1)$ Shooting	$f''(-1)$ Runge-Kutta-Fehlberg
0	0.5	2	0.2	0.3	1.900228462	1.900177948
10					1.489282916	1.489393986
20					1.098548787	1.098875165

The effect of Reynolds number R on velocity profile $f'(\eta)$ is presented in Figure 4.2. The profile presents that velocity profile diminished from the lower wall $\eta = -1$ of the channel to the focal point of the channel $\eta \approx 0$ but increased at the center of the channel to the upper wall given $R = 0, 10, 20, 30$. Figure 4.3 shows the effect of Casson parameter

β on velocity field $f'(\eta)$. It depicts the velocity decreased from $-1 \leq \eta < 0$ but increased afterwards $\eta > 0$ when Casson parameter $\beta = 0.1, 0.3, 0.7, 1.0$ is increasing. This behavior is caused by the lower wall's shrinking at a constant velocity. This shrinking increased the viscosity of the fluid particles resulting into the decrease of velocity near the lower wall of the channel to the center of the channel.
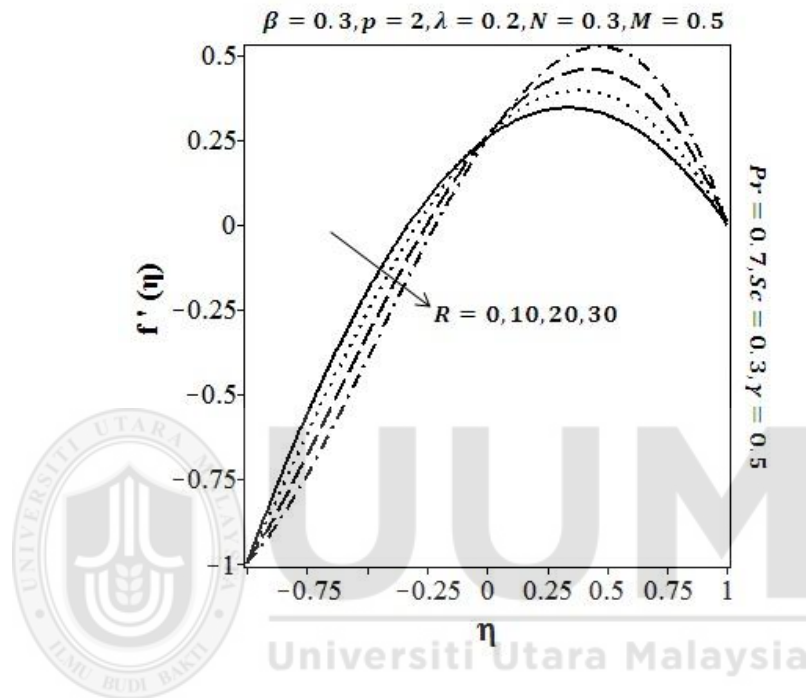
Figure 4.2. Effect of Reynolds number R on Velocity Profile $f'(\eta)$
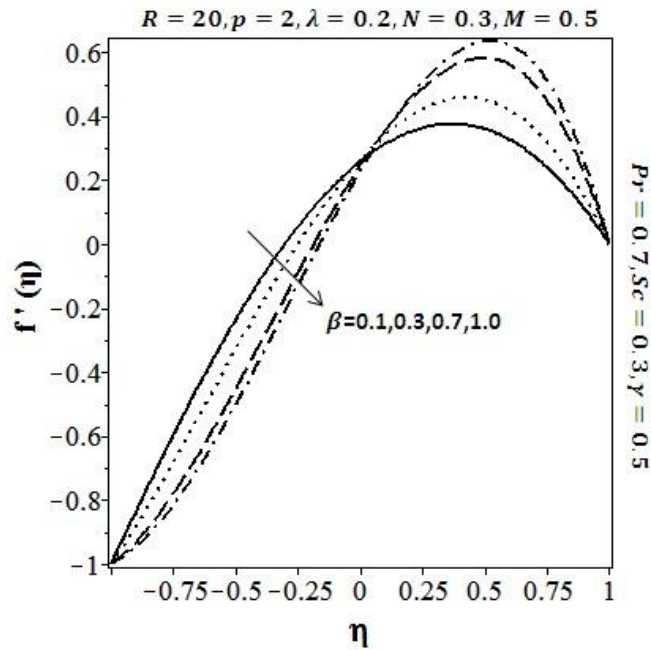
Figure 4.3. Effect of Casson parameter β on velocity profile $f'(\eta)$

The influence of the magnetic field M on the velocity profile $f'(\eta)$ for the fixed values of the other parameters is depicted from Figure 4.4. When the strength of magnetic field M is enhanced, the fluid is shifted towards the lower wall of the channel $\eta = -1$, so velocity of the fluid particles reduced till the center of the channel but increased later $\eta > 0$. A physical explanation for this is that, when magnetic field is connected to the Casson fluid, then the fluid viscosity increases because of the chain development of the particles. The chainlike structure retards the stream and decelerates the movement.

These outcomes demonstrated that the Casson fluid can be controlled proficiently by applying and differing magnetic field which results into numerous conceivable control based applications such as MHD power generator, manufacturing of metals, ion propulsion and so on. Velocity of the fluid particles decreases monotonically from lower wall to focal point of the channel and totally reverse phenomenon is observed

afterwards. This effect can be seen from Figure 4.5 with the increment in the numerical values of the porosity parameter $p = 0,2,4,6$.

The effect of Prandtl number Pr on temperature field $\theta(\eta)$ is plotted in Figure 4.6. From this graph, the temperature field increases monotonically from $\eta = -1$ to $\eta = 1$. The effect of Prandtl number may raise the temperature distribution to some extent which enhances the thermophorsis effect in the fluid's particles. The effect of Smith number Sc and chemical reaction rate γ on concentration field $\varphi(\eta)$ is shown in Figures 4.7 and 4.8 respectively. An increase in Smith number Sc and chemical reaction rate γ prompts the increment in the quantity of solute atoms experiencing substance reaction coming about the way that concentration of the fluid's molecule diminishes monotonically. The effect of Reynolds number on temperature and concentration field is shown in Figures 4.9 and 4.10 respectively. Figure 4.11 showed the comparison of the numerical results in the form of graphs of the present study with Sarojamma et al. (2014) and found the good agreement of the results by setting $\lambda = 0, p = 0, f'(-1) = 1, f'(1) = 1$.
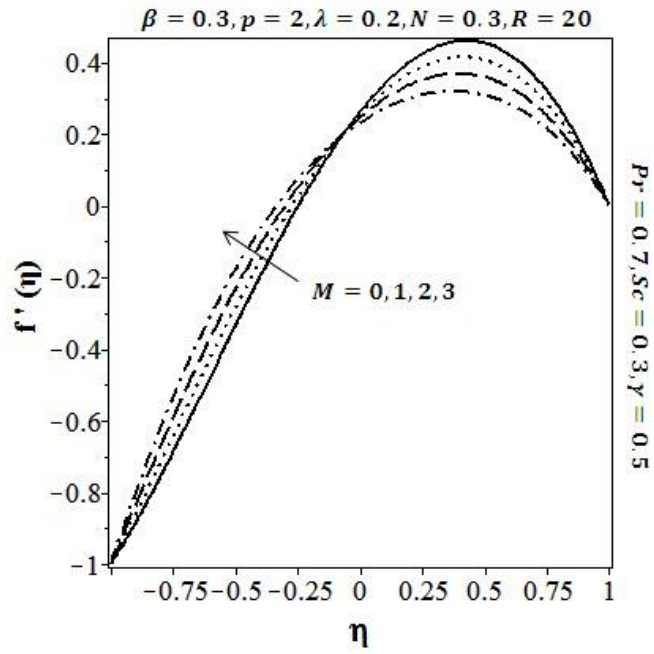
Figure 4.4. Effect of Magnetic field M on velocity profile $f'(\eta)$
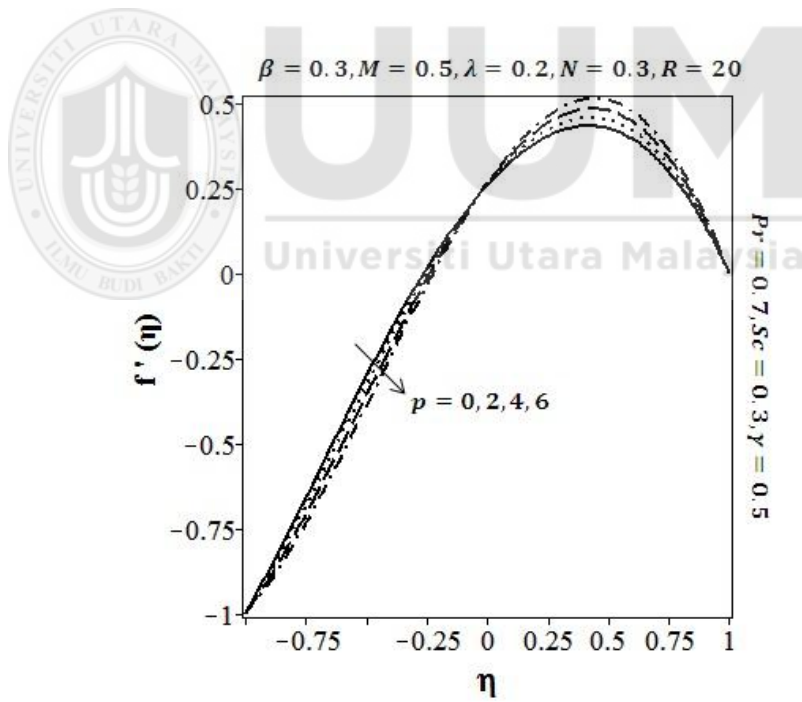
Figure 4.5. Effect of Porosity parameter p on velocity profile $f'(\eta)$
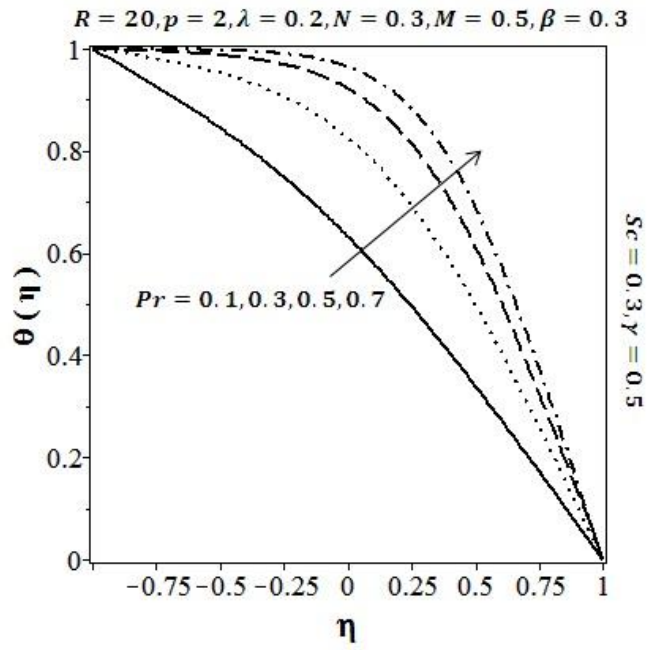
Figure 4.6. Effect of Prandtl number Pr on Temperature Profile $\theta(\eta)$
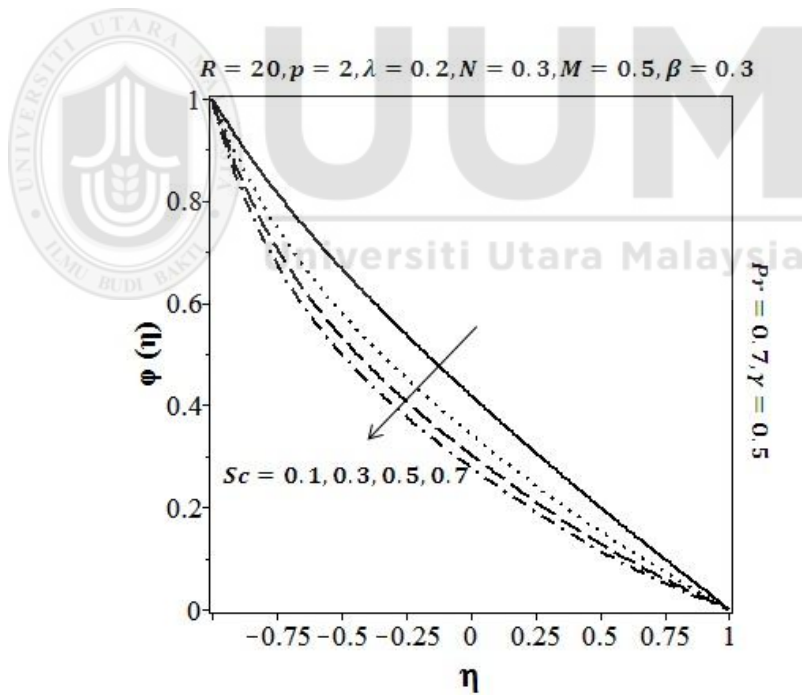
Figure 4.7. Effect of Smith number Sc on Concentration Profile $\varphi(\eta)$
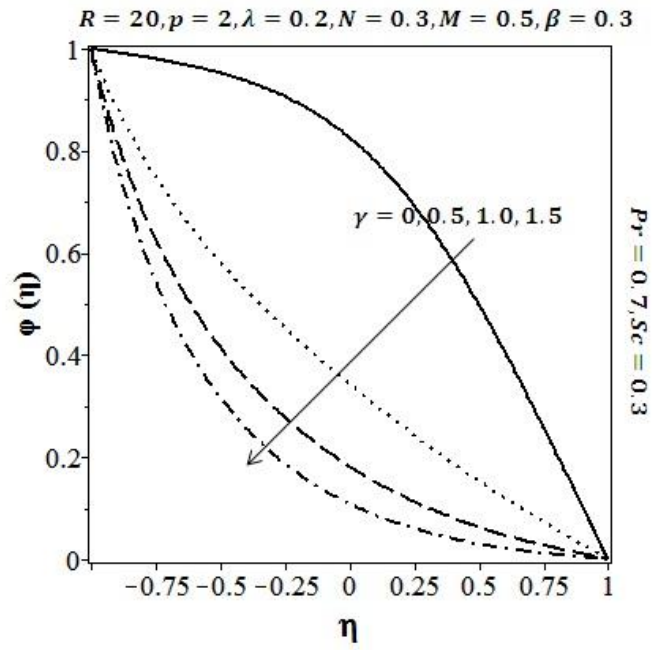
Figure 4.8. Effect of Chemical reaction γ on Concentration Profile $\varphi(\eta)$
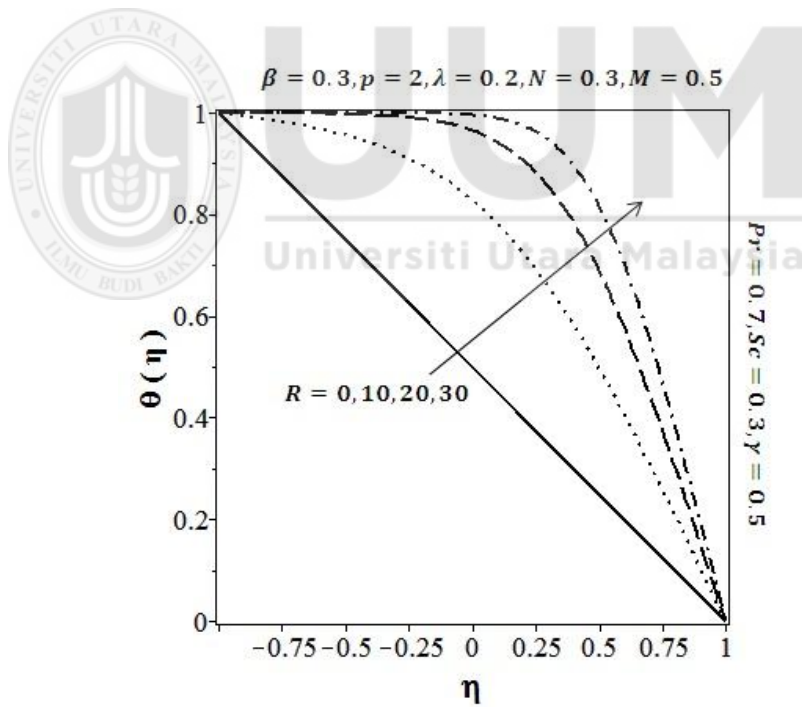
Figure 4.9. Effect of Reynolds number R on Temperature Profile $\theta(\eta)$

$$\beta = 0.3, p = 2, \lambda = 0.2, N = 0.3, M = 0.5$$
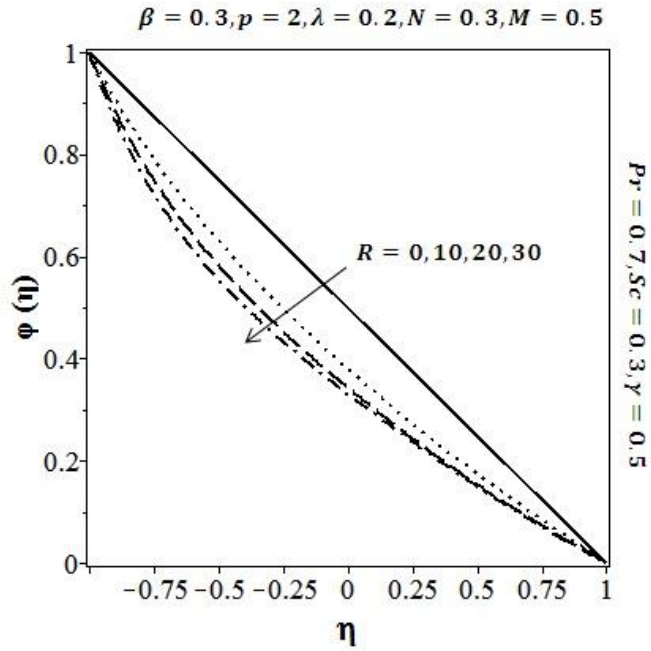
Figure 4.10. Effect of Reynolds number R on Concentration Profile $\varphi(\eta)$
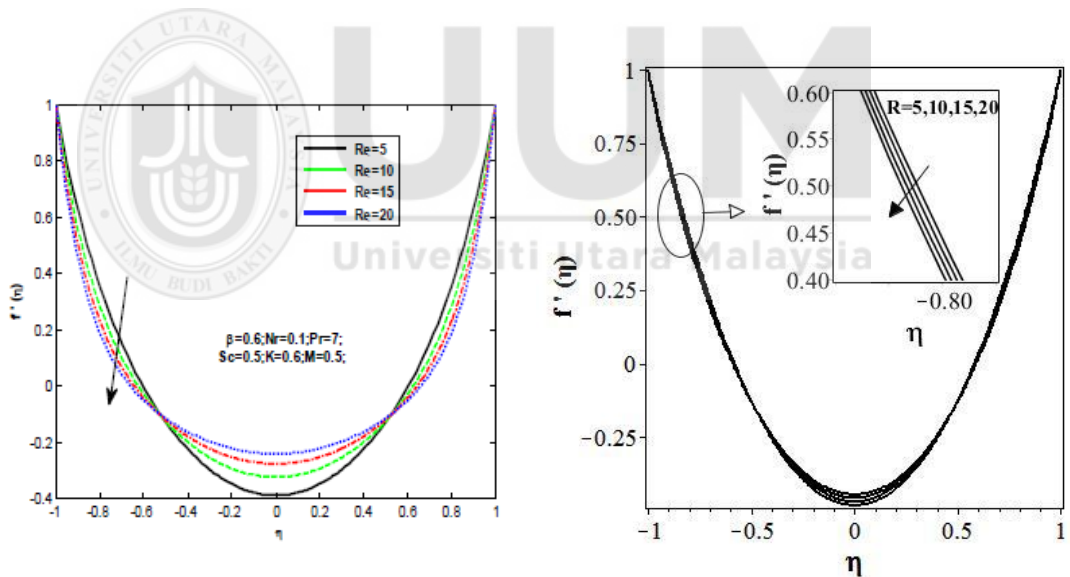
Sarojamma et al. (2014)

Present work by setting

$$\lambda = 0, p = 0, f'(-1) = 1, f'(1) = 1$$

Figure 4.11. Validation of physical model

4.3 Mixed Convective MHD Casson Fluid Flow in a Channel: Multiple Solutions

A numerical investigation is made to determine the occurrence of the multiple solutions of MHD Casson fluid in a porous channel. Governing PDEs of the proposed problem

are converted into nonlinear ODEs by using similarity transformation. Then, the shooting method is used to investigate the occurrence of the multiple solutions for the variations of different parameters and the effects of physical parameters on velocity profile, temperature, concentration and skin friction. Problem considered in this section is most relevant to Ganesh and Krishnambal (2006). They considered the problem of steady laminar incompressible viscous fluid in a porous channel under the influence of magnetic field. Governing equations were solved numerically by R-K- Gill method. Moreover, Ganesh and Krishnambal (2006) focused to examine the one solution, however, this study has succeeded to find the multiple solutions of the problem for the fixed values of the different physical parameters.

4.3.1 Problem Formulation

A steady, incompressible MHD flow of Casson fluid in a channel is considered. The *x*-axis is along the centerline of the channel, parallel to the channel surfaces and the *y*-axis is perpendicular to it. Lower wall of the channel is located at $y = -H$ and upper wall is at $y = H$. The fluid is injected into the channel and extracted out at a uniform velocity *V* (*V>0* suction, *V<0* injection) from upper wall and lower wall respectively. A uniform magnetic field of strength $B_\circ$ is applied perpendicular to the velocity field. The induced magnetic field is negligible as compared with the imposed field.

Under these assumptions, the governing equations for MHD boundary layer flow of Casson fluid are expressed as the following equations:

$$\frac{\partial u}{\partial x} + \frac{\partial v}{\partial y} = 0 \tag{4.38}$$

$$u \frac{\partial u}{\partial x} + v \frac{\partial u}{\partial y} = -\frac{1}{\rho} \frac{\partial p}{\partial x} + v \left(1 + \frac{1}{\beta}\right) \frac{\partial^2 u}{\partial y^2} - \frac{\sigma B_\circ^2 u}{\rho} \pm g \beta_T \big((T - T_2) + \beta_C (C - C_2)\big) \tag{4.39}$$

$$u\frac{\partial v}{\partial x} + v\frac{\partial v}{\partial y} = -\frac{1}{\rho}\frac{\partial p}{\partial y} + \upsilon\left(1 + \frac{1}{\beta}\right)\frac{\partial^2 v}{\partial x^2} \tag{4.40}$$

$$u\frac{\partial T}{\partial x} + v\frac{\partial T}{\partial y} = \frac{k}{\rho C_p}\frac{\partial^2 T}{\partial y^2} \tag{4.41}$$

$$u\frac{\partial C}{\partial x} + v\frac{\partial C}{\partial y} = D\frac{\partial^2 C}{\partial y^2} - \kappa_1 C \tag{4.42}$$

where ρ is density, μ is dynamic viscosity, υ is kinematic viscosity, σ is electrical conductivity, β is Casson fluid parameter, T is temperature of the fluid, k is thermal conductivity, κ_1 is reaction rate, D is mass diffusion and C is the concentration field.

The boundary conditions are:

$$u = 0, v = \frac{V}{2}, \ T = T_2, C = C_2 \ at \ y = H \tag{4.43}$$

$$\frac{\partial u}{\partial y} = 0, v = 0, T = T_1, C = C_1 \ at \ y = 0 \tag{4.44}$$

A stream function is introduced such that $\bar{u} = \frac{\partial \psi}{\partial y}, \bar{v} = \frac{-\partial \psi}{\partial x}$ and the pressure term is eliminated from Equations (4.39) - (4.40) by introducing vorticity ω resulting into:

$$u\frac{\partial \omega}{\partial x} + v\frac{\partial \omega}{\partial y} = \upsilon\left(1 + \frac{1}{\beta}\right)\left(\frac{\partial^2 \omega}{\partial x^2} + \frac{\partial^2 \omega}{\partial y^2}\right) - \frac{\sigma B_\circ^2 u'}{\rho} \pm \frac{\partial}{\partial y}\left(g\beta_T\big((T - T_2) + \beta_C(C - C_2)\big)\right)$$

where $\omega = \left(\frac{\partial \bar{v}}{\partial x} - \frac{\partial \bar{u}}{\partial y}\right)$

Defining $x^* = \frac{x}{H}, \ y^* = \frac{y}{H}, \ u = -Vx^*f'(y^*), \ v = Vf(y^*), \ \theta(y^*) = \frac{T-T_2}{T_1-T_2}, \ \phi(y^*) = \frac{C-C_2}{C_1-C_2}$

Then, the governing nonlinear momentum and energy equations of the proposed problem can be written as:

$$\left(1 + \frac{1}{\beta}\right)f'''' - M^2 f'' + R(f'f'' - ff''') + \lambda(\theta' + N\phi') = 0 \tag{4.45}$$

$$\theta'' - Prf\theta' = 0 \tag{4.46}$$

89

$$\varphi'' - Sc\gamma\varphi - Scf\varphi' = 0 \tag{4.47}$$

The boundary conditions in Eq. (4.43) - (4.44) are reduced into:

$$f(1) = \frac{1}{2}, f'(1) = 0, \theta(1) = 0, \varphi(1) = 0$$
$$f''(0) = 0, f(0) = 0, \theta(0) = 1, \varphi(0) = 1 \tag{4.48}$$

Here, $R = \frac{VH}{\nu}$ is Reynolds number ($R > 0$ for suction $R < 0$ for injection), $M^2 = \frac{\sigma B_\circ^2 H^2}{\mu}$ is Hartman number, $\lambda = \frac{Gr_x}{R^2}$ is the thermal buoyancy parameter, $Gr_x = \frac{VH^4 g\beta_T(T_1 - T_2)}{x\nu^3}$ is Grashof number, $N = \frac{\beta_C(C_1 - C_2)}{T_1 - T_2}$ is concentration buoyancy parameter, $Pr = \frac{\rho C_P HV}{\kappa}$ is Prantl number, $Sc = \frac{HV}{D}$ is Smith number, $\gamma = \frac{\kappa_1 H}{\nu}$ is chemical reaction rate.

4.3.2 Stability Analysis

For stability analysis, the steady flow solution $f(\eta) = f_\circ(\eta)$, $\theta(\eta) = \theta_\circ(\eta)$ which satisfies the boundary conditions in Eq. (4.48), is written as (Merkin 1986, Rosca & Pop 2013):

$$f(\eta) = f_\circ(\eta) + e^{-\lambda t} F(\eta, t) \tag{4.49}$$

$$\theta(\eta) = \vartheta_\circ(\eta) + e^{-\lambda t} G(\eta, t) \tag{4.50}$$

$$\varphi(\eta) = \varphi_\circ(\eta) + e^{-\lambda t} H(\eta, t) \tag{4.51}$$

where

$\tau = t$ and $0 < F(\eta, t) \ll 1$, $0 < G(\eta, t) \ll 1$ and λ is the unknown eigenvalues, $F(\eta, t)$, $G(\eta, t)$ and $H(\eta, t)$ are smallest relative to $f_\circ(\eta)$, $\theta_\circ(\eta)$ and $\varphi_\circ(\eta)$ respectively.

The governing equations of (4.45) – (4.47) for unsteady case are as follows:

$$\left(1 + \frac{1}{\beta}\right)\frac{\partial^4 f}{\partial \eta^4} + R\left[\frac{\partial f}{\partial \eta}\frac{\partial^2 f}{\partial \eta^2} - f\frac{\partial^3 f}{\partial \eta^3}\right] - M^2\frac{\partial^2 f}{\partial \eta^2} = \frac{\partial^3 f}{\partial \tau \partial \eta^2} \tag{4.52}$$

$$\frac{\partial^2 \theta}{\partial \eta^2} - Prf\frac{\partial \theta}{\partial \eta} = \frac{\partial \theta}{\partial \tau} \tag{4.53}$$

$$\frac{\partial^2 \varphi}{\partial \eta^2} - Sc\gamma\varphi - Scf\frac{\partial \varphi}{\partial \eta} = \frac{\partial \varphi}{\partial \tau} \tag{4.54}$$

Substituting Equations (4.49) - (4.51) into Equations (4.52) - (4.3654 and setting $\tau = 0$

(Merkin, 1986), will get:

$$\left(1 + \frac{1}{\beta}\right) F'''' + R[f_\circ' F'' + f_\circ'' F' - f_\circ F''' - F f_\circ'''] - M^2 F'' + \lambda F'' = 0 \tag{4.55}$$

$$G'' - Pr(f_\circ G' + F\theta_\circ') + \lambda G = 0 \tag{4.56}$$

$$H'' - Sc\gamma H - Sc(f_\circ H + F\varphi_\circ') + \lambda H = 0 \tag{4.57}$$

The boundary conditions are:

$$\begin{aligned} F(1) = 0, F'(1) = 0, G(1) = 1, H(1) = 1 \\ F''(0) = 0, F(0), G(0) = 0, H(0) = 0 \end{aligned} \tag{4.58}$$

$f_\circ(\eta)$, $\theta_\circ(\eta)$ and $\varphi_\circ(\eta)$ can be determined by the smallest eigenvalue λ due to the steady state flow solution. Therefore, the range of the possible eigenvalues can be determined by relaxing the boundary conditions on $f_\circ(\eta)$ and $\theta_\circ(\eta)$ as prescribed by Harris et al. (2009). So, by relaxing the boundary condition of $G(1) \to 0$ and solving the system of differential equation with a new boundary condition of $G'(0) = 1$.

4.3.3 Numerical Solution

The ODEs for stability in Eq. (4.55) – (4.57) are subjected to the boundary condition in Eq. (4.58) were also solved numerically using "*bvp4c*" from MATLAB.

Shooting method is employed to find the numerical solution of the proposed problem. The governing boundary value problem in Eq. (4.45) - (4.47) is reduced into initial value problem by assuming $x_1 = \eta, x_2 = f, x_3 = f', x_4 = f'', x_5 = f''', x_6 = \theta', x_7 = \varphi'$ then the following system is obtained:

91

$$
\begin{pmatrix} x_1' \\ x_2' \\ x_3' \\ x_4' \\ x_5' \\ x_6' \\ x_7' \end{pmatrix} = \begin{pmatrix} 1 \\ x_3 \\ x_4 \\ x_5 \\ \dfrac{\beta}{(1+\beta)}\left(M^2 x_4 - R(x_3 x_4 - x_2 x_5) - \lambda(x_6 + N x_7)\right) \\ Pr x_2 x_6 \\ Sc\gamma\varphi + Sc x_2 x_7 \end{pmatrix} \tag{4.59}
$$

The initial conditions are:

$$
\begin{pmatrix} x_1(1) \\ x_2(1) \\ x_3(1) \\ x_4(1) \\ x_5(1) \\ x_6(1) \\ x_7(1) \end{pmatrix} = \begin{pmatrix} 1 \\ 1 \\ \dfrac{1}{2} \\ 0 \\ \alpha_1 \\ \alpha_2 \\ \alpha_3 \\ \alpha_4 \end{pmatrix} \tag{4.60}
$$

Here, $\alpha_1, \alpha_2, \alpha_3, \alpha_4$ are the missing values. These values are similarly determined using shooting method aided by Maple 18. $\alpha_1, \alpha_2, \alpha_3, \alpha_4$

4.3.4 Results and Discussions

The main motive of this section is to investigate the multiple solutions of the proposed problems. Figures (4.12) - (4.17) are plotted to evaluate the effects of different physical quantities on the velocity, temperature and mass fraction. The effects include the existence of multiple solution, Reynolds number R, magnetic field M, Casson parameter β, Prandtl number Pr, Smith number Sc and chemical reaction rate γ.

Findings of multiple solutions concluded that there is only one solution in the case of $R < 0, \beta \in (0, \infty)$ and $\beta \in (0,5), R \in [0, \infty)$. However, multiple solutions exist at $\beta \in [5, \infty)$ and $R \in [31.07, \infty)$ for any value of magnetic number $M \in [0,2.0]$. So, this discovery shows that there is a critical value of Casson number β and suction parameter R such that $(\beta)_{critical} = 5$ and $(R)_{critical} = 31.07$. Thus, no multiple solutions exist if

$\beta < (\beta)_{critical}$ and $< (R)_{critical}$. The said phenomena can be observed from Figure 4.12 which shows the magnitude of skin friction $|f''(1)|$ against the values of Reynolds number R.
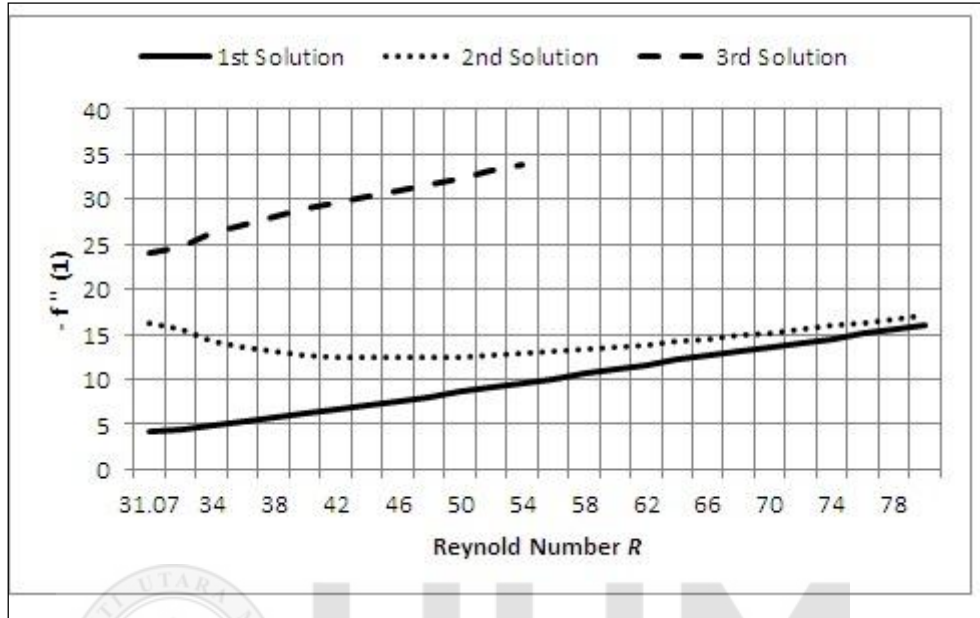
Figure 4.12. Skin friction $-f''(1)$ against the values of Reynolds number R

The effects of Reynolds number R on velocity profile $f'(\eta)$ for non-bouyant flow case $\lambda = 0$ are presented in Figure 4.13. For enhanced values of Reynolds number R, velocity profile $f'(\eta)$ decreases near the center of the channel for the 1st and the 3rd solutions but increases near the walls of the channel. However, a total reverse behavior is observed for 2nd solution. Furthermore, triple solutions exist only for $R \geq 31.07$. The effect of magnetic field M on velocity profile $f'(\eta)$ corresponding to forced convection or non-bouyant flow case $\lambda = 0$ is shown in Figure 4.14 where velocity profile $f'(\eta)$ for the 1st and the 2nd solutions decreases near the center of the channel $\eta \approx 0$,but increases near the channel walls. Since magnetic field is applied perpendicular to the channel walls, the effect of magnetic field is obvious near the channel walls of $\eta \approx 1$. The presence of magnetic field enhances the viscosity of the fluid due to the chain deformation of the fluid particles. The chainlike structure retards the flow and decelerates the motion. This

occurrence shows that fluid flow can be controlled by applying magnetic field resulting into many control based applications including MHD power generation, casting of metals, blood flow in arteries and many others. The effect of Casson parameter β on velocity profile $f'(\eta)$ for the case of forced convection $\lambda = 0$ is depicted in Figure 4.15. Velocity profile $f'(\eta)$ decreases gradually for the 1st and the 3rd solutions near the center of the channel but increases near the channel wall $\eta \approx 1$. However, velocity increases for the 2nd solution as the enhancement of the Casson parameter β is taken place about $\eta \approx 0$. Furthermore, $\beta \to \infty$ corresponds to the Newtonian fluid. Figure 4.16 presents the effect of Prandtl number Pr on temperature profile $\theta(1)$ for non-bouyant $\lambda = 0$ case. These profiles conclude that temperature profile $\theta(1)$ increases strictly monotonically as the Prandtl number Pr increases for the 1st and the 2nd solutions. On the other hand, temperature profile $\theta(1)$ decreases as the Prandtl number Pr increases for the 3rd solution. The effects of Smith number Sc on concentration profile $\phi(\eta)$ for $\lambda = 0$ (non-bouyant case) are plotted in Figure 4.17. The concentration profile $\phi(\eta)$ decreases by the increase of the strength of Smith number Sc for all triple solutions. In Figure 4.18, $\theta'(1)$ is plotted against the values of Reynolds number R for the case of forced convection $\lambda = 0$. It shows that the 1st and the 2nd solutions overlap as Reynolds number R increases. Figure 4.19 showed the validation of physical model with Ganesh and Krishnambal (2006). To validate this model, we set the parameters and boundary conditions as prescribed by Ganesh and Krishnambal (2006) i.e. $\lambda = 0, \beta \to \infty, f(-1) = -1, f'(-1) = 0, f(1) = 1, f'(1) = 0$ and found good agreement of the numerical results.
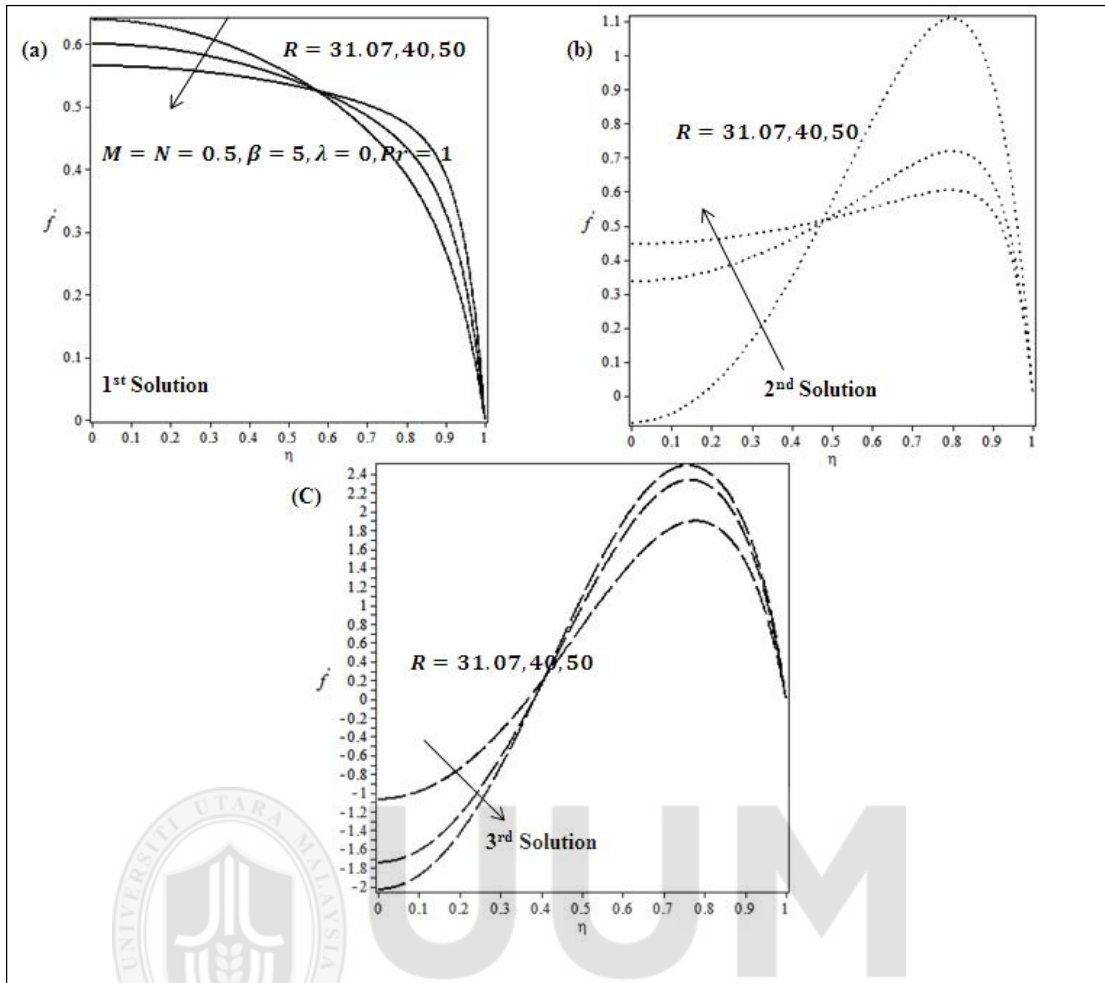
Figure 4.13. Effect of Reynolds number R on Velocity profile $f'(\eta)$
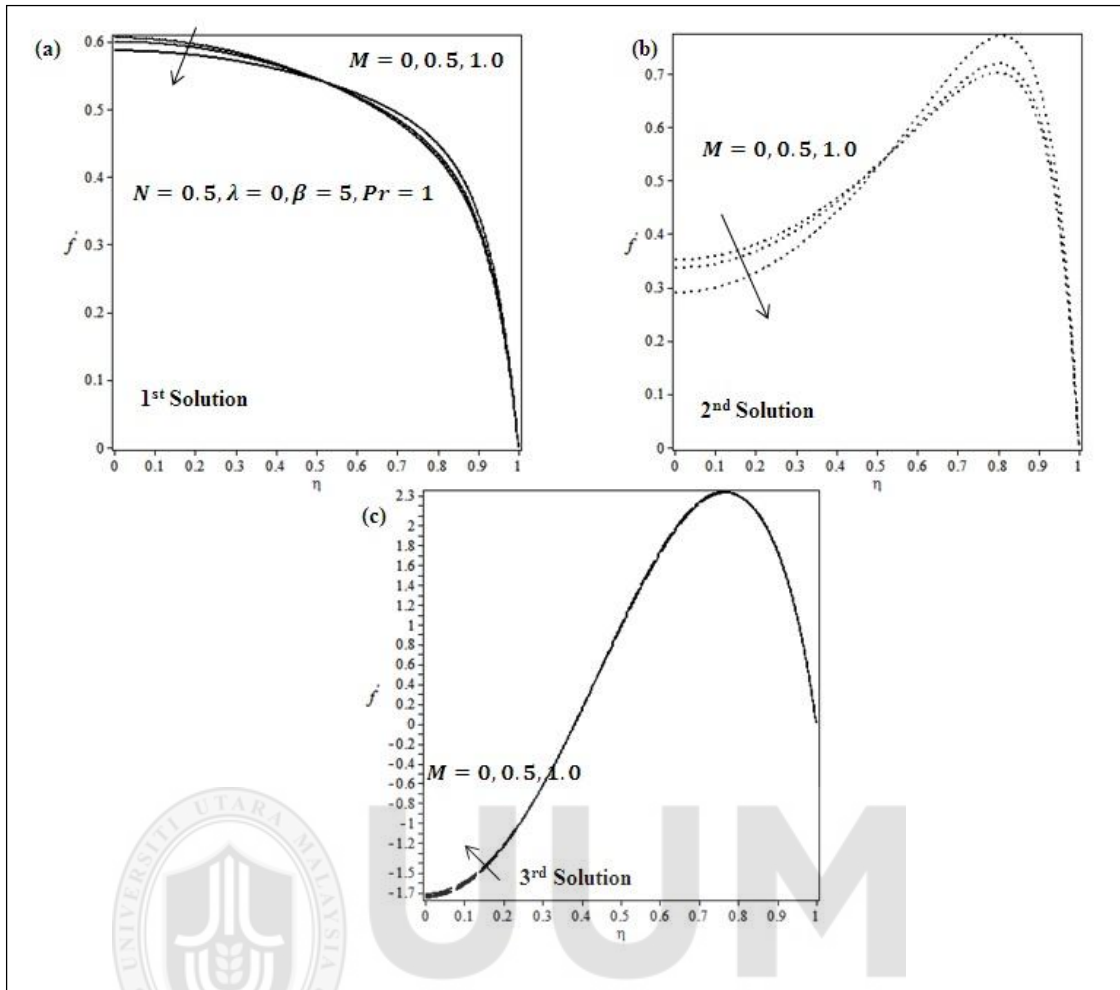
Figure 4.14. Effect of Magnetic field M on Velocity profile $f'(\eta)$

Table 4.5 and Table 4.6 represent the numerical values of skin friction $f''(1)$ and $\theta'(1)$ for the variations of different physical parameters. Specifically the Table 4.5 presents the numerical values of skin friction $f''(1)$ for the variation of buoyancy parameter λ by fixing $R = 36, M = N = 0.5, \beta = 5, Pr = 1, Sc = 1, \gamma = 1.2$. The magnitude of skin friction increases for the 1st and the 3rd solutions but decreases for the 2nd solution in the case of opposing flow $\lambda < 0$. Furthermore, the same behavior depicts the case of assisting flow of $\lambda > 0$. Therefore, the fluid velocity near the channel walls $\eta \approx 1$ increases. From Table 4.6, the magnitude of skin friction $f''(1)$ and $\theta'(1)$ increases and decreases respectively as Reynolds number increases for the case of assisting flow $\lambda > 0$ only for the 1st and the 3rd solutions by setting $M = N = 0.5, Pr = 1, Sc = 2, \gamma = 1.2$.

96

The numerical values of skin friction $f''(1)$ increase for the 1st and the 3rd solutions but decreases for the 2nd solution by varying Reynolds number for the case of opposing flow $\lambda < 0$ by setting $M = N = 0.5, Pr = 1, Sc = 2, \gamma = 1.2$.
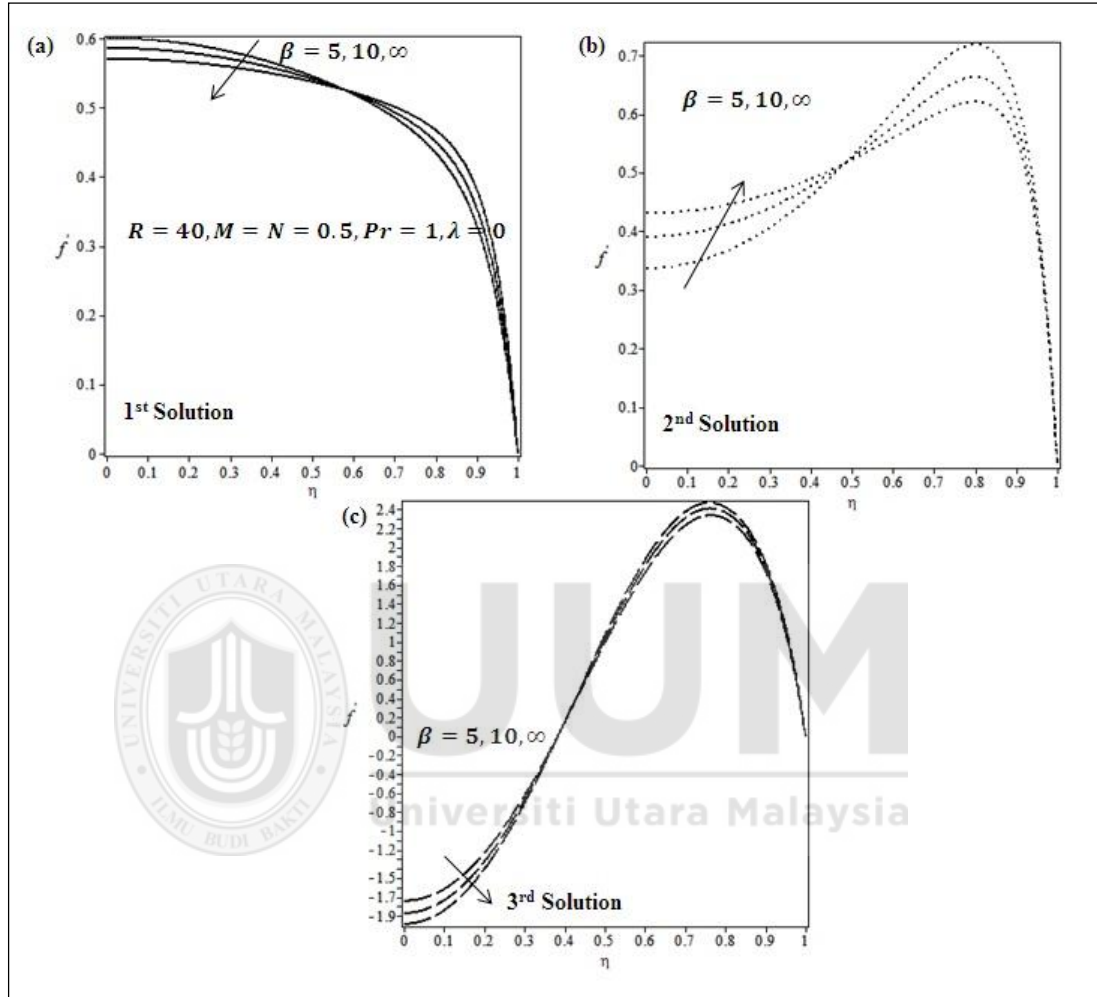
Figure 4.15. Effect of Casson parameter β on Velocity profile $f'(\eta)$
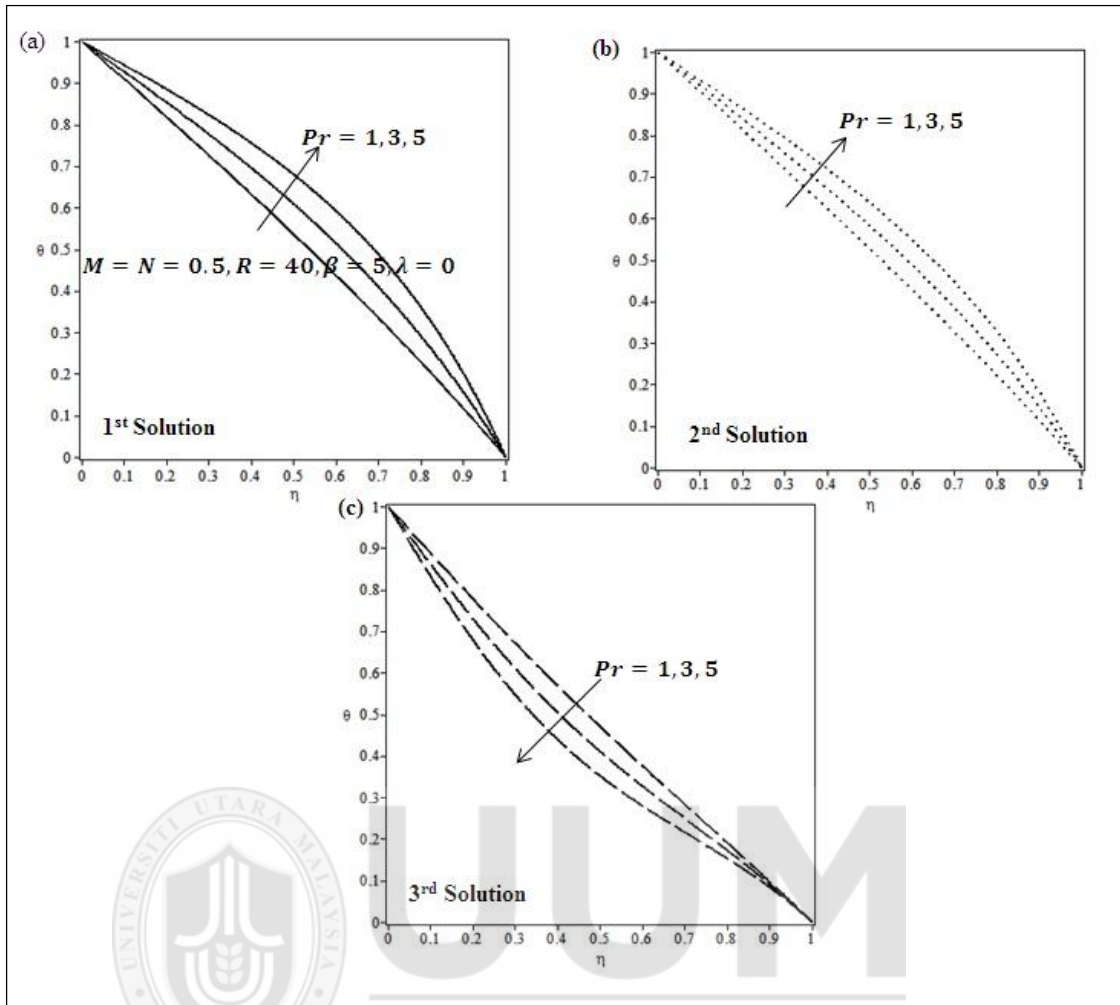
Figure 4.16. Effect of Prandtl number Pr on Temperature profile $\theta(\eta)$

Smallest eigenvalues λ are presented in Table 4.8 against several values of Reynolds number R. The numerical values of this table evidently show that eigenvalues of the 1st solution are positive, hence physically reliable. On the other hand, the 2nd and the 3rd solutions are physically unreliable because their eigenvalues are negative.
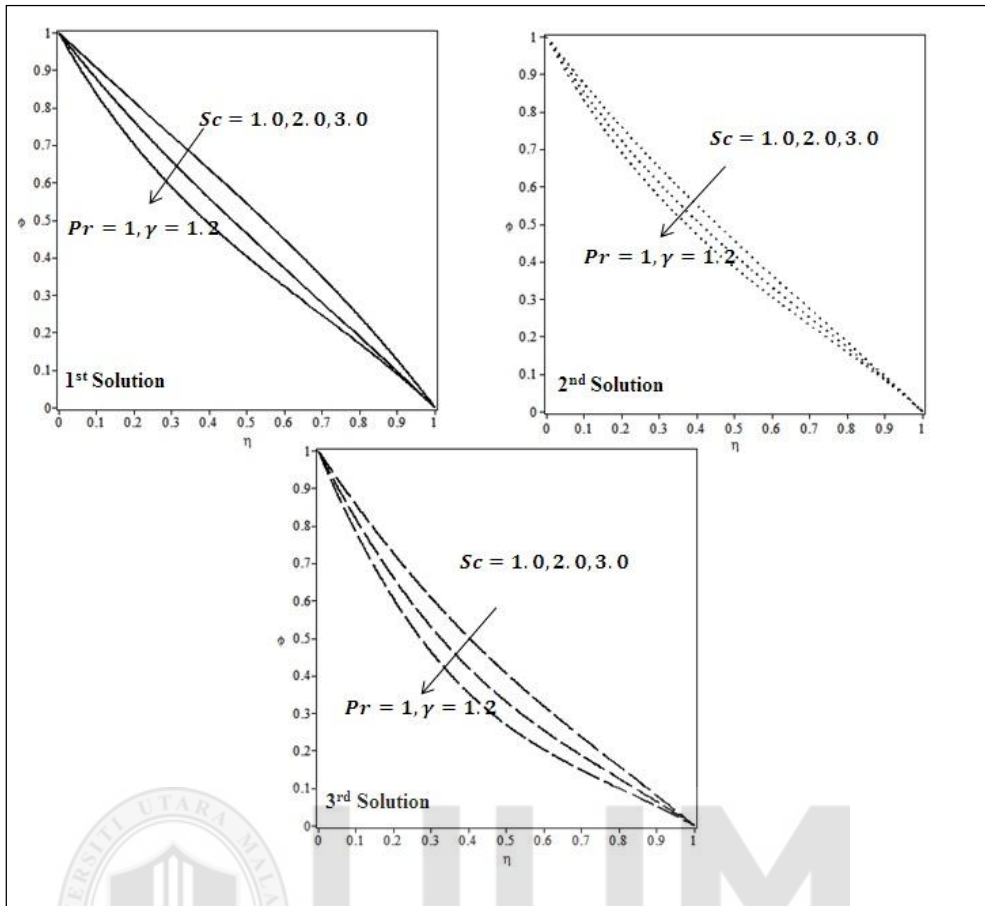
Figure 4.17. Effect of Smith number Sc on Concentration profile $\phi(\eta)$ for $\lambda = 0$
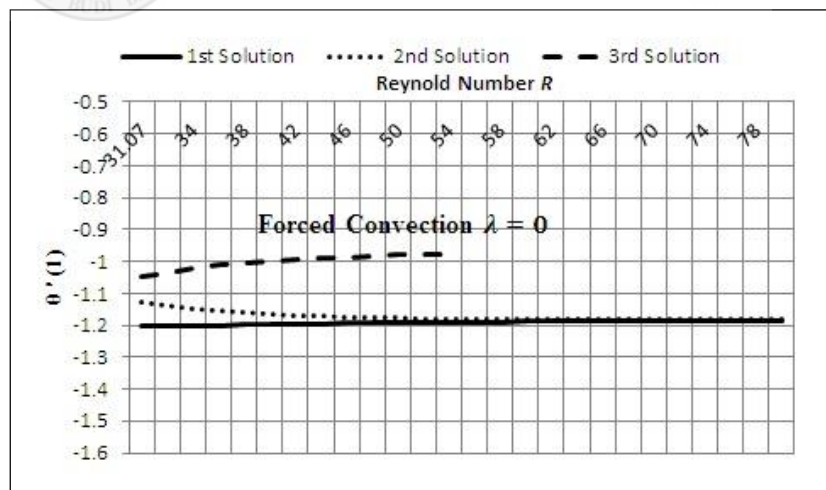
Figure 4.18. Effect of Reynolds number R on $\theta'(1)$

99
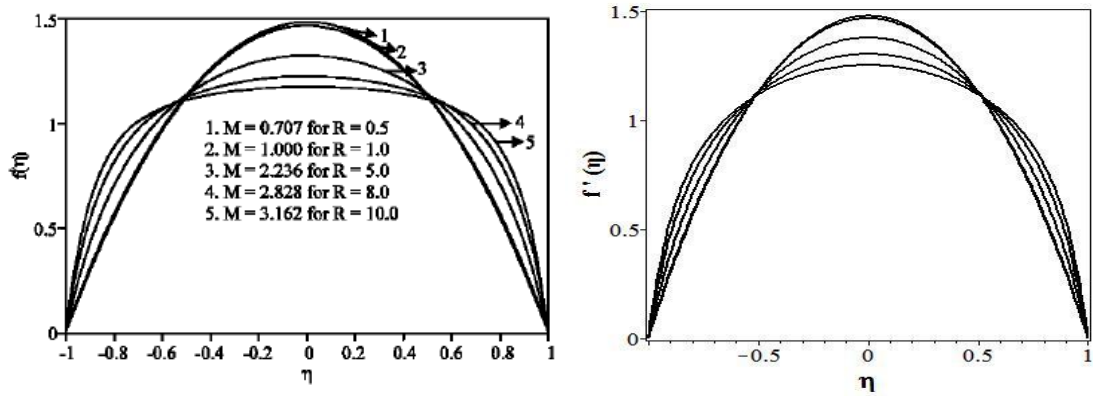
| Ganesh and Krishnambal (2006) | Present work for the same values of M and R (Ganesh & Krishnambal, 2006) by setting $\lambda = 0, \beta \rightarrow \infty, f(-1) = -1, f'(-1) = 0, f(1) = 1, f'(1) = 0$ |

Figure 4.19. Validation of physical model

Table 4.5

Skin friction for different values of buoyancy parameters for $R = 36, M = N = 0.5, \beta = 5, Pr = 1, Sc = 1, \gamma = 1.2$

λ	1st Solution $f''(1)$	2nd Solution $f''(1)$	3rd Solution $f''(1)$
-0.50	-3.29405873	-14.78794525	-27.20927012
-0.25	-4.19831393	-14.22940191	-27.20983823
0	-5.21362887	-13.55733409	-27.21039669
0.25	-6.42985179	-12.68188468	-27.21094599
0.50	-8.22263120	-11.22740570	-27.21148660

Table 4.6

Skin friction and temperature gradient for different values of Reynolds number R

R	λ	1st Solution $f''(1)$	2nd Solution $f''(1)$	3rd Solution $f''(1)$	1st Solution $\theta'(1)$	2nd Solution $\theta'(1)$	3rd Solution $\theta'(1)$
31.07		-3.56529871	-16.7538394	-23.89501535	-1.20630237	-1.12415316	-1.04645775
35	-0.25	-4.06923819	-14.50163765	-26.71544153	-1.20492033	-1.14909835	-1.01703703
40		-4.70569981	-13.72648291	-28.87613992	-1.20354537	-1.16169799	-0.99886321
31.07		-4.22815985	-16.33685245	-23.92995344	-1.20259758	-1.12723885	-1.045737
35	0	-5.00282319	-13.89608196	-26.71780315	-1.20017552	-1.15257708	-1.01679981
40		-6.10401248	-12.73103850	-28.87353590	-1.19720323	-1.16644810	-0.99874016
31.07		-4.93400210	-15.87676698	-23.96319996	-1.19862360	-1.13057525	-1.04504186
35	0.25	-6.08426152	-13.14036724	-26.72012735	-1.19463415	-1.15685896	-1.01656453
40		-8.28517017	-10.94971752	-28.87095120	-1.18721976	-1.17484905	-0.99861750

Table 4.7

Validation of numerical results

M	R	β	λ	N	$f''(-1)$ Shooting	$f''(-1)$ Runge-Kutta-Fehlberg
0.5	31.07	5	0	0.5	-4.228159853	-4.22815993
	40				-6.104012488	-6.10401289
	50				-8.557825396	-8.55782546

Table 4.8

Smallest eigenvaluesλ at several values of Reynolds number R

R	M	β	Pr	1st Solution λ	2nd Solution λ	3rd Solution λ
32.07				1.4477	-3.1621	-3.0968
34	5	0.5	0.7	1.4749	-3.2939	-3.9347
38				1.4939	-3.3634	-4.1715
42				1.5461	-3.8134	-4.4272

4.4 Casson Fluid Flow between Slowly Expanding and Contracting Walls: Multiple Solutions

This part focuses on Casson fluid flow in a channel of slowly expanding and contracting walls. The basic equations for the governing fluid flow are transformed into ODEs using suitable dimensionless variables. The resulting ODEs are solved numerically by employing shooting technique and triple solutions are obtained depending on Reynolds number, Casson fluid, expanding or contracting ratio and magnetic parameters considered. The work that has been done by Rahimi et al. (2015) is the most related reference for the problem considered for expanding or contracting walls. The difference between the present study and Rahimi et al. (2015) is the consideration of non-Newtonian fluid model (Casson fluid model). Furthermore, Rahimi et al. (2015) focused to investigate the single solution. However, this study has succeeded to find the different branches of the solution. Moreover, the study has found an excellent agreement to the literature of Berman (1953) by vanishing the wall expansion ratio $\alpha = 0$ and Casson parameter $\beta \to \infty$.

4.4.1 Problem Formulation

An unsteady, laminar and incompressible Casson fluid in a channel is considered. Both channel walls are considered equally permeable and can be expanded or contract uniformly with time dependent rate of $\dot{a}$. For the uniform wall suction/injection, the fluid is assumed to be symmetric about $y - axis$ and transverse magnetic field is applied perpendicular to the channel walls as described in physical model shown in Figure 4.20.
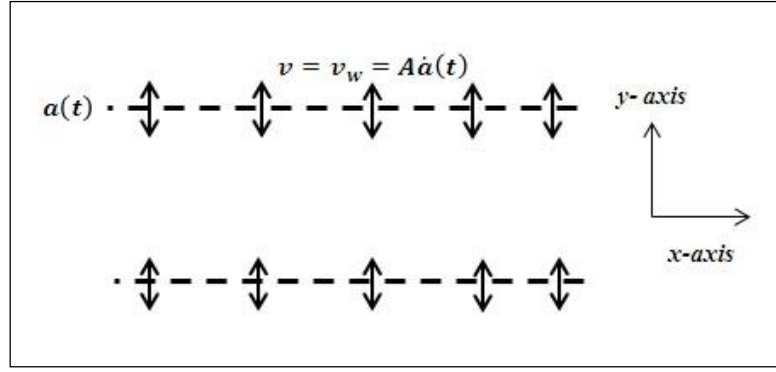
Figure 4.20: Physical Model of the Problem

By applying these assumptions, the governing equations for the proposed problem is written as:

$$\frac{\partial \bar{u}}{\partial x} + \frac{\partial \bar{v}}{\partial y} = 0 \tag{4.61}$$

$$\frac{\partial \bar{u}}{\partial t} + \bar{u}\frac{\partial \bar{u}}{\partial x} + \bar{v}\frac{\partial \bar{u}}{\partial y} = -\frac{1}{\rho}\frac{\partial p}{\partial x} + v\left(1 + \frac{1}{\beta}\right)\left(2\frac{\partial^2 \bar{u}}{\partial x^2} + \frac{\partial^2 \bar{u}}{\partial y^2} + \frac{\partial^2 \bar{u}}{\partial x \partial y}\right) - \frac{\sigma B_\circ^2 \bar{u}}{\rho} \tag{4.62}$$

$$\frac{\partial \bar{v}}{\partial t} + \bar{u}\frac{\partial \bar{v}}{\partial x} + \bar{v}\frac{\partial \bar{v}}{\partial y} = -\frac{1}{\rho}\frac{\partial p}{\partial y} + v\left(1 + \frac{1}{\beta}\right)\left(2\frac{\partial^2 \bar{v}}{\partial x^2} + \frac{\partial^2 \bar{v}}{\partial y^2} + \frac{\partial^2 \bar{v}}{\partial x \partial y}\right) \tag{4.63}$$

$$\frac{\partial T}{\partial t} + \rho C_p\left(u\frac{\partial T}{\partial x} + v\frac{\partial T}{\partial y}\right) = k_\circ\left(\frac{\partial^2 T}{\partial x^2} + \frac{\partial^2 T}{\partial y^2}\right) \tag{4.64}$$

The boundary conditions for expanding and contracting walls are:

$$\bar{u}(x, a) = 0, \qquad \bar{v}(a) = -v_w = -A\dot{a}, \qquad T = T_H \tag{4.65}$$

$$\frac{\partial \bar{u}}{\partial y}(x, 0) = 0, \qquad \bar{v}(0) = 0, \qquad T = T_w \tag{4.66}$$

At the channel walls, the fluid is assumed to be extracted or injected with a constant velocity v_w. Moreover, the coefficient of suction/injection $A \cong {v_w}/{\dot{a}}$ is a wall permeability parameter appears in Equation (4.65).

A stream function is introduced such that:

103

$$\bar{u} = \frac{\partial \psi}{\partial y}, \qquad \bar{v} = \frac{-\partial \psi}{\partial x} \tag{4.67}$$

The system of equations in Eq. (4.62) - (4.64) are solved. The pressure term is eliminated from Equations (4.62) - (4.63) by introducing vorticity ω:

$$\frac{\partial \omega}{\partial t} + u \frac{\partial \omega}{\partial x} + v \frac{\partial \omega}{\partial y} = \nu \left(1 + \frac{1}{\beta}\right) \left(\frac{\partial^2 \omega}{\partial x^2} + \frac{\partial^2 \omega}{\partial y^2}\right) - \frac{\sigma B_\circ^2 \bar{u}'}{\rho} \tag{4.68}$$

$$\omega = \left(\frac{\partial \bar{v}}{\partial x} - \frac{\partial \bar{u}}{\partial y}\right) \tag{4.69}$$

Similar solution of boundary conditions in Eq. (4.65) - (4.66) can be developed. For this purpose, $y \equiv \frac{\bar{y}}{a}$ is considered and stream function can be written as:

$$\psi = \frac{\upsilon}{a(t)} \bar{x} \bar{F}(\eta, t), where \; \eta = {}^{y}/_{a(t)} \tag{4.70}$$

By putting Equation (4.70) into Eq. (4.67) we get

$$\bar{u} = \frac{\upsilon \bar{x}}{a^2(t)} \bar{F}_\eta, \qquad \bar{v} = \frac{-\upsilon}{a(t)} \bar{F}(\eta, t), \qquad \theta(\eta) = \frac{T - T_H}{T_w - T_H} \tag{4.71}$$

where $\bar{F}_\eta$ is partial derivative of $\bar{F}$ with respect to η. By using Equation (4.71) into Equation (4.68), we have

$$\left(1 + {}^{1}/_{\beta}\right)(\bar{F})_{\eta\eta\eta\eta} + \alpha[\eta(\bar{F})_{\eta\eta\eta} + 3(\bar{F})_{\eta\eta}] + \bar{F}(\bar{F})_{\eta\eta\eta} - (\bar{F})_\eta (\bar{F})_{\eta\eta} - {}^{a^2}/_\upsilon (\bar{F})_{\eta\eta t}$$

$$-M^2 (\bar{F})_{\eta\eta} = 0 \tag{4.72}$$

where $\alpha = \frac{\dot{a} a}{\upsilon}$ is the wall expansion ratio and M is Hartman number.

The boundary conditions are:

$$\bar{F}_\eta = 0, \qquad \bar{F} = R, \qquad \theta = 0, \qquad \eta = 1 \tag{4.73}$$

$$\overline{F_{\eta\eta}} = 0, \qquad \bar{F} = 0, \qquad \theta = 1, \qquad \eta = 0 \tag{4.74}$$

where $R = \frac{a v_w}{v}$ is Reynolds number, such that $R > 0$ and $R < 0$ is for injection and suction respectively through the walls.

Uchida and Aoki (1977) and Dauenhauer and Majdalani (2003) developed a self-similar solution $f = \frac{\bar{F}}{R}$ with respect to space and time. This can be refined by considering: α is a constant and $f = f(\eta)$, which leads to $f_{\eta\eta t} = 0$. So Equation (4.72) becomes

$$\left(1 + \frac{1}{\beta}\right) f'''' + \alpha[\eta f''' + 3f''] + R(ff''' - f'f'') - M^2 f'' = 0 \tag{4.75}$$

$$\theta'' + (PrfR + \alpha\eta Pr)\theta' = 0 \tag{4.76}$$

$$\left.\begin{matrix} f(0) = 0, f''(0) = 0, \theta(0) = 1 \\ f(1) = 1, f'(1) = 0, \theta(1) = 0 \end{matrix}\right\} \tag{4.77}$$

Case 1:

As a specific case when $M = 0$ and $\beta \to \infty$, Equation (4.75) can be reduced to the case considered by Rahimi et al. (2015) as given in the following equation:

$$f'''' + \alpha[\eta f''' + 3f''] + R(ff''' - f'f'') = 0 \tag{4.78}$$

Subject to Equation (4.77)

Case 2:

Generalized Equation (4.75) can be transformed as (Berman, 1953) by setting $M = 0, \alpha = 0$ and $\beta \to \infty$. Mathematically:

$$f'''' + R(ff''' - f'f'') = 0 \tag{4.79}$$

Subject to Equation (4.77)

4.4.2 Stability Analysis

$f(\eta) = f_\circ(\eta)$, $\theta(\eta) = \theta_\circ(\eta)$ are introduced to the steady flow solution, which satisfies the boundary conditions in Eq. (4.77), using assumption from (Merkin 1986, Rosca and Pop 2013) and setting $\tau = t$:

$$f(\eta) = f_\circ(\eta) + e^{-\lambda t}F(\eta, t) \tag{4.80}$$

$$\theta(\eta) = \vartheta_\circ(\eta) + e^{-\lambda t}G(\eta, t) \tag{4.81}$$

$0 < F(\eta, t) \ll 1$, $0 < G(\eta, t) \ll 1$ and λ is the unknown eigenvalues, $F(\eta, t)$ and $G(\eta, t)$ are smallest relative to $f_\circ(\eta)$ and $\theta_\circ(\eta)$ respectively.

The governing equations of (4.75) and (4.76) for unsteady case are as follows:

$$\left(1 + \frac{1}{\beta}\right)\frac{\partial^4 f}{\partial \eta^4} + \left[\alpha\left(\eta\frac{\partial^3 f}{\partial \eta^3} + 3\frac{\partial^2 f}{\partial \eta^2}\right) + R\left(f\frac{\partial^3 f}{\partial \eta^3} - \frac{\partial f}{\partial \eta}\frac{\partial^2 f}{\partial \eta^2}\right)\right]$$

$$-M^2\frac{\partial^2 f}{\partial \eta^2} = \frac{\partial^3 f}{\partial \tau \partial \eta^2} \tag{4.82}$$

$$\frac{\partial^2 \theta}{\partial \eta^2} + Pr(Rf + \alpha\eta)\frac{\partial \theta}{\partial \eta} = \frac{\partial \theta}{\partial \tau} \tag{4.83}$$

Substituting Equations (4.80) and (4.81) into Equations (4.82) and (4.83) and setting $\tau = 0$ (Merkin, 1986), will get;

$$\left(1 + \frac{1}{\beta}\right)F'''' + R(f_\circ F''' + Ff_\circ''' - f_\circ'F'' - f_\circ''F') + \alpha(\eta F''' + 3F'')$$

$$-M^2 F'' + \lambda F'' = 0 \tag{4.84}$$

$$\theta'' + [PrRf_\circ + \alpha\eta Pr]\theta_\circ' + [PrRF + \alpha\eta Pr]G'' + \lambda G = 0 \tag{4.85}$$

The boundary conditions are:

$$\left.\begin{array}{l}F(1) = 0, F'(1) = 0, G(1) = 0 \\ \quad F''(0) = 0, F(0), G(0) = 1\end{array}\right\} \tag{4.86}$$

$f_\circ(\eta)$ and $\theta_\circ(\eta)$ can be determined by the smallest eigenvalue λ due to the steady state flow solution. Therefore, the range of the possible eigenvalues can be determined by relaxing the boundary conditions on $f_\circ(\eta)$ and $\theta_\circ(\eta)$ as prescribed by Harris et al. (2009)

by setting $G(1) \to 0$. The system of differential equations is solved using a new boundary condition of $G'(0) = 1$.

4.4.3 Numerical Solution

Governing equations for stability in Eq. (4.84) - (4.85) are also solved numerically with the help of "*bvp4c*" function from MATLAB using the boundary conditions in Eq. (4.86).

Shooting method is used to numerically solve the Equations (4.75) - (4.76) subjected to the boundary conditions in Eq. (4.77). Since Equation (4.75) is a fourth order nonlinear ODE so we have to change it into a system of 1st order ODEs such that:

$$\left.\begin{aligned} f' &= p, \\ p' &= q, \\ q' &= r, \\ r' &= \frac{1}{\left(1 + \frac{1}{\beta}\right)}\left(M^2 q - \alpha[\eta r + 3q] - R(pq - fr)\right) \\ \theta' &= s \\ s' &= -(PrfR + \alpha\eta Pr)\, s \end{aligned}\right\} \tag{4.87}$$

with boundary conditions of:

$$\left.\begin{aligned} f(1) &= 1, p(1) = 0, \theta(1) = 0 \\ q(1) &= s_1, r(1) = s_2, s(1) = s_3 \end{aligned}\right\} \tag{4.88}$$

s_1, s_2 and s_3 are unknown initial conditions that can be determined using shooting strategy. $q(1), r(1)s(1)$Afterwards the values for $f'(1)$ are calculated and compared with the given boundary conditions in Eq. (4.88).

4.4.4 Results and Discussions

The effects of the parameters on skin friction, velocity profile and temperature profile are presented in tabulation and pictorial representation. Calculated results are compared to (Rahimi et al. 2016) for $M = 0$ and $\beta \to \infty$ as shown in Figure 4.21 This figure shows that the computed results are in good agreement with previous study.

Figures (4.22-4.33) evaluate the effects of different physical parameters on skin friction $f''(\eta)$, $-\theta'(\eta)$ and velocity profile $f'(\eta)$. Figure 4.22 shows the skin friction coefficient $f''(1)$ verses suction Reynolds number $R < 0$ for $M = 0.4, \beta = 0.3, \alpha = 0.1$. The existence of triple solutions in $f''(1)$ with critical value (turning point) $R \approx -52.72$ is found from this figure. The 2nd solution shows that skin friction increases by increasing the magnitude of the Reynolds number. In other words, suction $(R < 0)$ increases the wall drag. The opposite happens to the 1st and the 3rd solutions of $f''(1)$ where the increases of suction will decrease the wall drag. Figure 4.23 reflects the effect of suction Reynolds number of $R < 0$ on $-\theta'(1)$ for $Pr = 0.3, M = 0.4, \beta = 0.3, \alpha = 0.1$. The numerical values of $-\theta'(1)$ for the 1st and the 2nd solutions increase gradually by increasing the values of Reynolds number R. However, a total opposite happens for the 3rd solution. The figures reveal the occurrence of triple solutions for the parameters considered. The effects of suction Reynolds number R on velocity profile $f'(\eta)$ for $\alpha = 0.1, M = 0.4, \beta = 0.3$ of slowly expanding walls and $\alpha = -0.1, M = 0.4, \beta = 0.3$ of slowly contracting walls are shown in Figures 4.24 - 4.25. These figures evidently demonstrate that the enhancement of magnitude of suction Reynolds number R decreases the velocity profile $f'(\eta)$ for the 1st and the 3rd solutions but increases for the 2nd solution. The velocity profile $f'(\eta)$ is noticeably fluctuated gradually for the 1st solution as compared to the other solutions because suction add up an extra forcing with Casson parameter β and wall expansion ratio α for the 2nd and the 3rd solutions. The

effect of wall expansion ratio $\alpha > 0$ and $\alpha < 0$ can be seen in Figures 4.26-4.27. In the case of expanding wall ($\alpha > 0$), as αincreases from 0.1 to 0.9, the enhancement of velocity profile $f'(\eta)$ is observed near the center $\eta \approx 0$ but detraction near the wall $\eta \approx 1$. This difference is caused by faster flow towards the center to make up for the space caused by the expansion of the wall. Similarly, for contracting wall ($\alpha < 0$), the velocity profile $f'(\eta)$ decreases near the center of the channel $\eta \approx 0$ but increases towards the wall of channel $\eta \approx 1$. However, both Figures 4.26-4.27 are self-similar to each other except the pattern that is observed and mentioned above. An increase value of Casson parameter of $\beta = 0.3, 0.5, 0.7$ makes velocity profile $f'(\eta)$ decreases for the 1st and the 3rd solutions but increases for 2nd solution in the quarter half of the channel for expanding and contracting walls as shown in figures 4.28 and 4.29. Figures 4.30 and 4.31 represent the effect of magnetic field M on velocity profile $f'(\eta)$ for fixed values of $R = -60, \beta = 0.3, \alpha = 1, -1$. Observation from these figures show that small changes exist in the velocity profile $f'(\eta)$ for all solutions. This observation is noted by the increment of velocity field f' near the wall for the 1st and 2nd solutions and adverse effect for the 3rd solution. Figure 4.32-4.33 demonstrate the effect of Prandtl number Pr on temperature profile $\theta(\eta)$. These figures present an increase in $\theta(\eta)$ when Pr is increased for the 1st and the 2nd solutions and decreases for the 3rd solution on both expanding and contracting walls.

Table 4.9 shows the smallest eigenvalue λ against different values of wall contraction parameter $\alpha < 0$ of fixed values of $R = 0, M = 0.4, \beta = 0.3$, and for $Pr = 0.7$. When the numerical values of wall contraction parameter $\alpha < 0$ is increased, the eigenvalues of the 1st solution are positive and hence the 1st solution is reliable. However, the eigenvalues for the 2nd and the 3rd solutions are negative; thus, physically unreliable.
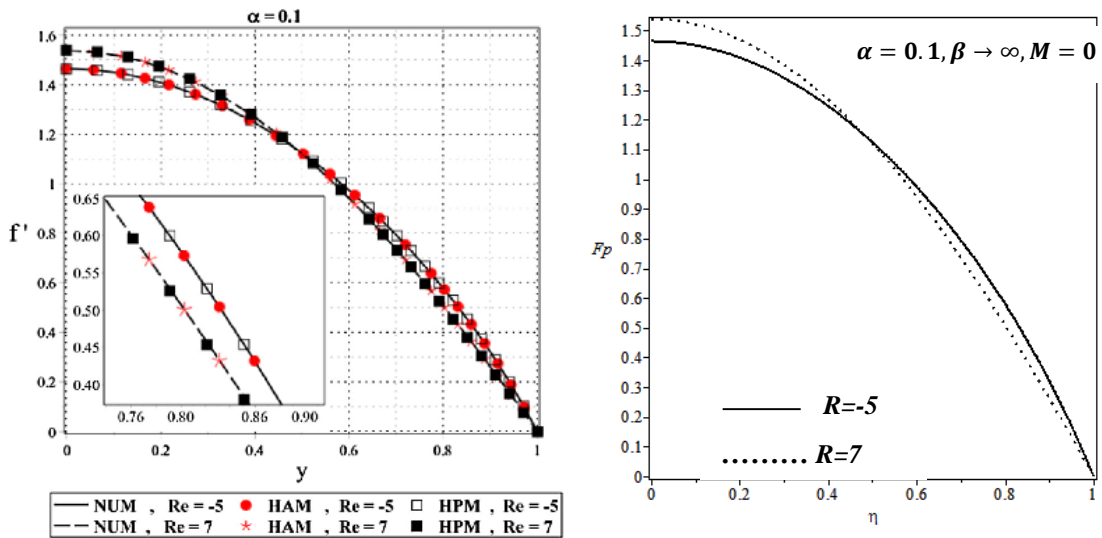
(a) Effect of Reynolds number R for slowly expanding wall on velocity profile $f'(\eta)$ (Rahimi et al., 2016)

(b) Effect of Reynolds number R for slowly expanding wall on velocity profile $f'(\eta)$ (Present Study)

Figure 4.21. Validation of present research work
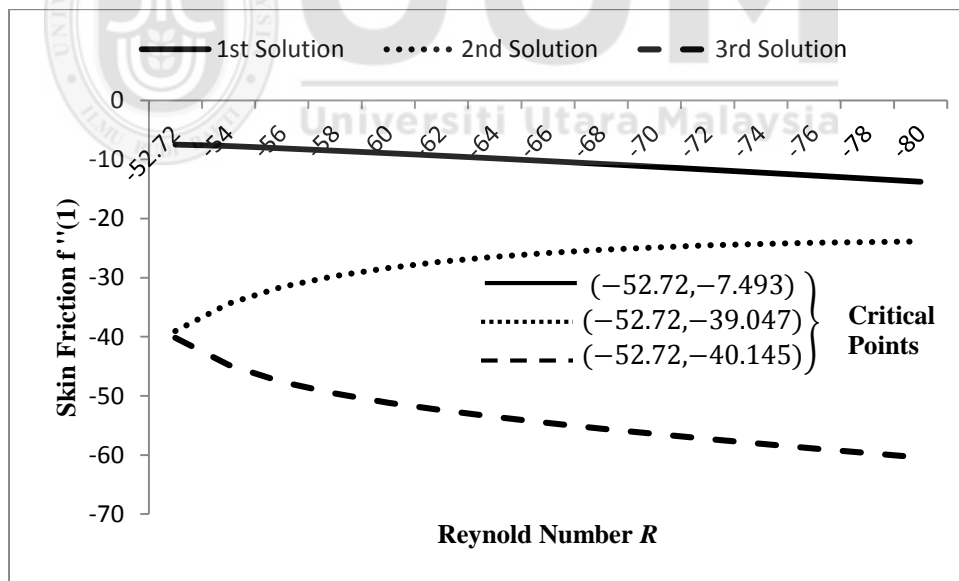
Figure 4.22. Variation of $f''(1)$ with Reynolds number R when $M = 0.4, \beta = 0.3, \alpha = 0.1$
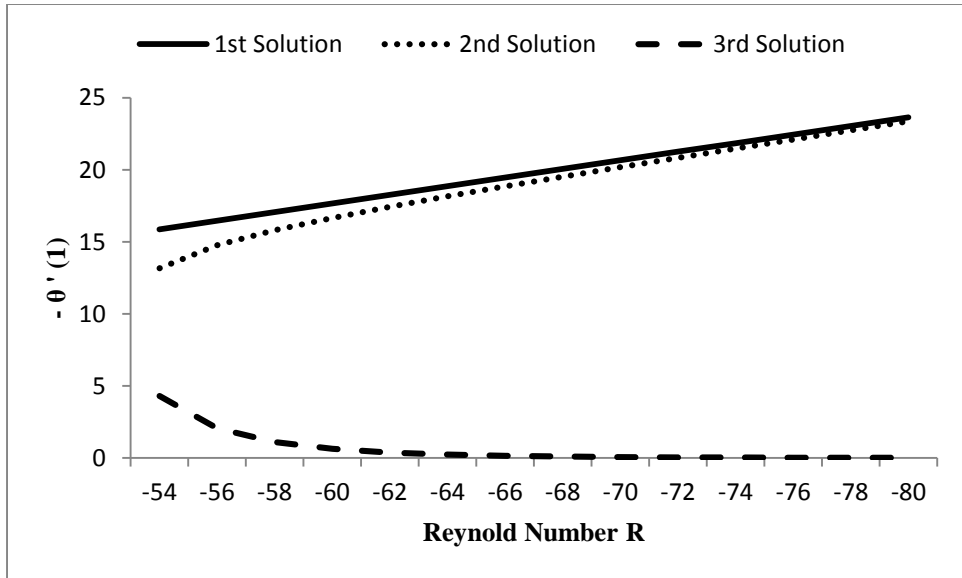
Figure 4.23. Variation of $-\theta'(1)$ with Reynolds number R when $Pr = 0.3, M = 0.4, \beta = 0.3, \alpha = 0.1$
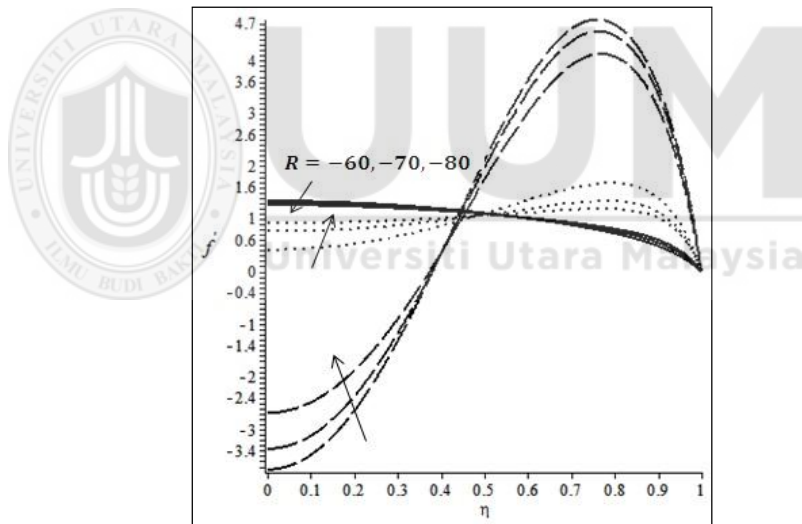
Figure 4.24. Effect of Suction on Velocity profile $f'(y)$ for $\alpha = 1, M = 0.4, \beta = 0.3$
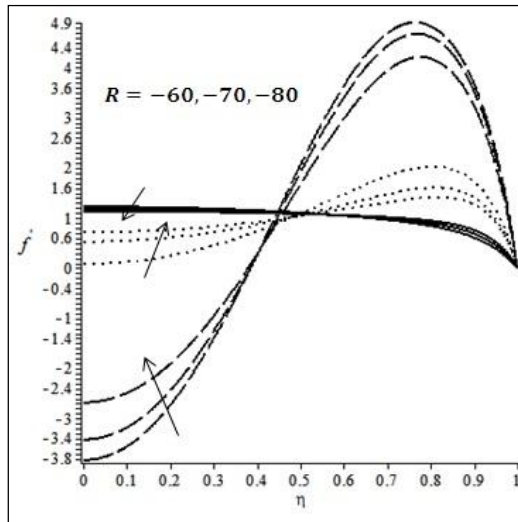
Figure 4.25. Effect of Suction on Velocity profile $f'(y)$ for $\alpha = -1, M = 0.4, \beta = 0.3$
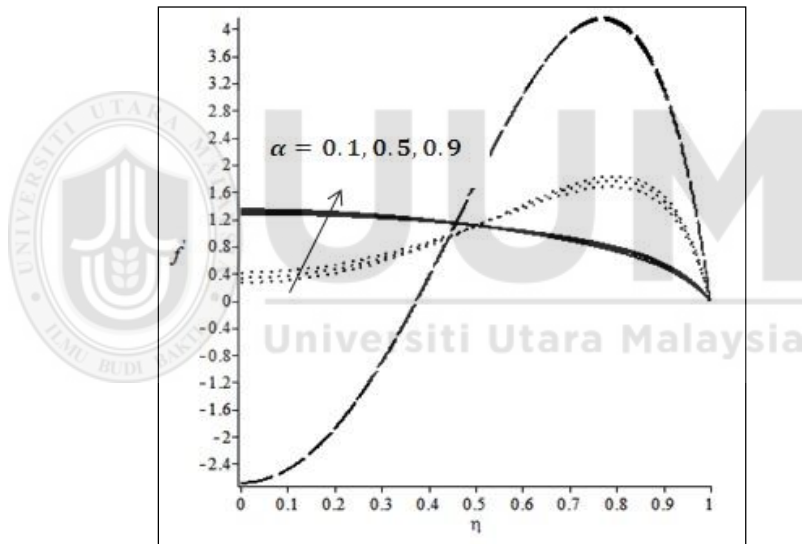
Figure 4.26. Effect of Wall expansion ratio $\alpha > 0$ on velocity profile $f'(\eta)$ for $R = -60, M = 0.4, \beta = 0.3$
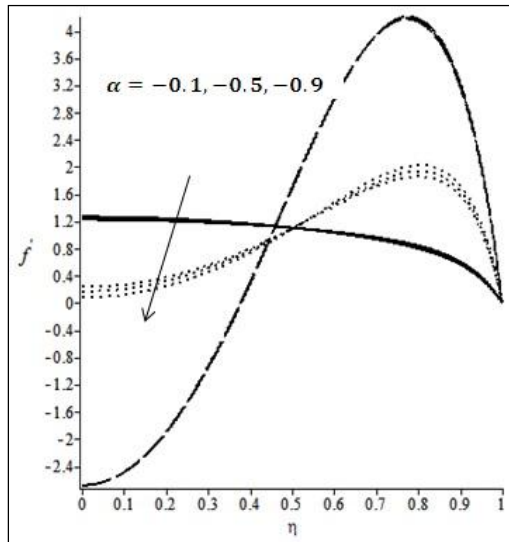
Figure 4.27. Effect of Wall expansion ratio $\alpha < 0$ on velocity profile $f'(\eta)$ for $R = -60, M = 0.4, \beta = 0.3$
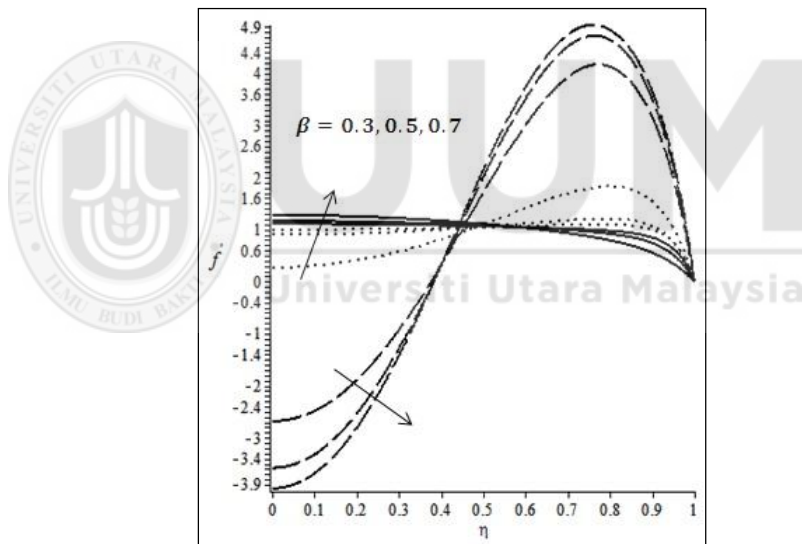
Figure 4.28. Effect of Casson Parameter β on velocity profile $f'(\eta)$ for $R = -60, M = 0.4, \alpha = 0.1$
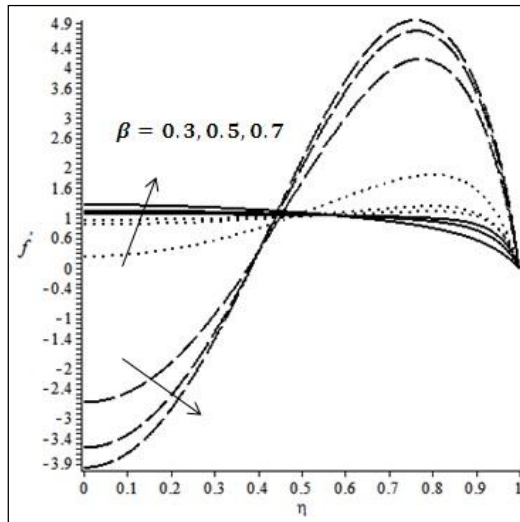
Figure 4.29. Effect of Casson Parameter β on velocity profile $f'(\eta)$ for $R = -60, M = 0.4, \alpha = -0.1$
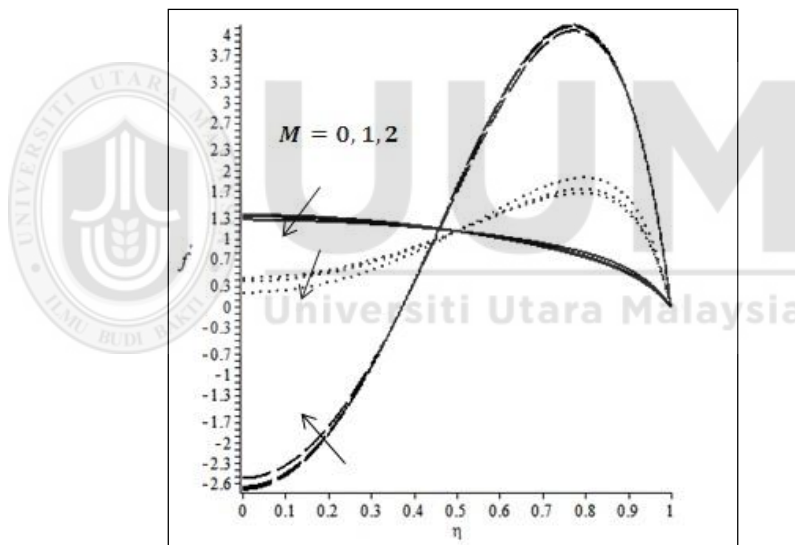
Figure 4.30. Effect of Magnetic field M on velocity profile $f'(\eta)$ for $R = -60, \beta = 0.3, \alpha = 1$
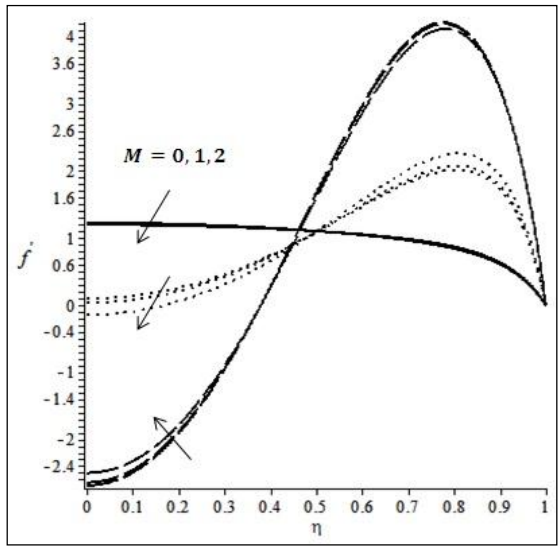
Figure 4.31. Effect of Magnetic field M on velocity profile $f'(\eta)$ for $R = -60, \beta = 0.3, \alpha = -1$
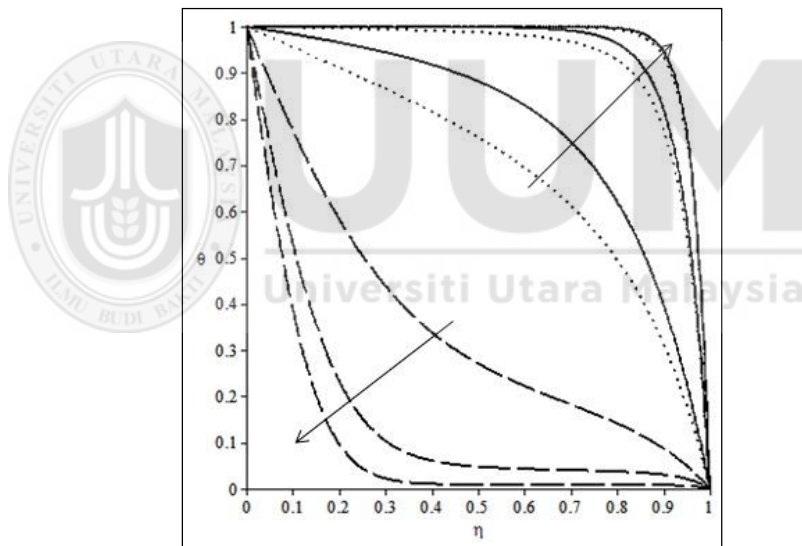
Figure 4.32. Effect of Prandtl number $Pr = 0.1, 0.3, 0.5$ on $\theta(\eta)$ for for $R = -60, \beta = 0.3, \alpha = 0.1, M = 0.4$

115
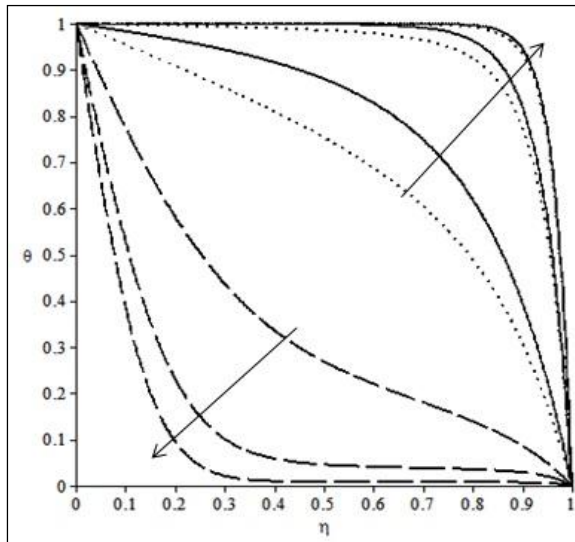
Figure 4.33. Effect of Prandtl number $Pr = 0.1, 0.3, 0.5$ on $\theta(\eta)$ for for $R = -60, \beta = 0.3, \alpha = -0.1, M = 0.4$

Table 4.9

Smallest eigenvalues against the various values of wall contraction parameter α

R	M	α	β	Pr	1st solution λ	2nd solution λ	3rd solution λ
		0			1.9257	-0.2597	-0.9465
-52.72	0.4		0.3				
		-0.1		0.7	2.1057	-0.2272	-0.8203
		-0.3			2.3957	-0.1947	-0.6941
		-0.5			2.4862	-0.0342	-0.5604

116

CHAPTER FIVE
NUMERICAL INVESTIGATIONS OF SOME PROBLEMS OF MICROPOLAR FLUID IN A CHANNEL

This chapter investigates the rheology of micropolar fluid in a channel of different walls' topologies. The effect on streamwise, microrotation, heat transfer and other physical parameters are briefly investigated. The classical Navier-Stokes model is inadequate to describe some modern engineering structures which are often made up of materials possessing and internal structure. The fluids containing additives, materials with fibrous or coarse grain structures and poly crystalline materials containing internal structure fall in this category. Hoyt and Fabula (1964) experimentally predicted that the fluid which cannot be characterized by Newtonian relationships indicates significant reduction of shear stress near a rigid body and it can be well explained in the micropolar model introduced by Eringen (1964).

5.1 Eringen Model for Micropolar fluid

In 1953, the theory of micropolar fluid was firstly introduced by Eringen. He stated that the impact of microration on microstructure model depicts micropolar fluid. These fluids have microscopic effects, coming from the local structure and micro motions of the fluid elements. These fluids are influenced by spin inertia and can support stress momentum and body momentum. Complicated fluid problems can be solved with the help of Eringen's theory including the flow of low concentration suspensions, blood, liquid crystals and turbulent shear flows. Micropolar fluids have five additional coefficients of viscosity as compared to classical Newtonian fluids. Physically micropolar fluids may represent fluids consisting of rigid, randomly oriented (or

117

spherical) particles suspended in a viscous medium, where the deformation of fluid particles is ignored. The fluids consisting of bar-like elements and certain anisotropic fluids, for example, liquid crystals which are made up of dumbbell molecules are of this type. Animal blood also falls into this category. Moreover, the mathematical model of polymeric fluids and fluids with certain additive may resemble the mathematical model of the micropolar fluids.

This model can cover many phenomena both in theory and applications than the classical Newtonian model. Polymeric suspensions, blood, colloids liquid crystals, muddy fluids, biological fluids are some examples of micropolar fluids whose bulk properties are different from those of Newtonian fluids. Micropolar fluids have five additional coefficients of viscosity as compared to the classical Newtonian fluids. Physically, these fluids may represent the fluid consisting of rigidly and randomly oriented particles suspended in a viscous medium possessing both translational and rotational motions. This matter have applications in blood flow, turbulent shear flows, lubricants, granular flows and flow in microchannels. A perturbation technique was used by Benis (1968) who considered the flow of non- Newtonian fluid through porous media in a narrow three-dimensional channels of varying gap. Rao and Iyengar (1981) investigated the slow stationary flow of incompressible micropolar fluid passing a spheroid (prolate and oblate) using the Stokesian approximation. These researchers obtained the velocity, microrotation, stress and couple stress analytically in an infinite series form. The drag on the body was determined and conclusion was made that no couple was exerted on the body, and micropolarity of the fluid has a supplementary effect on the drag. The laminar free convection boundary layer flow of a thermomicropolar fluid passing a non-isothermal vertical flat plate was examined by

Jena and Mathur (1981). They succeeded in finding a similarity solution by prescribing the plate temperature as a linear function of the streamwise coordinates. Meanwhile, Sastry and Rao (1982) discussed the effects of suction parameter on laminar micropolar fluid in a porous channel. Suitable similarity transformations were used to transform partial differential equations (PDEs) into ordinary differential equations (ODEs) and were solved numerically.

5.1.1 Mathematical Description of Micropolar Fluid

The general equations governing the motion of micropolar fluids as given (Eringen, 1964) may be expressed as:

$$\frac{\partial \rho}{\partial t} + \nabla \cdot (\rho \bar{V}) = 0 \tag{5.1}$$

$$(\lambda + 2\mu + \kappa)\nabla(\nabla \cdot \bar{V}) - (\mu + \kappa)\nabla \times \nabla \times \bar{V} + \kappa\nabla \times \bar{v} - \nabla p + \rho\bar{f} = \rho\dot{\bar{V}} \tag{5.2}$$

$$(\alpha + \beta + \gamma)\nabla(\nabla \cdot \bar{v}) - \gamma(\nabla \times \nabla \times \bar{v}) + \kappa\nabla \times \bar{V} - 2\kappa\bar{v} + \rho\bar{l} = \rho j\dot{\bar{v}} \tag{5.3}$$

$$\nabla \cdot \bar{B} = 0 \tag{5.4}$$

$$\nabla \times \bar{B} = \mu_m \bar{J}, \tag{5.5}$$

$$\nabla \times \bar{E} = 0 \tag{5.6}$$

$$\bar{J} = \sigma(\bar{E} + \bar{V} \times \bar{B}) \tag{5.7}$$

where $\bar{V}$ is the velocity field, $\bar{v}$ is the microrotation vector, ρ is the density, p is the pressure, $\bar{f}$ and $\bar{l}$ are the body force and body couple per unit mass respectively, j is the micro-inertia, $\lambda, \mu, \alpha, \beta, \gamma$ and κ are the micropolar material constants (or viscous coefficients), dot signifies material derivatives, $\bar{J}$ is the current density and $\bar{B}$ is total magnetic field so that $\bar{B} = \bar{B}_\circ + \bar{b}$, $\bar{b}$ is the conductivity of the fluid. Moreover, $\nabla \cdot \bar{J} = 0$ is obtained from Equations (5.4) - (5.5).

The uniform stationary magnetic field $\bar{B}$ is applied transverse in direction and magnetic Reynolds number is taken small (Shercliff, 1965). Consequently, the induced magnetic field $\bar{b}$ is negligible. Furthermore, polarization voltage is not applied, therefore electric field (i.e. $\bar{E} = 0$) is vanished. This vanishing means that the fluid follows conservation in energy (no energy is extracted or added to the fluid). Applying these assumptions, electromagnetic body force occurs in Equation (5.2) takes the following linearized form (Rossow, 1958):

$$\bar{f} = \bar{J} \times \bar{B} = \sigma[(\bar{V} \times \bar{B}_\circ) \times \bar{B}_\circ] = (-\sigma B_\circ^2 u, 0, 0) \tag{5.8}$$

Components of the velocity vector $\bar{V}$ and micro-rotation $\bar{v}$ are in the form of

$$\bar{V} = (u(x,y), v(x,y), 0) \qquad \bar{v} = (0,0, g(x,y)) \;,$$

where, g is the component of the micro-rotation normal to the xy-plane.

The governing equations of the flow for the proposed problem are:

$$\frac{\partial u}{\partial x} + \frac{\partial v}{\partial y} = 0 \tag{5.9}$$

$$u\frac{\partial u}{\partial x} + v\frac{\partial u}{\partial y} = \frac{-1}{\rho}\frac{\partial p}{\partial x} + \frac{\mu + \kappa}{\rho}\nabla^2 u + \frac{\kappa}{\rho}\frac{\partial g}{\partial y} - \frac{\sigma B_\circ^2 u}{\rho} \tag{5.10}$$

$$u\frac{\partial v}{\partial x} + v\frac{\partial v}{\partial y} = \frac{-1}{\rho}\frac{\partial p}{\partial y} + \frac{\mu + \kappa}{\rho}\nabla^2 v - \frac{\kappa}{\rho}\frac{\partial g}{\partial x} \tag{5.11}$$

$$\rho\bar{J}\left(u\frac{\partial g}{\partial x} + v\frac{\partial g}{\partial y}\right) = \gamma\nabla^2 g + \kappa\left(\frac{\partial v}{\partial x} - \frac{\partial u}{\partial y}\right) - 2\kappa g \tag{5.12}$$

5.2 Heat Transfer Analysis of MHD Micropolar Fluid in a Porous Channel

A numerical parameter study is conducted for MHD micropolar fluid in a porous channel to investigate different branches of the solutions. Rheology of micropolar fluid with heat transfer is analyzed. Governing PDEs were reduced into ODEs by applying

120

similarity transformation and then solved numerically with the help of shooting technique. The problem investigated by Ganesh and Krishnambal (2006) is the most appropriate and relevant reference of this problem. Ganesh and Krishnambal (2006) examined the flow of viscous fluid in a porous channel and discussed the numerical solution obtained from R-K-Gill method.

5.2.1 Problem Formulation

A steady, laminar and incompressible MHD micropolar fluid in a porous channel is considered. Fluid is taken in the direction of x-axis and channel walls are in the direction of y-axis. Lower and upper walls of the channel are at $y = -h$ and $y = h$ respectively. A uniform magnetic field is applied perpendicular to the channel walls and fluid can be injected or extracted from these porous walls. Moreover, magnetic field is negligible and tends to zero as compare with the imposed field.

The governing equations of the flow for the proposed problem are:

$$\frac{\partial u}{\partial x} + \frac{\partial v}{\partial y} = 0 \tag{5.13}$$

$$u\frac{\partial u}{\partial x} + v\frac{\partial u}{\partial y} = \frac{-1}{\rho}\frac{\partial p}{\partial x} + \frac{\mu + \kappa}{\rho}\nabla^2 u + \frac{\kappa}{\rho}\frac{\partial g}{\partial y} - \frac{\sigma B_\circ^2 u}{\rho} \tag{5.14}$$

$$u\frac{\partial v}{\partial x} + v\frac{\partial v}{\partial y} = \frac{-1}{\rho}\frac{\partial p}{\partial y} + \frac{\mu + \kappa}{\rho}\nabla^2 v - \frac{\kappa}{\rho}\frac{\partial g}{\partial x} \tag{5.15}$$

$$\rho\bar{J}\left(u\frac{\partial g}{\partial x} + v\frac{\partial g}{\partial y}\right) = \gamma\nabla^2 g + \kappa\left(\frac{\partial v}{\partial x} - \frac{\partial u}{\partial y}\right) - 2\kappa g \tag{5.16}$$

The boundary conditions for velocity and micro-rotation fields for the present problem are:

$$y = -h\colon u = 0, \qquad v = \frac{v_\circ}{2}, \qquad g = 0 \tag{5.17}$$

$$y = h: u = 0, \qquad v = \frac{v_\circ}{2}, \qquad g = 0 \tag{5.18}$$

Strong concentrated particle flows in which microelements close to the channel walls are unable to rotate is considered. The following equation introduces the similarity transformation:

$$u = -v_\circ \frac{x}{h} f'(\eta), v = v_\circ f(\eta), \eta = \frac{y}{h} \tag{5.19}$$

By inserting Equation (5.19) into Equations (5.13) - (5.16):

$$(1 + C_1) f^{iv} + C_1 g'' + R(f' f'' - f f''') + M^2 f'' = 0 \tag{5.20}$$

$$\left(1 + \frac{C_1}{2}\right) g'' - N(f'' + 2g) + R(f' g - f g') = 0 \tag{5.21}$$

where $C_1 = \frac{\kappa}{\mu}$ is vortex viscosity parameter, $N = \frac{\kappa h^2}{\mu j}$ is micro-inertia spin parameter, $M^2 = \frac{\sigma B_\circ^2 h^2}{\mu}$ is magnetic parameter and $R = \frac{v_\circ h}{\nu}$ is the Reynolds number, $R > 0$ is for suction and $R < 0$ is for injection.

$$y = \pm h: f' = 0, \qquad f = \frac{1}{2}, \qquad g = 0 \tag{5.22}$$

For the symmetric case:

$$y = 1: f' = 0, \qquad f = \frac{1}{2}, \qquad g = 0 \tag{5.23}$$

$$y = 0: f'' = 0, \qquad f = 0, \qquad g = 0 \tag{5.24}$$

5.2.2 Heat Transfer

For temperature distribution in the flow field, the governing energy equation can be written as:

$$\rho C_P \left(u \frac{\partial T}{\partial x} + v \frac{\partial T}{\partial y}\right) = k_\circ \frac{\partial^2 T}{\partial y^2} \tag{5.25}$$

where T is the temperature, $k_\circ$ is the thermal conductivity and C_P is the specific heat.

The appropriate boundary conditions are:

$$y = 0: T = T_1 \tag{5.26}$$

$$y = h: T = T_2 \tag{5.27}$$

where, T_1 and T_2 are fixed temperatures of the lower and upper channel walls, respectively.

A dimensionless temperature θ is introduced such that:

$$\theta(\eta) = \frac{T - T_2}{T_1 - T_2}$$

where $T_2 = T_1 - Ax$ and A is the constant.

Using similarity transformation, Equation (5.19) reduces to:

$$\theta'' + Pe_h f' \theta - Pe_h f \theta' = 0 \tag{5.28}$$

where, $Pe_h = Pr \cdot R$ is Peclet number for the diffusion of heat and $Pr = \frac{\rho C_p h v_\circ}{\kappa_\circ}$ is the Prandtl number. Boundary conditions for θ can be obtained from Equations (5.26) - (5.27) as:

$$y = 0: \theta = 1 \tag{5.29}$$

$$y = 1: \theta = 0 \tag{5.30}$$

5.2.3 Stability Analysis

The analysis uses a steady flow solution of $f(\eta) = f_\circ(\eta)$ and $\theta(\eta) = \theta_\circ(\eta)$ which satisfies the boundary conditions in Eq. (5.23) - (5.24) and (5.29) – (5.30) and setting $\tau = t$ (Merkin 1986, Rosca & Pop 2013), such that;

$$f(\eta) = f_\circ(\eta) + e^{-\lambda t} F(\eta, t) \tag{5.31}$$

123

$$g(\eta) = g_\circ(\eta) + e^{-\lambda t}G(\eta,t) \tag{5.32}$$

$$\theta(\eta) = \theta_\circ(\eta) + e^{-\lambda t}H(\eta,t) \tag{5.33}$$

where

$0 < F(\eta,t) \ll 1,\ 0 < G(\eta,t) \ll 1$, λ is the unknown eigenvalues, $F(\eta,t)$, $G(\eta,t)$ and $H(\eta,t)$ are smallest relative to $f_\circ(\eta)$, $\theta_\circ(\eta)$ and $\varphi_\circ(\eta)$ respectively.

The governing equations of (5.20), (5.21) and (5.28) for unsteady case are as follows:

$$(1+c_1)\frac{\partial^4 f}{\partial \eta^4} + c_1\frac{\partial^2 g}{\partial \eta^2} + R\left(f\frac{\partial^3 f}{\partial \eta^3} - \frac{\partial f}{\partial \eta}\frac{\partial^2 f}{\partial \eta^2}\right) - M^2\frac{\partial^2 f}{\partial \eta^2} = \frac{\partial^3 f}{\partial \tau \partial \eta^2} \tag{5.34}$$

$$\left(1+\frac{c_1}{2}\right)\frac{\partial^2 g}{\partial \eta^2} - N\left(\frac{\partial^2 f}{\partial \eta^2} + 2g\right) + R\left(g\frac{\partial f}{\partial \eta} - f\frac{\partial g}{\partial \eta}\right) = 0 \tag{5.35}$$

$$\frac{\partial^2 \theta}{\partial \eta^2} + Pe_h\theta\frac{\partial f}{\partial \eta} - Pe_h f\frac{\partial \theta}{\partial \eta} = \frac{\partial \theta}{\partial \tau} \tag{5.36}$$

Substituting Equations (5.31) – (5.33) into Equations (5.34) - (5.36) and setting $\tau = 0$ (Merkin, 1986), resulting;

$$(1+c_1)F'''' + c_1 G'' + R(f_\circ F'' + F'f_\circ'' - f_\circ F''' - Ff_\circ''') + M^2 F'' + \lambda F'' = 0 \tag{5.37}$$

$$\left(1+\frac{c_1}{2}\right)G'' - N(f_\circ''G + F''g_\circ) + R(f_\circ'G + F'g_\circ - f_\circ G' - Fg_\circ') = 0 \tag{5.38}$$

$$H'' + Pe_h(f_\circ'H + F'\theta_\circ) - Pe_h(f_\circ H' + F\theta_\circ') + \lambda H = 0 \tag{5.39}$$

The boundary conditions are:

$$\begin{aligned}F(1) = 0, F'(1) = 0, G(1) = 0, H(1) = 1\\ F''(0) = 0, F(0), G(0) = 0, H(0) = 0\end{aligned} \tag{5.40}$$

$f_\circ(\eta)$, $\theta_\circ(\eta)$ and $\varphi_\circ(\eta)$ can be determined by the smallest eigenvalue λ due to the steady state flow solution. Therefore, the range of the possible eigenvalues can be determined by relaxing the boundary conditions on $f_\circ(\eta)$ and $\theta_\circ(\eta)$ as prescribed by Harris et al. (2009). Therefore, the boundary condition is relaxed to $G(1) \to 0$ and the system of differential equation new boundary condition $G'(0) = 1$ is solved.

5.2.4 Numerical Computation

Similar MATLAB function is used to reduce the Equations (5.37) - (5.39) into 1st order differential equation system. Shooting method is then applied to solve and to implore the multiple solutions of Equation (5.20) - (5.21) of boundary conditions in Equations (5.23) - (5.24). Converting Equation (5.20) – (5.21) of boundary value problem into initial value problem by setting:

$$Z_1 = \eta, Z_2 = f, Z_3 = f', Z_4 = f'', Z_5 = f''', Z_6 = g, Z_7 = g', Z_8 = \theta, Z_9 = \theta'$$

Then the following system of differential equations is obtained,

$$
\begin{pmatrix} Z_1' \\ Z_2' \\ Z_3' \\ Z_4' \\ Z_5' \\ Z_6' \\ Z_7' \\ Z_8' \\ Z_9' \end{pmatrix}
=
\begin{pmatrix}
1 \\
Z_3 \\
Z_4 \\
Z_5 \\
\frac{-C_1}{(1+C_1)}\left(\frac{N}{\left(1+\frac{C_1}{2}\right)}(Z_4 + 2Z_6) - \frac{R}{\left(1+\frac{C_1}{2}\right)}(Z_3 Z_6 - Z_2 Z_7) \right) - \frac{R}{(1+C_1)}(Z_3 Z_4 - Z_2 Z_5) - \frac{M^2}{(1+C_1)}Z_4 \\
Z_7 \\
\frac{N}{\left(1+\frac{C_1}{2}\right)}(Z_4 + 2Z_6) - \frac{R}{\left(1+\frac{C_1}{2}\right)}(Z_3 Z_6 - Z_2 Z_7) \\
Z_9 \\
Pe_h f Z_9 - Pe_h Z_3 \theta
\end{pmatrix}
\quad (5.41)
$$

with initial conditions:

$$
\begin{pmatrix} Z_1 \\ Z_2 \\ Z_3 \\ Z_4 \\ Z_5 \\ Z_6 \\ Z_7 \\ Z_8 \\ Z_9 \end{pmatrix}
=
\begin{pmatrix} 1 \\ \frac{1}{2} \\ 0 \\ \alpha \\ \beta \\ 0 \\ \gamma \\ 1 \\ \delta \end{pmatrix}
\quad (5.42)
$$

α, β and γ and δ are unknown initial conditions and can be determined using shooting strategy. Once slope of α, β and γ is obtained, then numerical integration is made for the initial value problem and accuracy of missing initial conditions is then checked by comparing calculated value with the given terminal point.

5.2.5 Results and Discussions

This section presents the effect of suction $R > 0$, magnetic field M, vortex viscosity parameter C_1 and micro-inertia spin parameter N on skin friction, velocity and microrotation profiles.

Figure 5.1 shows a plot of skin friction $f''(1)$ against the values of Reynolds number $R > 0$ for the fixed values of $C_1 = 0.3, N = 0.2$ and for $M = 0.5$. The computed results show multiple solutions of the proposed problem only for the numerical value of Reynolds number $R = 26.56$. The critical values is depicted at $R = R_{crtical} = 26.56$, which shows multiple solutions occurred only for $R \geq R_{critical}$. Moreover, single solution only exists in the case of injection < 0. These results are presented in the form of pictorial representation in Figure 5.1. The effect of vortex viscosity parameter C_1 on velocity profile $f'(\eta)$ is presented in Figure 5.2. Velocity of the fluid particles decreases near the walls of the channel $\eta \approx 1$ for I-Type and III-Type of the solutions by increasing the numerical values of C_1. This behavior was described by Eringen (1964), Hoyt and Fabula (1964) that non-Newtonian fluid near the rigid body offers great reduction of the fluid velocity. However, totally reverse trend is observed for the II-Type of the solution. Figure 5.3 exposed the effect of vortex viscosity parameter C_1 on micro-rotation profile $g(\eta)$. The effect of vortex viscosity parameter C_1 on micro-rotation profile $g(\eta)$ is naturally parabolic. When the values of C_1 profile increases, the micro-rotation also increases with strictly monotonic and exhibits parabolic

126

characteristics for I-Type of solution. On the other hand, quite opposite behavior is flattering for the case of II-Type solution. For the III-Type of solution, the profile is concave down for the values of $C_1 = 0.1, 0.3$ and concave up for the value of $C_1 = 0.5$. Figure 5.4 and 5.5 elucidate the effect of micro-inertia spin parameter N on velocity profile $f'(\eta)$ and micro-rotation profile $g(\eta)$ for $C_1 = 0.3, M = 0.5$ and for $R = 50$. No significant effect on velocity of the fluid particles for I-Type and III-Type of solutions but II-Type solution shows fluid particles decreases near the center of the channel $\eta \approx 0$ by increasing the values of N. Micro-rotation profile for I-Type of the solution increases by the enhancement of the numerical values of N and opposite trend is observed for the rest of the solutions. The effect of Reynolds number $R > 0$ (suction) on velocity and micro-rotation profile is depicted from Figures 5.6 and 5.7 for $C_1 = 0.3, N = 0.2$ and for $M = 0.5$. The velocity of the micropolar fluid increases monotonically near the channel walls $\eta \approx 1$ for I-Type and III-Type of solutions but decreases for II-Type when the strength of the suction is increased. Micro-rotation profiles are parabolic for multiple solutions. The velocity profile of $f'(\eta)$ decreases near the channel wall $\eta \approx 1$ by increasing the strength of the magnetic field M for I-Type and II-Type of solutions as shown in Figure 5.8. This is caused by the magnetic field at the channel wall so fluid's viscosity increases but the velocity decreases. The effect of magnetic field M on micro-rotation is depicted in Figure 5.9 by setting $C_1 = 0.1, N = 0.2$ and $R = 50$.

The variations of $\theta'(1)$ against the values of Reynolds number are presented in Figure 5.10. The profile of multiple solutions can be seen clearly in this pictographic representation. The effect of Peclet number Pe_h on temperature profile $\theta(\eta)$ is shown in Figure 5.11. From this topographical presentation, temperature profile $\theta(\eta)$ increases monotonically by increasing the values of Peclet number Pe_h throughout $0 \le \eta \le 1$ for

I-Type and II-Type of solutions. However, for III-Type of solution temperature profile $\theta(\eta)$ is split into two phases. In the first phase, $0 \leq \eta < 0.5$, the temperature profile $\theta(\eta)$ decreases by the enhancement of Peclet number Pe_h from 0.5 to 2.5. In the second phase $0 < \eta \leq 1$, totally opposite trend is observed. Figure 5.12 plotted to present the validation of the numerical results with previously published results of Ganesh and Krishnambal (2006). For this purpose, we set $C_1 = 0$, $N = 0$, $f(-1) = -1$, $f'(-1) = 0$, $f(1) = 1$, $f'(1) = 0$ and found an excellent agreement with the results of Ganesh and Krishnambal (2006) in the form of graph.

Numerical values of skin friction $f''(1)$ and shear stress $g'(1)$ at the channel wall is shown in Table 5.1 for various values of $R > 0$, magnetic field M, vortex viscosity parameter C_1 and micro-inertia spin parameter N. Heat transfer rate is presented in Table 5.2 for variations of Peclet number Pe_h. From these numerical data, the magnitude of the heat transfer rate is increasing as the value of Peclet number Pe_h is increased for I and II-Type of solutions. However, totally opposite trend of heat transfer rate is observed for III-Type of solution. Table 5.4 presents the smallest eigenvalue against several values of Reynolds number R. Table 5.4 depicts that eigenvalues of the 1st solution increase monotonically and positive, but decrease for the 2nd and the 3rd solutions. These results demonstrated that the 1st solution is physically reliable compared to the 2nd or the 3rd solutions
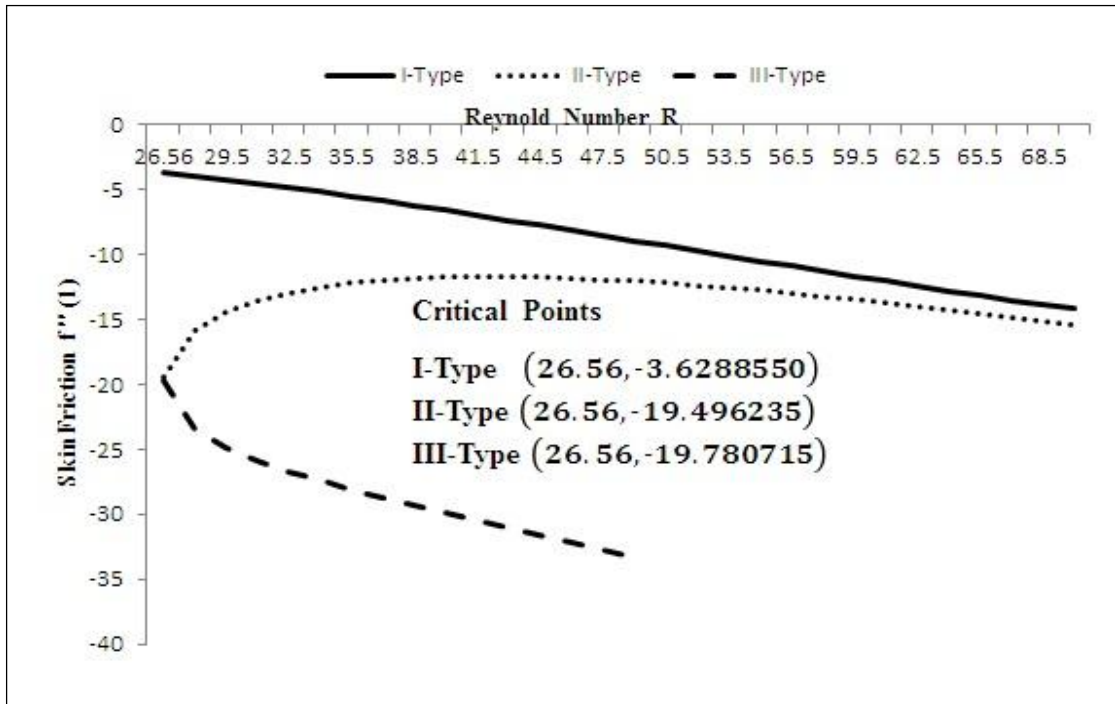
Figure 5.1. Skin friction at the wall against Reynolds number
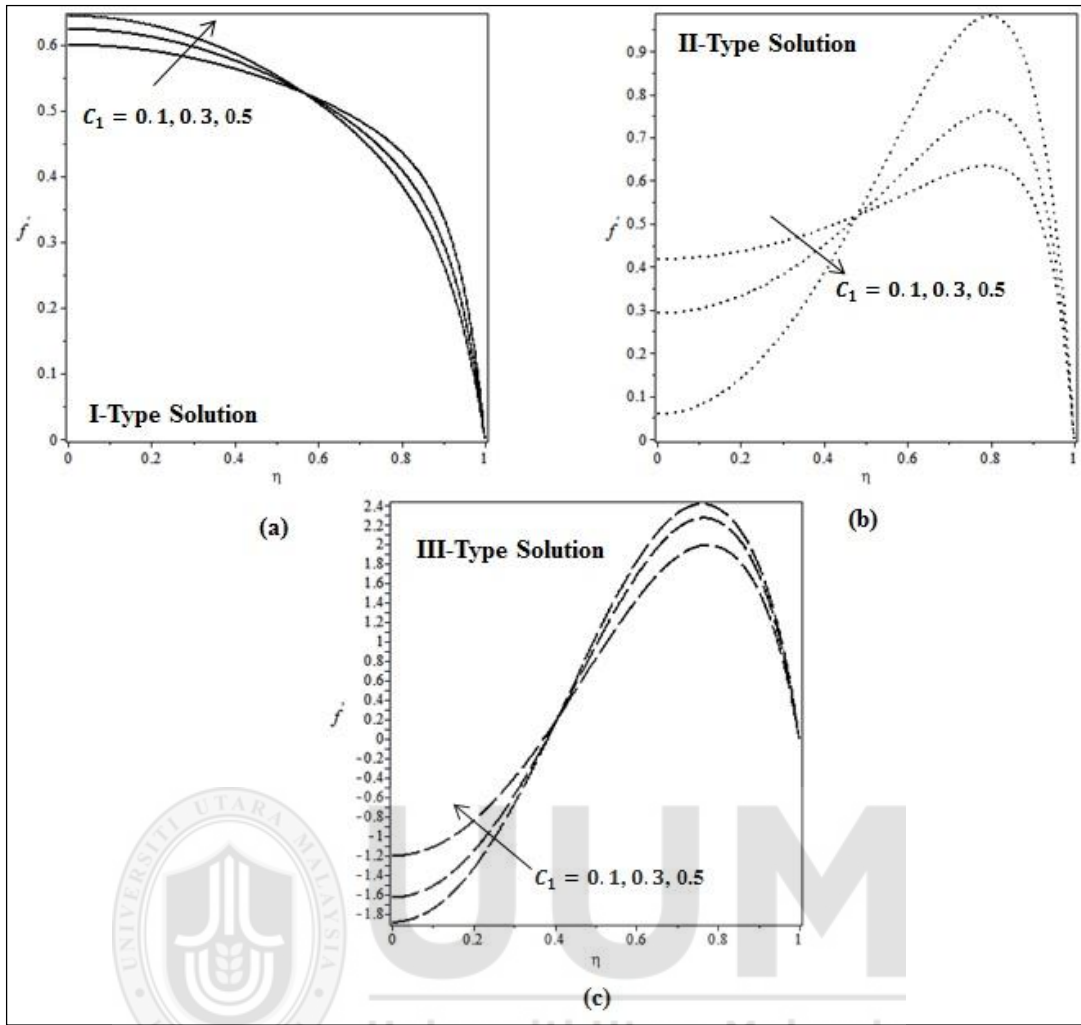
Figure 5.2. Effect of C_1 on streamwise velocity $f'(\eta)$ for $N = 0.2, M = 0.5$ and $R = 50$
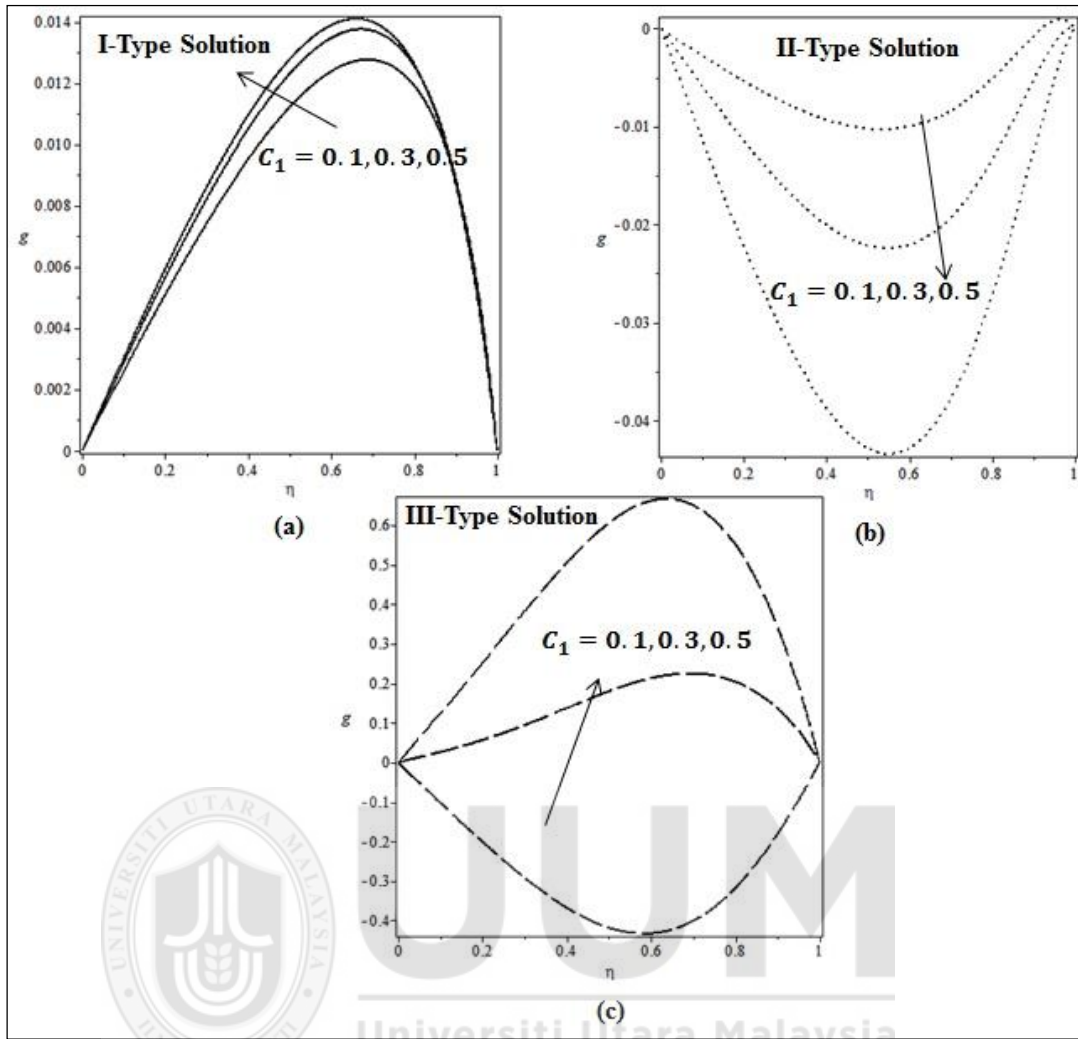
Figure 5.3. Effect of C_1 on microrotation profile $g(\eta)$ for $N = 0.2, M = 0.5$ and $R = 50$
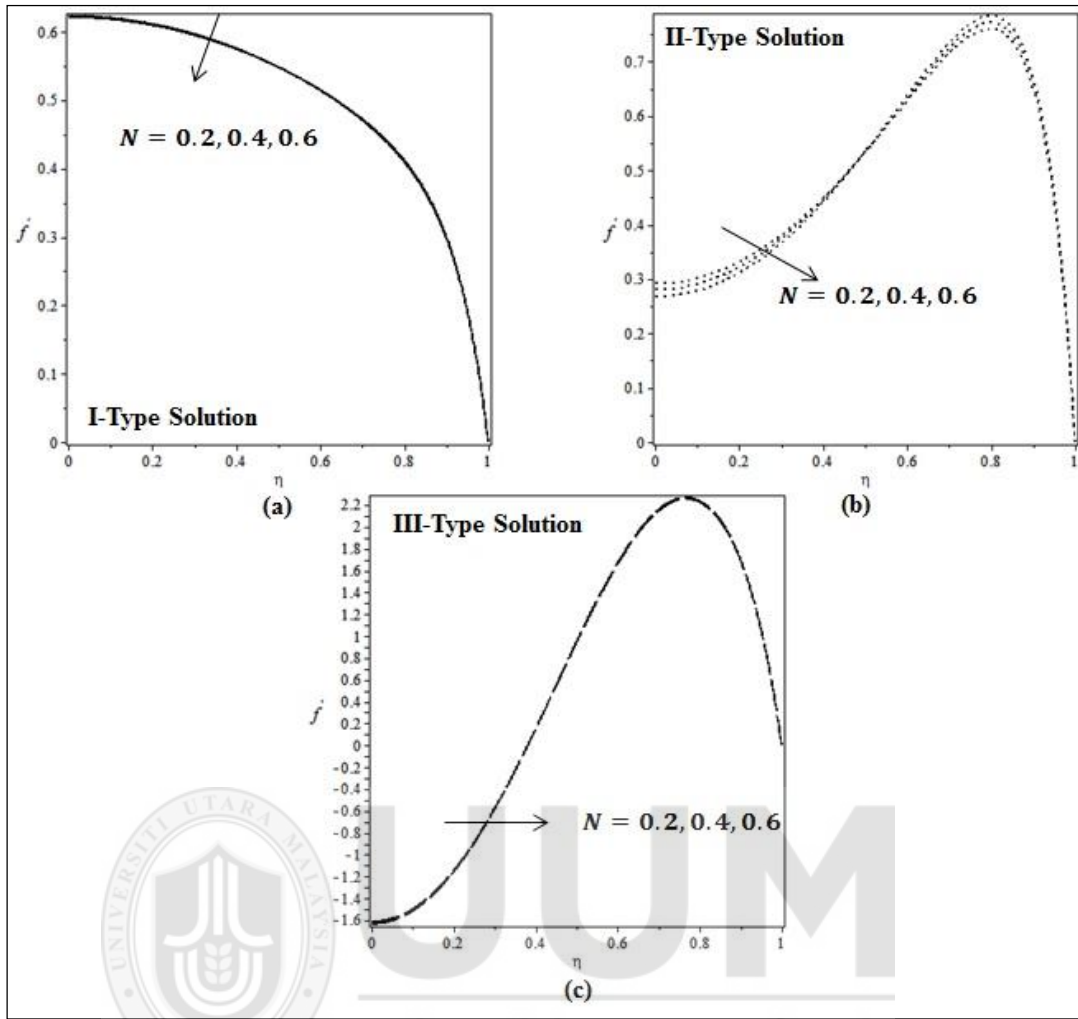
Figure 5.4. Effect of N on streamwise velocity $f'(\eta)$ for $C_1 = 0.3, M = 0.5$ and $R = 50$
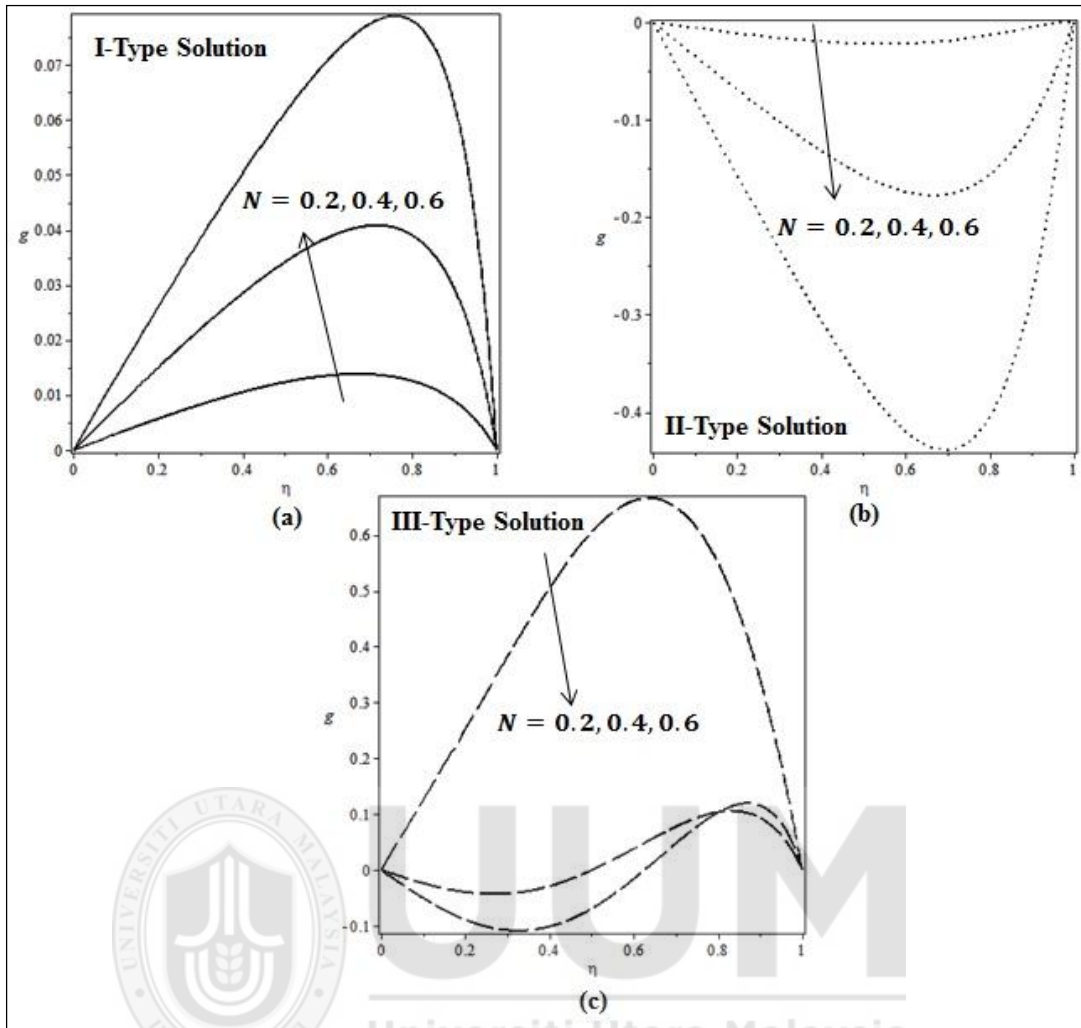
Figure 5.5. Effect of N on microrotation profile $g(\eta)$ for $C_1 = 0.3, M = 0.5$ and $R = 50$
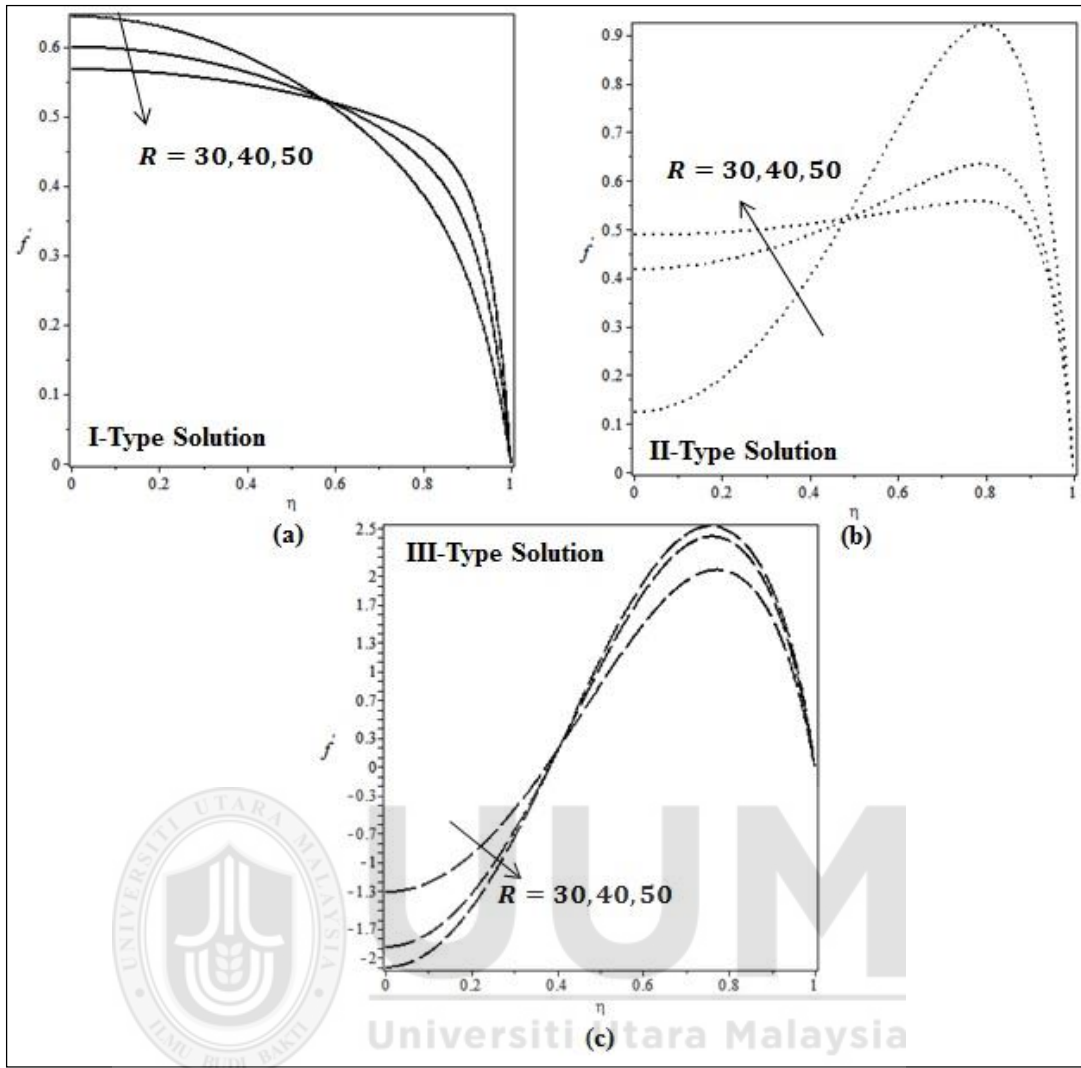
Figure 5.6. Effect of Reynolds number R on velocity profile $f'(\eta)$ for $C_1 = 0.3, N = 0.2$ and $M = 0.5$
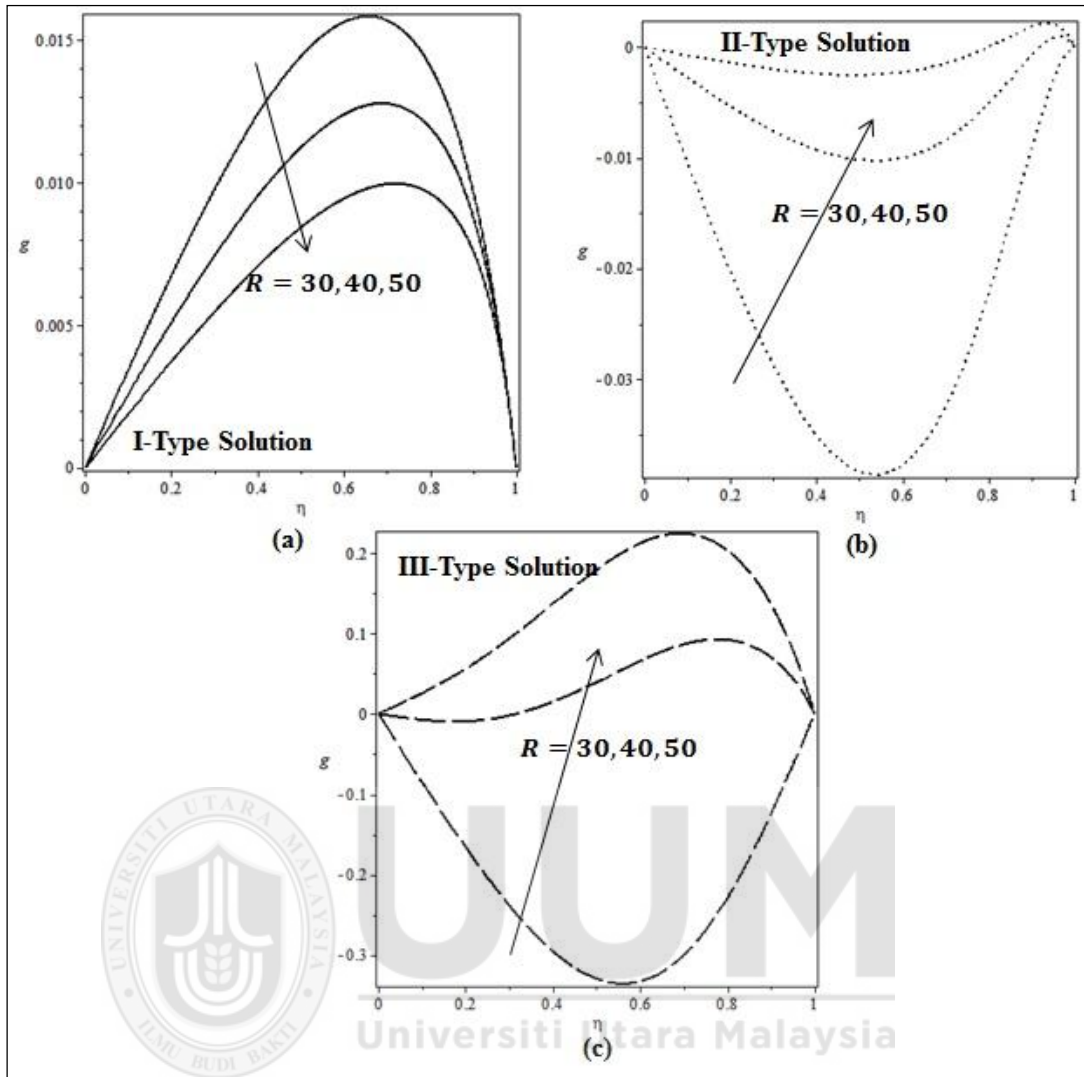
Figure 5.7. Effect of Reynolds number R on Microrotation $g(\eta)$ for $C_1 = 0.3, N = 0.2$ and $M = 0.5$
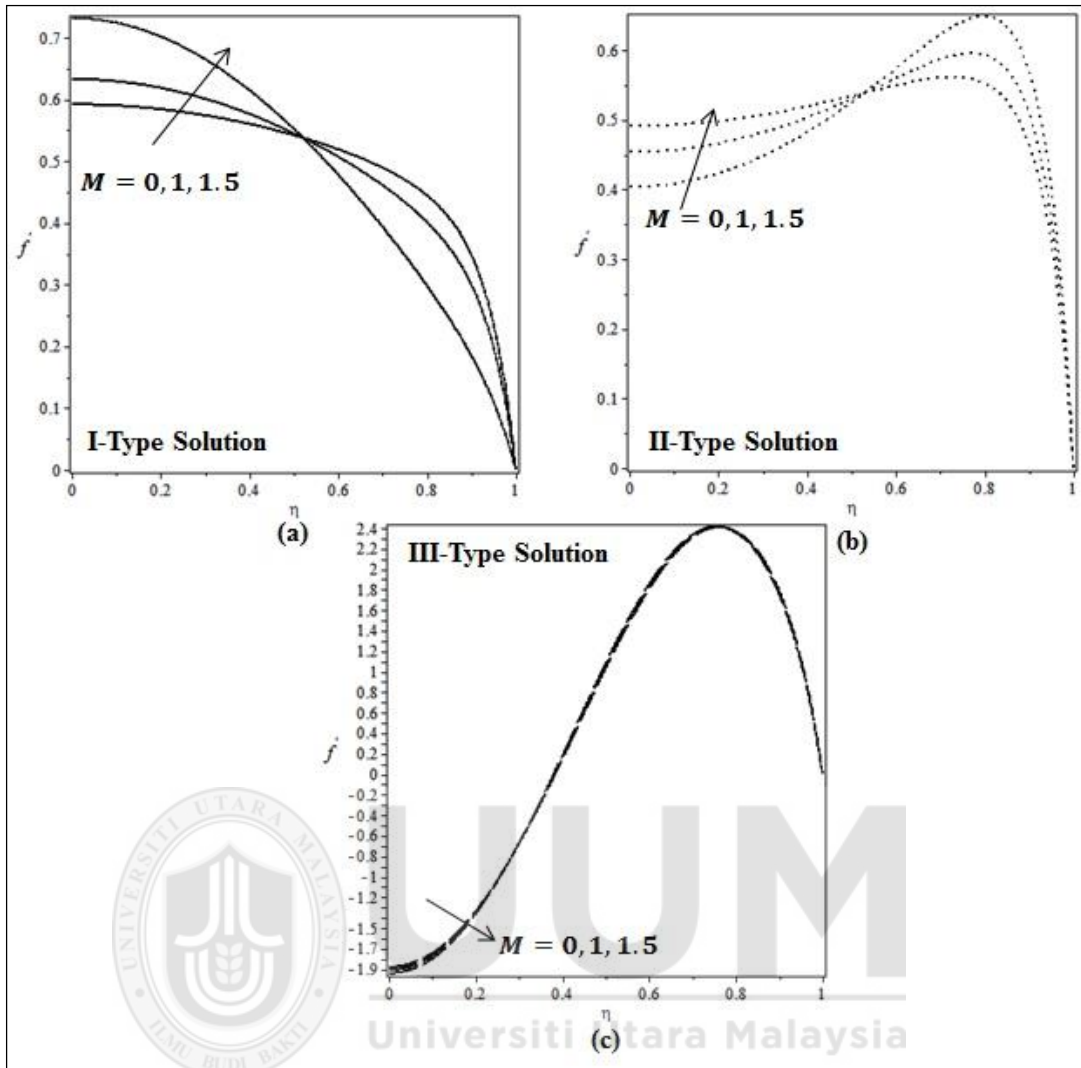
Figure 5.8. Effect of magnetic field M on velocity profile $f'(\eta)$ for $C_1 = 0.1, N = 0.2$ and $R = 50$
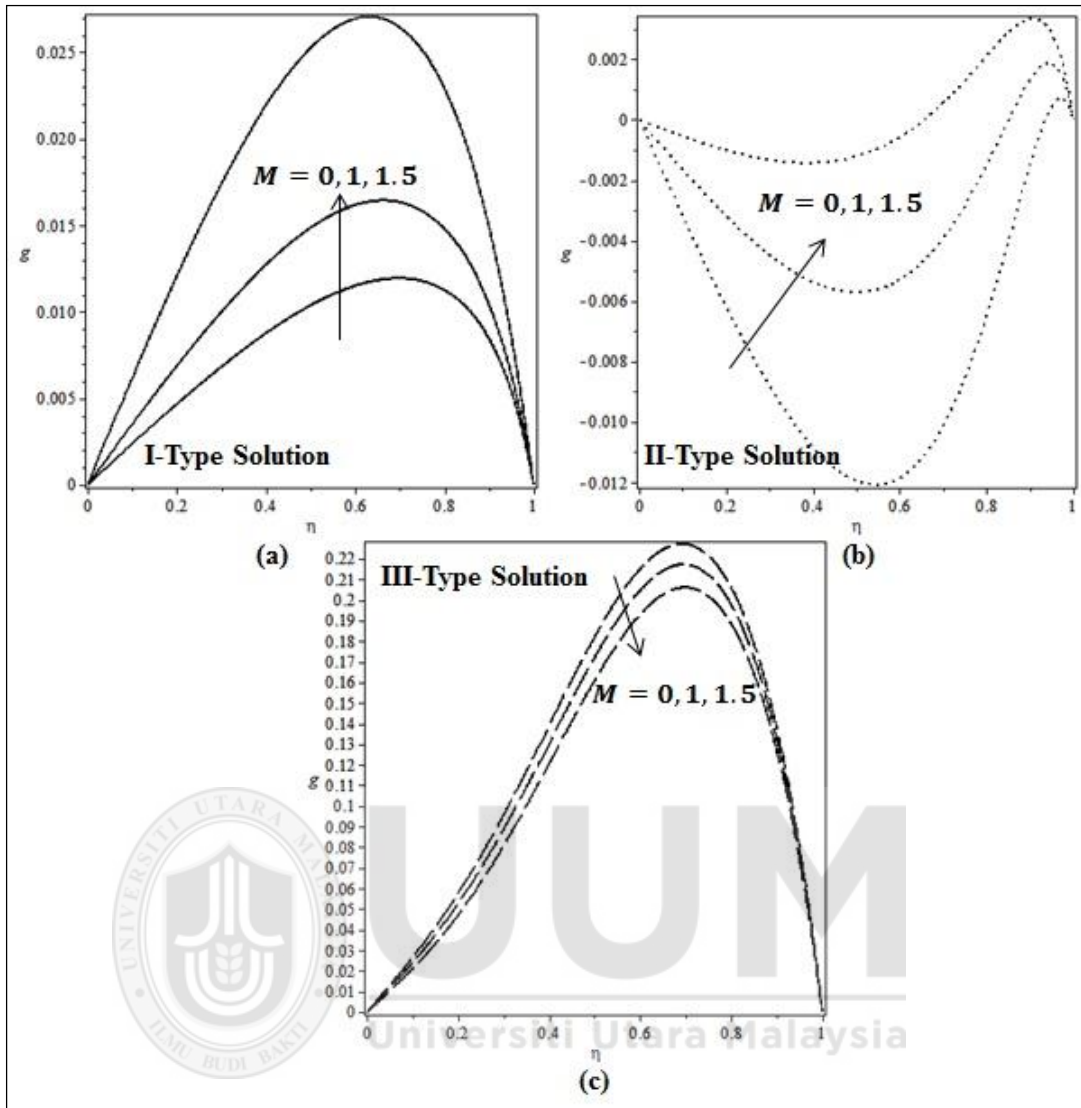
Figure 5.9. Effect of magnetic field M on microrotation profile $g(\eta)$ for $C_1 = 0.1, N = 0.2$ and $R = 50$
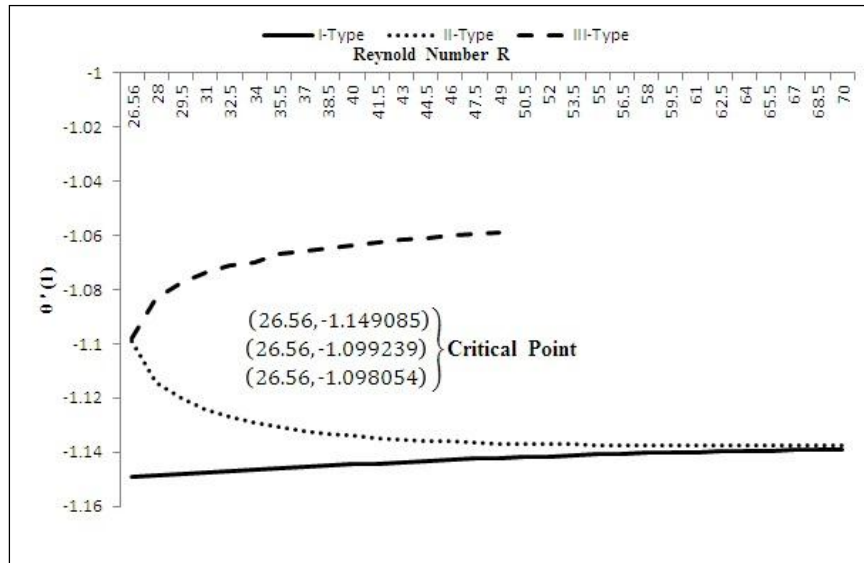
Figure 5.10. Variations of $\theta'(1)$ against the values of Reynolds number
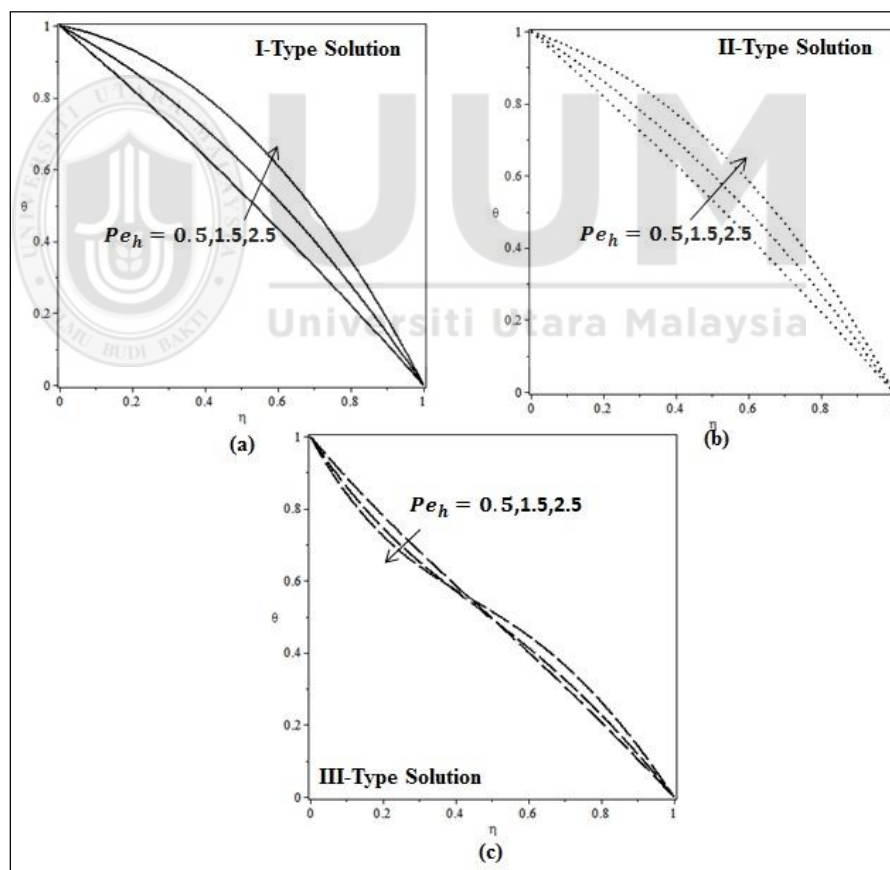
Figure 5.11. Effect of Peclet number Pe_h on temperature profile $\theta(\eta)$
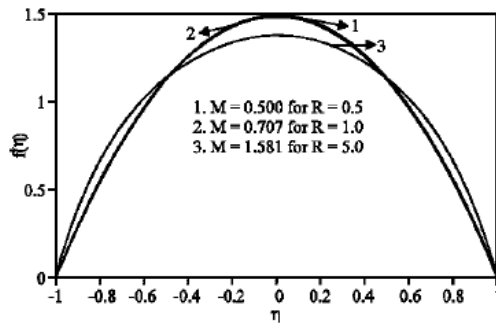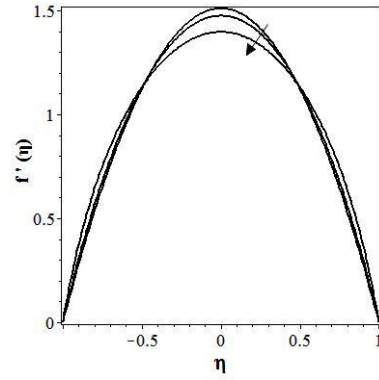
| Ganesh and Krishnambal (2006) | Present results for the same values of M and R |

Figure 5.12. Validation of physical model

Table 5.1

Effect of different parameters on shear and couple stresses

R	C_1	N	M	I-Type Solution		II-Type Solution		III-Type Solution	
				$f''(1)$	$g'(1)$	$f''(1)$	$g'(1)$	$f''(1)$	$g'(1)$
30	0.1	0.2	0.5	-4.487078	-0.143457	-13.560205	-0.002105	-25.914736	1.903009
40				-6.582673	-0.147967	-11.709335	-0.061752	-29.952809	-1.863112
50				-8.925834	-0.148068	-12.039470	-0.087899	-33.358408	-1.121543
40	0.1	0.2	0.5	-6.582673	-0.147967	-11.709335	-0.061752	-29.952809	-1.863112
	0.3			-5.156178	-0.138164	-12.646054	-0.011976	-27.542480	-4.250628
	0.5			-4.216380	-0.127789	-14.821986	0.063632	-24.638763	1.975517
40	0.1	0.2	0.5	-6.582673	-0.147967	-11.709335	-0.061752	-29.952809	-1.863112
		0.4		-6.602342	-0.508449	-11.757211	0.3503649	-29.961577	-1.749161
		0.6		-6.609633	-1.186382	-11.788404	5.7429194	-29.974608	-2.736792
40	0.1	0.2	0	-5.301661	-0.136253	-13.004141	-0.004558	-27.633910	-4.404887
			1	-4.605545	-0.145356	-11.609194	-0.032481	-27.264065	-3.854517
			1.5	-3.136794	-0.163974	-10.115760	-0.059702	-26.785785	-3.356378

139

Table 5.2

Heat transfer rate at the wall for various values of Peclet number Pe_h

Peclet number Pe_h	I-Type Solution $\theta'(1)$	II-Type Solution $\theta'(1)$	III-Type Solution $\theta'(1)$
0.5	-1.144657095	-1.134002697	-1.069150103
1.5	-1.498759072	-1.459761183	-1.063403522
2.5	-1.960434424	-1.881982339	-1.234055583

Table 5.3
Validation of Numerical Results

R	C_1	N	M	Pe	$f''(1)$ Shooting	$f''(1)$ Runge-Kutta-Fehlberg
0	0.1	0.2	0.5	0.5	-1.475429846	-1.475429746
10					-1.791018764	-1.791018974
20					-2.623877833	-2.623877952

Table 5.4

Smallest eigenvalues λ at several values of vortex viscosity parameter c_1

c_1	M	N	R	1st Solution λ	2nd Solution λ	3rd Solution λ
0				1.2821	-2.8243	-2.0638
0.1				1.2853	-2.8936	-2.6782
0.3	0.5	0.2	26.56	1.2868	-3.0352	-3.2452
0.5				1.2891	-3.1283	-3.5147

5.3 Micropolar Fluid in a Channel with Changing Walls: Multiple Solutions

This numerical study is performed to investigate the multiple solutions of micropolar fluid in a channel of changing walls. Mathematical modeling of laws of conservation of mass, momentum, angular momentum and energy is performed and governing PDEs

are converted into self-similar ODEs by applying suitable similarity transformation and then solved numerically using shooting method. A new branch of solutions is found and presented graphically and numerically for the various values of parameters, which has never been reported. DTM solution for two dimensional flow of micropolar fluid in a channel with expanding or contracting walls is investigated by Mosayebidorcheh (2014) and this study is relative to the problem considered in this section. Nevertheless, Mosayebidorcheh (2014) examined only the behavior of single solution but in this study we succeeded to find the different branches of the solution and find triple solutions. Moreover, we employed linear stability to check which solution is physically reliable.

5.3.1 Problem Formulation

Let us consider unsteady, laminar and incompressible micropolar fluid in a channel. Both the channel walls are considered equally permeable and can be expanded or contracted uniformly with time dependent rate $\dot{a}$. For the uniform wall suction/injection we assume that fluid is symmetric about $y - axis$ to the channel walls as described in physical model Figure 5.13.
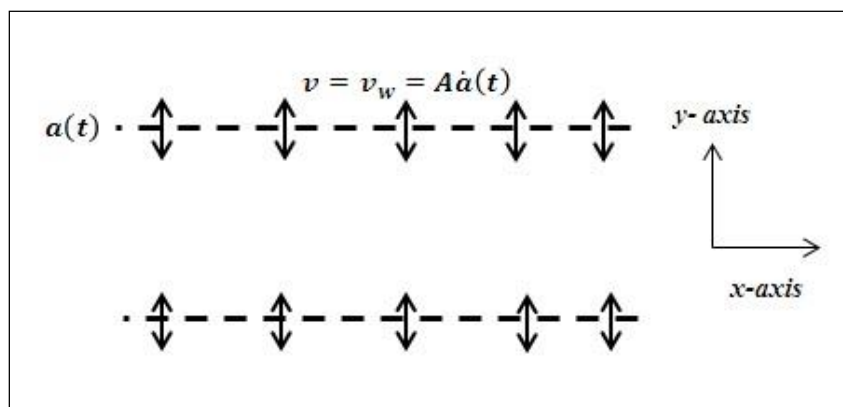
Figure 5.13. Physical model of the proposed problem

Governing equations of the flow for the proposed problem are:

$$\frac{\partial u}{\partial x} + \frac{\partial v}{\partial y} = 0 \tag{5.43}$$

$$u\frac{\partial u}{\partial x} + v\frac{\partial u}{\partial y} = \frac{-1}{\rho}\frac{\partial p}{\partial x} + \frac{\mu+\kappa}{\rho}\nabla^2 u + \frac{\kappa}{\rho}\frac{\partial g}{\partial y} \tag{5.44}$$

$$u\frac{\partial v}{\partial x} + v\frac{\partial v}{\partial y} = \frac{-1}{\rho}\frac{\partial p}{\partial y} + \frac{\mu+\kappa}{\rho}\nabla^2 v - \frac{\kappa}{\rho}\frac{\partial g}{\partial x} \tag{5.45}$$

$$\rho\bar{J}\left(u\frac{\partial g}{\partial x} + v\frac{\partial g}{\partial y}\right) = \gamma\nabla^2 g + \kappa\left(\frac{\partial v}{\partial x} - \frac{\partial u}{\partial y}\right) - 2\kappa g \tag{5.46}$$

with boundary conditions of:

$$\bar{u}(x,a) = 0, \bar{v}(a) = -v_w = -A\dot{a} \tag{5.47}$$

$$\frac{\partial\bar{u}}{\partial y}(x,0) = 0, \bar{v}(0) = 0 \tag{5.48}$$

Assumption at the channel walls is made such that fluid can be extracted or injected with the constant velocity v_w. Moreover, the coefficient of suction/injection $A \cong {v_w}/{\dot{a}}$ is a wall permeability parameter appears in Equation (5.47).

We can develop similar solution in the light of boundary conditions of Equation (5.47) - (5.48). For this purpose, $y \equiv \frac{\bar{y}}{a}$ is considered and stream function can be written as;

$$\psi = \frac{v}{a(t)}\bar{x}\bar{F}(\eta,t), g = va^{-3}xG(\eta,t) \text{ where } \eta = {y}/{a(t)} \tag{5.49}$$

Putting Equations (5.49) into Equations (5.43) - (5.46), we get:

$$(1+C_1)F_{\eta\eta\eta\eta} - C_1 G_{\eta\eta} + 3\alpha F_{\eta\eta} + \alpha\eta F_{\eta\eta\eta} + (F_\eta F_{\eta\eta} - FF_{\eta\eta\eta}) - v^{-1}a^2 F_{\eta\eta t} = 0 \tag{5.50}$$

$$\left(1+\frac{C_1}{2}\right)G_{\eta\eta} + N\alpha(3G+\eta G_\eta) + NF_\eta G - NFG_\eta - C_1(2G - F_{\eta\eta})$$

$$-v^{-1}a^2 G_t = 0 \tag{5.51}$$

where $\alpha = \frac{a\dot{a}}{v}$ is the wall expansion ratio; $\alpha > 0$ is for expansion and $\alpha < 0$ is for contraction, C_1 is vortex viscosity parameter, and N is micro-inertia spin parameter. $\alpha > 0\alpha < 0$

$R = \frac{av_w}{v}$ is the crossflow Reynolds number; $R > 0$ is for injection and $R < 0$ for suction through the walls.

For self-similar solution, we consider $f = \frac{\bar{F}}{R}$ and $g = \frac{G}{R}$ by the transformation introduced by Uchida & Aoki (1977), Dauenhauer & Majdalani (2003). This leads us to consider the case α is a constant and $f = f(\eta)$. Therefore, $f_{\eta\eta t} = 0$.

In the light of above provisions, Equations (5.50) and (5.51) becomes:

$$(1 + C_1)f'''' - C_1 g'' + 3\alpha f'' + \alpha \eta f''' + R(f'f'' - ff''') = 0 \tag{5.52}$$

$$\left(1 + \frac{C_1}{2}\right)g'' + N\alpha(3g + \eta g') + NR(f'g - fg') - C_1(2g - f'') = 0 \tag{5.53}$$

Appropriate boundary conditions are:

$$f'(1) = 0, f(1) = 1, g(1) = 0 \tag{5.54}$$

$$f(0) = f''(0) = g(0) = 0 \tag{5.55}$$

5.3.2 Heat Transfer

For the temperature distribution in the flow field, the governing energy equation can be written as:

$$\frac{\partial T}{\partial t} + \rho C_p \left(u \frac{\partial T}{\partial x} + v \frac{\partial T}{\partial y}\right) = k_\circ \left(\frac{\partial^2 T}{\partial x^2} + \frac{\partial^2 T}{\partial y^2}\right) \tag{5.56}$$

where, T is the temperature, $k_\circ$ is the thermal conductivity and C_P is the specific heat.

The appropriate boundary conditions are:

$$T = T_H \ at \ y = a \tag{5.57}$$

$$T = T_w \ at \ y = 0 \tag{5.58}$$

The dimensionless temperature θ is introduced as $\theta(\eta) = \frac{T - T_H}{T_w - T_H}$, and using similarity transformation, the Equation (5.56) becomes:

$$\theta'' + (PrfR + \alpha \eta Pr)\theta' = 0 \tag{5.59}$$

where $Pr = \frac{\rho C_p}{\kappa_\circ}$ is the Prandtl number. Boundary conditions for θ can be obtained from such that:

$$y = 0: \theta = 1 \tag{5.60}$$

$$y = 1: \theta = 0 \tag{5.61}$$

5.3.3 Stability Analysis

A steady flow solution $f(\eta) = f_\circ(\eta)$, $g(\eta) = g_\circ(\eta)$ and $\theta(\eta) = \theta_\circ(\eta)$ which satisfies the boundary conditions of Eq. (5.54) - (5.55) taken from (Merkin 1986, Rosca & Pop 2013) is expressed as:

$$f(\eta) = f_\circ(\eta) + e^{-\lambda t} F(\eta, t) \tag{5.62}$$

$$g(\eta) = g_\circ(\eta) + e^{-\lambda t} G(\eta, t) \tag{5.63}$$

$$\theta(\eta) = \theta_\circ(\eta) + e^{-\lambda t} H(\eta, t) \tag{5.64}$$

where $\tau = t$ and $0 < F(\eta, t) \ll 1$, $0 < G(\eta, t) \ll 1$ and λ is the unknown eigenvalues, $F(\eta, t)$, $G(\eta, t)$ and $H(\eta, t)$ are smallest relative to $f_\circ(\eta)$, $\theta_\circ(\eta)$ and $\varphi_\circ(\eta)$ respectively.

The governing equations of (5.52), (5.53) and (5.59) for unsteady case are as follows:

$$(1 + c_1)\frac{\partial^4 f}{\partial \eta^4} + c_1\frac{\partial^2 g}{\partial \eta^2} + 3\alpha\frac{\partial^2 f}{\partial \eta^2} + \alpha\eta\frac{\partial^3 f}{\partial \eta^3} + R\left(f\frac{\partial^3 f}{\partial \eta^3} - \frac{\partial f}{\partial \eta}\frac{\partial^2 f}{\partial \eta^2}\right) = \frac{\partial^3 f}{\partial \tau \partial \eta^2} \tag{5.65}$$

$$\left(1 + \frac{c_1}{2}\right)\frac{\partial^2 g}{\partial \eta^2} + N\alpha\left(3g + \eta\frac{\partial g}{\partial \eta}\right) - c_1\left(\frac{\partial^2 f}{\partial \eta^2} + 2g\right) + NR\left(g\frac{\partial f}{\partial \eta} - f\frac{\partial g}{\partial \eta}\right) = 0 \tag{5.66}$$

$$\frac{\partial^2 \theta}{\partial \eta^2} + (PrfR + \alpha \eta Pr)\frac{\partial \theta}{\partial \eta} = \frac{\partial \theta}{\partial \tau} \tag{5.67}$$

Substituting Equations (5.62) – (5.64) into Equations (5.65) – (5.67) and setting $\tau = 0$ (Merkin, 1986), will get;

$$(1 + c_1)F'''' - c_1 G'' + 3\alpha F'' + \alpha \eta F''' +$$

$$R(f_\circ' F'' + F' f_\circ'' - f_\circ F''' - F f_\circ''') + \lambda F'' = 0 \tag{5.68}$$

$$\left(1 + \frac{c_1}{2}\right)G'' + N\alpha(3G + \eta G') - c_1(2G - F'')$$

$$+NR(f_\circ' G + F' g_\circ - f_\circ G' - F g_\circ') = 0 \tag{5.69}$$

$$\theta'' + [PrRf_\circ + \alpha\eta Pr]\theta_\circ' + [PrRF + \alpha\eta Pr]G'' + \lambda G = 0 \tag{5.70}$$

The boundary conditions are:

$$\left.\begin{array}{l} F(1) = 0, F'(1) = 0, G(1) = 0, H(1) = 0 \\ F''(0) = 0, F(0), G(0) = 0, H(0) = 1 \end{array}\right\}$$

$f_\circ(\eta)$ and $\theta_\circ(\eta)$ can be determined by the smallest eigenvalue λ due to the steady state flow solution. Therefore, the range of the possible eigenvalues can be determined by relaxing the boundary conditions on $f_\circ(\eta)$ and $\theta_\circ(\eta)$ as prescribed by Harris et al. (2009). Relaxing the boundary condition by $H(1) \to 0$ and the system of differential equation of new boundary condition $H'(0) = 1$ is solved.

5.3.4 Numerical Solutions

Stability equations in Eq. (5.67) - (5.70) are solved numerically using *"bvp4c"* function from MATLAB and reduced into a system of 1st order ordinary differential equations of $y' = f(x, y)$.

Shooting method is used to solve and to investigate the multiple solutions of Equation (5.52 - 5.53) and (5.59) subjected to the boundary conditions in Equations (5.54 - 5.55) and (5.60 - 5.61).

This is done by converting Equation (5.52 - 5.53) and (5.59) boundary value problem into initial value problem by setting:

$$\chi_1 = \eta, \chi_2 = f, \chi_3 = f', \chi_4 = f'', \chi_5 = f''', \chi_6 = g, \chi_7 = g', \chi_8 = \theta, \chi_9 = \theta'$$

$$
\begin{pmatrix}
\chi_1' \\
\chi_2' \\
\chi_3' \\
\chi_4' \\
\chi_5' \\
\chi_6' \\
\chi_7' \\
\chi_8' \\
\chi_9'
\end{pmatrix}
=
$$

$$
\begin{pmatrix}
1 \\
\chi_3 \\
\chi_4 \\
\chi_5 \\
\dfrac{1}{(1+C_1)}\left(\dfrac{C_1}{\left(1+\frac{C_1}{2}\right)}\left(-N\alpha(3\chi_6 + \chi_1\chi_7) - NR(\chi_3\chi_6 - \chi_2\chi_7) + C_1(2\chi_6 - \chi_4)\right) - 3\alpha\chi_4 - \alpha\chi_1\chi_5 - R(\chi_3\chi_4 - \chi_2\chi_5)\right) \\
\chi_7 \\
\dfrac{C_1}{\left(1+\frac{C_1}{2}\right)}\left(-N\alpha(3\chi_6 + \chi_1\chi_7) - NR(\chi_3\chi_6 - \chi_2\chi_7) + C_1(2\chi_6 - \chi_4)\right) \\
\chi_9 \\
-(Pr\chi_2 + \alpha\chi_1 Pr)\chi_9
\end{pmatrix}
$$

with initial conditions of:

$$
\begin{pmatrix}
\chi_1 \\
\chi_2 \\
\chi_3 \\
\chi_4 \\
\chi_5 \\
\chi_6 \\
\chi_7 \\
\chi_8 \\
\chi_9
\end{pmatrix}
=
\begin{pmatrix}
1 \\
1 \\
0 \\
\beta \\
\gamma \\
0 \\
\delta \\
0 \\
\varepsilon
\end{pmatrix}
\tag{5.72}
$$

where β, γ, δ and ε are unknown initial conditions which can be determined using shooting method such that solution of the system (5.71) satisfies the given boundary conditions. Once the slope of β, γ, δ and ε are obtained, then numerical integration is made for the initial value problem and accuracy of missing initial conditions is then checked by comparing calculated value with the given terminal point.

5.3.5 Results and Discussions

This section studies the effects of Reynolds number R, vortex viscosity parameter C_1, wall expansion ratio α and Prandtl number Pr on velocity $f'(\eta)$, micro-rotation $g(\eta)$ and temperature profile $\theta(\eta)$. Moreover, the effect of these parameters on shear and couple stresses is also discussed in the form of tabulation representation. Table 5.4 presents the effects of Reynolds number R, vortex viscosity parameter C_1 and wall expansion ratioα on shear and couple stress at the wall. This table manifests that the magnitude of the shear stress decreases gradually by the increasing values of wall expansion ratio $\alpha \in [-0.5, 0.5]$. Physically speaking, the fluid velocity increases due to decreasing trend of wall drag because wall expansion $\alpha \geq -0.5$ decrease the boundary layer thickness and allows the fluid to move in a channel freely causing an increase in the velocity. The effects of Reynolds number R and vortex viscosity parameter C_1 on shear and couple stress is also discussed in this table only for the expanding wall $\alpha > 0$. Furthermore, numerical values of the skin friction at the wall $f''(1)$ increases which causes the falloff the velocity of the fluid near the channel wall for I-Type and III-Type solutions. This result is in good agreement to the previously published experimental work of Hayt and Fabula (1964). They claimed that non-Newtonian fluids offered great reduction in the velocity of the fluid near the rigid body. Thus, without loss of any generality we can say that our obtained numerical results are up to the mark and tally with the previously published work. Table 5.5 presents the numerical values of heat transfer rate at the walls for various values of Prandtl number. From this representation, the numerical values of heat transfer naturally decreasing by the increasing values of Prandtl number for all the branches of the solutions. Smallest eigenvalues λ are presented in Table 5.8 against several values of wall contraction parameters. This table shows that the eigenvalues of the 1st solution are positive; hence, physically reliable.

On the other hand, the 2nd and the 3rd solutions are unreliable because their eigenvalues are negative.

Figure 5.14 plots the values of skin friction $f''(1)$ against the values of wall expansion ratio α for fixed values of $R = 40, C_1 = 0.3$ and for $N = 1$. The value of skin friction $f''(1)$ is increasing monotonically for all solutions. This means that an increase in the wall expansion ratio $\alpha > 0$ provides some space for the fluid to flow easily in a channel. However, a totally opposite behavior is observed for wall contraction case $\alpha < 0$. Figure 5.15 shows the effect of Reynolds number R on heat transfer at the channel wall. It presents I-Type and II-Type of solutions behave asymptotically to the horizontal axis $y = 0$ as the values of suction increase. An explanation is that heat transfer of $|\theta'(1)|$ decreases and tends to zero as the values of Reynolds number increase. However, for III-Type solution, the heat transfer increases initially but gradually decrease. As indicated by Mishra and DebRoy (2011), multiple solutions exist for many complex fluid flow problems in fluid dynamics and heat transfer because their highly nonlinear. Computing the unstable states as well as stable ones is necessary, since solution emerging from bifurcations along unstable solutions often connect with stable solution delivering generally mystifying phenomena. The transition process provides valuable information regarding flow evolution and can be used to confirm flow stability. The transition to multiplicity of solutions takes place below any threshold to chaos or turbulence. For example, in heat transfer engineering, the flow multiplicity and instability may strongly influence the quality and structure of the final product in material processing. Therefore, a better insight about the development of stability and multiplicity of flow states can serve to stimulate innovations as well as lead to improvements in the performance, reliability and costs of many practical flow problems such as crystal growth processes and rotating machines. For some special cases from

148

two-dimensional unsteady boundary-layer equations, five different solutions of the governing equations exist. Figure 5.16 and 5.17 present the effects of wall expansion $\alpha > 0$ on velocity profile $f'(\eta)$ and micro-rotation $g(\eta)$ respectively for $C_1 = 0.3, R = 40$ and for $N = 1$. The velocity of fluid particles near the channel walls decreases as the values of wall expansion $\alpha > 0$ increase for all multiple solutions. Profile of the micro-rotation $g(\eta)$ is increasing by the enhancement of the $\alpha > 0$ for I-Type and II-Type solutions. However, for III-Type solution, its profile is twisted into two phases and can be seen clearly in Figure 5.17. Furthermore, effect of wall contraction $\alpha < 0$ on velocity profile $f'(\eta)$ is shown in Figure 5.18 and observed that the effect of wall contraction $\alpha < 0$ on velocity profile $f'(\eta)$ is opposite to the effect of wall expansion $\alpha > 0$. Micro-rotation $g(\eta)$ increases by the increasing of numerical values of wall contraction $\alpha < 0$ for the I-Type of solution and decreases for the II-Type and III-Type solutions. The effect of C_1 on velocity profile $f'(\eta)$ for $\alpha = 0.3, R = 40$ and for $N = 1$ is identified in Figure 5.20. This figure shows that the velocity of the fluids decreases near the channel wall for the I-Type and III-Type of solutions by increasing the values of C_1. This behavior is caused by micropolar fluids which offer great resistance near the rigid body. However, totally opposite trend is seen for the II-Type of solution. The effect of C_1 on micro-rotation $g(\eta)$ for $\alpha = 0.3, R = 40$ and for $N = 1$ is viewed in Figure 5.21. Figure 5.22 illustrated the effects of Reynolds number R on velocity profile $f'(\eta)$ for $\alpha = 0.3, C_1 = 0.3$ and for $N = 1$. From this figure, the velocity of the fluid increases near the channel wall by increasing the numerical values of Reynolds number for I-Type and III-Type solutions and opposite effect can be seen for II-Type solution. The effect of Reynolds number R on micro-rotation $g(\eta)$ for $\alpha = 0.3, C_1 = 0.3$ and for $N = 1$ is depicted in Figure 5.23. Microrotation profile squeezes for I-Type and II-Type solutions but naturally increasing for III-Type solution. Figure 5.24 reflects the effect of Prandtl

149

number Pr on Temperature profile $\theta(\eta)$. An increase in the strength of Prandtl number reduces the temperature profile $\theta(\eta)$ for I-Type and II-Type solutions. For III-Type of solution, the temperature profile $\theta(\eta)$ decreases near the channel wall $\eta \approx 1$ but increases far from the wall. Figure 5.25 shows the validity of numerical results in the form of graph. Numerical results are compared with the previously published results of Mosayebidorcheh (2014) by setting $C_1 = 0.1, N = 1.0, R = 1.0, f(-1) = -1, f'(-1) = 0, f(1) = 1, f'(1) = 0$.

Table 5.5

Effects of Reynolds number R, vortex viscosity parameter C_1 and wall expansion ratio α on shear and couple stress at the wall

R	C_1	α	I-Type Solution		II-Type Solution		III-Type Solution	
			$f''(1)$	$g'(1)$	$f''(1)$	$g'(1)$	$f''(1)$	$g'(1)$
40	0.3	-0.5	-8.005579	0.155951	-15.69354	1.582672	-32.220054	0.643720
		-0.3	-7.647417	0.240592	-14.191112	1.389367	-31.348314	0.643122
		-0.1	-7.133580	0.449830	-12.73455	1.111721	-30.48721	0.642870
		0.1	-6.328660	1.048944	-11.42021	0.787151	-29.63664	0.642993
		0.3	-5.034100	2.770737	-10.37298	0.505138	-28.79648	0.643519
		0.5	-3.105862	6.145867	-9.637289	0.324069	-27.96660	0.644481
40	0.1	0.1	-6.328660	1.048944	-11.420211	0.7871513	-29.636649	0.642993
	0.3		-4.879977	1.812693	-12.232172	2.203667	-27.101721	1.653356
	0.5		-3.916973	2.181498	-14.242791	2.998649	-24.352902	2.439703
30	0.1	0.1	-4.116602	0.668627	-13.84659	0.638262	-24.936474	0.537415
40			-6.328660	1.048944	-11.420211	0.7871513	-29.636649	0.642993
50			-8.809910	1.556109	-11.860050	0.7912084	-33.437599	0.791893

Table 5.6

Effect of Prandtl number Pr on $\theta'(1)$

Pr	I-Type Solution $\theta'(1)$	II-Type Solution $\theta'(1)$	III-Type Solution $\theta'(1)$
0.5	-0.010247437	-0.019265008	-0.51147143
1.5	-2.47E-07	-2.14E-06	-0.0336541
2.5	-4.44E-12	-1.80E-10	-0.00302957

Table 5.7
Validation of Numerical Results

R	C_1	α	N	M	Pr	$f''(1)$ Shooting	$f''(1)$ Runge-Kutta-Fehlberg
0	0.1	0.1	1.0	0.5	1.0	-1.461987586	-1.461989886
10						-1.759790129	-1.759791329
20						-2.552850081	-2.552861081

Table 5.8

Smallest eigenvalues λ at several values of α

α	c_1	N	R	1st Solution λ	2nd Solution λ	3rd Solution λ
0				1.0725	-1.9867	-1.9575
-0.1				1.3595	-2.1535	-2.0959
-0.5	0.3	1.0	40.0	1.6465	-2.3204	-2.2103
-1.0				1.9335	-2.6545	-2.3447
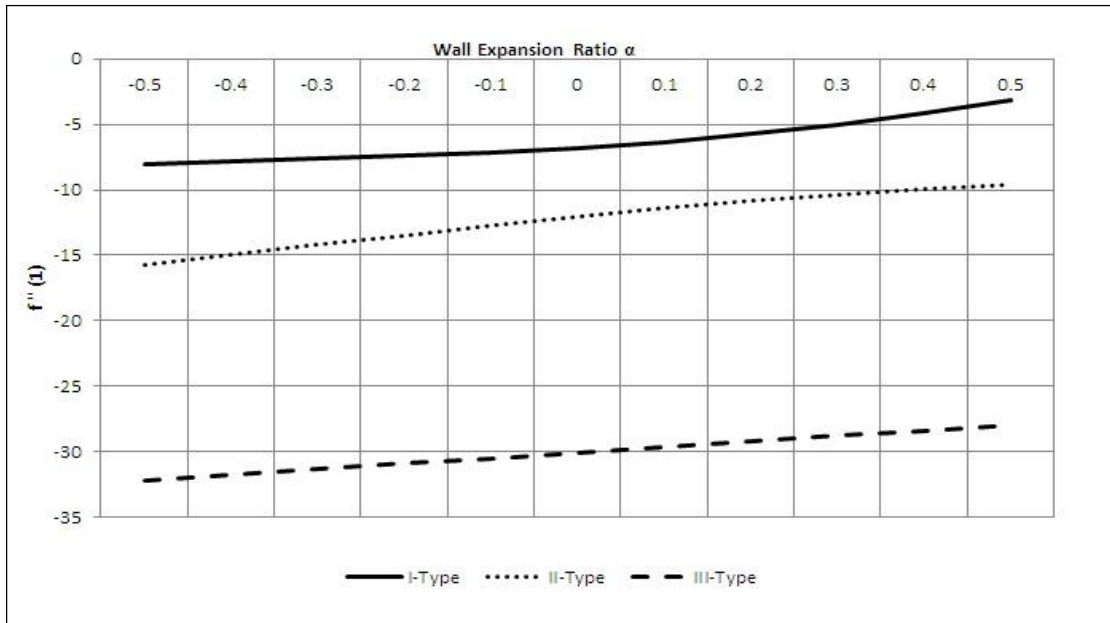
Figure 5.14. Skin friction against the values of wall expansion ratio
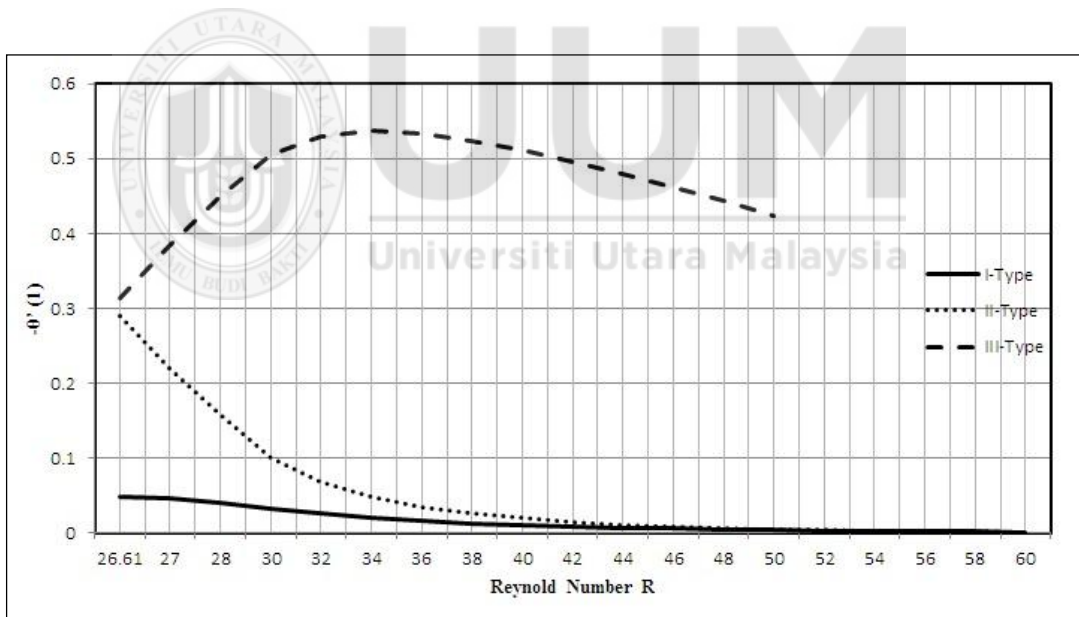
Figure 5.15. Heat transfer $|\theta'(1)|$ against the values of Reynolds number R

153
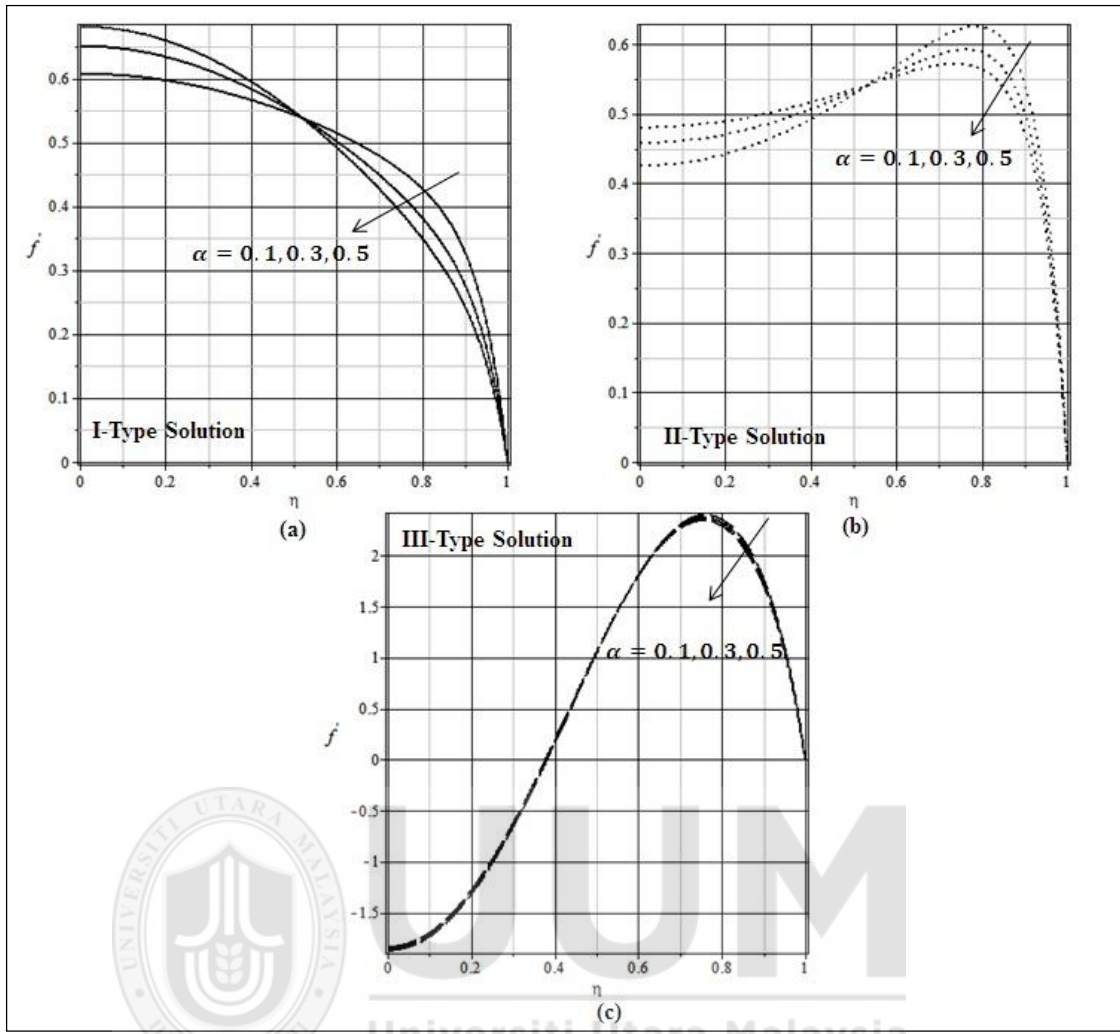
Figure 5.16. Effect of wall expansion $\alpha > 0$ on velocity profile $f'(\eta)$ for $C_1 = 0.3, R = 40$ and $N = 1$
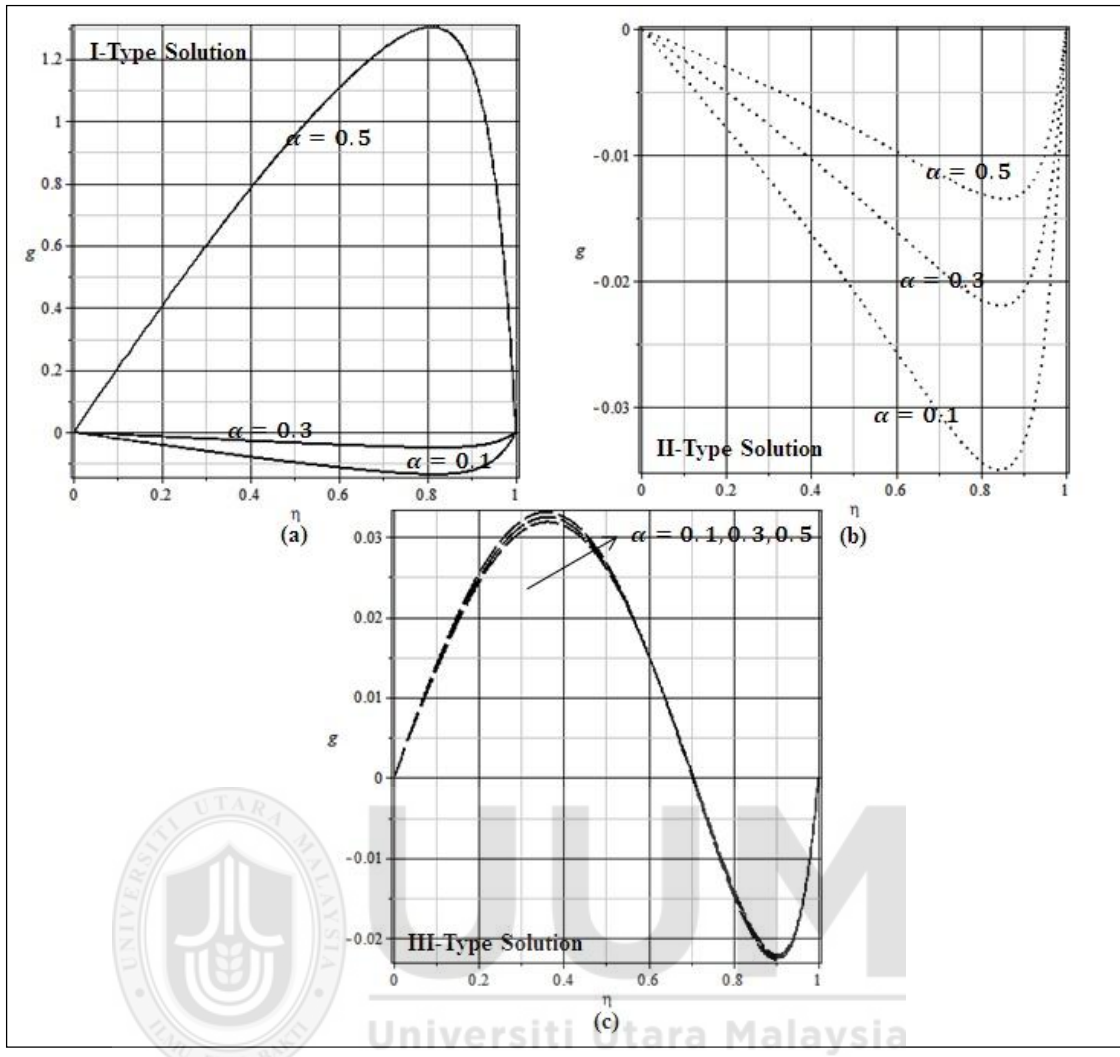
Figure 5.17. Effect of wall expansion $\alpha > 0$ on micro-rotation $g(\eta)$ for $C_1 = 0.3, R = 40$ and $N = 1$
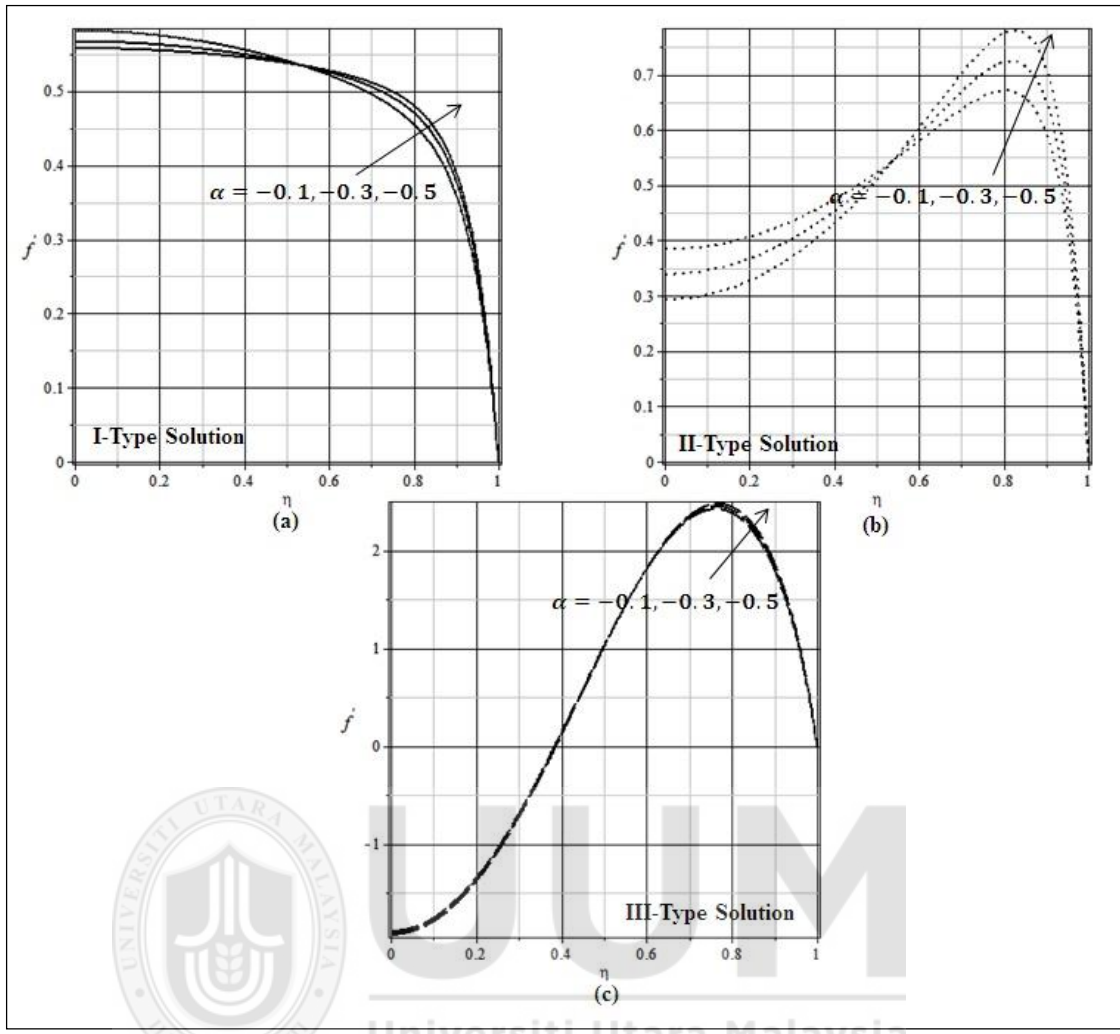
Figure 5.18. Effect of wall contraction $\alpha < 0$ on velocity profile $f'(\eta)$ for $C_1 = 0.3, R = 40$ and $N = 1$
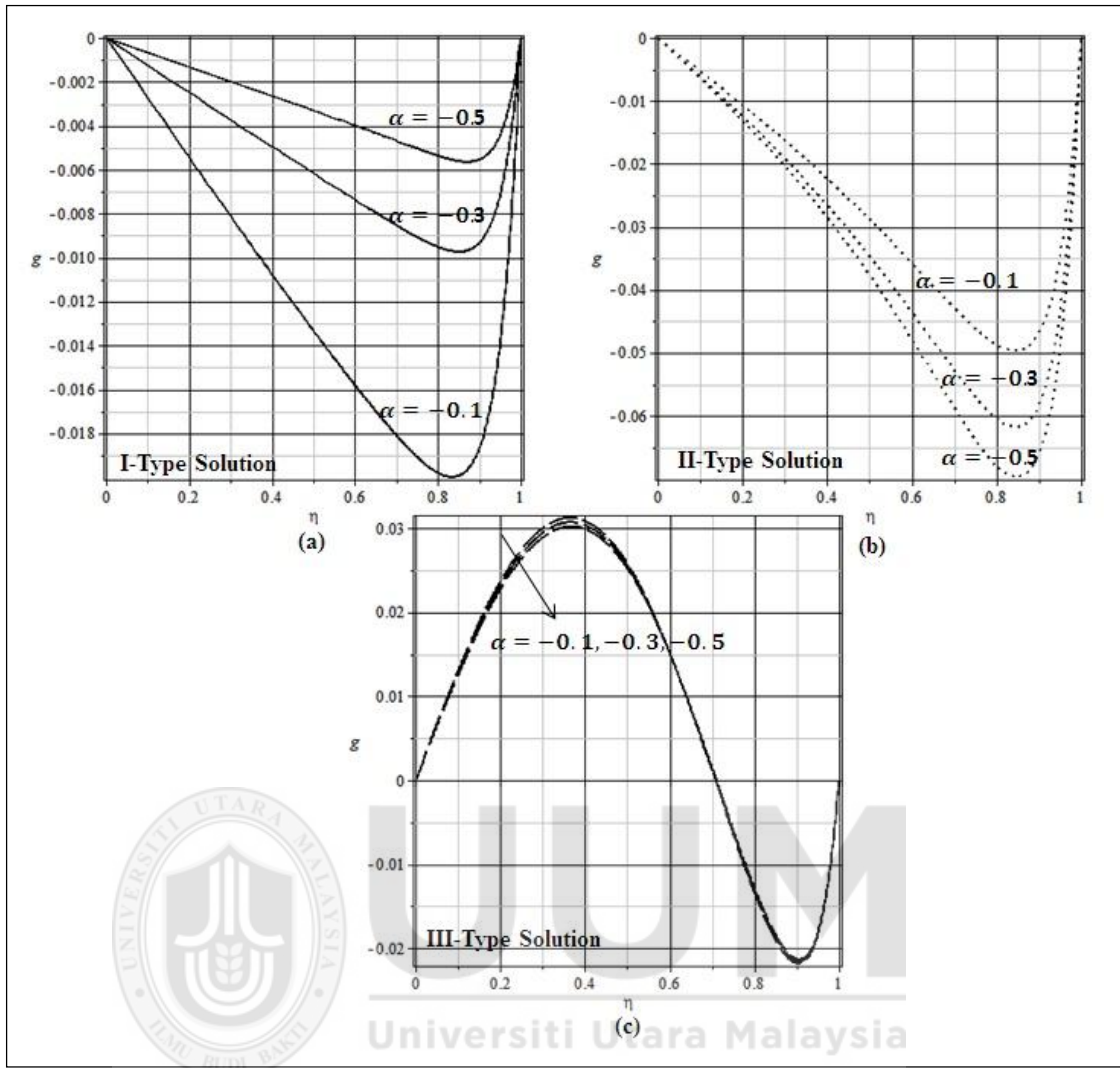
Figure 5.19. Effect of wall expansion $\alpha < 0$ on micro-rotation $g(\eta)$ profile $f'(\eta)$ for $C_1 = 0.3, R = 40$ and $N = 1$
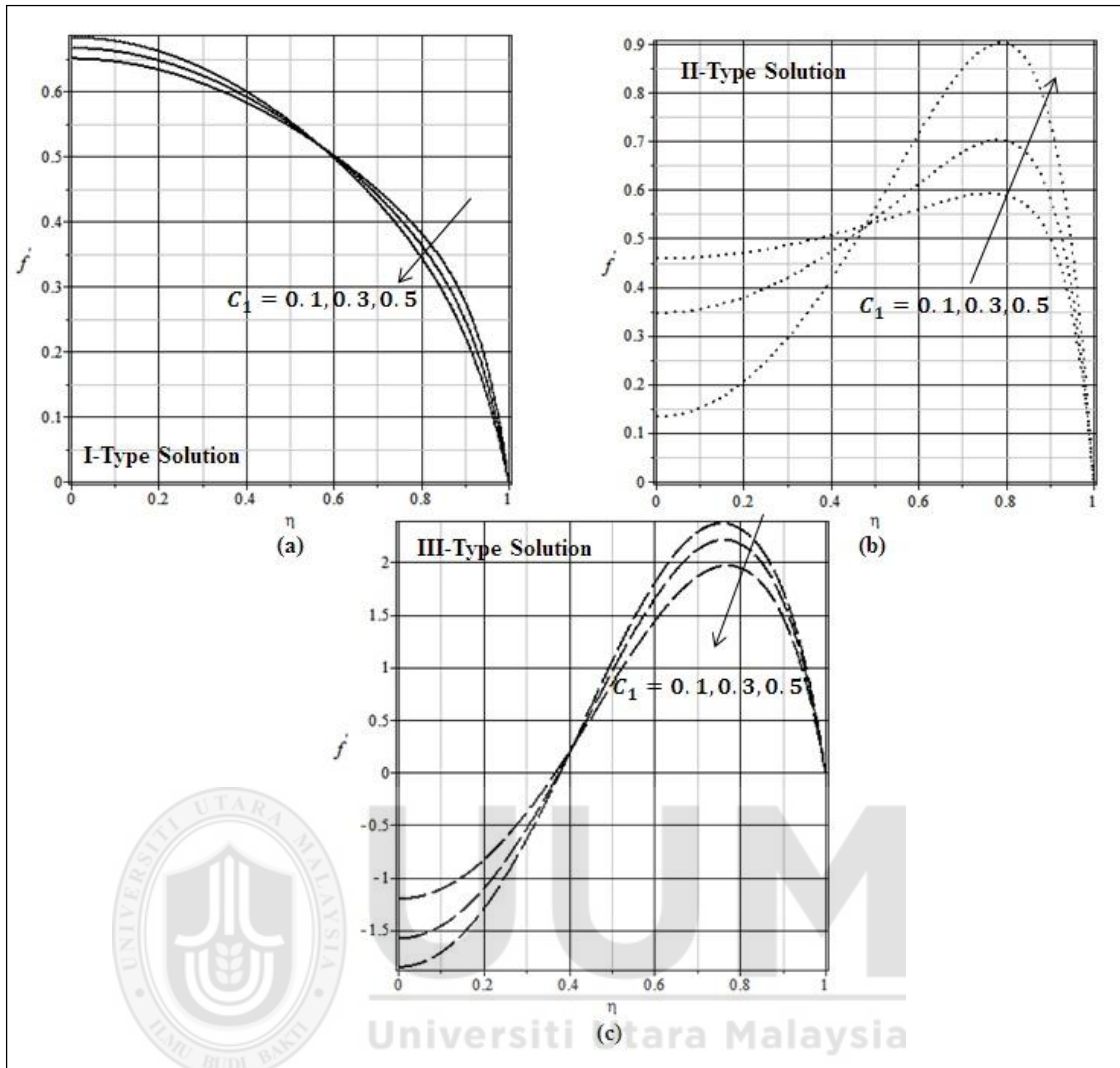
Figure 5.20. Effect of C_1 on velocity profile $f'(\eta)$ for $\alpha = 0.3, R = 40$ and $N = 1$
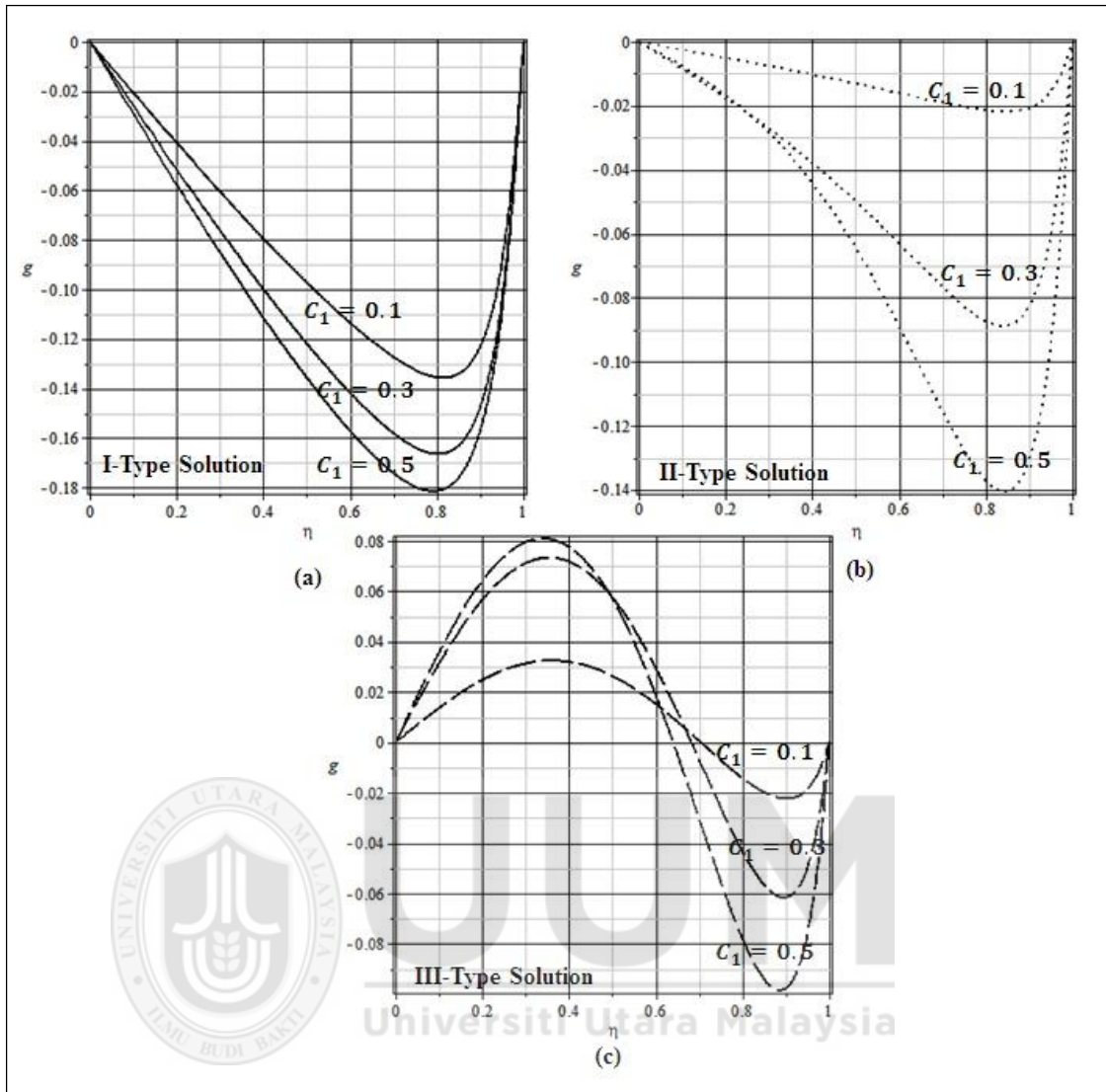
Figure 5.21. Effect of C_1 on micro-rotation $g(\eta)$ for $\alpha = 0.3, R = 40$ and $N = 1$
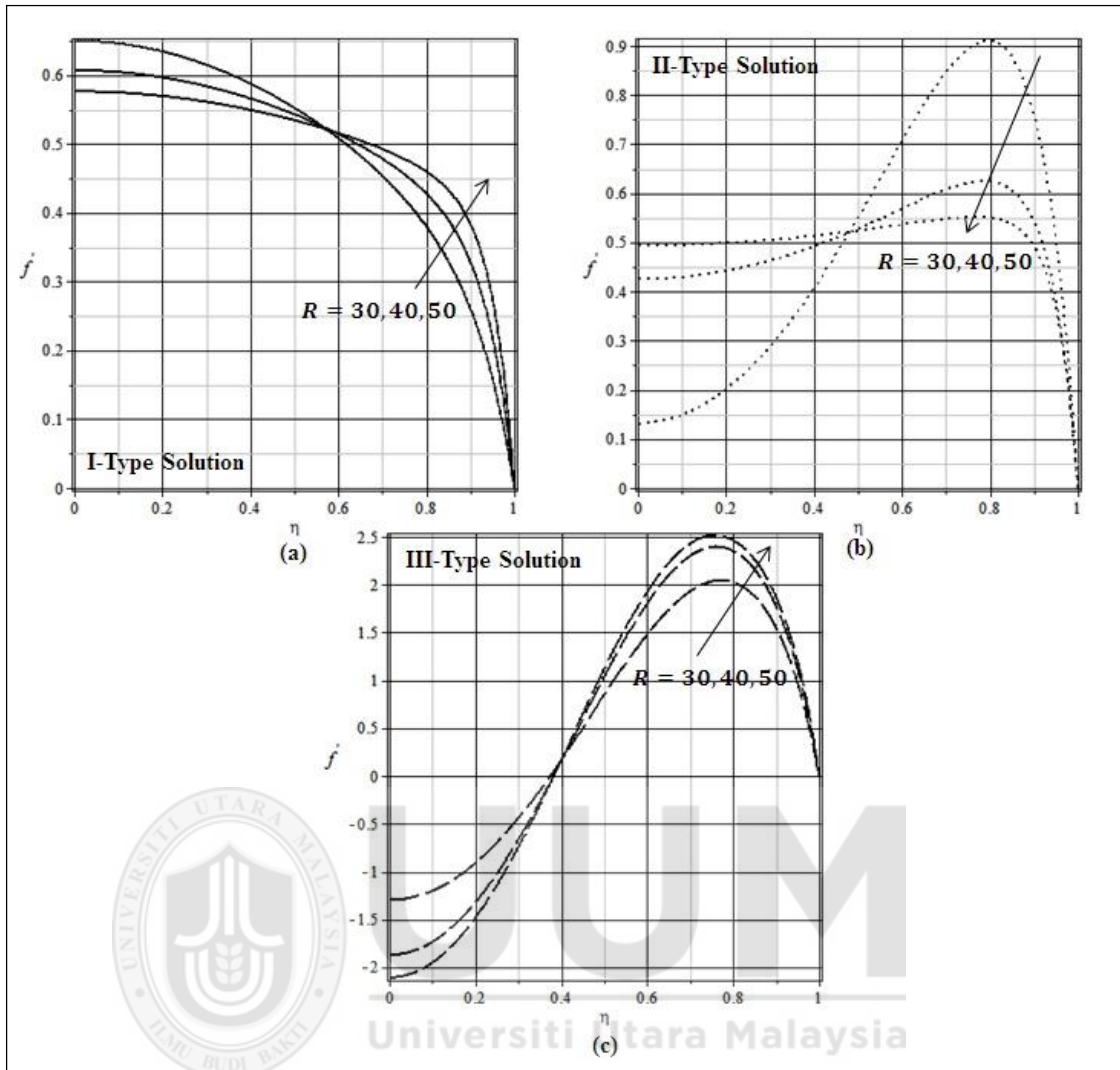
Figure 5.22. Effect of Reynolds number R on velocity profile $f'(\eta)$ for $\alpha = 0.3, C_1 = 0.3$ and $N = 1$
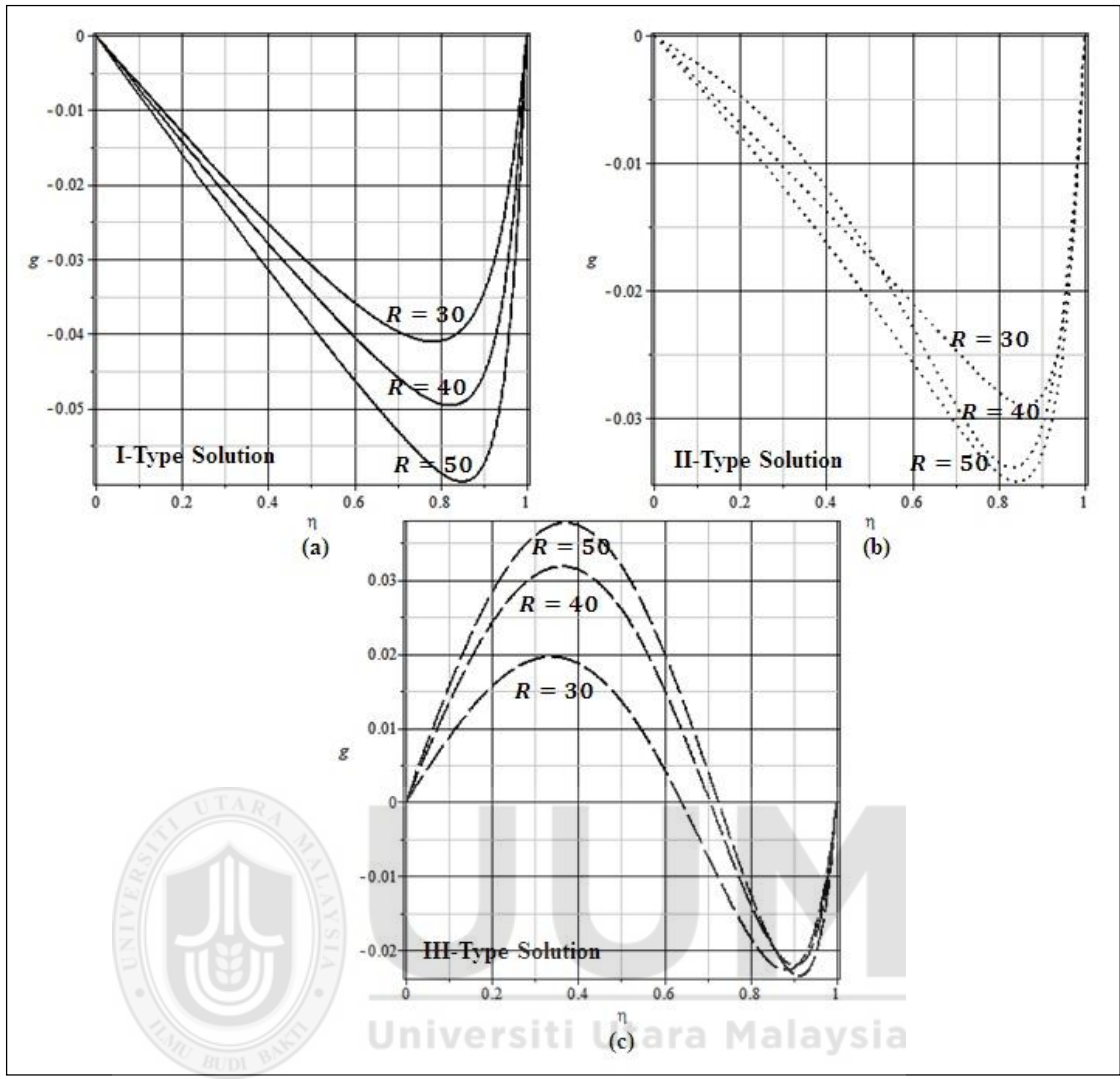
Figure 5.23. Effect of Reynolds number R on micro-rotation $g(\eta)$ for $\alpha = 0.3, C_1 = 0.3$ and $N = 1$
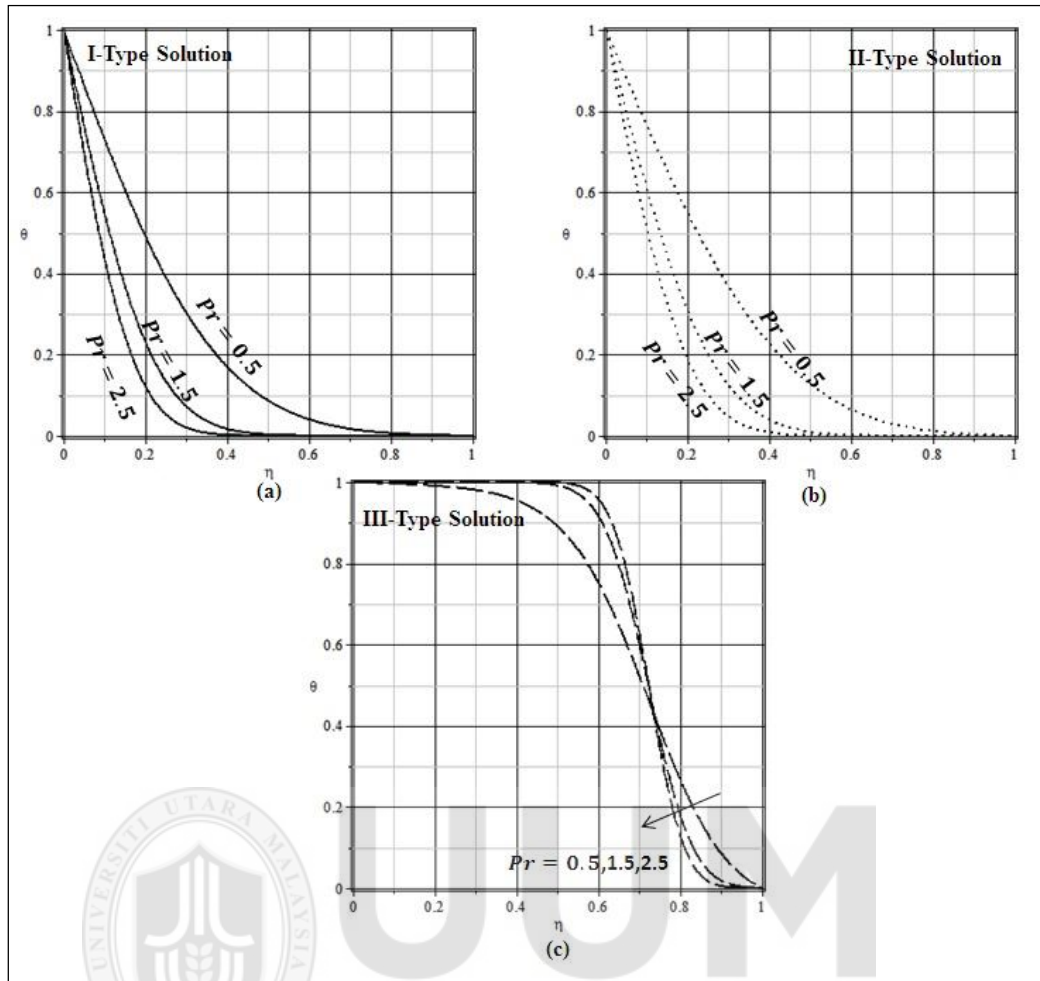
Figure 5.24. Effect of Prandtl number Pr on Temperature profile $\theta(\eta)$
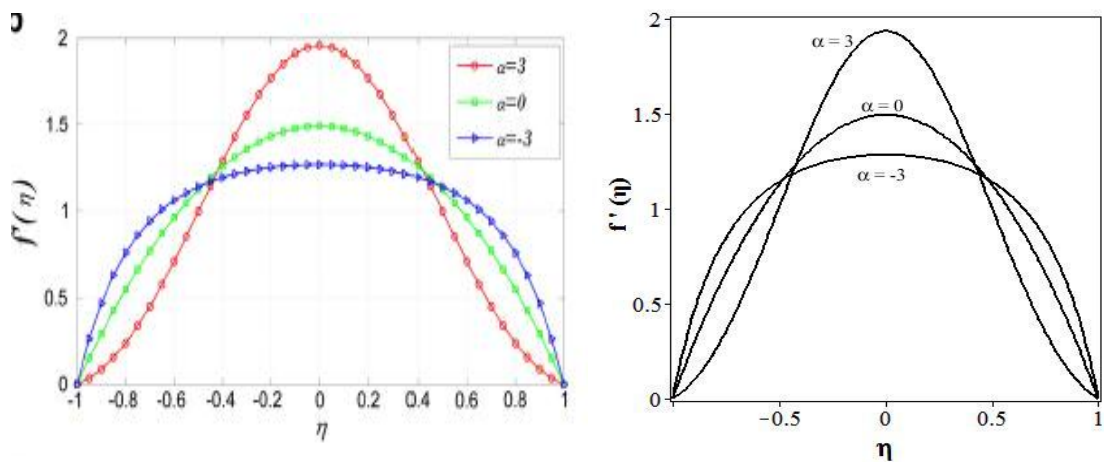
Mosayebidorcheh (2014)

Present results for $C_1 = 0.1, N = 1.0,$
$R = 1.0, f(-1) = -1, f'(-1) = 0,$
$f(1) = 1, f'(1) = 0$

Figure 5.25. Validation of physical model

5.4 Micropolar Fluid in a Channel with Permeable Walls: Multiple Solutions

The aim of this section is to investigate further branches of solution of micropolar fluid in a channel of permeable walls. The governing PDEs of momentum and angular momentum are reduced into ODEs by applying dimensionless parameters and then solved numerically with the help of shooting technique. Simultaneous effect of suction Reynolds number and vortex viscosity parameter on velocity and micro-rotation profile is examined for different branches of solution making the analysis more interesting. The study reveals that various branches of the solution of the proposed problem exist only for the case of strong suction. The problem of micropolar fluid in a channel with permeable walls was investigated numerically by Ashraf et al. (2011) is the most relevant reference of the current problem. The contribution of the current problem is to examine the multiple solutions and apply stability analysis in order to check the physical reliability of the solutions. Nevertheless, we found our results in a good agreement of the previously published results of Ashraf et al. (2011) in term of qualitative representation.

5.4.1 Problem Formulation

A two-dimensional laminar, incompressible micropolar fluid in a porous channel is considered. The width of the channel is taken $2h$ such that its lower wall of the channel is located at $y = -h$ and its upper wall is at $y = h$ as shown in Figure 5.26. Let the flow be driven by the constant inlet velocity U with constant pressure. Fluid is considered symmetric in both axes. Moreover, fluid can be inserted or extracted into a channel through porous walls at constant velocity $\frac{V}{2}$. The body forces and body couples of the fluid are neglected.
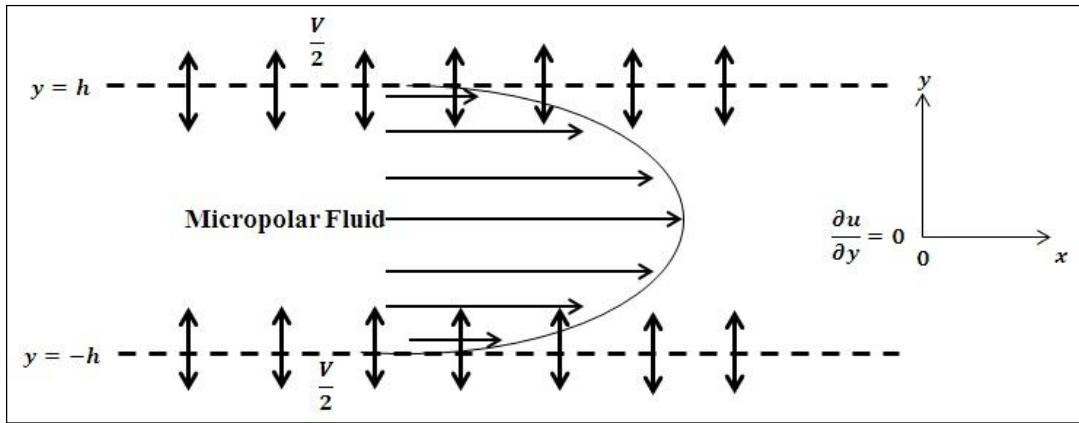
Figure 5.26. Physical Model of the Proposed Problem

The governing equations of the flow for the proposed problem are given as:

$$\frac{\partial u}{\partial x} + \frac{\partial v}{\partial y} = 0 \tag{5.73}$$

$$u\frac{\partial u}{\partial x} + v\frac{\partial u}{\partial y} = \frac{-1}{\rho}\frac{\partial p}{\partial x} + \frac{\mu + \kappa}{\rho}\nabla^2 u + \frac{\kappa}{\rho}\frac{\partial g}{\partial y} \tag{5.74}$$

$$u\frac{\partial v}{\partial x} + v\frac{\partial v}{\partial y} = \frac{-1}{\rho}\frac{\partial p}{\partial y} + \frac{\mu + \kappa}{\rho}\nabla^2 v - \frac{\kappa}{\rho}\frac{\partial g}{\partial x} \tag{5.75}$$

$$\rho\bar{j}\left(u\frac{\partial g}{\partial x} + v\frac{\partial g}{\partial y}\right) = \gamma\nabla^2 g + \kappa\left(\frac{\partial v}{\partial x} - \frac{\partial u}{\partial y}\right) - 2\kappa g \tag{5.76}$$

These correspond to the boundary conditions at the lower and upper walls of:

$$\left.\begin{array}{l} u(x, \pm h) = 0 \\ v(x, \pm h) = \dfrac{V}{2} \\ g(x, \pm h) = 0 \end{array}\right\} \tag{5.77}$$

Such that $V > 0$ corresponds to suction and $V < 0$ is for injection. Moreover, micro-rotation component g is taken to be zero because we neglect body coupling near the channel walls (i.e. $\nabla \times \bar{V} = 0$).

The governing PDEs (5.73 - 5.76) are converted into ODEs by using the following similarity variables suggested by Berman (1953) as:

164

$$\psi(x, y) = (Uh - Vx)f(\eta), \quad g(x, y) = -\left(U - \frac{Vx}{h}\right)\frac{\varphi(\eta)}{h}, \quad \eta = \frac{y}{h} \tag{5.78}$$

resulting the following nonlinear system of ODEs

$$f'''' - C_1\varphi'' + R(f'f'' - ff''') = 0 \tag{5.79}$$

$$\varphi'' + C_2(f'' + 2\varphi) - C_3(f'\varphi - f\varphi') = 0 \tag{5.80}$$

with appropriate boundary conditions of:

$$\left.\begin{array}{c} f(1) = \dfrac{1}{2}, f'(1) = 0, \varphi(1) = 0 \\ f''(0) = 0, \varphi(0) = 0 \end{array}\right\} \tag{5.81}$$

where $R = \frac{\rho Vh}{(\mu + \kappa)}$ is Reynolds number ($R > 0$ suction, $R < 0$ injection), $C_2 = \frac{\kappa h^2}{\gamma}$ is spin

gradient viscosity and $C_3 = \frac{\rho j Vh}{\gamma}$ is micro-inertia density.

5.4.2 Stability Analysis

The stability analysis of steady flow solutions of $f(\eta) = f_\circ(\eta)$, $g(\eta) = g_\circ(\eta)$ and $\theta(\eta) = \theta_\circ(\eta)$ that satisfies the boundary conditions (5.81) is carried by setting $\tau = t$ (Merkin 1986, Rosca & Pop 2013) such that:

$$f(\eta) = f_\circ(\eta) + e^{-\lambda t}F(\eta, t) \tag{5.82}$$

$$g(\eta) = g_\circ(\eta) + e^{-\lambda t}G(\eta, t) \tag{5.83}$$

where

$0 < F(\eta, t) \ll 1$, $0 < G(\eta, t) \ll 1$ and λ is the unknown eigenvalues, $F(\eta, t)$, $G(\eta, t)$ and $H(\eta, t)$ are smallest relative to $f_\circ(\eta)$, $\theta_\circ(\eta)$ and $\varphi_\circ(\eta)$ respectively.

The governing equations of (5.79) and (5.80) for unsteady case are as follows:

$$(1 + c_1)\frac{\partial^4 f}{\partial \eta^4} - c_1\frac{\partial^2 g}{\partial \eta^2} + R\left(f\frac{\partial^3 f}{\partial \eta^3} - \frac{\partial f}{\partial \eta}\frac{\partial^2 f}{\partial \eta^2}\right) = \frac{\partial^3 f}{\partial \tau \partial \eta^2} \tag{5.84}$$

$$\left(1 + \frac{c_1}{2}\right)\frac{\partial^2 g}{\partial \eta^2} + c_2\left(\frac{\partial^2 f}{\partial \eta^2} + 2g\right) - c_3\left(g\frac{\partial f}{\partial \eta} - f\frac{\partial g}{\partial \eta}\right) = 0 \tag{5.85}$$

165

Substituting Equations (5.82) and (5.83) into Equations (5.84) and (5.85) and setting

$\tau = 0$ (Merkin, 1986), will get;

$$(1 + c_1)F'''' + c_1 G'' + R(f_\circ' F'' + F' f_\circ'' - f_\circ F''' - F f_\circ''') + M^2 F'' + \lambda F'' = 0 \quad (5.86)$$

$$G'' + c_2(F'' + 2G) - c_3(f_\circ' G + F' g_\circ - f_\circ G' - F g_\circ') = 0 \quad (5.87)$$

Along with the boundary conditions,

$$\begin{aligned} F(1) = 0, F'(1) = 0, G(1) = 0, \\ F''(0) = 0, F(0), G(0) = 0, \end{aligned} \quad (5.88)$$

$f_\circ(\eta)$, $\theta_\circ(\eta)$ and $\varphi_\circ(\eta)$ can be determined by the smallest eigenvalue λ due to the steady state flow solution. Therefore, the range of the possible eigenvalues can be determined by relaxing the boundary conditions on $f_\circ(\eta)$ and $\theta_\circ(\eta)$ as prescribed by Harris et al. (2009). Therefore, we relaxed the boundary condition $G(1) \to 0$ and solved the system of differential equation with the new boundary condition $G'(0) = 1$.

5.4.3 Numerical Solution

Equations (5.86) and (5.87) subjected to the boundary conditions in Eq. (5.88) are solved using the same function in MATLAB. Equations (5.79 - 5.80) subjected to boundary condition (5.81) are numerically solved by employing shooting technique. This technique converts the given equations into 1st order initial value problem by setting $\Gamma_1 = \eta, \Gamma_2 = f, \Gamma_3 = f', \Gamma_4 = f'', \Gamma_5 = f''', \Gamma_6 = \varphi, \Gamma_7 = \varphi'$

$$\begin{pmatrix} \Gamma_1' \\ \Gamma_2' \\ \Gamma_3' \\ \Gamma_4' \\ \Gamma_5' \\ \Gamma_6' \\ \Gamma_7' \end{pmatrix} = \begin{pmatrix} 1 \\ \Gamma_3 \\ \Gamma_4 \\ \Gamma_5 \\ C_1\big(C_3(\Gamma_3\Gamma_6 - \Gamma_2\Gamma_7) - C_2(\Gamma_4 + 2\Gamma_6)\big) - R(\Gamma_3\Gamma_4 - \Gamma_2\Gamma_5) \\ \Gamma_7 \\ C_3(\Gamma_3\Gamma_6 - \Gamma_2\Gamma_7) - C_2(\Gamma_4 + 2\Gamma_6) \end{pmatrix} \quad (5.89)$$

with initial conditions of:

$$
\begin{pmatrix} \Gamma_1 \\ \Gamma_2 \\ \Gamma_3 \\ \Gamma_4 \\ \Gamma_5 \\ \Gamma_6 \\ \Gamma_7 \end{pmatrix} = \begin{pmatrix} 1 \\ 1 \\ 2 \\ 0 \\ \alpha \\ \beta \\ 0 \\ \gamma \end{pmatrix} \tag{5.90}
$$

where, α, β and γ are unknown initial conditions. These initial conditions are shot with some arbitrary slope such that solution of the system (5.89) satisfies the given conditions at the boundary until they satisfy the given tolerance. Once slope of α, β and γ are obtained, then numerical integration is made for the initial value problem and accuracy of missing initial conditions is then checked by comparing calculated value with the given terminal point.

5.4.4 Results and Discussions

The main objective of this section is to investigate different branches of the solution for variation of suction Reynolds number R and vortex viscosity parameter C_1. Figures are drawn by varying numerical values of one parameter at a time while fixing the other parameter. The effects of C_2 and C_3 on velocity and micro-rotation has no significant contribution, therefore $C_2 = 0.1$ and $C_3 = 0.3$ are fixed throughout this study. Table 5.10 shows the smallest eigenvalues γ for several values of Reynolds number. This table shows that the eigenvalues of the 1st solution is positive but negative for the 2nd and the 3rd solutions. This stability analysis shows that the 1st solution is stable and physically reliable but the others are physically unreliable.

167
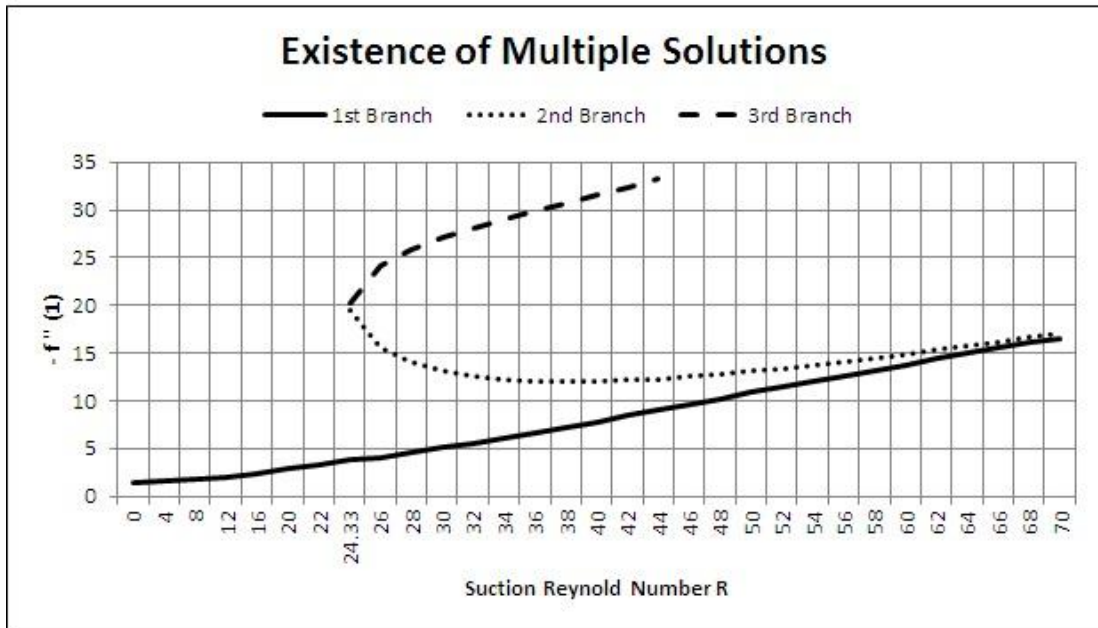
Figure 5.27. Skin friction $-f''(1)$ at the wall against suction Reynolds number R

Figure 5.27 plots the skin friction $-f''(1)$ at the wall against suction Reynolds number of $R > 0$ by setting $C_1 = C_2 = 0.1, C_3 = 0.3$. Based on the findings of multiple solutions of the proposed problem, the solution satisfies the existence and the uniqueness theorem for $0 \leq R < 24.33$. Thus, from this pictorial representation of numerical investigation, only single solution exists within the range of $0 \leq R < 24.33$. Whereas, for $24.33 \leq R < \infty$ three solutions exist for every value of suction Reynolds number R. Therefore, $R = R_{critical} = 24.33$ is the critical value of the suction Reynolds number R where solutions has more than one branch and it can be seen clearly in Figure 5.27. Furthermore, for $R \geq 70$, the 1ˢᵗ branch of solution is conspired with the 2ⁿᵈ branch of solution. Without loss of any generality, triple solutions of the proposed problem exist only for $R \geq R_{critical} = 24.33$. Figure 5.28 plots the effect of suction Reynolds number R on velocity profile $f'(\eta)$ for $C_1 = 0.5$, for different branches of solutions. This figure shows that the velocity profile $f'(\eta)$ increases near the channel wall $\eta \approx 1$ by the enhancement of suction Reynolds number $R = 30, 35, 40$ for the 1ˢᵗ and the 3ʳᵈ branch of the solutions.

168

This is caused by extra forcing agents from suction to the fluid particles thus the velocity boosts up further incalculably by increasing R. However, totally opposite behavior is observed near the wall for the 2nd branch of the solution. Figure 5.29 depicts the behavior of micro-rotation in a channel for different values of suction Reynolds number R. Profiles of micro-rotation for different branches of solution are seemed naturally parabolic. Micro-rotation profile is amassed upwards by increasing the values of suction Reynolds number $R = 30, 35, 40$ for the 1st and the 3rd branches of the solutions. Profile of the 1st branch is concave up and concave down for the 2nd and the 3rd branches. Micro-rotation profile for the 2nd branch decreasing as the increase of suction Reynolds number R. Point of concavity $\eta \approx 0.8$ where micro-rotation changes its sign from negative to positive is the point where shear stresses due to the suction resulting in zero micro-rotation. Before the inflection point, the micro-rotation profile decreases and afterwards its increases.
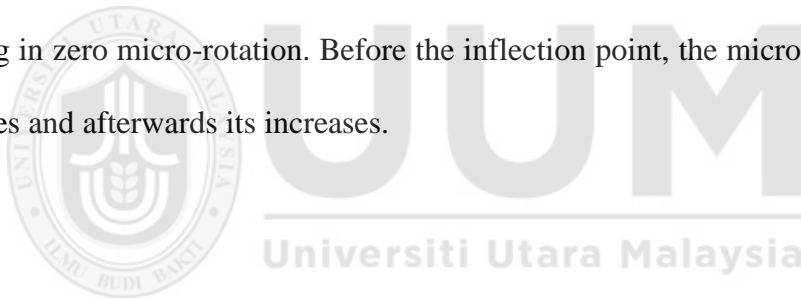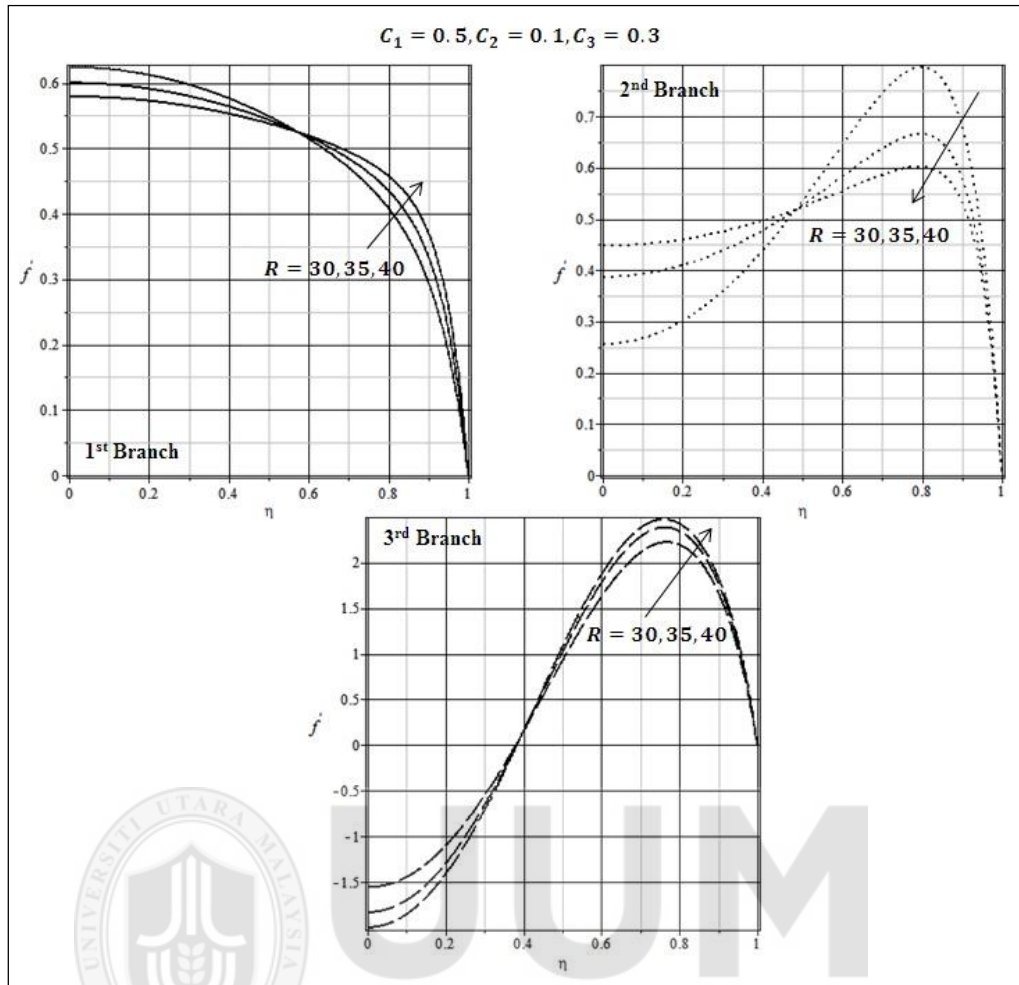
Figure 5.28. Effect of suction Reynolds number R on velocity profile $f'(\eta)$

The effect of vortex viscosity parameter C_1 on velocity and micro-rotation profile for $R = 30, C_2 = 0.1$ and $C_3 = 0.3$ is presented in Figures 5.30 and 5.31 respectively. These figures show the velocity profile $f'(\eta)$ is shifted away from the channel wall as we increase in the strength of vortex viscosity parameter $C_1 = 0.5,5,10$. This shift means velocity increases near the center of the channel $\eta \approx 0$ for the 1st and the 2nd branches. Physically speaking, the shear stress at the wall $f''(1)$ decreases by increasing the values of C_1, which resemble the results derived by Hayt & Fabula (1964). However, totally reversed phenomena is observed for the 3rd branch.

170
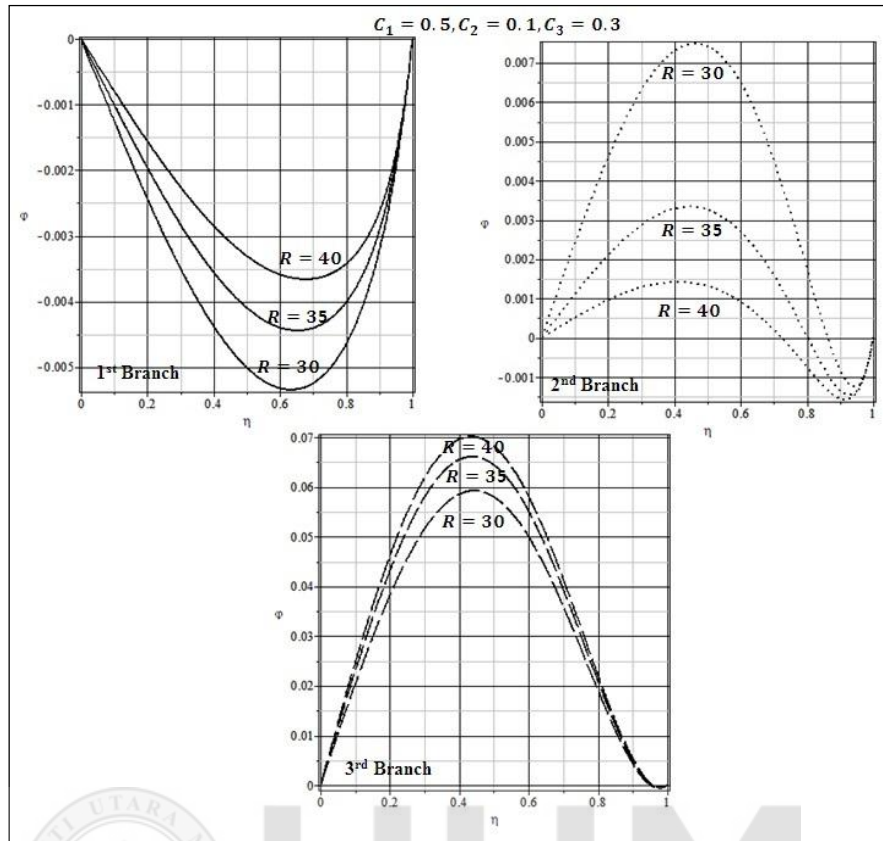
Figure 5.29. Effect of suction Reynolds number R on micro-rotation profile $\varphi(\eta)$
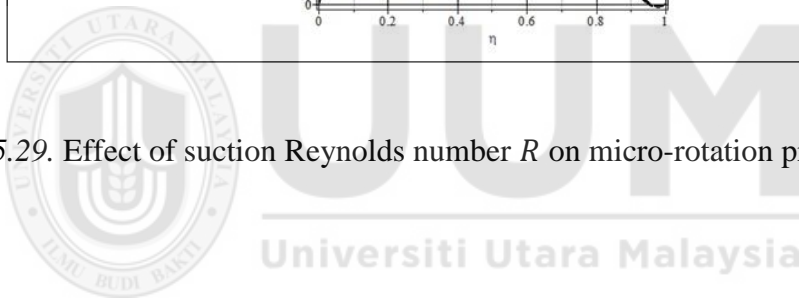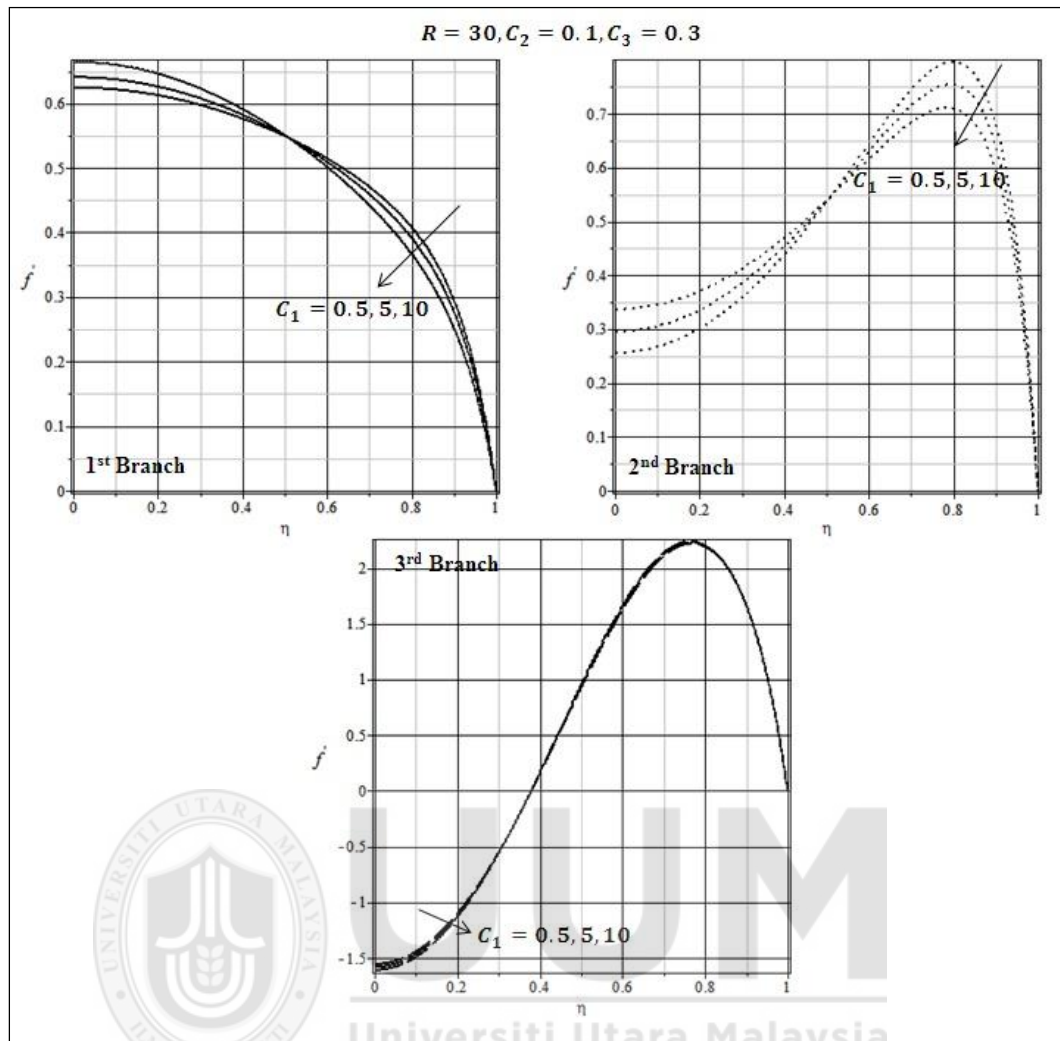
Figure 5.30. Effect of C_1 on velocity profile $f'(\eta)$

Micro-rotation profile $\varphi(\eta)$ decreases for the 1st and the 2nd branches by increasing the values of vortex viscosity parameter C_1, because couple stress $\varphi'(\eta)$ increases by increasing the numerical values of $C_1 = 0.5, 5, 10$. Validation of physical model in the form of graphical representation is presented in Fig. 32. For this we set $f(-1) = 0, f'(-1) = 0, \varphi(-1) = 0, f(1) = 1, f'(1) = 0, \varphi(1) = 0$ and taking the same values of the micropolar parameters as taken by Ashraf et al. (2011).
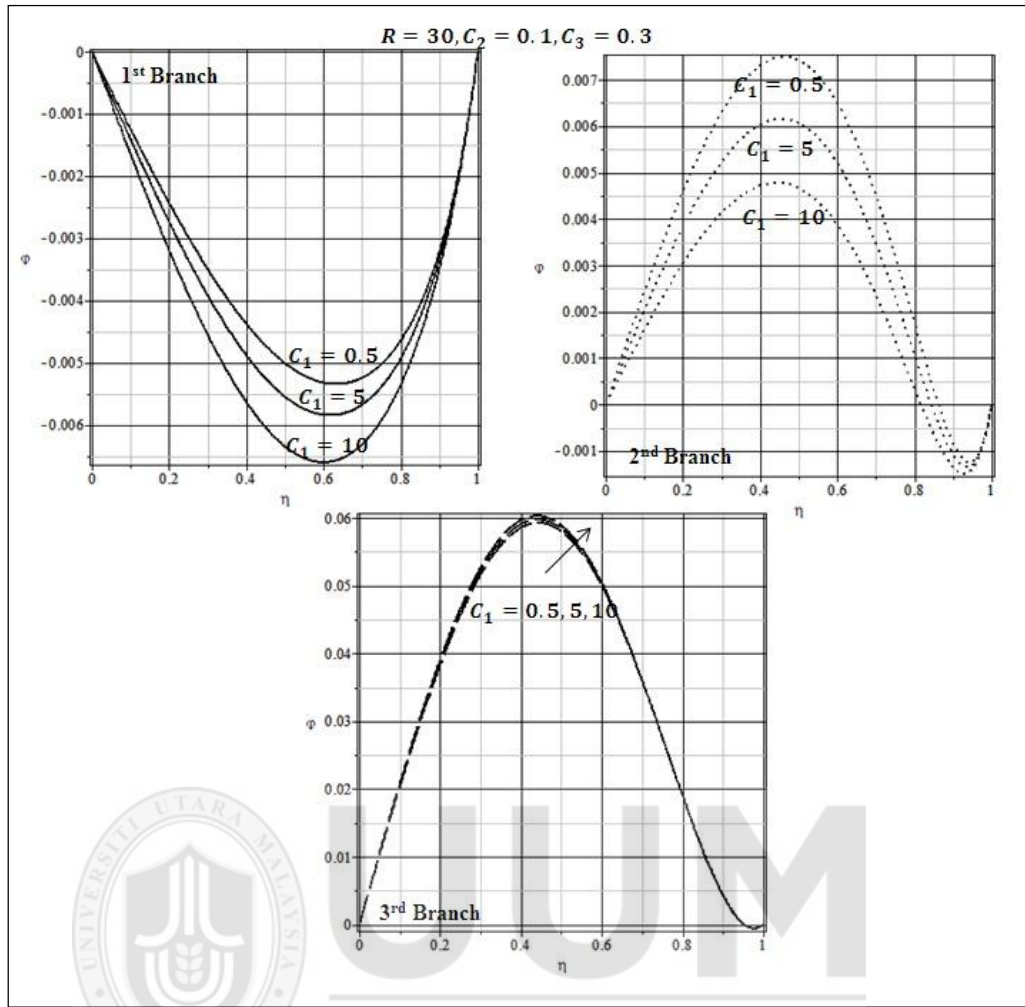
Figure 5.31. Effect of C_1 on micro-rotation profile $\varphi(\eta)$
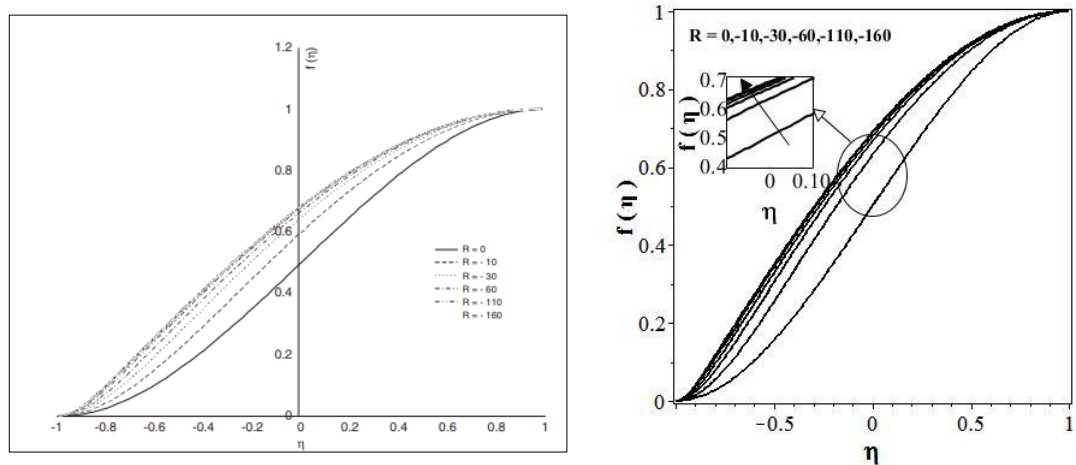
R=-10 Ashraf et al. (2011)   Present results

Figure 5.32. Validation of physical model

Table 5.9
Validation of Numerical Results

R	C_1	C_2	C_3	$f''(1)$ Shooting	$f''(1)$ Runge-Kutta-Fehlberg
0	0.1	0.1	0.3	-1.499002275	-1.499002285
2				-1.546998475	-1.546998438
4				-1.607444473	-1.607444451
4	0	0.1	0.3	-1.608792213	-1.608792189
	0.5			-1.602041617	-1.602041595
	1.0			-1.595261094	-1.595261071

Table 5.10

Smallest eigenvalues λ at several values of R

R	c_1	c_2	c_3	1st Solution λ	2nd Solution λ	3rd Solution λ
26.56				1.6321	-2.0642	-2.7686
30				1.6814	-2.1211	-2.9785
35	0.5	0.1	0.3	1.7323	-2.4186	-3.0194
40				1.7819	-2.8358	-3.2178
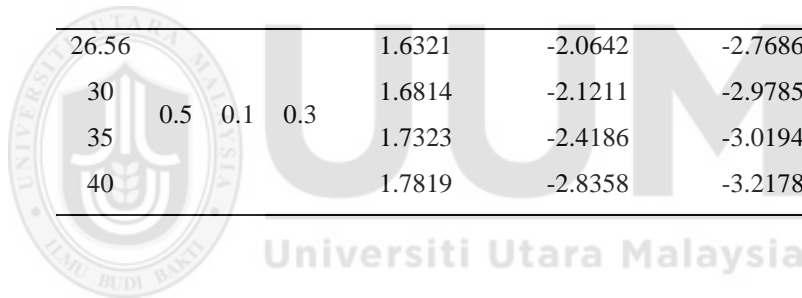
CHAPTER SIX
CONCLUSIONS

6.1 Summary of the Research

This study has examined the numerical solutions and the occurrence of multiple similarity solutions of different non-Newtonian fluids in a channel under some physical effects such as magnetic field, heat and mass transfer, Joules heating and viscous dissipation. The examined non-Newtonian fluids are (1) Nanofluids (2) Casson Fluid (3) Micropolar Fluid. All problems are studied theoretically, and the solutions are obtained numerically using shooting technique and verified by RK- Fehlberg Method.

Chapter 1 consists of general introduction and an overview of the research including the basic concept of fluids, non-Newtonian fluid, nanofluid, Casson fluid, micropolar fluid, channel, types of channel, motivation of study, problem statement, objectives, significance and scope of study. Then, Chapter 2 deals with previous studies regarding flow in a channel, techniques of solving boundary value problem (BVPs) and the tabulation representation of the literature review.

In Chapter 3, some problems regarding nanofluids in a topologylike channel are discussed. From the numerical results we have drawn some important remarks.

Heat transfer of MHD copper-water nanofluid in a channel is studied in problem 3.1. The effects of different parameters on velocity profile and temperature profile are demonstrated in pictorial representation. The following considerations are made for the bases of our numerical results. Enhancement of solid volume friction φ from 0 to 0.9 increases the velocity profile $f'(\eta)$ from lower wall to the center of the channel but decreases afterwards. Stretching the Reynolds number $R > 0$ will increase the velocity profile prior to the half of channel but

gradually decrease afterwards. Solid volume fraction φ decreases the skin friction $f''(-1)$ which implies that fluid near the lower wall is under high influence of slip effect increasing the velocity of the fluid. Rising the strength of Prandtl number Pr increases the heat transfer rate of $-\theta'(-1)$. Problem 3.2 dealt with multiple solutions of MHD flow of nanofluid in a porous channel. The effects of different physical parameters on velocity $f'(\eta)$ and temperature $\theta(\eta)$ are shown. The following observations have been made; Triple solutions of MHD flow of nanofluid in a porous channel occurred only for the case of suction such that $R \geq 21.1$. For injection, only single solution exists. Solid volume fraction φ and Reynolds number R on velocity profile $f'(\eta)$ have similar effect for all solutions. An increase in the magnetic field M reduces the fluid motion and enhances the heat transfer.

Two-dimensional flow of nanofluid in slowly expanding or contracting walls is studied in problem 3.3 and the effects of different physical parameters were analyzed. Conclusion from these effects is made such that; in the case of injection $R > 0$ through porous walls for any value of expanding walls ($\alpha > 0$), contracting walls ($\alpha < 0$) and solid volume fraction $\varphi > 0$, only single solution exists. The velocity of the nanofluid particles increases at the center of the channel $\eta \approx 0$ as the channel walls expands $\alpha > 0$ and decreases as the channel walls contracts $\alpha < 0$. The effect of solid volume fraction φ on the velocity profile $f'(\eta)$ and temperature profile $\theta(\eta)$ for both contracting and expanding walls ($\alpha < 0 \; and \; \alpha > 0$) are the same.

A numerical investigation is carried out for the problem of MHD mixed convection flow of Casson fluid in a channel embedded with porous medium in Problem 4.1. Heat and mass transfer analysis is also made to check the physical behavior of fluid. Summary from numerical results is made such that; the effect of Reynolds number R, Casson parameter β and the porosity parameter p on velocity profile is naturally the same. The velocity of the fluid particles increases near the lower wall $\eta \approx -1$ of the channel with an enhancement in the strength of the magnetic field M. Thermal buoyancy parameter $\lambda \geq 0$ increases the skin friction $f''(\pm 1)$ and heat transfer $\theta'(\pm 1)$ at the channel walls. Concentration field $\varphi(\eta)$ decreases monotonically

176

by the increasing values of Smith number Sc and chemical reaction rate γ. Multiple solutions of MHD for Casson fluid flow in a channel with heat and mass transfer is analyzed in Problem 4.2. Moreover, crucial observations have also been engendered in the light of the numerical investigation. Only single solution is found in the case of injection $R < 0$ for any value of Casson number β or Hartman number M. Then, multiple solutions only for $\beta \in [5, \infty)$ and $R \in [31.07, \infty)$ for any value of magnetic number $M \in [0, 2.0]$. The effect of Casson number $\beta \geq 5$ and Reynolds number $R > 31.06$ on velocity profile $f'(\eta)$ increases for the 1st and the 3rd solutions near the channel wall $\eta \approx 1$ and the effect of Reynolds number R on skin friction $f''(1)$ and $\theta'(1)$ is the same for assisting flow $\lambda > 0$ and opposing flow $\lambda < 0$.

Multiple solutions of MHD for Casson fluid flow in a channel with heat and mass transfer is analyzed in problem 4.3. In this problem, we have concluded that for high Casson number $\beta \to \infty$ and magnetic field $M = 0$, the proposed problem gives accurate results in terms of multiple solutions as investigated by Robinson (1976). Moreover, only single solution is found in the case of injection $R < 0$ for any value of Casson number β or Hartman number M. The effect of Casson number $\beta \geq 5$ and suction Reynolds number $R > 14.68$ on velocity profile $f'(\eta)$ is the same in all cases of multiple solutions. The magnitude of couple stresses at the lower wall $|f''(-1)|$ increases strictly monotonically for the 1st and the 3rd solutions but decreases for the 2nd solution by the enhancement of suction Reynolds number R and Casson number β. Finally, the effect of Smith number Sc and chemical reaction rate γ on concentration field $\phi(\eta)$ is the same for all solutions. Problem 4.4 presented the problem of MHD for Casson fluid in a channel with stretching walls under the influence of Joules heating and viscous dissipation. From the numerical results, some remarks are made such that; in Figure 4.33, the effects of Casson parameter β on velocity profile $f'(\eta)$ decreases from lower wall $\eta = -1$ to the center of the channel $\eta = 0$. Lower wall is under the influence of the injection therefore velocity profile shifted towards the channel wall as the values of Casson parameter β is increased. Furthermore, velocity profile decreases from lower wall of the channel to center of the channel as the values of stretching Reynolds number increase and totally opposite behavior is depicted afterwards.

177

Fluid velocity $f'(\eta)$ near the upper channel wall $\eta \approx 1$ is reduced and increased near the center of the channel $\eta \approx 0$ as the enhancement of the strength in magnetic field M. However, negligible effect of magnetic field M is observed near the lower wall of the channel $\eta \approx -1$ due to stretching and injection. An increase in the strength of the injection of the fluid monotonically reduces the fluid velocity on more than half of the channel $-1 \leq \eta < 0.5$. Negligible effect is observed near the upper wall of the channel $\eta = 1$ because injection is only taken place at the lower wall of the channel $\eta = -1$.

Problem 5.1 investigates multiple solutions of micropolar fluid in a channel under the influence of transverse magnetic field. The effect of Reynolds number R, magnetic field M, vortex viscosity parameter C_1, micro-rotational spin parameter N and Peclect number Pe_h is presented and deeply discussed. Some important observations which have been engendered in the light of numerical investigation are made such that; the existence of multiple solutions occurs only for the case of suction i.e. for $R \geq R_{critical} = 26.56$. For the case of injection $R < 0$, existence and uniqueness theorem for the solution is satisfied. Hence, without loss of any generality, single solution only exists in the case of injection. Magnitude of the heat transfer at the wall $|\theta'(1)|$ decreases for I-Type and II-Type solutions by increasing in the strength of Peclect number Pe_h but decreases for III-Type solution. Investigation on the multiple solutions of micropolar fluid in a channel with changing walls is presented in problem 5.2. This numerical study revealed that the magnitude of the shear stress decreases gradually by the increasing values of wall expansion ratio $\alpha \in [-0.5,0.5]$. Furthermore, numerical values of the skin friction at the wall $f''(1)$ increases which causes the fall off the velocity of the fluid near the channel wall for I-Type and III-Type solutions. This result is in good argument with Hayt & Fabula (1964).

Problem 5.3 is motived to investigate the multiple solutions of a micropolar fluid in a channel with porous walls. Numerical study is carried out to find different branches of the solution for the variation of suction Reynolds number R on the shear stresses and micro-rotation field. Based

on the findings of numerical investigation, the following conclusion has been engendering such that; Multiple solutions of the problem occurs only for the case of large suction within the range of $24.33 \leq R < \infty$. The velocity profile $f'(\eta)$ increases near the wall of the channel $\eta \approx 1$ for the 1st and the 3rd branches of solution. Enhancement of the vortex viscosity parameter C_1 reduces the velocity of the fluid particles near the channel wall, this result is tally with Hayt & Fabula (1964) as well. Furthermore, micro-rotation profile $\varphi(\eta)$ decreases by increasing the values of $C_1 = 0.5, 5, 10$ for the 1st and the 2nd branches of solution.

6.2 Suggestions for Future Study

In the current research, the study performed only for three types of non-newtonian fluids which are Nanofluids, Casson fluids and Micropolar fluids, and it can be expanded into the following:

- Different Non-Newtonian fluids can be considered such as, Williamson nanofluid, Jeffrey nanofluids etc.
- Hybrid nanofluid model can be incorporated in the same geometry.
- Various nanoparticles (silver, gold, carbon nanotubes, TiO_2, graphene) can be considered in three dimensional flows in a channel.

REFERENCES

Afikuzzaman, M., Ferdows, M., & Alam, M. M. (2015). Unsteady MHD Casson fluid flow through a parallel plate with Hall current. *Procedia Engineering*, *105*, 287–293.

Abbasi, M., Domiri Ganji, D., & Taeibi Rahni, M. (2014). MHD flow in a channel using new combination of order of magnitude technique and HPM. Tehnički vjesnik, 21(2), 317-321.

AbdEl-Gaied, S. M., & Hamad, M. A. A. (2013). MHD forced convection laminar boundary layer flow of alumina-water nanofluid over a moving permeable flat plate with convective surface boundary condition. Journal of Applied Mathematics, 2013 (2013), 1-8, doi:10.1155/2013/403210.

Ahmad, S., & Pop, I. (2010). Mixed convection boundary layer flow from a vertical flat plate embedded in a porous medium filled with nanofluids. International Communications in Heat and Mass Transfer, 37(8), 987-991.

Ahmed, M. E. S., & Attia, H. A. (1998). Magnetohydrodynamic flow and heat transfer of a non-Newtonian fluid in an eccentric annulus. *Can. J. Phys*, *76*, 391–401.

Akbar, N. S., Raza, M., & Ellahi, R. (2015). Influence of induced magnetic field and heat flux with the suspension of carbon nanotubes for the peristaltic flow in a permeable channel. *Journal of Magnetism and Magnetic Materials*, *381*, 405–415.

Ashraf, M., Syed, K. S., & Anwar Kamal, M. (2011). Numerical simulation of flow of micropolar fluids in a channel with a porous wall. *International Journal for Numerical Methods in Fluids*, *66*(7), 906-918.

Aski, F. S., Nasirkhani, S. J., Mohammadian, E., & Asgari, A. (2014). Application of Adomian decomposition method for micropolar flow in a porous channel. *Propulsion and Power Research*, *3*(1), 15-21.

Attia, H., & Sayed-Ahmed, M. E. (2010). Transient MHD Couette flow of a Casson fluid between parallel plates with heat transfer. *Italian J Pure Appl Math*, *27*, 19–38.

Balu, R. (1980). An application of Keller's method to the solution of an eighth-order nonlinear boundary value problem. *International Journal for Numerical Methods in Engineering*, *15*(8), 1177–1186.

Batra, R. L., & Jena, B. (1991). Flow of a Casson fluid in a slightly curved tube. *International Journal of Engineering Science*, *29*(10), 1245–1258.

Bég, O. A., Prasad, V. R., & Vasu, B. (2013). Numerical study of mixed bioconvection in porous media saturated with nanofluid containing oxytactic microorganisms. *Journal of Mechanics in Medicine and Biology*, *13*(04), 1350067.

Benis, A. M. (1968). Theory of non-Newtonian flow through porous media in narrow three-dimensional channels. *International Journal of Non-Linear Mechanics*, *3*(1), 31-46.

Berman, A. S. (1953). Laminar flow in channels with porous walls. *Journal of Applied Physics*, *24*(9), 1232–1235.

Bethune, D. S., Kiang, C. H., De Vries, M. S., Gorman, G., Savoy, R., Vazquez, J., & Beyers, R. (1993). Cobalt-catalysed growth of carbon nanotubes with single-atomic-layer walls. *Nature*, *363*(6430), 605.

Bhatti, M. M., Abbas, T., & Rashidi, M. M. (2016). Entropy analysis on titanium magneto-nanoparticles suspended in water-based nanofluid: a numerical study. *Computational Thermal Sciences: An International Journal*, 8(5), 457-468.

Bockrath, M., Cobden, D. H., McEuen, P. L., Chopra, N. G., Zettl, A., Thess, A., & Smalley, R. E. (1997). Single-electron transport in ropes of carbon nanotubes. *Science*, *275*(5308), 1922–1925.

Brady, J. F. (1984). Flow development in a porous channel and tube. *Physics of Fluids (1958-1988)*, *27*(5), 1061–1067.

Brinkman, H. C. (1952). The viscosity of concentrated suspensions and solutions. *The Journal of Chemical Physics*, *20*(4), 571.

Bujurke, N. M., Pai, N. P., & Jayaraman, G. (1998). Computer extended series solution for unsteady flow in a contracting or expanding pipe. *IMA Journal of Applied Mathematics*, *60*(2), 151–165.

Buongiorno, J. (2006). Convective transport in nanofluids. *Journal of Heat Transfer*, *128*(3), 240–250.

Casson, N. (1959). *A flow equation for pigment-oil suspensions of the printing ink type*. Pergamon press.

Chamkha, A. J., & Aly, A. M. (2010). MHD free convection flow of a nanofluid past a vertical plate in the presence of heat generation or absorption effects. *Chemical Engineering Communications*, *198*(3), 425–441.

Chang, H. N., Ha, J. S., Park, J. K., Kim, I. H., & Shin, H. D. (1989). Velocity field of pulsatile flow in a porous tube. *Journal of Biomechanics*, *22*(11), 1257–1262.

Choi, S. U. S. (2009). Nanofluids: from vision to reality through research. *Journal of Heat Transfer*, *131*(3), 33106.

Cox, S. M. (1991). Analysis of steady flow in a channel with one porous wall, or with accelerating walls. *SIAM Journal on Applied Mathematics*, *51*(2), 429–438.

Croisille, J.-P. (2002). Keller's box-scheme for the one-dimensional stationary convection-diffusion equation. *Computing*, *68*(1), 37–63.

Das, M., Mahato, R., & Nandkeolyar, R. (2015). Newtonian heating effect on unsteady hydromagnetic Casson fluid flow past a flat plate with heat and mass transfer. *Alexandria Engineering Journal*, *54*(4), 871–879.

Dash, R. K., Mehta, K. N., & Jayaraman, G. (1996). Casson fluid flow in a pipe filled with a homogeneous porous medium. International Journal of Engineering Science, 34(10), 1145-1156.

Dauenhauer, E. C., & Majdalani, J. (2003). Exact self-similarity solution of the Navier--Stokes equations for a porous channel with orthogonally moving walls. *Physics of Fluids (1994-Present)*, *15*(6), 1485–1495.

Dogonchi, A. S., Alizadeh, M., & Ganji, D. D. (2017). Investigation of MHD Go-water nanofluid flow and heat transfer in a porous channel in the presence of thermal radiation effect. *Advanced Powder Technology,* 28(7), 1815-1825.

Eldabe, N. T., Elbashbeshy, E. M. A., & Elsaid, E. M. (2013). Effects of Magnetic Field and Heat Generation on Viscous Flow and Heat Transfer over a Nonlinearly Stretching Surface in a Nanofluid. *International Journal of Applied Mathematics*, *28*(1), 1130.

Eldabe, N. T. M., Saddeck, G., & El-Sayed, A. F. (2001). Heat transfer of MHD non-Newtonian Casson fluid flow between two rotating cylinders. *Mechanics and Mechanical Engineering*, *5*(2), 237–251.

Ellahi, R., Hassan, M., & Zeeshan, A. (2015). Shape effects of nanosize particles in Cu--H2O nanofluid on entropy generation. *International Journal of Heat and Mass Transfer*, *81*, 449–456.

Eringen, A. C. (1964). Simple microfluids. *International Journal of Engineering Science*, *2*(2), 205–217.

Fan, C., & Chao, B.-T. (1965). Unsteady, laminar, incompressible flow through rectangular ducts. *Zeitschrift F{ü}r Angewandte Mathematik Und Physik ZAMP*, *16*(3), 351–360.

Fakour, M., Vahabzadeh, A., Ganji, D. D., & Hatami, M. (2015). Analytical study of micropolar fluid flow and heat transfer in a channel with permeable walls. *Journal of Molecular Liquids*, *204*, 198-204.

Freidoonimehr, N., Rostami, B., & Rashidi, M. M. (2015). Predictor homotopy analysis method for nanofluid flow through expanding or contracting gaps with permeable walls. *International Journal of Biomathematics*, *8*(04), 1550050.

Ganesh, S., & Krishnambal, S. (2006). Magnetohydrodynamic flow of viscous fluid between two parallel porous plates. *Journal of Applied Sciences*, *6*(11), 2420-2425.

Goto, M., & Uchida, S. (1990). Unsteady flows in a semi-infinite expanding pipe with injection through wall. *Japan Society for Aeronautical and Space Sciences, Journal (ISSN 0021-4663),* Vol. 38, No. 434, 1990, P. 131-138. In Japanese, with Abstract in English., 38, 131–138.

Hamad, M. A. A., Pop, I., & Ismail, A. I. M. (2011). Magnetic field effects on free convection flow of a nanofluid past a vertical semi-infinite flat plate. *Nonlinear Analysis: Real World Applications*, *12*(3), 1338–1346.

Haq, R. U., Khan, Z. H., & Khan, W. A. (2014). Thermophysical effects of carbon nanotubes on MHD flow over a stretching surface. *Physica E: Low-Dimensional Systems and Nanostructures*, *63*, 215–222.

Haq, R. U., Nadeem, S., Khan, Z. H., & Noor, N. F. M. (2015). Convective heat transfer in MHD slip flow over a stretching surface in the presence of carbon nanotubes. *Physica B: Condensed Matter*, *457*, 40–47.

Harris, S. D., Ingham, D. B., & Pop, I. (2009). Mixed convection boundary-layer flow near the stagnation point on a vertical surface in a porous medium: Brinkman model with slip. *Transport in Porous Media*, *77*(2), 267-285.

Hatami, M., Sahebi, S. A. R., Majidian, A., Sheikholeslami, M., Jing, D., & Domairry, G. (2015). Numerical analysis of nanofluid flow conveying nanoparticles through expanding and contracting gaps between permeable walls. *Journal of Molecular Liquids*, *212*, 785-791.

Hauke, G., & Moreau, R. (2008). *An introduction to fluid mechanics and transport phenomena* (Vol. 86). Springer.

Hayat, T., & Abbas, Z. (2008). Heat transfer analysis on the MHD flow of a second grade fluid in a channel with porous medium. *Chaos, Solitons & Fractals*, *38*(2), 556–567.

Hayat, T., Imtiaz, M., Alsaedi, A., & Mansoor, R. (2014). MHD flow of nanofluids over an exponentially stretching sheet in a porous medium with convective boundary conditions. *Chinese Physics B*, *23*(5), 54701.

Hewitt, R. E., Duck, P. W., & Al-Azhari, M. (2003). Extensions to three-dimensional flow in a porous channel. *Fluid Dynamics Research*, *33*(1), 17–39.

Hossain, M., Roy, N. C., & Hossain, A. (2013). Boundary layer flow and heat transfer in a micropolar fluid past a permeable at plate. *Theoretical and Applied Mechanics*, *40*(3), 403–425.

Hoyt, J. W., & Fabula, A. G. (1964). *The effect of additives on fluid friction* (NOTS-TP-3670). Naval ordnance test station china lake calif, United States

Hussain, S., & Ahmad, F. (2014). MHD Flow of Micropolar Fluids over a Shrinking Sheet with Mass Suction. *Basic Appl. Sci. Res*, *4*(2), 174–179.

Iijima, S., & Ichihashi, T. (1993). Single-shell carbon nanotubes of 1-nm diameter. *nature*, *363*(6430), 603-605.

Iijima, S., & others. (1991). Helical microtubules of graphitic carbon. *Nature*, *354*(6348), 56–58.

Ishak, A. and Nazar, R. (2010). Effects of suction and injection on the stagnation point flow over a stretching sheet in a micropolar fluid. In *Proc. 2nd Int. Conf. Mathematical Sciences ICMS2* (Vol. 1, p. 7).

Ishak, A., Nazar, R., & Pop, I. (2006). Flow of a micropolar fluid on a continuous moving surface. *Archives of Mechanics*, *58*(6), 529–541.

Jafaryar, M., Farkhadnia, F., Mohammadian, E., Hosseini, M., & Khazaee, A. M. (2014). Analytical investigation of laminar flow through expanding or contracting gaps with porous walls. *Propulsion and Power Research*, *3*(4), 222–229.

J. Phillips, W. Bowen, E. Cagin, W. Wang (2011). Electronic and Optoelectronic Devices Based on Semiconducting Zinc Oxide. *Reference Module in Materials Science and Materials Engineering,* 6(2011), 101-127.

Jaluria, Y., & Torrance, K. E. (2002). Computational Heat Transfer (Series in Computational and Physical Processes in Mechanics and Thermal Sciences).

Jat, R. N., Saxena, V., & Rajotia, D. (2013). MHD flow and heat transfer near the stagnation point of a micropolar fluid over a stretching surface with heat generation/absorption. *Indian J. Pure Appl. Phys*, *51*, 683–689.

Jena, S. K., & Mathur, M. N. (1981). Similarity solutions for laminar free convection flow of a thermomicropolar fluid past a non-isothermal vertical flat plate. *International Journal of Engineering Science*, *19*(11), 1431-1439.

Kameswaran, P. K., Shaw, S., & Sibanda, P. (2014). Dual solutions of Casson fluid flow over a stretching or shrinking sheet. *Sadhana*, *39*(6), 1573–1583.

Kandelousi, M. S. (2014). Effect of spatially variable magnetic field on ferrofluid flow and heat transfer considering constant heat flux boundary condition. *The European Physical Journal Plus*, *129*(11), 1–12.

Kataria, H. R., & Patel, H. R. (2016). Radiation and chemical reaction effects on MHD Casson fluid flow past an oscillating vertical plate embedded in porous medium. *Alexandria Engineering Journal*, *55*(1), 583–595.

Kelson, N. A., Desseaux, A., & Farrell, T. W. (2003). Micropolar flow in a porous channel with high mass transfer. *ANZIAM Journal*, *44*, 479–495.

Khan, U., Ahmed, N., & Mohyud-Din, S. T. (2015). Heat transfer effects on carbon nanotubes suspended nanofluid flow in a channel with non-parallel walls under the effect of velocity slip boundary condition: a numerical study. *Neural Computing and Applications*, 1–10.

Khan, U., Ahmed, N., & Mohyud-Din, S. T. (2016). Stoke's First Problem for Carbon Nanotubes Suspended Nanofluid Flow Under the Effect of Slip Boundary Condition. *Journal of Nanofluids*, *5*(2), 239–244.

Khodashenas, B., & Ghorbani, H. R. (2014). Synthesis of copper nanoparticles: An overview of the various methods. *Korean Journal of Chemical Engineering*, *31*(7), 1105-1109.

Konieczny, J., & Rdzawski, Z. (2012). Antibacterial properties of copper and its alloys. *Archives of Materials Science and Engineering*, *56*(2), 53-60.

Kishan, N., & Jagadha, S. (2013). MHD effects on non-Newtonian micro polar fluid with uniform suction/blowing and heat generation in the presence of chemical reaction and thermophoresis. *International Journal of Research in Engineering and Technology*, *2*(9), 350–358.

Kleinstreuer, C., Li, J., & Koo, J. (2008). Microfluidics of nano-drug delivery. *International Journal of Heat and Mass Transfer*, *51*(23), 5590–5597.

Kumar, J. P., Umavathi, J. C., Chamkha, A. J., & Pop, I. (2010). Fully-developed free-convective flow of micropolar and viscous fluids in a vertical channel. *Applied Mathematical Modelling*, *34*(5), 1175–1186.

Kumar, N., Jain, T., & Gupta, S. (2012). Effects of Radiation, Free Convection and Mass Transfer on an Unsteady Flow of a Micropolar Fluid Over a Vertical Moving Porous Plate Immersed in a Porous Medium With Time Varying Suction. *International Journal of Theoretical and Applied Science*, *4*(1), 23–29.

Kuznetsov, A. V., & Nield, D. A. (2010). Natural convective boundary-layer flow of a nanofluid past a vertical plate. *International Journal of Thermal Sciences*, *49*(2), 243–247.

Liu, J. B., Gao, W., Siddiqui, M. K., & Farahani, M. R. (2016). Computing three topological indices for Titania nanotubes. *AKCE International Journal of Graphs and Combinatorics*, *13*(3), 255-260.

Majdalani, J., & Zhou, C. (2003). Moderate-to-large injection and suction driven channel flows with expanding or contracting walls. *ZAMM*, *83*(3), 181–196.

Makanda, G., Shaw, S., & Sibanda, P. (2015). Diffusion of chemically reactive species in Casson fluid flow over an unsteady stretching surface in porous medium in the presence of a magnetic field. *Mathematical Problems in Engineering*, *2015*.

Marsden, J. E., & Ratiu, T. S. (1999). Introduction to Mechanics and Symmetry, volume 17 of Texts in Applied Mathematics, 17,1994.

Meade, D. B., Haran, B. S., & White, R. E. (1996). The shooting technique for the solution of two-point boundary value problems. *Maple Technical Newsletter*, *3*(1).

Mekheimer, K. S., & El Kot, M. A. (2008). The micropolar fluid model for blood flow through a tapered artery with a stenosis. *Acta Mechanica Sinica*, *24*(6), 637–644.

Merkin, J. H. (1986). On dual solutions occurring in mixed convection in a porous medium. *Journal of engineering Mathematics*, *20*(2), 171-179.

Merrill, E. W., Benis, A. M., Gilliland, E. R., Sherwood, T. K., & Salzman, E. W. (1965). Pressure-flow relations of human blood in hollow fibers at low flow rates. *Journal of Applied Physiology*, *20*(5), 954–967.

Mehmood, R., Nadeem, S., & Masood, S. (2016). Effects of transverse magnetic field on a rotating micropolar fluid between parallel plates with heat transfer. *Journal of Magnetism and Magnetic Materials*, *401*, 1006-1014.

Misra, J. C., Shit, G. C., & Rath, H. J. (2008). Flow and heat transfer of a MHD viscoelastic fluid in a channel with stretching walls: Some applications to haemodynamics. *Computers & Fluids*, *37*(1), 1–11.

Mukhopadhyay, S. (2013). Casson fluid flow and heat transfer over a nonlinearly stretching surface. *Chinese Physics B*, *22*(7), 74701.

Mukhopadhyay, S., Moindal, I. C., & Hayat, T. (2014). MHD boundary layer flow of Casson fluid passing through an exponentially stretching permeable surface with thermal radiation. Chinese Physics B, 23(10), 104701.

Muraviev, D. N., Macanás, J., Farre, M., Munoz, M., & Alegret, S. (2006). Novel routes for inter-matrix synthesis and characterization of polymer stabilized metal nanoparticles for molecular recognition devices. *Sensors and Actuators B: Chemical*, *118*(1-2), 408-417.

Mustafa, M., & Khan, J. A. (2015). Model for flow of Casson nanofluid past a non-linearly stretching sheet considering magnetic field effects. AIP Advances, 5(7), 077148.

Na, T. Y. (1980). *Computational methods in engineering boundary value problems* (Vol. 145). Academic Press.

Nadeem, S., Haq, R. U., Akbar, N. S., & Khan, Z. H. (2013). MHD three-dimensional Casson fluid flow past a porous linearly stretching sheet. Alexandria Engineering Journal, 52(4), 577-582.

Nichols, W., O'Rourke, M., & Vlachopoulos, C. (2011). *McDonald's blood flow in arteries: theoretical, experimental and clinical principles*. CRC Press.

Nouri, R., Ganji, D. D., & Hatami, M. (2013). MHD Nanofluid Flow Analysis in a Semi-Porous Channel by a Combined Series Solution Method. *Transport Phenomena in Nano and Micro Scales*, *1*(2), 124–137.

Parveen, S., Misra, R., & Sahoo, S. K. (2012). Nanoparticles: a boon to drug delivery, therapeutics, diagnostics and imaging. *Nanomedicine: Nanotechnology, Biology and Medicine*, *8*(2), 147-166.

Prathap K., J., Umavathi, J. C., & Shreedevi, K. (2014). Chemical Reaction Effects on Mixed Convection Flow of Two Immiscible Viscous Fluids in a Vertical Channel. *Open Journal of Heat, Mass and Momentum Transfer,* 2(2), 28-46.

Pritchard, P. J., & Mitchell, J. W. (2011). Fox and McDonald's Introduction to Fluid Mechanics. Wiley, Hoboken, NJ.

Qi, X. G., Scott, D. M., & Wilson, D. I. (2008). Modelling laminar pulsed flow in rectangular microchannels. *Chemical Engineering Science*, *63*(10), 2682–2689.

Raju, C. S. K., Sandeep, N., Sugunamma, V., Babu, M. J., & Reddy, J. R. (2016). Heat and mass transfer in magnetohydrodynamic Casson fluid over an exponentially permeable stretching surface. *Engineering Science and Technology, an International Journal*, *19*(1), 45-52.

Rahimi, E., Rahimifar, A., Mohammadyari, R., Rahimipetroudi, I., & Rahimi-Esbo, M. (2016). Analytical approach for solving two-dimensional laminar viscous flow between slowly expanding and contracting walls. Ain Shams Engineering Journal, 7(4), 1089-1097.

Ramesh, K., & Devakar, M. (2015). Some analytical solutions for flows of Casson fluid with slip boundary conditions. *Ain Shams Engineering Journal*, *6*(3), 967–975.

Rangi, R. R., & Ahmad, N. (2012). Boundary layer flow past a stretching cylinder and heat transfer with variable thermal conductivity. *Applied mathematics*, *3*(3), 205-209.

Rao, S. L., & Iyengar, T. K. V. (1981). The slow stationary flow of incompressible micropolar fluid past a spheroid. *International Journal of Engineering Science*, *19*(2), 189-220.

Rauf, A., Siddiq, M. K., Abbasi, F. M., Meraj, M. A., Ashraf, M., & Shehzad, S. A. (2016). Influence of convective conditions on three dimensional mixed convective hydromagnetic boundary layer flow of Casson nanofluid. *Journal of Magnetism and Magnetic Materials*, *416*, 200-207.

Saidulu, N., & Lakshmi, A. V. (2016). Slip effects on MHD flow of casson fluid over an exponentially stretching sheet in presence of thermal radiation, heat source/sink and chemical reaction. *European journal of advances in engineering and technology*, *3*(1).

Rashidi, S., Dehghan, M., Ellahi, R., Riaz, M., & Jamal-Abad, M. T. (2015). Study of stream wise transverse magnetic fluid flow with heat transfer around an obstacle embedded in a porous medium. *Journal of Magnetism and Magnetic Materials*, *378*, 128–137.

Reddy, C. R., Rao, C. V., & Surender, O. (2015). Soret, joule heating and Hall effects on free convection in a Casson fluid saturated porous medium in a vertical channel in the presence of viscous dissipation. *Procedia Engineering*, *127*, 1219–1226.

Reddy, K. R., & Raju, G. S. S. (2014). Fully developed free convection flow of a third grade fluid through a porous medium in a vertical channel. *Int J Concept Comput Inf Technol*, *2*, 2345-9808.

Richmond, W. R., Jones, R. L., & Fawell, P. D. (1998). The relationship between particle aggregation and rheology in mixed silica–titania suspensions. *Chemical Engineering Journal*, *71*(1), 67-75.

Robinson, W. A. (1976). The existence of multiple solutions for the laminar flow in a uniformly porous channel with suction at both walls. *Journal of Engineering Mathematics*, *10*(1), 23–40.

Rohni, A. M., Omar, Z., & Ibrahim, A. (2008). Free Convection over a Vertical Plate in a Micropolar Fluid Subjected to a Step Change in Surface Temperature. *Modern Applied Science*, *3*(1), 22.

Rohni, A.M. (2013). Multiple similarity solutions of Steady and unsteady Convection boundary layer flows in Viscous fluids and nanofluids (Doctoral thesis). Universiti Sains Malaysia (USM), Pulau Pinang, Malaysia.

Roşca, A. V., & Pop, I. (2013). Flow and heat transfer over a vertical permeable stretching/shrinking sheet with a second order slip. *International Journal of Heat and Mass Transfer*, *60*, 355-364.

Rossow, V. J. (1958). *On flow of electrically conducting fluids over a flat plate in the presence of a transverse magnetic field* (NACA-TR-1358). National Advisory Committee for Aeronautics. Ames Aeronautical Lab.; Moffett Field, CA, United States

Sadek, H. A. A., Khami, M. J., & Obaid, T. A. S. (2013). Computer Simulation of Blood Flow in Large Arteries by a Finite Element Method. *Science and Engineering (IJCSE)*, *2*(4), 171–184.

Sajid, M., Abbas, Z., & Hayat, T. (2009). Homotopy analysis for boundary layer flow of a micropolar fluid through a porous channel. *Applied Mathematical Modelling*, *33*(11), 4120-4125.

Sarif, N. M., Salleh, M. Z., & Nazar, R. (2013). Numerical solution of flow and heat transfer over a stretching sheet with Newtonian heating using the Keller box method. *Procedia Engineering*, *53*, 542–554.

Sarojamma, G., Vasundhara, B., & Vendabai, K. (2014). MHD Casson fluid flow, heat and mass transfer in a vertical channel with stretching Walls. *Int. J. Sci and Innovative Mathhematical Res*, *2*(10), 800-810.

Sastry, V. U. K., & Rao, V. R. M. (1982). Numerical solution of micropolar fluid flow in a channel with porous walls. *International Journal of Engineering Science*, *20*(5), 631-642.

Shateyi, S., & Prakash, J. (2014). A new numerical approach for MHD laminar boundary layer flow and heat transfer of nanofluids over a moving surface in the presence of thermal radiation. *Boundary Value Problems*, *2014*(1), 1–12.

Shehzad, S. A., Hayat, T., Qasim, M., & Asghar, S. (2013). Effects of mass transfer on MHD flow of Casson fluid with chemical reaction and suction. *Brazilian Journal of Chemical Engineering*, *30*(1), 187–195.

Sheikholeslami, M., & Ganji, D. D. (2013). Heat transfer of Cu-water nanofluid flow between parallel plates. *Powder Technology*, 235, 873-879.

Sheikholeslami, M., Ashorynejad, H. R., Ganji, D. D., & Rashidi, M. M. (2014). Heat and mass transfer of a micropolar fluid in a porous channel. *Communications in Numerical Analysis*, *2014*.

Sheikholeslami, M., Ashorynejad, H. R., & Rana, P. (2016). Lattice Boltzmann simulation of nanofluid heat transfer enhancement and entropy generation. *Journal of Molecular Liquids*, *214*, 86–95.

Sheikholeslami, M., & Ellahi, R. (2015). Three dimensional mesoscopic simulation of magnetic field effect on natural convection of nanofluid. *International Journal of Heat and Mass Transfer*, *89*, 799–808.

Sheikholeslami, M., & Ganji, D. D. (2014a). Numerical investigation for two phase modeling of nanofluid in a rotating system with permeable sheet. *Journal of Molecular Liquids*, *194*, 13–19.

Sheikholeslami, M., & Ganji, D. D. (2014b). Three dimensional heat and mass transfer in a rotating system using nanofluid. *Powder Technology*, *253*, 789–796.

Sheikholeslami, M., & Ganji, D. D. (2015). Nanofluid flow and heat transfer between parallel plates considering Brownian motion using DTM. *Computer Methods in Applied Mechanics and Engineering*, *283*, 651–663.

Sheikholeslami, M., Hatami, M., & Ganji, D. D. (2014). Micropolar fluid flow and heat transfer in a permeable channel using analytical method. *Journal of Molecular Liquids*, *194*, 30-36.

Sheikholeslami, M., Ganji, D. D., Javed, M. Y., & Ellahi, R. (2015). Effect of thermal radiation on magnetohydrodynamics nanofluid flow and heat transfer by means of two phase model. *Journal of Magnetism and Magnetic Materials*, *374*, 36–43.

Sheikholeslami, M., Hatami, M., & Ganji, D. D. (2013). Analytical investigation of MHD nanofluid flow in a semi-porous channel. *Powder Technology*, *246*, 327–336.

Sheikholeslami, M., Rashidi, M. M., & Ganji, D. D. (2015a). Effect of non-uniform magnetic field on forced convection heat transfer of--water nanofluid. *Computer Methods in Applied Mechanics and Engineering*, *294*, 299–312.

Sheikholeslami, M., Rashidi, M. M., & Ganji, D. D. (2015b). Numerical investigation of magnetic nanofluid forced convective heat transfer in existence of variable magnetic field using two phase model. *Journal of Molecular Liquids*, *212*, 117–126.

Sheikholeslami, M., Soleimani, S., & Ganji, D. D. (2016). Effect of electric field on hydrothermal behavior of nanofluid in a complex geometry. *Journal of Molecular Liquids*, *213*, 153–161.

Sheikholeslami, M., Vajravelu, K., & Rashidi, M. M. (2016). Forced convection heat transfer in a semi annulus under the influence of a variable magnetic field. *International Journal of Heat and Mass Transfer*, *92*, 339–348.

Sheikholeslami, M., & Bhatti, M. M. (2017). Active method for nanofluid heat transfer enhancement by means of EHD. *International Journal of Heat and Mass Transfer*, 109, 115-122.

Sheikholeslami, M., Ganji, D. D., & Rashidi, M. M. (2015). Ferrofluid flow and heat transfer in a semi annulus enclosure in the presence of magnetic source considering thermal radiation. *Journal of the Taiwan Institute of Chemical Engineers*, 47, 6-17.

Sheremet, M. A., Grosan, T., & Pop, I. (2015). Free convection in a square cavity filled with a porous medium saturated by nanofluid using Tiwari and Das' nanofluid model. *Transport in Porous Media*, *106*(3), 595-610.

Shercliff, J. A. (1965). *Textbook of magnetohydrodynamics*. Pergamon Press, New York

Shi, P., He, P., Teh, T. K. H., Morsi, Y. S., & Goh, J. C. H. (2011). Parametric analysis of shape changes of alginate beads. *Powder Technology*, *210*(1), 60–66.

Shrestha, G. M., & Terrill, R. M. (1968). Laminar flow with large injection through parallel and uniformly porous walls of different permearility. *The Quarterly Journal of Mechanics and Applied Mathematics*, *21*(4), 413–432.

Si, X., Zheng, L., Zhang, X., & Chao, Y. (2010). Perturbation solution to unsteady flow in a porous channel with expanding or contracting walls in the presence of a transverse magnetic field. *Applied Mathematics and Mechanics*, *31*, 151–158.

Soleimani, S., Sheikholeslami, M., Ganji, D. D., & Gorji-Bandpay, M. (2012). Natural convection heat transfer in a nanofluid filled semi-annulus enclosure. *International Communications in Heat and Mass Transfer*, *39*(4), 565–574.

Sreenadh, S., Kishore, S. N., Srinivas, A. N. S., & Reddy, R. H. Flow of an Incompressible Micropolar Fluid Through a Channel Bounded By a Permeable Bed. *International Journal of Mathematics And Scientific Computing*, 2(1), 2012.

Tamoor, M., Waqas, M., Khan, M. I., Alsaedi, A., & Hayat, T. (2017). Magnetohydrodynamic flow of Casson fluid over a stretching cylinder. *Results in physics*, *7*, 498-502.

Tans, S. J., Devoret, M. H., Dai, H., Thess, A., Smalley, R. E., Georliga, L. J., & Dekker, C. (1997). Individual single-wall carbon nanotubes as quantum wires. *Nature* 386 (6624), 474-477.

Tans, S. J., Verschueren, A. R. M., & Dekker, C. (1998). Room-temperature transistor based on a single carbon nanotube. *Nature*, *393*(6680), 49–52.

Tiwari, R. K., & Das, M. K. (2007). Heat transfer augmentation in a two-sided lid-driven differentially heated square cavity utilizing nanofluids. *International Journal of Heat and Mass Transfer*, *50*(9), 2002–2018.

Uchida, S., & Aoki, H. (1977). Unsteady flows in a semi-infinite contracting or expanding pipe. *Journal of Fluid Mechanics*, *82*(02), 371–387.

Uddin, M. S. (2013). Chemically Reactive Solute Transfer over a Plate in Porous Medium in Presence of Suction. *Journal of Physical Sciences*, 17, 97-109.

Walawender, W. P., Chen, T. Y., & Cala, D. F. (1975). An approximate Casson fluid model for tube flow of blood. *Biorheology*, *12*(2), 111–119.

Watson, E. B. B., Banks, W. H. H., Zaturska, M. B., & Drazin, P. G. (1990). On transition to chaos in two-dimensional channel flow symmetrically driven by accelerating walls. *Journal of Fluid Mechanics*, *212*, 451–485.

Wong, K. V, & De Leon, O. (2010). Applications of nanofluids: current and future. *Advances in Mechanical Engineering*, *2*, 519659.

Yadav, D., Agrawal, G. S., & Bhargava, R. (2011). Thermal instability of rotating nanofluid layer. *International Journal of Engineering Science*, *49*(11), 1171–1184.

Ziabakhsh, Z., & Domairry, G. (2008). Homotopy analysis solution of micropolar flow in a porous channel with high mass transfer. *Adv. Theor. Appl. Mech*, *1*(2), 79–94.

APPENDIX-A

DERIVATION OF THE PROBLEM 3.3

$$\frac{\partial u}{\partial x} + \frac{\partial v}{\partial y} = 0 \tag{1}$$

$$\left(\rho_f(1-\varphi) + \rho_s\right)\left(u\frac{\partial u}{\partial x} + v\frac{\partial u}{\partial y}\right) = -\frac{\partial p}{\partial x} + \left(\frac{\mu_f}{(1-\varphi)^{2.5}}\right)\frac{\partial^2 u}{\partial y^2} - \sigma_{nf}B_\circ^2 u \tag{2}$$

$$\left(\rho_f(1-\varphi) + \rho_s\right)\left(u\frac{\partial v}{\partial x} + v\frac{\partial v}{\partial y}\right) = -\frac{\partial p}{\partial y} + \left(\frac{\mu_f}{(1-\varphi)^{2.5}}\right)\frac{\partial^2 v}{\partial x^2} \tag{3}$$

$$u\frac{\partial T}{\partial x} + v\frac{\partial T}{\partial y} = \frac{k_f}{\left(\rho C_p\right)_{nf}}\left(\frac{k_s + 2k_f - 2\varphi(k_f - k_s)}{k_s + 2k_f + 2\varphi(k_f - k_s)}\right)\frac{\partial^2 T}{\partial y^2} \tag{4}$$

where u and v are the velocity component along x and y axes respectively, σ_{nf} is effective electrical conductivity of nanofluid, ρ_{nf} is effective density, μ_{nf} is the effective dynamic viscosity, $\left(\rho C_p\right)_{nf}$ is heat capacitance and k_{nf} thermal conductivity of the nanofluid. These physical quantities described mathematically as:

$$\rho_{nf} = \rho_f(1-\varphi) + \rho_s \tag{5}$$

$$\mu_{nf} = \frac{\mu_f}{(1-\varphi)^{2.5}} \tag{6}$$

$$\left(\rho C_p\right)_{nf} = \left(\rho C_p\right)_f(1-\varphi) + \left(\rho C_p\right)_s\varphi \tag{7}$$

$$\frac{k_{nf}}{k_f} = \frac{k_s + 2k_f - 2\varphi(k_f - k_s)}{k_s + 2k_f + 2\varphi(k_f - k_s)} \tag{8}$$

$$\frac{\sigma_{nf}}{\sigma_f} = 1 + \frac{3\left(\frac{\sigma_s}{\sigma_f} - 1\right)\varphi}{\left(\frac{\sigma_s}{\sigma_f} + 2\right) - \left(\frac{\sigma_s}{\sigma_f} - 1\right)\varphi} \tag{9}$$

Here φ is the solid volume fraction, φ_s is for nanosolid-particles and φ_f is for base fluid. The associated wall conditions are of the form:

$$u = 0, \; v = \frac{V}{2}, \; T = T_w, C = C_w \qquad \text{at} \qquad y = 0 \tag{10}$$

$$\frac{\partial u}{\partial y} = 0, \; v = 0, \; T = T_H, \; C = C_H \qquad \text{at} \qquad y = H. \tag{11}$$

Introduce the following similarity transformation,

$$x^* = \frac{x}{H}, y^* = \frac{y}{H}, u = -Vx^*f'(y^*), v = Vf(y^*), \theta(y^*) = \frac{T-T_H}{T_w-T_H}, \vartheta(y^*) = \frac{C-C_H}{C_w-C_H},$$

So, equation (2) becomes:

$$\frac{-Vx}{H}f'\left(\frac{-V}{H}f'\right) + Vf\left(\frac{-Vx}{H^2}f''\right) = \frac{\overline{1}}{\rho_{nf}}\frac{\partial p}{\partial x} + v_{nf}\left(\frac{-Vx}{H^3}f'''\right) + \frac{\sigma_{nf}B^2}{\rho_{nf}}\left(\frac{Vx}{H}\right)f'$$

191

Simplifying the above equation:

$$\frac{VH}{\nu_f}\left(f'^2 - ff''\right) = \frac{-1}{\rho_{nf}}\frac{\partial p}{\partial x} - f''' + \frac{\sigma_{nf}B_\circ^2 H^2}{\mu_{nf}}f' \tag{12}$$

Similarly, from equation (3), and taking derivative w.r.t x, we have:

$$\frac{\partial^2 p}{\partial x \partial y} = 0 \tag{13}$$

Taking derivative of equation (12), w.r.t y and put equation (13), we get:

$$f^{iv} + RA_1(1-\varphi)^{2.5}(f'f'' - ff''') + B^\circ M^2(1-\varphi)^{2.5}f'' = 0 \tag{14}$$

where $R = \frac{VH}{\nu}$ is Reynolds number ($R > 0$ for suction $R < 0$ for injection), $M^2 = \frac{\sigma B_\circ^2 H^2}{\mu_f}$ is Hartman number, and, the values of A_1, A_2, A_3 are:

$$A_1 = \frac{\rho_{nf}}{\rho_f} = (1-\varphi) + \frac{\rho_s}{\rho_f}\varphi \tag{15}$$

$$A_2 = \frac{(\rho C_p)_{nf}}{(\rho C_p)_f} = (1-\varphi) + \frac{(\rho C_p)_s}{(\rho C_p)_f}\varphi \tag{16}$$

$$A_3 = \frac{\kappa_{nf}}{\kappa_f} = \frac{\kappa_s + 2\kappa_f - 2\varphi(\kappa_f - \kappa_s)}{\kappa_s + 2\kappa_f + 2\varphi(\kappa_f - \kappa_s)} \tag{17}$$

Moreover, boundary conditions becomes

$$f(1) = \frac{1}{2}, f'(1) = 0$$

$$f''(0) = 0, f(0) = 0 \tag{18}$$

DERIVATION OF THE STABILITY ANALYSIS FOR SECTION 3.3.2

For stability, similarity variables defined as:

$$u = -Vx^* f'(y^*), v = Vf(y^*), \theta(y^*) = \frac{T-T_H}{T_w-T_H} \text{ where } x^* = \frac{x}{H}, y^* = \frac{y}{H} \qquad (17)$$

The governing equations of (3.56) – (3.57) for unsteady case $\tau = t$, can be written as:

$$\frac{\partial^4 f}{\partial \eta^4} + RA_1(1-\varphi)^{2.5}\left[\frac{\partial f}{\partial \eta}\frac{\partial^2 f}{\partial \eta^2} - f\frac{\partial^3 f}{\partial \eta^3}\right] + M^2(1-\varphi)^{2.5}\frac{\partial^2 f}{\partial \eta^2} = \frac{\partial^3 f}{\partial \tau \partial \eta^2} \qquad (18)$$

$$\frac{\partial^2 \theta}{\partial \eta^2} + Pr\frac{A_2}{A_3}f\frac{\partial \theta}{\partial \eta} = \frac{\partial \theta}{\partial \tau} \qquad (19)$$

The stability analysis of the steady flow solution $f(\eta) = f_\circ(\eta)$ and $\theta(\eta) = \theta_\circ(\eta)$.

$$f(\eta) = f_\circ(\eta) + e^{-\lambda t}F(\eta, t) \qquad (20)$$

$$\theta(\eta) = \vartheta_\circ(\eta) + e^{-\lambda t}G(\eta, t) , \qquad (21)$$

Where $0 < F(\eta, t) \ll 1, 0 < G(\eta, t) \ll 1$ and λ is the unknown eigenvalues, $F(\eta, t)$ and $G(\eta, t)$ are the smallest relative to $f_\circ(\eta)$ and $\theta_\circ(\eta)$ respectively.

Taking derivative of Eqs. (20) and (21)

$$\left.\begin{aligned}
\frac{\partial f}{\partial \eta} &= f_\circ' + e^{-\lambda t}F' \\
\frac{\partial^2 f}{\partial \eta^2} &= f_\circ'' + e^{-\lambda t}F'' \\
\frac{\partial^3 f}{\partial \eta^3} &= f_\circ''' + e^{-\lambda t}F''' \\
\frac{\partial^4 f}{\partial \eta^4} &= f_\circ'''' + e^{-\lambda t}F'''' \\
\frac{\partial^3 f}{\partial \eta^2 \partial \tau} = \frac{\partial}{\partial \tau}\left(\frac{\partial^2 f}{\partial \eta^2}\right) = \frac{\partial}{\partial \tau}\left(f_\circ'' + e^{-\lambda t}F''\right) &= te^{-\lambda t}\left(\frac{\partial F''}{\partial \tau}\right)\frac{\partial t}{\partial \tau} - \lambda e^{-\lambda t}F'' \\
\frac{\partial \theta}{\partial \eta} &= \theta_\circ' + e^{-\lambda t}G' \\
\frac{\partial^2 \theta}{\partial \eta^2} &= \theta_\circ'' + e^{-\lambda t}G''
\end{aligned}\right\} \qquad (22)$$

Use the above relation into (18) – (19) and assume $\tau = 0$.

From Eq. (18),

$$\left(f_\circ'''' + e^{-\lambda t}F''''\right) + RA_1(1-\varphi)^{2.5}\left[\left(f_\circ' + e^{-\lambda t}F'\right)\left(f_\circ'' + e^{-\lambda t}F''\right) - \left(f_\circ(\eta) + \right.\right.$$

$$\left.\left. e^{-\lambda t}F\right)\left(f_\circ'' + e^{-\lambda t}F''\right)\right] + M^2(1-\varphi)^{2.5}\left(f_\circ'' + e^{-\lambda t}F''\right) + \lambda e^{-\lambda t}F'' = 0,$$

Expand the equation,

$$f_\circ'''' + RA_1(1-\varphi)^{2.5}(f_\circ'f_\circ'' - f_\circ f_\circ''') + M^2(1-\varphi)^{2.5}f_\circ'' + e^{-\lambda t}F'''' + RA_1(1-$$

$$\varphi)^{2.5}\left[(f_\circ'F''e^{-\lambda t} + f_\circ''F'e^{-\lambda t} + F'F''e^{-2\lambda t}) - (f_\circ F'''e^{-\lambda t} + FF'''e^{-\lambda t})\right] + M^2(1-$$

$$\varphi)^{2.5}e^{-\lambda t}F'' + \lambda e^{-\lambda t}F'' = 0,$$

Since we have assumed that $F(\eta, t)$ is small, therefore the product of their derivatives are also small. So by neglecting the terms and considering the steady state:

$$f_\circ'''' + RA_1(1-\varphi)^{2.5}(f_\circ'f_\circ'' - f_\circ f_\circ''') + M^2(1-\varphi)^{2.5}f_\circ'' = 0$$

The stability equation becomes:

$$F'''' + RA_1(1-\varphi)^{2.5}[(f_\circ'F'' + f_\circ''F') - (f_\circ F''' + Ff_\circ''')]$$

$$+M^2(1-\varphi)^{2.5}F'' + \lambda F'' = 0 \tag{23}$$

Similarly from (19),

$$\left(\theta_\circ'' + e^{-\lambda t}G''\right) + Pr\frac{A_2}{A_3}\left(f_\circ(\eta) + e^{-\lambda t}F\right)\left(\theta_\circ' + e^{-\lambda t}G'\right) + \lambda e^{-\lambda t}G = 0,$$

Expand and rearrange the equation:

$$\theta_\circ'' + Pr\frac{A_2}{A_3}(f_\circ\theta_\circ') + e^{-\lambda t}G'' + Pr\frac{A_2}{A_3}\left(fG'e^{-\lambda t} + e^{-\lambda t}F\theta_\circ' + e^{-2\lambda t}FG'\right) = 0,$$

Since, we have assumed that $G(\eta, t)$ and $F(\eta, t)$ are small, therefore the product of their derivatives are also small. So by neglecting the terms and considering the steady state:

$$\theta_\circ'' + Pr\frac{A_2}{A_3}(f_\circ\theta_\circ') = 0$$

The stability equation becomes:

$$G'' + Pr\frac{A_2}{A_3}(fG' + F\theta_\circ') + \lambda G = 0. \tag{24}$$

Boundary equations becomes:

At wall $y = H$

$$u = 0 \Rightarrow = -Vx^*f'(y^*) = 0 \Rightarrow f'\left(\frac{y}{H}\right) = 0 \Rightarrow f'(1) = 0 \tag{25}$$

$$, v = \frac{V}{2} = Vf(y^*) \Rightarrow f\left(\frac{y}{H}\right) = \left(\frac{1}{2}\right) = f(1) = \frac{1}{2} \tag{26}$$

194

$$\theta(y^*) = \frac{T - T_H}{T_w - T_H} => \theta(1) = 1 \text{ as } T = T_w \tag{27}$$

At $y = 0$

$$\frac{\partial u}{\partial y} = 0 => \frac{-V}{H} x^* f^{''}(y^*) => f^{''}(0) = 0 \tag{28}$$

$$v = 0 = V f(y^*) => f\left(\frac{y}{H}\right) = 0 => f(0) = 0 \tag{29}$$

$$\theta(y^*) = \frac{T - T_H}{T_w - T_H} => \theta(0) = 0 \text{ as } T = T_H \tag{30}$$

Put Eqns. (25) – (30) into Eqns. (20) - (21) and use $\tau = t$, we get the boundary conditions for stability:

$$\left.\begin{array}{l} F(1) = \frac{1}{2}, F'(1) = 1, G(1) = 1 \\ F''(0) = 0, F(0), G(0) = 0 \end{array}\right\} \tag{31}$$

APPENDIX C

MAPLE PROGRAM

This maple program solves the problem of steady laminar incompressible nanofluid in a porous channel with the help of shooting method.

> $restart$;

> $Shootlib := $ "D:\\nanofluid/";

$$Shootlib := \text{"D:\\nanofluid/"}$$

> $libname := Shootlib, libname$;

$$libname := \text{"D:\\nanofluid/"}, \text{"C:\\Program Files\\Maple 18\\lib"}, \text{"."}$$

> $with(\, Shoot\,)$;

$$[shoot]$$

> $with(\, plots\,)$:

> $M := 1.5; R := 30.0; \varphi := 0.03; s := 0.5; \sigma_f := 0.05; \sigma_s := 5980000; S_1 := 0.0; S_2 := 0.0;$

$$M := 1.5$$
$$R := 30.0$$
$$\varphi := 0.03$$
$$s := 0.5$$
$$\sigma_f := 0.05$$
$$\sigma_{0.5} := 5980000$$
$$S_1 := 0.$$
$$S_2 := 0.$$

> $Pr := 6.0; \rho_s := 8933; \rho_f := 997.1; C_{ps} := 385; C_{pf} := 4179; K_s := 401; K_f := 0.613;$

$$Pr := 6.0$$
$$\rho_{0.5} := 8933$$
$$\rho_f := 997.1$$
$$C_{ps} := 385$$
$$C_{pf} := 4179$$
$$K_{0.5} := 401$$
$$K_f := 0.613$$

> $A_1 := (1 - \varphi) + \dfrac{\rho_s}{\rho_f} \cdot \varphi;$

$$A_1 := 1.238769431$$

> $A_2 := (1 - \varphi) + \dfrac{\rho_s \cdot C_{ps}}{\rho_f \cdot C_{pf}} \cdot \varphi;$

$$A_2 := 0.9947610029$$

> $A_3 := \dfrac{\left(K_s + 2 \cdot K_f - 2 \cdot \varphi \cdot \left(K_f - K_s\right)\right)}{\left(K_s + 2 \cdot K_f + 2 \cdot \varphi \cdot \left(K_f - K_s\right)\right)};$

$$A_3 := 1.127038834$$

> $blt1 := 1;\ blt2 := 5;\ blt3 := 6;$

$$blt1 := 1$$
$$blt2 := 5$$
$$blt3 := 6$$

> $B^{\circ} := \left(1 + \left(\dfrac{3 \cdot \left(\dfrac{\sigma_s}{\sigma_f} - 1\right) \cdot \varphi}{\left(\dfrac{\sigma_s}{\sigma_f} + 2\right) - \left(\dfrac{\sigma_s}{\sigma_f} - 1\right) \cdot \varphi}\right)\right);$

$$B^{\circ} := 1.092783503$$

> $FNS := \{F(\eta), Fp(\eta), Fpp(\eta), Fppp(\eta), \theta(\eta), \theta p(\eta)\};$

$$FNS := \{F(\eta), Fp(\eta), Fpp(\eta), Fppp(\eta), \theta(\eta), \theta p(\eta)\}$$

>
$$ODE := \Big\{ diff(F(\eta), \eta) = Fp(\eta), diff(Fp(\eta), \eta) = Fpp(\eta), diff(Fpp(\eta), \eta) = Fppp(\eta),$$
$$diff(Fppp(\eta), \eta) = -M^2 \cdot (1 - \varphi)^{2.5} \cdot Fpp(\eta) - R \cdot A_1 \cdot (1 - \varphi)^{2.5} \cdot \big(Fp(\eta) \cdot Fpp(\eta)$$
$$- F(\eta) \cdot Fppp(\eta)\big), diff(\theta(\eta), \eta) = \theta p(\eta), \frac{1}{Pr} \cdot diff(\theta p(\eta), \eta) = -\frac{A_2}{A_3} \cdot F(\eta) \cdot \theta p(\eta) \Big\};$$

$$ODE := \Big\{ 0.1666666667 \left(\frac{d}{d\eta}\, \theta p(\eta)\right) = -0.8826324106\, F(\eta)\, \theta p(\eta), \frac{d}{d\eta} F(\eta) = Fp(\eta),$$
$$\frac{d}{d\eta} Fp(\eta) = Fpp(\eta), \frac{d}{d\eta} Fpp(\eta) = Fppp(\eta), \frac{d}{d\eta} Fppp(\eta) = -2.085027819\, Fpp(\eta)$$
$$- 34.43824966\, Fp(\eta)\, Fpp(\eta) + 34.43824966\, F(\eta)\, Fppp(\eta), \frac{d}{d\eta} \theta(\eta) = \theta p(\eta) \Big\}$$

> $IC1 := \{F(1) = s, Fp(1) = S_1 \cdot \alpha,\ Fpp(1) = \alpha, Fppp(1) = \beta, \theta(1) = 0, \theta p(1) = \Omega\};$

$$IC1 := \{F(1) = 0.5, Fp(1) = 0., Fpp(1) = \alpha, Fppp(1) = \beta, \theta(1) = 0, \theta p(1) = \Omega\}$$

> $BC1 := \{F(0) = 0, Fpp(0) = 0,\ \theta(0) = 1\};$

$$BC1 := \{F(0) = 0, Fpp(0) = 0, \theta(0) = 1\}$$

>

> $infolevel[shoot] := 1 :$

> $S1 := shoot(ODE, IC1, BC1, FNS, [\alpha = -27.87843544811985, \beta = -330.38790947783133, \Omega = 0.1]) :$

197

shoot: Step # 1

shoot: Parameter values : alpha = -27.87843544811985 beta = -330.38790947783133 Omega = .1

shoot: Step # 2

shoot: Parameter values : alpha = HFloat(-26.36175378243866) beta = HFloat(-311.6398759119528) Omega = HFloat(-0.8809866159927399)

shoot: Step # 3

shoot: Parameter values : alpha = HFloat(-26.462859744145767) beta = HFloat(-314.26358245169484) Omega = HFloat(-0.9304574939017813)

shoot: Step # 4

shoot: Parameter values : alpha = HFloat(-27.754039617817263) beta = HFloat(-332.54815889671147) Omega = HFloat(-0.9428238639736823)

shoot: Step # 5

shoot: Parameter values : alpha = HFloat(-27.894451024208035) beta = HFloat(-334.82037068238213) Omega = HFloat(-0.9429413671505218)

shoot: Step # 6

shoot: Parameter values : alpha = HFloat(-28.06597704207974) beta = HFloat(-337.31819029760845) Omega = HFloat(-0.9442871983658467)

shoot: Step # 7

shoot: Parameter values : alpha = HFloat(-28.070360342937857) beta = HFloat(-337.38663667071324) Omega = HFloat(-0.9443028164268538)

shoot: Step # 8

shoot: Parameter values : alpha = HFloat(-28.07044734864878) beta = HFloat(-337.3879094575454) Omega = HFloat(-0.9443034815316692)

shoot: Step # 9

shoot: Parameter values : alpha = HFloat(-28.07044734997453) beta = HFloat(-337.3879094779187) Omega = HFloat(-0.9443034815374989)

$>$ p1 := odeplot$\left(S1, \left[\eta, \mathrm{Fp}(\eta) \right], 0 \,.. \,blt1, numpoints = 500 \right)$:

$>$ p2 := odeplot$\left(S1, \left[\eta, \mathrm{F}(\eta) \right], 0 \,..blt1, numpoints = 500 \right)$:

$>$ p3 := odeplot$\left(S1, \left[\eta, \theta(\eta) \right], 0 \,..blt1, numpoints = 500 \right)$:

$>$

$>$ p4 := odeplot$\left(S1, \left[\eta, Fppp(\eta) \right], 0 \,..blt1, numpoints = 500 \right)$:
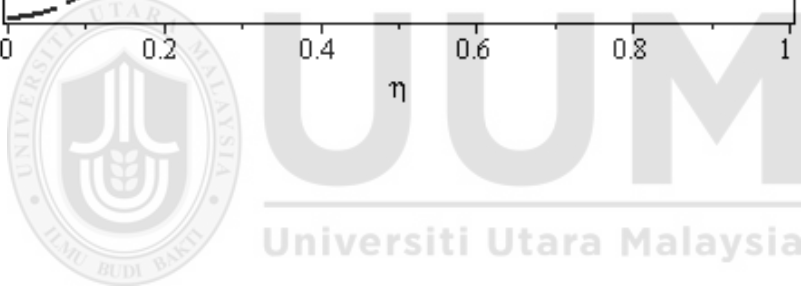
$>$

$>$ **display(p1);**

198

>
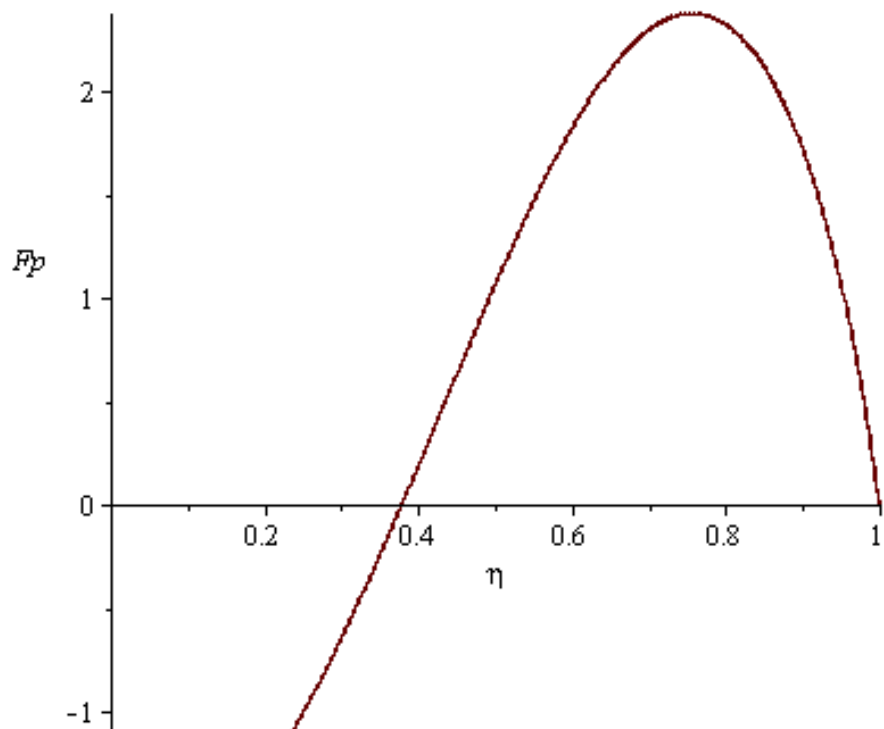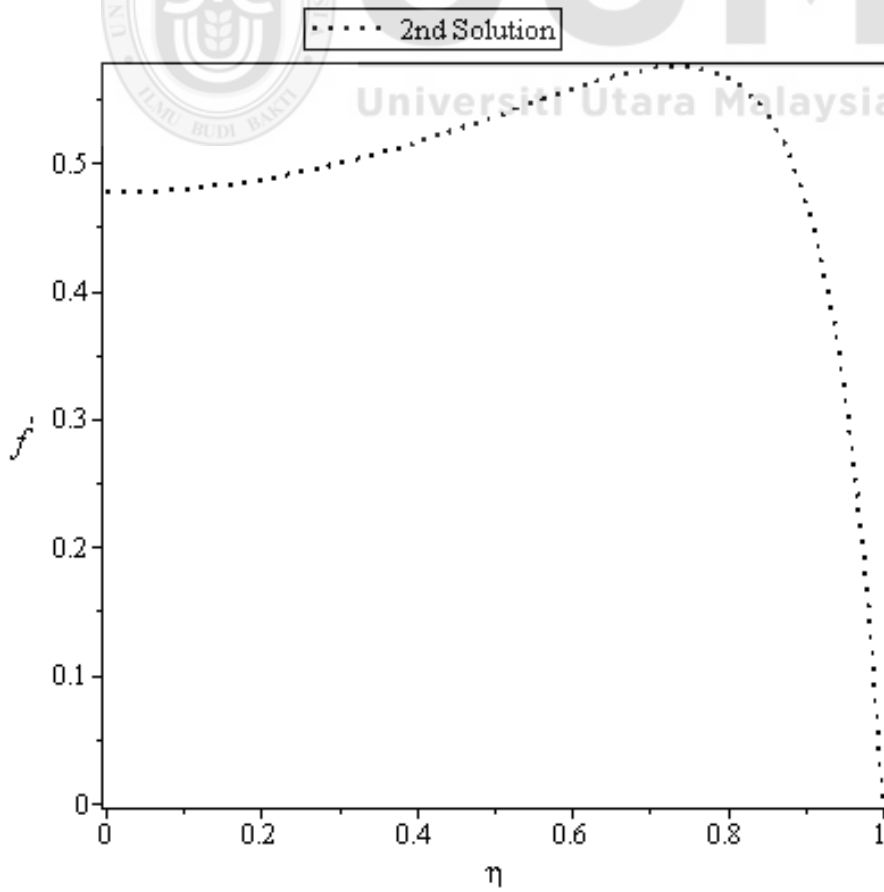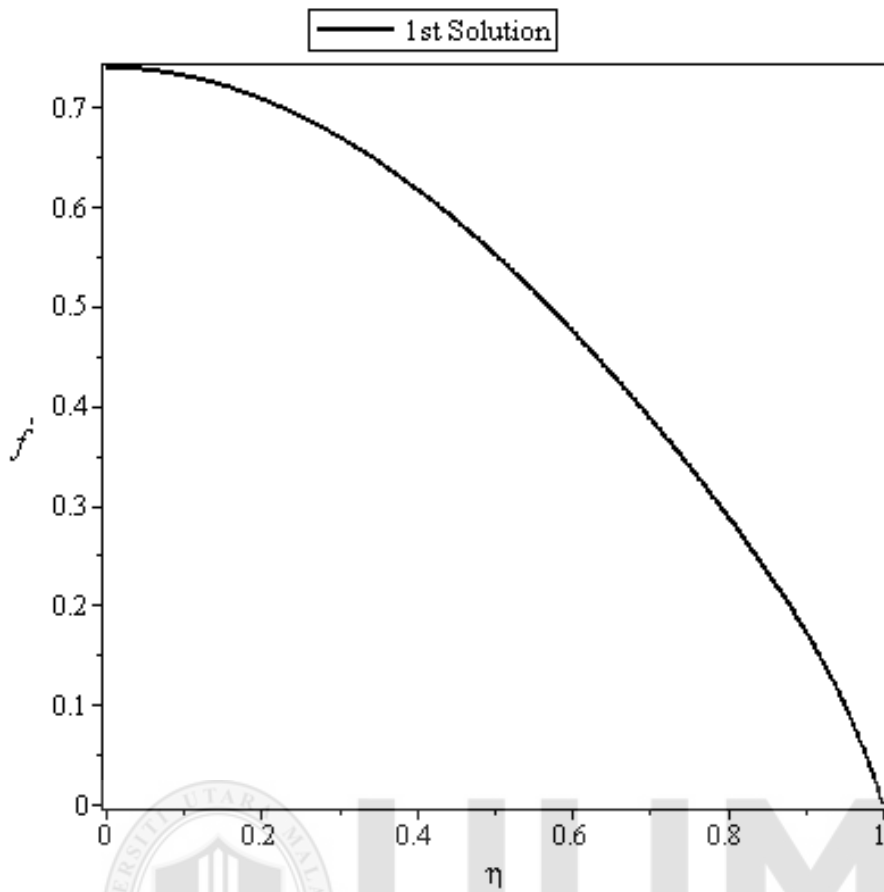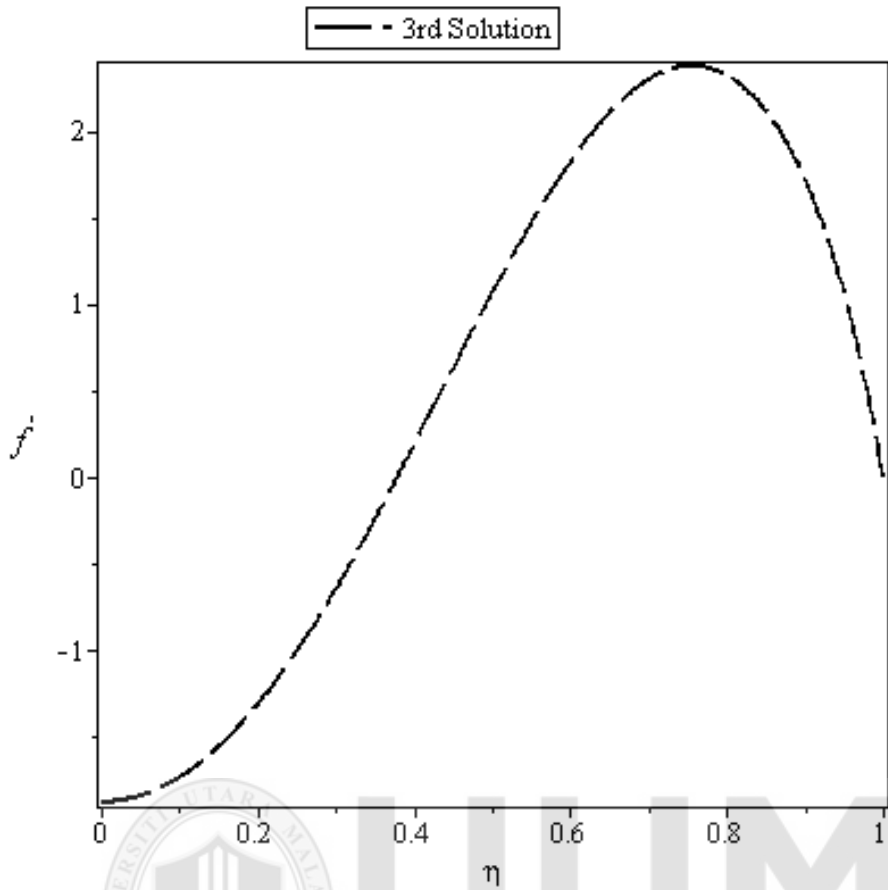
APPENDIX D

Stability Program for Section 3.3.2

This MATLAB program solves the problem of steady laminar incompressible nanofluid in a

porous channel with the help of 3-Stage Lobatto III-A Formula:

```matlab
function first_solution
clear all;
clc;
global R phi M a b Pr ros rof cps cpf ks kf A1 A2 A3
ros = 8933; rof = 991.1; cps = 385; cpf = 4179; kf = 0.613; ks =
401;Pr=6.2;
phi = 0.03; R = 33.0; M=0.4;
A1 = (1-phi)+(ros/rof)*phi;
A2 = (1-phi)+ ((ros*cps)/(rof*cpf))*phi;
A3 = (ks+2*kf-2*phi*(kf-ks))/(ks+2*kf+phi*(kf-ks));


a = 0;
b = 1;

solinit = bvpinit(linspace(a,b,5),@guess);
options = bvpset('stats','on','RelTol',1e-7);
sol = bvp4c(@nano_ode,@nano_bc,solinit,options);
figure(1)
plot(sol.x,sol.y(2,:),'b')
xlabel('\eta')
ylabel ('f''(\eta)')
hold on

figure(2)
plot(sol.x,sol.y(5,:),'r')
xlabel('\eta')
ylabel('\theta(\eta)')
hold on

descris=[sol.x; sol.y];
save 'first_sol_casson.txt' descris -ascii
%save first_sol_casson.mat '-struct' 'sol';

fprintf('f(1) = %7.3f.\n', sol.y(1,end));
fprintf('f''(1) = %7.3f.\n', sol.y(2,end));
fprintf('f"(1) = %7.3f.\n', sol.y(3,end));
fprintf('f""(1) = %7.3f.\n', sol.y(4,end));
fprintf('thetha(1) = %7.3f.\n', sol.y(5,end));
fprintf('thetha''(1) = %7.3f.\n', sol.y(6,end));


%-------------------------------------------------------------------
-----
```

```matlab
function dydx = nano_ode(x,y,R,M,phi,A1,A2,A3,Pr)
global R phi A1 A2 A3 M Pr


dydx = [y(2)
    y(3)
    y(4)
    -(M^2)*((1-phi)^2.5)*y(3)-R*A1*((1-phi)^2.5)*(y(2)*y(3)-
y(1)*y(4))
    y(6)
    -(Pr)*(A2/A3)*y(1)*y(6)];
%---------------------------------------------------------------------
-----
function BC = nano_bc(ya,yb)

BC = [ya(1)
    ya(3)
    ya(5)-1
    yb(1)-0.5
    yb(2)
    yb(5)];
%---------------------------------------------------------------------
------


function v = guess(x)

%v = [0 0 0 2 0 1];
v = [-1*exp(-x) sin(x) sin(-x) 2*cos(x) sin(x) cos(x)];



function second_solution
clear all;
clc;
global R phi M a b Pr ros rof cps cpf ks kf A1 A2 A3
ros = 8933; rof = 991.1; cps = 385; cpf = 4179; kf = 0.613; ks =
401;Pr=6.2;
phi = 0.03; R = 33.0; M=0.4;
A1 = (1-phi)+(ros/rof)*phi;
A2 = (1-phi)+ ((ros*cps)/(rof*cpf))*phi;
A3 = (ks+2*kf-2*phi*(kf-ks))/(ks+2*kf+phi*(kf-ks));



a = 0;
b = 1;

solinit = bvpinit(linspace(a,b,5),@guess);
options = bvpset('stats','on','RelTol',1e-7);
sol = bvp4c(@nano_ode,@nano_bc,solinit,options);
figure(1)
plot(sol.x,sol.y(2,:),'b')
xlabel('\eta')
ylabel ('f''(\eta)')
hold on

figure(2)
plot(sol.x,sol.y(5,:),'r')
xlabel('\eta')
```

```matlab
ylabel('\theta(\eta)')
hold on

descris=[sol.x; sol.y];
save 'second_sol_casson.txt' descris -ascii
%save 'second_sol_casson.mat' '-struct' 'sol';

fprintf('f(1) = %7.3f.\n', sol.y(1,end));
fprintf('f''(1) = %7.3f.\n', sol.y(2,end));
fprintf('f"(1) = %7.3f.\n', sol.y(3,end));
fprintf('f""(1) = %7.3f.\n', sol.y(4,end));
fprintf('thetha(1) = %7.3f.\n', sol.y(5,end));
fprintf('thetha''(1) = %7.3f.\n', sol.y(6,end));



%----------------------------------------------------------------------
-----

function dydx = nano_ode(x,y,R,M,phi,A1,A2,A3,Pr)
global R phi A1 A2 A3 M Pr


dydx = [y(2)
    y(3)
    y(4)
    -(M^2)*((1-phi)^2.5)*y(3)-R*A1*((1-phi)^2.5)*(y(2)*y(3)-
y(1)*y(4))
    y(6)
    -(Pr)*(A2/A3)*y(1)*y(6)];
%----------------------------------------------------------------------
-----
function BC = nano_bc(ya,yb)

BC = [ya(1)
    ya(3)
    ya(5)-1
    yb(1)-0.5
    yb(2)
    yb(5)];
%----------------------------------------------------------------------
------

function v = guess(x)

%v = [1 0.5 -4 204 0 0]; %2nd solution
v = [-2*exp(x) sin(x) 4*sin(-x) cos(x) sin(x) cos(-4*x)];



function third_solution
clear all;
clc;
global R phi M a b Pr ros rof cps cpf ks kf A1 A2 A3
ros = 8933; rof = 991.1; cps = 385; cpf = 4179; kf = 0.613; ks =
401;Pr=6.2;
phi = 0.03; R = 33.0; M=0.4;
A1 = (1-phi)+(ros/rof)*phi;
```

204

```matlab
A2 = (1-phi)+ ((ros*cps)/(rof*cpf))*phi;
A3 = (ks+2*kf-2*phi*(kf-ks))/(ks+2*kf+phi*(kf-ks));



a = 0;
b = 1;


solinit = bvpinit(linspace(a,b,5),@guess);
options = bvpset('stats','on','RelTol',1e-7);
sol = bvp4c(@nano_ode,@nano_bc,solinit,options);
figure(1)
plot(sol.x,sol.y(2,:),'b')
xlabel('\eta')
ylabel ('f''(\eta)')
hold on

figure(2)
plot(sol.x,sol.y(5,:),'r')
xlabel('\eta')
ylabel('\theta(\eta)')
hold on

descris=[sol.x; sol.y];
save 'third_sol_casson.txt' descris -ascii
%save 'third_sol_casson.mat' '-struct' 'sol';

fprintf('f(1) = %7.3f.\n', sol.y(1,end));
fprintf('f''(1) = %7.3f.\n', sol.y(2,end));
fprintf('f"(1) = %7.3f.\n', sol.y(3,end));
fprintf('f""(1) = %7.3f.\n', sol.y(4,end));
fprintf('thetha(1) = %7.3f.\n', sol.y(5,end));
fprintf('thetha''(1) = %7.3f.\n', sol.y(6,end));



%-----------------------------------------------------------------
-----


function dydx = nano_ode(x,y,R,M,phi,A1,A2,A3,Pr)
global R phi A1 A2 A3 M Pr


dydx = [y(2)
    y(3)
    y(4)
    -(M^2)*((1-phi)^2.5)*y(3)-R*A1*((1-phi)^2.5)*(y(2)*y(3)-
y(1)*y(4))
    y(6)
    -(Pr)*(A2/A3)*y(1)*y(6)];
%-----------------------------------------------------------------
-----
function BC = nano_bc(ya,yb)

BC = [ya(1)
    ya(3)
    ya(5)-1
    yb(1)-0.5
    yb(2)
    yb(5)];
```

```matlab
%-----------------------------------------------------------------------
------

function v = guess(x)

%v= [0 0.5 -8 204 0 0]; % 3rd solution
%v = [exp(x) -1*exp(x) -4*exp(x) 204+exp(x) -20+cos(x) -20*sin(-x)];
v = [-4*exp(-2*x) 2*exp(-x) 4*sin(-x) cos(x) sin(x) cos(-4*x)];


function velocity_nano
clear all;
clc;
global R phi M a b Pr ros rof cps cpf ks kf A1 A2 A3
ros = 8933; rof = 991.1; cps = 385; cpf = 4179; kf = 0.613; ks =
401;Pr=6.2;
phi = 0.03; R = 33.0; M=0.4;
A1 = (1-phi)+(ros/rof)*phi;
A2 = (1-phi)+ ((ros*cps)/(rof*cpf))*phi;
A3 = (ks+2*kf-2*phi*(kf-ks))/(ks+2*kf+phi*(kf-ks));


a = 0;
b = 1;
for R = 33.0:0.1:34.0
    if R == 33.0
        lo = load ('first_sol_casson.txt');
        solinit.x=lo(1,:);solinit.y=lo(2:7,:);
        else
      solinit.x = sol.x; solinit.y=sol.y;
end


options = bvpset('stats','off','RelTol',1e-10);
sol = bvp4c(@nano_ode,@nano_bc,solinit,options);


end
figure(1)
 plot(sol.x,sol.y(2,:),'k')
 hold on
figure(2)
 plot(sol.x,sol.y(4,:),'k')
 hold on
save ('first_sol_casson.mat', '-struct', 'sol');

%-----------------------------------------------------------------------
-----

for R = 33.0:0.1:34.0
    if R == 33.0
        lo = load ('second_sol_casson.txt');
        solinit.x=lo(1,:);solinit.y=lo(2:7,:);
        else
      solinit.x = sol.x; solinit.y=sol.y;
end


options = bvpset('stats','off','RelTol',1e-10);
sol = bvp4c(@nano_ode,@nano_bc,solinit,options);
```

206

```matlab
end
figure(1)
 plot(sol.x,sol.y(2,:),'k')
 hold on
figure(2)
 plot(sol.x,sol.y(4,:),'k')
 hold on
save ('second_sol_casson.mat', '-struct', 'sol');



%-----------------------------------------------------------------------
-----


for R = 33.0:0.1:34.0
    if R == 33.0
        lo = load ('third_sol_casson.txt');
        solinit.x=lo(1,:);solinit.y=lo(2:7,:);
        else
      solinit.x = sol.x; solinit.y=sol.y;
end

options = bvpset('stats','off','RelTol',1e-10);
sol = bvp4c(@nano_ode,@nano_bc,solinit,options);



end
figure(1)
 plot(sol.x,sol.y(2,:),'k')
 hold on
figure(2)
 plot(sol.x,sol.y(4,:),'k')
 hold on
save ('third_sol_casson.mat', '-struct', 'sol');



%-----------------------------------------------------------------------
-----
function dydx = nano_ode(x,y,R,M,phi,A1,A2,A3,Pr)
global R phi A1 A2 A3 M Pr


dydx = [y(2)
    y(3)
    y(4)
    -(M^2)*((1-phi)^2.5)*y(3)-R*A1*((1-phi)^2.5)*(y(2)*y(3)-
y(1)*y(4))
    y(6)
    -(Pr)*(A2/A3)*y(1)*y(6)];
%-----------------------------------------------------------------------
-----
function BC = nano_bc(ya,yb)

BC = [ya(1)
    ya(3)
    ya(5)-1
    yb(1)-0.5
    yb(2)
```

207

```matlab
    yb(5)];
%----------------------------------------------------------------
------

function v = guess(x)

%v = [0 0 0 2 0 1];
%v = [exp(x) sin(x) sin(-x) 2*cos(x) sin(x) cos(x)];
%v = [-1*exp(x) exp(-x) 4*sin(-x) cos(x) sin(x) cos(-4*x)];
%v = [exp(x) -1*exp(x) -4*exp(x) 204+exp(x) -20+cos(x) -20*sin(-x)];
v = [-4*exp(-2*x) 2*exp(-x) 4*sin(-x) cos(x) sin(x) cos(-4*x)];



function stability_nano
format long g

clear all;
clc;
global R phi M a b Pr ros rof cps cpf ks kf A1 A2 A3 D gamma
ros = 8933; rof = 991.1; cps = 385; cpf = 4179; kf = 0.613; ks =
401;Pr=6.2;
phi = 0.03; R = 33.0; M=0.4;
A1 = (1-phi)+(ros/rof)*phi;
A2 = (1-phi)+ ((ros*cps)/(rof*cpf))*phi;
A3 = (ks+2*kf-2*phi*(kf-ks))/(ks+2*kf+phi*(kf-ks));



a = 0;
b = 1;

D = load('first_sol_casson.mat');
%D=load('first_sol_casson.mat');
%D=load('second_sol_casson.mat');%gamma = -5.1979:-0.0001:-5.1985
%D=load('third_sol_casson.mat');
%D=descris;

err = [];
gam = [];

for gamma = 12.2:0.0001:12.3
    solinit = bvpinit(linspace(a,b,5),@guess);

sol = bvp4c(@nano_ode,@nano_bc,solinit);
figure(1)
plot(sol.x,sol.y(2,:),'b')
hold on
plot(sol.x,sol.y(1,:),'r')
hold on
sol.y;
disp([gamma,abs(sol.y(5,end))]);
err = [err,abs(sol.y(5,end))];
gam = [gam,gamma];



end
figure(2)
plot(gam,err, 'LineWidth', 1.5);
hold on
```

208

```matlab
min(err)
%fprinitf ('eigen value = %7.3f.\n',sol.parameters);


%-------------------------------------------------------------------
---

function dydx = nano_ode(x,y,R,M,phi,A1,A2,A3,Pr,gamma)
global R phi A1 A2 A3 M Pr s D gamma
[s,sp] = deval(D,x);

dydx = [y(2)
    y(3)
    y(4)
    -(M^2)*((1-phi)^2.5)*s(3)-R*A1*((1-
phi)^2.5)*(y(2)*s(3)+s(2)*y(3)-y(1)*s(4)-s(1)*y(4))-gamma*s(3)
    y(6)
    -(Pr)*(A2/A3)*(y(1)*s(6)+s(1)*y(6))-gamma*s(5)];
%-------------------------------------------------------------------
-----


function BC = nano_bc(ya,yb)

BC = [ya(1)
    ya(3)
    ya(5)-1
    ya(6)-1
    yb(1)-0.5
    yb(2)
    ];
%-------------------------------------------------------------------
-----

function v = guess(x,gamma)

v = [-1*exp(-x) sin(x) sin(-x) 2*cos(x) sin(x) cos(x)]; %first
solution
%v = [exp(x) exp(x) -4*exp(x) 208*exp(x) sin(x) sin(-x)]; %2nd
solution
%v = [cos(x) exp(x) -8*exp(x) 204+exp(x) sin(x) sin(-x)]; %3rd
solution
```

209